

Efficient numerical methods to solve some reaction-diffusion problems arising in biology

Owolabi Kolade Matthew



A Thesis submitted in partial fulfillment of the requirements for the degree of Doctor of Philosophy in the Department of Mathematics and Applied Mathematics at the Faculty of Natural Sciences, University of the Western Cape

Supervisor: Prof. Kailash C. Patidar

November 2013

KEYWORDS

Reaction-Diffusion equations

Competitive models

Exponential time differencing methods

Finite difference approximations

Pattern formation

Predator-prey models

Spatiotemporal chaos

Stability analysis

Higher order numerical methods.



ABSTRACT

Efficient numerical methods to solve some reaction-diffusion problems arising in
biology

by

Owolabi Kolade Matthew

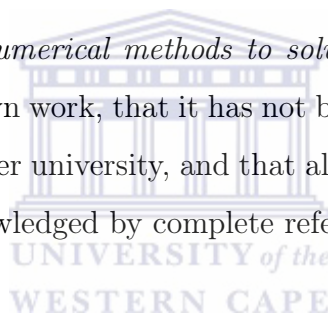
PhD thesis, Department of Mathematics and Applied Mathematics, Faculty of
Natural Sciences, University of the Western Cape

In this thesis, we solve some time-dependent partial differential equations, and systems of such equations, that governs reaction-diffusion models in biology. we design and implement some novel exponential time differencing schemes to integrate stiff systems of ordinary differential equations which arise from semi-discretization of the associated partial differential equations. We split the semi-linear PDE(s) into a linear, which contains the highly stiff part of the problem, and a nonlinear part, that is expected to vary more slowly than the linear part. Then we introduce higher-order finite difference approximations for the spatial discretization. Resulting systems of stiff ODEs are then solved by using exponential time differencing methods. We present stability properties of these methods along with extensive numerical simulations for a number of different reaction-diffusion models, including single and multi-species models. When the diffusivity is small many of the models considered in this work are found to exhibit a form of localized spatiotemporal patterns. Such patterns are correctly captured by our proposed numerical schemes. Hence, the schemes that we have designed in this thesis are dynamically consistent. Finally, in many cases, we have compared our results with those obtained by other researchers.

November 2013.

DECLARATION

I declare that *Efficient numerical methods to solve some reaction-diffusion problems arising in biology* is my own work, that it has not been submitted before for any degree or examination at any other university, and that all sources I have used or quoted have been indicated and acknowledged by complete references.



Kolade Matthew Owolabi

November 2013

Signed

ACKNOWLEDGEMENT

I wish to express my sincere gratitude and appreciation to certain individual and organization who in one way or the other have contributed and helped to make this research work a reality.

First of all, I would like to thank my supervisor, an icon of knowledge, a living legend, Professor Kailash C. Patidar for his leadership, enthusiasm, continuous support, practicality and insightful direction coupled with his sense of humor and willingness to explain things as many times as required were indispensable. May God be with you and your family.

I would like to appreciate the partial financial support of the Federal Government of Nigeria under the Year 2009 Education Trust Fund Academic Staff Training and Development (ASTD) Intervention. Additional funding was provided by Ekiti State government through the Ekiti State scholarship board, Nigeria.

I would like to specially appreciate people like Professor L.N. Trefethen (Oxford University, UK), Professor Ixaru (National Institute of Physics and Nuclear Engineering, Bucharest, Romania), Professor Bengt Fornberg (University of Colorado, Boulder, USA), Professor Emeritus W.E. Schiessser (Lehigh University, Pennsylvania, USA), Professor P.C. Matthews (University of Nottingham, UK), Professor M. Garvie (University of Guelph, Canada) and Assistant Professor R. Sassi (McMaster University, Canada) for their help as and when needed.

Special thanks to my dear wife Mrs Owolabi Toluwalope, her support and ceaseless prayers saw me through the thick and thin of this work. Also to my children, brothers, sisters and friends at home and away, I deeply love you all.

Lastly, my true appreciation also goes to my colleagues in the Department of Mathe-

mathematical Sciences, Federal University of Technology Akure, Ondo-State Nigeria, for their cooperation and understanding in the course of my PhD pursuit in the department of Mathematics and Applied Mathematics, University of the Western Cape, South Africa. I thank you all.



DEDICATION

Dedicated to my **wife, children, mother** and in honour of my late **father**.



Contents

Keywords	i
Abstract	ii
Declaration	iii
Aknowledgement	v
Dedication	vi
List of Tables	x
List of Figures	xxi
List of Publications	xxii
1 General introduction	1
1.1 Reaction-diffusion systems in nature	2
1.2 A quick tour to reaction-diffusion problems and their derivation	3
1.3 Nonlinear reaction-diffusion model	11
1.4 Literature review	16
1.5 Outline of the thesis	21
2 Numerical simulation of some scalar reaction-diffusion models in one and two dimensions	23
2.1 Introduction	24



2.2	Numerical methods	28
2.3	Analysis of the numerical methods	38
2.4	Numerical results	43
2.5	Summary and discussions	63
3	Numerical solution of systems of reaction-diffusion models	65
3.1	Introduction	66
3.2	Model problems	71
3.3	Numerical method	73
3.4	Numerical results	75
3.5	Summary and discussions	97
4	Numerical simulations of reaction-diffusion models in ecology	99
4.1	Introduction	99
4.2	Model problems	102
4.3	Numerical method	120
4.4	Numerical results	121
4.5	Summary and discussions	122
5	Higher-order numerical methods for time-dependent reaction-diffusion equations	125
5.1	Introduction	126
5.2	Qualitative analysis of model problems	128
5.3	Numerical methods	131
5.4	Numerical results	138
5.5	Summary and discussions	152
6	Further exploration of higher order numerical methods for other classes of reaction-diffusion problems	154
6.1	Introduction	155
6.2	Qualitative analysis of model problems	158
6.3	Numerical method	162

6.4	Numerical results	169
6.5	Summary and discussions	184
7	Concluding remarks and scope for future research	186
	Bibliography	190



List of Tables

2.4.1 Error norm L_2 at some selected time steps for solving KISS equation (2.4.3). Parameter values are $T = 1$, $D = 0.5$, $\tau = 0.5$ and $\alpha = 2$ on interval $[-1,1]$ for $N = 200$. We present CPU times for each of the schemes to check competitiveness of the methods.	48
2.4.2 Maximum relative error for Fisher's equation (2.4.5) at various step-sizes for $\delta = 1/8$, final time $T = 1$, $N = 250$ and $x \in [-150, 150]$	60
3.4.1 Absolute relative error for autocatalysis equation (3.4.4) for parameter values $\epsilon = 0.1$, $m = 9$, final time $T = 1$, $L = 50$, $N = 100$	95
5.3.1 Butcher s -stage implicit-explicit Runge-Kutta tableau.	135
5.3.2 Fourth-order implicit (Table(6.5) of [69]) and explicit (Equation (14) of [30]) Runge-Kutta Methods.	136

List of Figures

1.3.1	Time series solution of equation (1.3.4): (a) obtained at $t = 50$ and (b) obtained at $t = 200$. Plot (c) represents the logistic population growth (1.2.13): at $t = 1$, $\tau = 0.9$, $K = 2$. Plot (d) is the phase plane limit circle obtained at $t = 400$, with ratio $\frac{\tau}{D} = 1$	13
1.3.2	Time series solutions and phase plane trajectory of (1.3.10).	16
2.3.1	Stability regions of the ETDADAMS4 scheme (2.2.19) in (a) the complex x plane and (b) the real (x, y) plane.	40
2.3.2	Stable and unstable regions of the ETDADAMS4 scheme in the real (x, y) plane at $y = \pm 1$	41
2.3.3	Boundary of stability regions in the complex x plane for the ETDRK4 scheme (2.2.20).	43
2.4.1	Numerical solutions of one-dimensional KISS model (2.4.3): Time dependent density profiles $u(x, t)$ versus position x on interval $-l \leq x \leq l$ for $D = \tau = \alpha = 1$	45
2.4.2	Diffusion-driven spatial pattern in one-dimensional KISS model (2.4.3) as it changes with both spatial domain x with varying time t	46
2.4.3	Solutions of two-dimensional KISS model (2.4.4) on different spatial domain.	47
2.4.4	Solutions of two-dimensional KISS model (2.4.4) on different spatial domain. The initial data is $u_0(x, y) = \exp(1/10)(\cos x + \sin y)$. Other parameters are $T = 0.05$ $D = 1$, $\tau = 0.01$ and $\alpha = 2$ on (a) $l = 8$ and (b) $l = 14$	49

2.4.5	Solutions of two-dimensional KISS model (2.4.4) on different spatial domain. The initial data is $u_0(x, y) = \sin(\sqrt{(x/\pi)^2 + (y/\pi)^2})$. Other parameters are $D = 1$, $\tau = 0.01$ and $\alpha = 2$ on (a) $l = 10$, $T = 1$; (b) $l = 20$, $T = 0.05$; (c) $l = 40$, $T = 0.05$, and (d) $l = 80$, $T = 0.05$	49
2.4.6	Performance of ETDRK4, ETDM4, ETDM5, ETDM6 and ETDADAMS4 methods for solving the KISS equation (2.4.3) with parameter values $T = 1$, $D = 0.5$, $\tau = 0.5$ and $\alpha = 2$ on interval $[-1,1]$ for $N = 200$	50
2.4.7	Monotonically increasing (a) and decreasing (b) travelling wave solutions of Fisher-KPP equation that switches between two equilibrium points 0 and 1 on $-\infty < x < \infty$	51
2.4.8	Fisher's equation (2.4.5): solution is obtained on interval $-L \leq x \leq L$, for $L = 150$; simulation runs for $N = 250$. Parameter values: Panels (a) at $\delta = 1/8$, $T = 12$ and surface plot (b) is obtained at $T = 40$ when $\delta = 1$, notice the variation at the peaks of (a) and (b).	51
2.4.9	Fisher's equation (2.4.5): Panels (a) and (b) show the profiles of $u(x, t)$ at unit time intervals $T = 1(1)12$ for $\delta = 1/8$ and $\delta = 8$ respectively. Surface plot C is obtained at parameter values $\delta = 1/8$ with final time $T = 1$. D is the solution at $T = 10$ for $\delta = 1/8$. We took $N = 200$	52
2.4.10	Plots of $u(x, t)$ for the first kind in problem (2.4.8) on $-L \leq x \leq L$	53
2.4.11	Various behavioural patterns of traveling waves emanating as a result of the perturbation of the second (2.4.11) and third (2.4.12) kinds of waves for problem (2.4.8).	54
2.4.12	Numerical solutions of equation (2.4.13) for different parameters values of diffusion coefficient D , carrying capacity κ , growth rate τ and time t for initial condition (2.4.6) with $\delta = 1/8$	59
2.4.13	Numerical solutions of Nagumo equation (2.4.23) for different parameter values of D , α , β and time t	61

2.4.14	The top and lower panels show the relative errors as a function of time-step k for various higher-order time stepping methods for Fisher equation (2.4.5). The parameter values are: $\delta = 1/8$, $T=1$, $N = 250$ and $x \in [-150, 150]$	62
3.1.1	Bifurcation curves showing the saddle-node (<i>solid line</i>) and the Hopf bifurcation curve (<i>dotted line</i>). The area enclosed to the left and right of the bifurcation curves described the stable and unstable regions. . .	71
3.4.1	Surface plots of $u(x, t)$ and $v(x, t)$, propagation of pulses and shedding phenomena are observed in the numerical simulation of (3.4.1) at $t = 2000$. . .	77
3.4.2	Propagation of pulses and shedding phenomena of problem (3.4.1) at re-scaled values for $A = \epsilon a$ and $B = \epsilon^{1/3}b$	78
3.4.3	Plots (a)-(d) showing self-replicating patterns and pulse splitting procedures in (3.4.1) for the species u and v	79
3.4.4	Spatially periodic stationary solutions of (3.4.1) observed basically in the positive quadrant. Numerical simulations are obtained with $A = \epsilon a$, $B = \epsilon^{1/\alpha}b$; where $a = 9$, $b = 0.4$ and $\alpha = 1$	80
3.4.5	The dynamic of multiple pulse-splitting process, spatially periodic stationary states of (3.4.1) obtained with $a = 9$, $b = 0.4$, $A = \epsilon a$, $B = \epsilon^{\alpha/3}b$, $\alpha = 1$	81
3.4.6	Front solutions showing amplitudes of u and v at $\epsilon = 0.1$. In panels (a) and (b): The solid curves show $U(\xi) = U(x - ct)$ and the dotted curves show $V(\xi) = V(x - ct)$ at different time.	82
3.4.7	Contour plots showing an unstable eigenfunction of the perturbation $\xi(u, v)$ for $\epsilon = 0.1$, $m = 9$ and the eigenvalue $\lambda = (0.01, 0.2)$	83
3.4.8	Results for the autocatalytic model (3.4.4) with $\epsilon = 0.1$, $m = 9$ at $t = 500$ in panels (a, b) and $m = 9$, $\epsilon = 0$ at time $t = 100$ in panels (c) and (d) for the chemical species u and v . Panels (e) and (f) represent respective surface plots that illustrate the extent at which autocatalytic specie $u(x, t)$ eats into the reactant $v(x, t)$. The parameters chosen here are $\epsilon = 0.1$, $m = 9$ at time $t=100$	84

3.4.9	Contour plots (3.4.4) indicating the spatial behavior of the travelling fronts of the two species. The parameter values are: For panels (a) and (b): $\epsilon = 0.5$, $m = 9$, $L = 50$. Panel (c) and (d): $\epsilon = 0.01$, $m = 9$, $L = 150$; for (e): $\epsilon = 0.1$, $m = 9$, $L = 100$, and for (f): $\epsilon = 0.2$, $m = 9$, $L = 100$	85
3.4.10	Panels (a) and (b): Show typical result of autocatalytic model (3.4.4), at $t = 100$, $\epsilon = 0$ and $m = 7.649$. In (c,d), clearly, the rate at which $u(x, t)$ gains dominance over $v(x, t)$ has been reduced for choosing the parameters $m = 13$, $\epsilon = 0.5$. Panels (c) and (d) describe how u eats into v for $m = 9$, $\epsilon = 0.001$	86
3.4.11	Plots indicating the behavioural patterns of the two species u and v in equation (3.4.4) during the process of their interactions in space. Different parameter values of $m > 0$ and $\epsilon > 0$ are used in a specified domain $-L \leq x \leq L$	87
3.4.12	Results for Gierer-Meinhardt equation (3.4.8) at various parameter values.	88
3.4.13	Concentration profiles for <i>Case I</i> of the Gierer-Meinhardt reaction kinetics (3.4.10) describing the interaction between the activator $u(x, t)$ and inhibitor $v(x, t)$	90
3.4.14	Concentration profiles for <i>Case II</i> of the Gierer-Meinhardt (3.4.11) reaction kinetics describing the interaction between the activator $u(x, t)$ and inhibitor $v(x, t)$	92
3.4.15	Solution for <i>Case III</i> of the Gierer-Meinhardt equation (3.4.13) indicating reaction kinetics between two competing species with concentrations $u(x, t)$ as the activator and $v(x, t)$ that stands for the inhibitor.	93
3.4.16	Solution of Gierer-Meinhardt equation (3.4.16) for <i>Case IV</i> that describes the effect of slowly and mild nonlinear term introduced to the reaction kinetics between two competing chemicals with concentrations $u(x, t)$ as the activator and $v(x, t)$ that stands for the inhibitor.	94

3.4.17 (a) Results for Gray-Scott (3.4.1), autocatalytic (3.4.4) and Gierer-Meinhardt (3.4.11) equations obtained by ETDRK4 scheme at $T = 2$	
(b) Comparative results for autocatalytic equation (3.4.4) obtained by ETDRK4, ABM4 and RK4 schemes at $T = 1$	96
3.4.18 Comparative results for Gray-Scott equation (3.4.1) obtained by ETDRK4, ETDM4, ETDM5, ETDM6 and ETDADAMS4 schemes at $T = 2$, $L = 50$, $A = 9\epsilon$, $B = 2\epsilon^{1/3}$, $\epsilon = 0.001$, $N = 200$, $x \in [0, 100]$	96
3.4.19 Comparative results for Gierer-Meinhardt equation (3.4.11) obtained by ETDRK4, ETDM4, ETDM5, ETDM6 and ETDADAMS4 schemes at $T = 1$, $D = 1$, $\epsilon = 0.01$, $p = 2$, $q = 1$, $m = 2$, $s = 1$ and $N = 250$ for $x \in [-1, 1]$	97
4.2.1 (a) Bifurcation diagram for $\mu > 0$ and $\phi > 0$, for $\phi = \sqrt{\mu^2 + 4\mu} + \mu - 1$. (b) Phase plane trajectory for prey-predator system (4.2.10) for parameter value $\mu = 1.025$, $\phi = 0.3$ and $\psi = 0.05$	106
4.2.2 Typical phase trajectories for (b) the unrealistic prey-predator system (4.2.8). Plots (a), (c), (d) are the various periodic behaviour of the prey u and predator v populations. Parameter values: $\mu = 0.8$, $\psi = 2$, $\phi = 0.4$, which give a steady state at $\hat{u} = 1.5$, $\hat{v} = 0.1$ for (a) at $t = 100$, (b) $t=8000$, (c) $t=500$ and (d) $t=8000$	107
4.2.3 Typical phase trajectories for (b), (f) and (h) for the realistic prey-predator system (4.2.8). Plots (a), (c), (d), (e) and (g) are the various periodic behaviour of the prey u and predator v populations. Parameter values: $\mu = 1.5$, $\psi = 0.08$, $\phi = 0.01$, which give a steady state at $\hat{u} = 1.5$, $\hat{v} = 0.1$ for (a) at $t = 400$, (b) $t=7000$, (c) $t=1500$ and (d) $t=8000$. By taking $\hat{u} = \hat{v} = 0.35$, $\mu = 1$, $\psi = 0.05$, $\phi = 0.2$, we obtain (e) for $t = 100$, (f) for $t = 1000$ and (g) for $t = 300$. For (h), $\mu = 1.025$, $t = 8000$. . .	108
4.2.4 A graph depicting stable equilibrium between two competing species of system (4.2.20).	111

4.2.5	A decline population density associated with the competitive system (4.2.19). Parameter values: (a) $\hat{u} = \hat{v} = 1, \mu = 0.5, \phi = 0.5, \psi = 0.5$ at $t = 5$ and (b) $\hat{u} = \hat{v} = 1, \mu = 0.5, \phi = 0.15, \psi = 0.15$ at $t = 40$. Other parameters are as in (b) except at $\hat{v} = 0.8, t = 40$ for (c) and $t = 20000$ for (d).	113
4.2.6	Phase plane trajectory that represents a nontransitive interactions between three-species in the May-Leonard competition model. The $u_i - u_j$ phase plane for $i \neq j$, indicates that species u_i eliminates u_j and that, there are no two-species positive equilibria. The solutions tend to equilibrium at points $u_i = 1$ and $u_j = 0$	114
4.2.7	Typical phase trajectory limit circle solutions (a), (d)and (f) for the May-Leonard three-species competition system (4.2.28). Plots (a), (c), (e), (g) and (h) show some of the local chaotic behaviours of the three competing species u, v and w population densities.	117
4.2.8	Plots describing individual (chaotic) behaviours in the May-Leonard three-species competition system (4.2.28).	118
4.2.9	Phase trajectories of the two-species mutualism model (4.2.35) with limited carrying capacities. (a) With $\phi\psi > 1$, the system experience an unbounded growth as $u \rightarrow \infty$ and $v \rightarrow \infty$. (b) With $\phi\psi < 1$, all trajectories tend to a positive steady state P with $\hat{u} > 1$ and $\hat{v} > 1$. . .	120
4.2.10	Phase plane trajectory for mutualism system (4.2.35). (a) Linear behaviour of species u and v . Each species experienced an unbounded population growth since the existence of one has no effect on the other and their relationship is linear as in (b). Parameter values are; $u_0 = v_0 = 1, \mu = 1/2, \phi = \psi = 0.15$ at $t = 5$	121

4.4.1	Absolute errors obtained by the computational methods ETDRK4, ETDADAMS4, ETDM4, ETDM5 and ETDM6 at various time steps, Panel (a): when applied to the prey-predator system (4.2.10) at parameter values $t = 1$, $\mu = 0.1$, $\psi = 0.08$, $\phi = 0.01$, $\delta = 0.01$, $N = 200$ and $x \in [-5, 5]$. Panel (b): when applied to the competitive system (4.2.20) with $t = 1$, $\mu = 0.5$, $\psi = 0.15$, $\phi = 0.15$, $\delta = 0.5$, $N = 200$ and $x \in [-5, 5]$.	122
4.4.2	Absolute errors obtained by the computational methods ETDRK4, ETDADAMS4, ETDM4, ETDM5 and ETDM6 at various time steps. Panel (a): when applied to the mutualism system (4.2.34) at parameter values $t = 1$, $\mu = 0.5$, $\psi = 0.5$, $\phi = 0.5$, $\delta = 0.1$, $N = 200$ and $x \in [-1, 1]$. Panel (b): when applied to the competing three species system (4.2.28) with $t = 1$, $\alpha = 0.1$, $\beta = 0.5$, $\zeta_1 = 0.05$, $\zeta_2 = 0.015$, $N = 200$ and $x \in [0, 1]$.	123
5.4.1	Geometric decay of the three species described in problem (5.4.1). Solution is obtained at $t = 20$ for parameter values $\phi = \varphi = \psi = 0$, $\lambda_1 = 0.1$, $\lambda_2 = 0.5$, $\lambda_3 = 0.5$ with initial size 1.5, 0.6, 1.3 for u , v and w respectively.	139
5.4.2	Surface plot of the solutions of (5.4.1) at $t = 0.00007$, for the case when the diffusion coefficients are treated to be equal and taken as $\epsilon = 0.001$.	140
5.4.3	Surface plot of the solutions as a result of coexistence of species A and B to produce C at different time steps: (a) $t = 0.00007$, $\epsilon = 0.001$, $x \in [0, 1]$, (b) $t = 0.009$, $\epsilon = 1$, $x \in [0, 1]$, (c) $t = 2$, $\epsilon = 1$, $x \in [0, 1]$, (d) $t = 0.00007$, $\epsilon = 1$, $x \in [0, 0.2]$, (e) $t = 0.009$, $\epsilon = 1$, $x \in [0, 0.2]$ and (f) $t = 1.086$, $\epsilon = 1$, $x \in [0, 0.2]$, in (5.4.1), where ϵ is defined as diffusivity ratio and $k = 500$, the number of solutions attained between $t_{initial}$ and t_{final} .	141
5.4.4	Plot of the reaction rate e^q , $q = \lambda uv$ in the interval $0 \leq x \leq 1$, $k = 5$, at different time steps: (a) $t = 0.00007$, $\lambda = 10^{-3}$, (b) $t = 0.009$, $\lambda = 0.5$, (c) $t = 0.015$, $\lambda = 0.5$, (d) $t = 0.02$, $\lambda = 0.5$ in problem (5.4.1), when the diffusion coefficients $\phi = \varphi = \psi = 1$.	142

5.4.5	Plot of the reaction rate q at different time steps in the interval $0 \leq x \leq 1$ for (5.4.1). Panels (a) $t = 1, k = 1, \lambda = 0.5$ (b) $t = 50, k = 300, \lambda = 0.5$ and (c) $t = 100, k = 500, \lambda = 0.5$. Panels (d) $t = 0.00007, k = 5, \lambda = 10^3$, (e) $t = 0.009, k = 5, \lambda = 0.5$, and contour plot (f) $t = 0.00007, k = 500, \lambda = 10^3$	143
5.4.6	Comparative relative errors of ETDRK and various IMEX methods when applied to (5.4.1).	144
5.4.7	Local phase planes (a)-(d) for equation (5.4.5), showing spatial distribution of the species at parameter values $\alpha = \beta = \gamma = 0$, for $t = 0.8, u_0 = 2, v_0 = w_0 = 0.8, \tau_1 = \tau_3 = 2, \tau_2 = \tau_4 = 0.8$ and $\tau_5 = \tau_6 = 0.1$. . .	145
5.4.8	Concentration profiles of (5.4.5), obtained at $\tau_1 = \tau_3 = 4.10^{-2}, \tau_2 = \tau_4 = 10^4, \tau_5 = \tau_6 = 3.10^7, \alpha = \beta = \gamma = 1$ for the three species for case I initial condition at $t = 0.01, N = 200, k = 1000$ for panels (a)-(c). Panels (d) and (e) are obtained at time steps $t=0.05$ and $t=0.1$ respectively.	146
5.4.9	Concentration profiles in phase for the three species in case II of problem (5.4.5).	147
5.4.10	Various density profiles of equation (5.4.5) for the three species taken with $N = 250$ when a steady pattern has been obtained in the domain as a result of dynamic evolution from some initial perturbation. The parameters values are: (a) $\tau_1 = \tau_3 = 0.01, \tau_2 = \tau_4 = 0.15, \tau_5 = \tau_6 = 0.3, \alpha = \beta = \gamma = 0.05$, at $t = 1$; (b), (c) and (d) $\tau_1 = \tau_3 = 4.10^{-2}, \tau_2 = \tau_4 = 10^4, \tau_5 = \tau_6 = 3.10^7, \alpha = \beta = \gamma = 2.10^{-2}$ at $t = 5.10^{-4}$	148
5.4.11	Plots showing the spatial distribution of (a) species u , (b) species v and (c) species w obtained at $t = 3000$ for parameters $\alpha = 0.0, \beta = 0.0, \gamma = 0.0, \delta_{11} = 0.01, \delta_{12} = 0.02, \delta_{13} = -0.01, \delta_{21} = 0.1, \delta_{22} = 0.0, \delta_{23} = 0.0, \delta_{31} = 0.1, \delta_{32} = 0.0, \delta_{33} = 0.01, \tau_1 = 0.05, \tau_2 = -0.15, \tau_3 = -0.15, \epsilon_1 = 0.03, \epsilon_2 = 0.06, \epsilon_3 = 0.02$ with initial size $u_0 = v_0 = w_0 = 1$. The local phase plane of model (5.4.10) is shown in plates (d)-(f). The parameter values are the same as above.	149

5.4.12	Density profiles for the three species, modelled through (5.4.10), taken at $t = 30, 60, 210$ for plots (a), (b) and (c) respectively. Panel (d) is showing the oscillation of v concentration at $t = 180$. Parameter values are: $\alpha = 0.005, \beta = 0.1, \gamma = 0.1, \delta_{11} = 0.08, \delta_{12} = -0.08, \delta_{13} = -0.01, \delta_{21} = -0.1, \delta_{22} = 0.0, \delta_{23} = 0.0, \delta_{31} = 0.1, \delta_{32} = 0.0, \delta_{33} = 0.01, \tau_1 = 0.05, \tau_2 = -0.15, \tau_3 = -0.25, \epsilon_1 = 0.03, \epsilon_2 = 0.06, \epsilon_3 = 0.02$	150
5.4.13	Plots showing the dynamical evolution of the three species in (5.4.10), obtained as a result of some small initial perturbations of (5.4.12) to obtain a steady (periodic) state. The parameter values here are same to those used for Figure 5.4.12 but notice the scales on the vertical axes for different amplitudes in the surface plot panels.	151
5.4.14	Concentration profiles for the three species model (5.4.10) taken at (a) $t = 80$ (b) $t = 100$ (c) $t = 100$ and (d) $t = 100$. Parameter values are: $\alpha = 0.007, \beta = 0.001, \gamma = 0.2, \delta_{11} = 0.01, \delta_{12} = 0.02, \delta_{13} = -0.01, \delta_{21} = 0.1, \delta_{22} = 0.0, \delta_{23} = 0.0, \delta_{31} = 0.1, \delta_{32} = 0.0, \delta_{33} = 0.01, \tau_1 = 0.05, \tau_2 = -0.15, \tau_3 = -0.15, \epsilon_1 = 0.03, \epsilon_2 = 0.06, \epsilon_3 = 0.02$	152
6.2.1	Solution of (6.1.1), with $\nu = 0.0015, \alpha = \beta = 0, t = 0.2(0.2)1.8, N = 200$ and $x \in [-10, 10]$	160
6.2.2	Traveling wave solution for equation (6.2.13).	162
6.3.1	Stability regions of (a) IMEXLM1 (6.3.10) and (b) IMEXPC1 (6.3.12)-(6.3.13).	169
6.4.1	Numerical solution for Burgers-Fisher equation (6.1.1) at different parameter values for $N = 200$ with time-step $k = 0.0001$, (a) $\alpha = 1, \beta = 1, \delta = 1, \nu = 1, t = 0.1, 0.2, \dots, 0.9$, (b) surface plot at time $t = 0.9, \alpha = 1, \beta = 1, \delta = 1, \nu = 1$. Panel (c) is obtained at $t = 0.6, \beta = 5, 7, 9, 11, \nu = 1, \alpha = 2$ and $\delta = 2$. Surface plot (d) shows solution at time $t = 0.6, \beta = 11, \delta = 2, \nu = 1$ and $\alpha = 2$	171
6.4.2	Performance of IMEXLM1, IMEXLM2, IMEXPC1 and IMEXPC2 when applied to solve Burger's-Fisher equation (6.1.1) at parameter values $\nu = 0.5, \alpha = 2, \beta = 5, \delta = 2, t = 1$, and $N = 250$ for $x \in [-50, 50]$	171

6.4.3	Numerical solution of Burgers equation (6.4.5) at different parameter values and for $u(x, 0) = \sin(32\pi x)$	172
6.4.4	Numerical solution of Burgers equation (6.4.5) for different parameter values and $u(x, 0) = e^{-10 \sin(\frac{x}{2})^2}$	172
6.4.5	Solution of inviscid Burgers equation (6.1.6) for different parameter values and different initial conditions.	173
6.4.6	Performance of IMEXLM1, IMEXLM2, IMEXPC1 and IMEXPC2 when applied to solve Burgers equation (6.4.5). Other parameter values are $\nu = 0.001$, $\beta = 0.2$, $t = 1$, and $N = 200$ for $x \in [-20, 20]$	173
6.4.7	Numerical solution of Fisher's equation (6.4.6) for various initial conditions.	174
6.4.8	Performance of IMEXLM1, IMEXLM2, IMEXPC1 and IMEXPC2 when applied to solve Fisher's equation (6.4.6) for parameter values $\nu = 0.5$, $\beta = 0.15$, $t = 1$, and $N = 250$ for $x \in [-5, 5]$	175
6.4.9	One soliton solution for KdV equation (6.4.8), using initial condition (6.4.12) and with $N = 200$, $x \in [-15, 5]$. The parameter values used are: (a) $t = 0.0005$, $c = 20$ and $\beta = 1$, (b) $t = 0.005$, $c = 5$ and $\beta = 0.05$	177
6.4.10	One soliton solution for KdV equation (6.4.8) using initial condition (6.4.13), for $\beta = 1, B = 20$ and with parameter values (a) $t = 0.00005$, $\nu = 0.1$, (b) $t = 0.01, \dots, 0.05$, $\nu = 0.9$ and (c) $t = 0.005$, $\nu = 0.05$	177
6.4.11	Two soliton solutions for KdV equation (6.4.8), for $t = 0.0001$, $A = 25$, $B = 16$ and $\beta = 1$, and using initial condition (6.4.14).	178
6.4.12	Two soliton solutions for KdV equation (6.4.8) using initial condition (6.4.15), for $\beta = 1$	178
6.4.13	Solitons travelling from $x = -\infty$ to $x = \infty$ with different phase for KdV equation (6.4.8).	179
6.4.14	Interaction of (a) one and (b) two solitons for KdV equation (6.4.8).	180
6.4.15	Three solitons solutions for KdV equation (6.4.8): (a) $t=0.005$, (b) $t=0.0001$	180

6.4.16 Time evolution for the Allen-Cahn equations (6.4.17)-(6.4.19), for $\omega = 16$, $0 \leq t \leq 100$, the x -axis runs from $x = -1$ to $x = 1$ with diffusion coefficient in the range $[0.001,0.01]$	182
6.4.17 Performance of ETDRK4, ETDM4, ETDM5, ETDM6 and ETDADAMS4 methods for solving the Allen-Cahn equation with $N = 200$, $\delta = 0.5$ and $T = 1$ on $[-1,1]$	183
6.4.18 A typical spatiotemporally chaotic structure of the solution of the Kuramoto-Sivashinsky equation (6.4.20) emerging from smooth initial data on interval of length $L = 32\pi$	183
6.4.19 Time evolution of the Kuramoto-Sivashinsky equation (6.4.20) at some initial conditions for $L = 32\pi$	184



List of Publications

Part of this thesis has been submitted in the form of the following research papers to international journals for publications.

1. K.M. Owolabi and K.C. Patidar, Efficient numerical simulation of Fisher's equation in a localized domain, submitted for publication.
2. K.M. Owolabi and K.C. Patidar, Numerical solution of singular patterns in one-dimensional Gray-Scott-like models, submitted for publication.
3. K.M. Owolabi and K.C. Patidar, Higher-order time-stepping methods for time-dependent reaction-diffusion equations arising in biology, submitted for publication.
4. K.M. Owolabi and K.C. Patidar, On the numerical exploration of Burgers-Fisher equations with implicit-explicit schemes, submitted for publication.
5. K.M. Owolabi and K.C. Patidar, Numerical exploration of nonlinear stiff higher-order PDEs, submitted for publication.
6. K.M. Owolabi and K.C. Patidar, Numerical simulations of some ecological models with exponential time differencing schemes, submitted for publication.
7. K.M. Owolabi and K.C. Patidar, Numerical simulations of KISS models in one and two-dimensional space, submitted for publication.

Chapter 1

General introduction

The field of mathematical biology has become very large with some specialized areas and disciplines like biofluid mechanics, theoretical ecology and so on. So, it is unrealistic and totally inappropriate to think that a single thesis work would cover the whole areas, for this reason, we are restricted in this work to some time dependent partial differential equations that are found largely in application areas of mathematical biology.

In development, for instance, it is true that researchers are still a long way from being able to reliably simulate some biological models due to the theory that abound their formulations which still seems to be poorly understood. We are motivated in this thesis to explore numerically some of the time-dependent reaction-diffusions problems in attempt to address some of the points and queries that naturally arise.

We are thus involved in simulating frameworks on which we can hang our understanding. The model equations, the mathematical analysis and the numerical simulations that follow serve to reveal both quantitatively and qualitatively the consequences of the logical patterns.

Clearly, as more data (variables that are seen as the central players) emerge from the biological system, the models become more sophisticated and the mathematics increasingly challenging. The aim of this thesis is far beyond deriving the mathematical models, though we intend to present the general review of the method of derivation of reaction-diffusion equations. Our goal is to seek for an accurate numerical methods that would capture the essence of various interactions and provide a more fully

understanding of such models.

1.1 Reaction-diffusion systems in nature

Reaction-diffusion equations are regarded as an important class of partial differential equations (PDEs) for which the independent variables are time, t , and space, x . Reaction-diffusion systems are further classify as mathematical models which explains how the concentration of one or more substances or species of organisms, distributed in space changes under the influence of two processes termed reaction and the diffusion. This type of system has a wide application areas, examples are mostly found in biology, geology, physics and ecology.

Mathematically, reaction-diffusion system take the form of semi-linear parabolic differential equations presented in the form


$$\partial_t u = D \nabla^2 u + F(u), \quad (1.1.1)$$

where $u(x, t)$ is the concentration or density of a substance, or simply the vector of dependent variables, D is the diagonal matrix of diffusion coefficients, and F (stands for all the local reactions), is a nonlinear vector-valued function of u (called the reaction terms) and ∇^2 is the laplacian operator. The solution of this class of equation has displayed a wide range of behaviours, such as the formation of travelling waves, self-organised patterns like spots and stripes, replicating patterns and many other dissipative structures. Many of these models are very complex and therefore cannot be solved analytically. To this end, numerical solution of some of these problems will be presented later in this work.

1.2 A quick tour to reaction-diffusion problems and their derivation

Reaction-diffusion systems are used as models in population dynamics, genetics, epidemiology, nerve conduction and combustion theory as well as chemical reactions. Often, these systems are coupled systems of parabolic partial differential equations that are largely encountered in various fields of science, engineering and technology. From ecological point of view, u is regarded as population densities, $F(u)$ represents the effect of predator-prey interactions (relationships), competition or in the form of symbiosis association that describes the mutual benefit and co-existence between two organisms.

The diffusion terms may represent molecular diffusion or some random movement of individuals in a population. For applications of such equations to chemical reactor, see [9, 23, 47]. Applications to biological systems may be in the areas of modeling of infectious diseases such as HIV, cholera, etc, pattern formation on growing domains, mammalian coat [139], single and multi-species waves pursuit and evasions in predator-prey models [120, 137, 146, 181, 190], model for epidermal wound [140] and population dynamics [23, 102] among many others.

This thesis is primarily concerned with the mathematical reaction-diffusion models, we shall outline the derivation of the reaction-diffusion equation of a single-specie system in one spatial dimension from the basic principles. Assume $u(x, t)dx$ is an equivalence of number of individuals located in the interval $(x, x + dx)$ at time t . Following the discussions in [23, 102], we can write the rate of change of the number of individuals in a given interval of space as

$$\frac{\partial}{\partial t}[u(x, t)\Delta x] = \text{growth rate}(x, x + \Delta x) + \text{rate of entry}(x) - \text{rate of departure}(x + \Delta x),$$

where Δx is the spatial interval. Written in mathematical terms, this gives

$$\frac{\partial u}{\partial t} \Delta x = f(x, t) \Delta x + J(x, t) - J(x + \Delta x, t), \quad (1.2.1)$$

where $f(x, t)$ is the growth rate of the population per unit length and $J(x, t)$ is the positive *flux* of individuals to the left and right at position x and time t . Dividing both sides of (1.2.1) by Δx , we obtain

$$\frac{\partial u}{\partial t} = f(x, t) - \left(\frac{J(x + \Delta x, t) - J(x, t)}{\Delta x} \right). \quad (1.2.2)$$

Taking the limit as Δx tends to zero, we get

$$\frac{\partial u}{\partial t} = f(x, t) - \frac{\partial J}{\partial x}, \quad (1.2.3)$$

which is the conservation law for the density of individuals. Specifically, the flux J plays the role of the heat flux in heat transport, or a concentration flux for a chemical reactor, and so on.

Above can be generalized into higher spatial dimensions. Consider Ω to be some, more or less arbitrary region in space with boundary $\delta\Omega$, and let organisms move into and out of this region in any direction, that is,

Change of u in Ω = flux through + change due to birth, death.

In mathematical terms, this means that

$$\frac{d}{dt} \int_{\Omega} u dV = \int_{\Omega} f dV - \int_{\delta\Omega} \mathbf{J} \cdot d\mathbf{S}, \quad (1.2.4)$$

where f comes from the application of the law of mass action to the reactions taking place (describes birth and death), dV denotes integration over space \mathbb{R}^n and $d\mathbf{S}$ denotes surface integration in \mathbb{R}^{n-1} and \mathbf{J} is a flux vector [23]. With the aid of divergence theorem, we convert the third integral in (1.2.4) into a volume integral,

$$\int_{\delta\Omega} \mathbf{J} \cdot d\mathbf{S} = \int_{\Omega} \nabla \cdot \mathbf{J} \cdot d\mathbf{V}, \quad (1.2.5)$$

which, along with (1.2.4) yields

$$\int_{\Omega} \left(\frac{\partial u}{\partial t} - f + \nabla \cdot \mathbf{J} \right) dV = 0. \quad (1.2.6)$$

Since the above integral is zero for arbitrary Ω , we have

$$\frac{\partial u}{\partial t} = f - \nabla \cdot \mathbf{J}. \quad (1.2.7)$$

If u is only a function of (x, t) and f is $f(u)$, we have one-dimensional:

$$\frac{\partial u}{\partial t} = fu(x, t) - \frac{\partial J}{\partial x}, \quad (1.2.8)$$

two-dimensional:

$$\frac{\partial u}{\partial t} = fu(x, y, t) - \nabla \cdot \mathbf{J}, \quad (1.2.9)$$

and three-dimensional:

$$\frac{\partial u}{\partial t} = fu(x, y, z, t) - \nabla \cdot \mathbf{J}, \quad (1.2.10)$$

models.

In deriving these models, some reasonable assumptions have been made by different researchers (see [23, 50, 139]). Often, such reaction-diffusion equations are used to describe the spread of populations in space. In biology, most of these equations are typical time-dependent reaction-diffusion equations where reasonable choices are made for the growth rate $f(u)$, which depends on the independent variables, space and time. We present some of the cases here:

1. No births/death, only flux:

$$f(u) = 0, \quad (1.2.11)$$

2. Exponential growth:

$$f(u) = \tau u, \quad (1.2.12)$$

for $\tau = \text{constant}$ (the growth rate).

3. Logistic growth:

$$f(u) = \tau u \left(1 - \frac{u}{K}\right), \quad (1.2.13)$$

adding a carrying capacity K as limitation of growth.

4. Logistic growth with parameters variation in space:

$$f(u) = \tau(x)u(x, t) \left[1 - \frac{u(x, t)}{K(x)}\right]. \quad (1.2.14)$$

5. Hutchinson-Wright equation:

$$f(u) = \tau u(x, t) \left[1 - \frac{u(x, t - \tau)}{K}\right]. \quad (1.2.15)$$

6. Allee effect:

$$f(u) = \tau u \left(\frac{u}{K_0} - 1\right) \left(1 - \frac{u}{K}\right), \quad (1.2.16)$$

where K_0 is the initial carrying capacity. The basis of this model approach is still the logistic growth, but if the population is too low, it will also die out (extinction). In this circumstance, such phenomena may appear due to the necessity to find a mate for reproduction, or to defend the group against predators. This actually leads to the additional factor $(u/K_0 - 1)$, known as the reaction term. It is paramount to investigate the impact of flux, this is achieved by considering the advection or convection, random motion or diffusion and density-dependent diffusion. Below we briefly describe each of these cases.

Advection or convection:

The advection equation can be derived from the continuity equation, which states that the rate of change for a scalar quantity in a differential control volume is given by flow and diffusion into and out of that part of the system along with any generation or consumption inside the control volume [23]. One can imagine organisms that move

horizontally (advection) or vertically (convection) with velocity $v = v(x)$, so that

$$J = J_A = v(x)u(x, t). \quad (1.2.17)$$

Thus, we can write equation (1.2.8) in the form

$$\frac{\partial u}{\partial t} + \frac{\partial}{\partial x}[v(x)u] = f(u). \quad (1.2.18)$$

For two and three dimensions, we respectively have

$$J_A = v(x, y)u(x, y, t) \text{ and } J_A = v(x, y, z)u(x, y, z, t), \quad (1.2.19)$$

which, in general compactly written after simplifying for organism that moves with a constant velocity in the form

$$\frac{\partial u}{\partial t} + v \frac{\partial u}{\partial x} = f(u), \quad (1.2.20)$$

for one space dimension,

$$\frac{\partial u}{\partial t} + v \cdot \nabla = f(u), \quad v \cdot \nabla = v(x, y), \quad (1.2.21)$$

for two space dimensions, and

$$\frac{\partial u}{\partial t} + v \cdot \nabla = f(u), \quad v \cdot \nabla = v(x, y, z), \quad (1.2.22)$$

for the three space dimensions.

Random motion or diffusion:

Diffusion is one of several transport phenomena that occur in nature. A distinguishing feature of diffusion is that it results in mixing or mass transport, without requiring bulk motion [23, 139]. Thus, diffusion should not be confused with convection, or advection, which are other transport mechanisms that utilize bulk motion to move particles from one place to another. Literarily, diffusion means 'spread out'. Biological

species are often reminiscent of chemical species. Many chemical species move down a density gradient, from high to low concentration regions. The flux in these species is proportional to the negative concentration gradient of density.

There are two ways to introduce the notion of diffusion: either a phenomenological approach starting with Fick's laws of diffusion and their mathematical consequences, or a physical and atomistic one, by considering the random walk of the diffusing particles. Relating this description to the classical approach, namely, Fickian diffusion, this says that the flux, J , of material, which can be cells, amount of chemical, number of animals and so on, is proportional to the gradient of the concentration of the material [139]. That is in one dimension

$$J \propto -\frac{\partial u}{\partial x} \Rightarrow J_D = -D \frac{\partial u}{\partial x}, \quad (1.2.23)$$

where $u(x, t)$ is the concentration or population density of the species and D is its diffusivity. The minus sign simply indicates that diffusion transports matter from a high to low concentration. The movement of $u(x, t)$ is called the flux of the population density, which is a vector. The *high to low* principle now means that, the flux always points to the most rapid decreasing direction of $u(x, t)$, which is the negative gradient of $u(x, t)$.

Using (1.2.23) along with (1.2.8), we obtain

$$\frac{\partial u}{\partial t} = D \frac{\partial^2 u}{\partial x^2} + f(u), \quad (1.2.24)$$

where D is the proportionality constant or diffusion coefficient, $f(u)$ is the reaction term that could take any of the six cases discussed above. The diffusive flux can also be written as

$$J_D = -D \nabla u. \quad (1.2.25)$$

Hence, we have the general balance equation in the form

$$\frac{\partial u}{\partial t} = D \nabla^2 u + f(u), \quad (1.2.26)$$

where $\nabla^2 u$, is the Laplacian operator defined as

$$\nabla^2 u = \frac{\partial^2 u}{\partial x^2} + \frac{\partial^2 u}{\partial y^2}$$

and

$$\nabla^2 u = \frac{\partial^2 u}{\partial x^2} + \frac{\partial^2 u}{\partial y^2} + \frac{\partial^2 u}{\partial z^2}$$

in two and three dimensions respectively.

Some of the examples of diffusion equations in the literature are

- (a) The diffusion or heat equation

$$\frac{\partial u}{\partial t} = D \frac{\partial^2 u}{\partial x^2}, \quad (1.2.27)$$

it has no reaction term $f(u)$ and simple Fickian diffusion [139].

- (b) The simple linear model

$$\frac{\partial u}{\partial t} = \tau u + D \frac{\partial^2 u}{\partial x^2}, \quad (1.2.28)$$

called the KISS (Kierstead, Slobodkin and Skellam) model. This equation has been used to describe the outbreak of red tide [97].

- (c) The simple nonlinear model with logistic growth and simple Fickian diffusion,

$$\frac{\partial u}{\partial t} = \tau u \left(1 - \frac{u}{K}\right) + D \frac{\partial^2 u}{\partial x^2}, \quad (1.2.29)$$

popularly known as the Fisher-Kolmogoroff equation after Fisher [51] who proposed the one-dimensional version as a model for spread of an advantageous gene in a population and Kolmogorov et al. [100] who studied the equation in depth and obtained some basic analytical results. Equation (1.2.29) gives a typical example of a scalar reaction-diffusion equation with a simple traveling wave solution. This is one of the main equations we study in detail later in this work.

(d) The bistable nonlinear model

$$\frac{\partial u}{\partial t} = u(1-u)(u-a) + D \frac{\partial^2 u}{\partial x^2}, \quad (1.2.30)$$

is called the Nagumo equation [141] which is related to the FitzHugh-Nagumo model for nerve action potential.

Density-dependent diffusion:

There are situations where the diffusivity D is not a constant but depends instead on the density of the organisms. It is also possible for diffusion of one species to affect the rate of production of another, so in the course of solving this type of problem the diffusion matrix D cannot be treated as diagonal [102]. A natural extension to incorporate density-dependent diffusion is thus, in one-dimensional situation, where we write the diffusive flux as

$$J_D = -D_0 u^m \frac{\partial u}{\partial x}, \quad (1.2.31)$$

where $D(u) = D_0 u^m$, stands for the density of the organisms, with D_0 and m positive constants. This along with (1.2.8) leads to

$$\frac{\partial u}{\partial t} = D_0 \frac{\partial}{\partial x} \left(u^m \frac{\partial u}{\partial x} \right) + f(u). \quad (1.2.32)$$

To generalize this, let us describe here a situation where functions $f(u)$ have two zeros, say one at $u = 0$ and the other at $u = 1$. Specifically, we consider $f(u) = ku^\alpha(1-u^\beta)$, where α and β are positive constants. Parameters k and D_0 can be eliminated by suitably rescaling t and x so that we have a general form

$$\frac{\partial u}{\partial t} = u^\alpha(1-u^\beta) + \frac{\partial}{\partial x} \left[u^m \frac{\partial u}{\partial x} \right], \quad (1.2.33)$$

where α , β and m are positive parameters. Writing out the diffusion terms in full we get

$$\frac{\partial u}{\partial t} = u^\alpha(1-u^\beta) + mu^{m-1} \left(\frac{\partial u}{\partial x} \right)^2 + u^m \frac{\partial^2 u}{\partial x^2} \quad (1.2.34)$$

which shows that the nonlinear diffusion can be thought as contributing an equivalent convection with velocity $-mu^{m-1}\partial u/\partial x$.

1.3 Nonlinear reaction-diffusion model

We present briefly here some information on the local dynamics of the reaction-diffusion equation (1.2.29). This idea enhances conditions on the parameters necessary for the solutions to have biologically meaningful equilibria as well as a perfect guide for the choice of parameters in the numerical simulations. We consider in this section the solutions of the popular Fisher equation (1.2.29) that contains logistic growth and simple Fickian diffusion for both steady states and the travelling wave solutions.

Steady state solution:

In one-dimension, we write equation (1.2.29) in the form

$$\left. \begin{aligned} u_t &= Du_{xx} + \tau u \left[1 - \frac{u}{\kappa}\right], & 0 \leq x \leq L, \\ u(0, t) &= u(L, t) = 0, \\ u(x, 0) &= u_0(x), \end{aligned} \right\} \quad (1.3.1)$$

where τ , κ and D remain the growth rate, the carrying capacity and the diffusion coefficient respectively. We shall investigate the numerical study of dynamics of the solution of (1.3.1) with a view in the context of biology, that is the main reason for setting out the domain here to include just only the positive half plane, that is $u > 0$, actually corresponds to biologically meaningful solutions. For simplicity, the three parameters r , κ and D can be eliminated by rescaling the dependent and independent variables, this can be achieved by setting the parameters as $\hat{u} \equiv u/\tau$, $\hat{t} \equiv \tau t$, $\hat{x} \equiv \sqrt{\tau/D}x$. After dropping the hats and without loss of generality especially in the context of biology, we only rescale the density as $u \equiv u/\kappa$ but leave both space and

time alone. So, the system take the form

$$\left. \begin{aligned} u_t &= Du_{xx} + \tau u(1 - u), & 0 \leq x \leq L, \\ u(0, t) &= u(L, t) = 0, \\ u(x, 0) &= u_0(x). \end{aligned} \right\} \quad (1.3.2)$$

System (1.3.2) is steady if it is independent of time.

$$\left. \begin{aligned} \tau u(1 - u) + Du'' &= 0, \\ u(0) = 0, \quad u(L) &= 0. \end{aligned} \right\} \quad (1.3.3)$$

We sought solutions around equation (1.3.3) that are equilibrium in time for which $u(x) \geq 0$. The case $u = 0$ is the trivial case that satisfy the system for all values of L . For the nontrivial state, with a new variable $v = du/dx$, we reduce equation (1.3.3) to a system of first order ordinary differential equations

$$u' = v, \quad v' = -\frac{\tau}{D}u(1 - u), \quad (1.3.4)$$

with Dirichlet boundary conditions $u(0) = 0, u(L) = 0, v(0) = 0, v(L) = 0$. It is noticeable that this system of ODEs has two phase-plane equilibria at say, $Q_1 = (0, 0), Q_2 = (1, 0)$. This system has purely imaginary eigenvalues $\lambda_{a,b} = \pm i\sqrt{\frac{\tau}{D}}$. So, Q_1 is the center - for the linear system. Again, linearization about Q_2 yields

$$Df(1, 0) = \begin{pmatrix} 0 & 1 \\ \frac{\tau}{D} & 0 \end{pmatrix}, \quad (1.3.5)$$

with $\lambda_{a,b} = \pm \frac{\tau}{D}$. Hence, Q_2 is called a saddle point. Since $(1, 0)$ is a saddle for the linearization, it is also regarded as a saddle for the original nonlinear system.

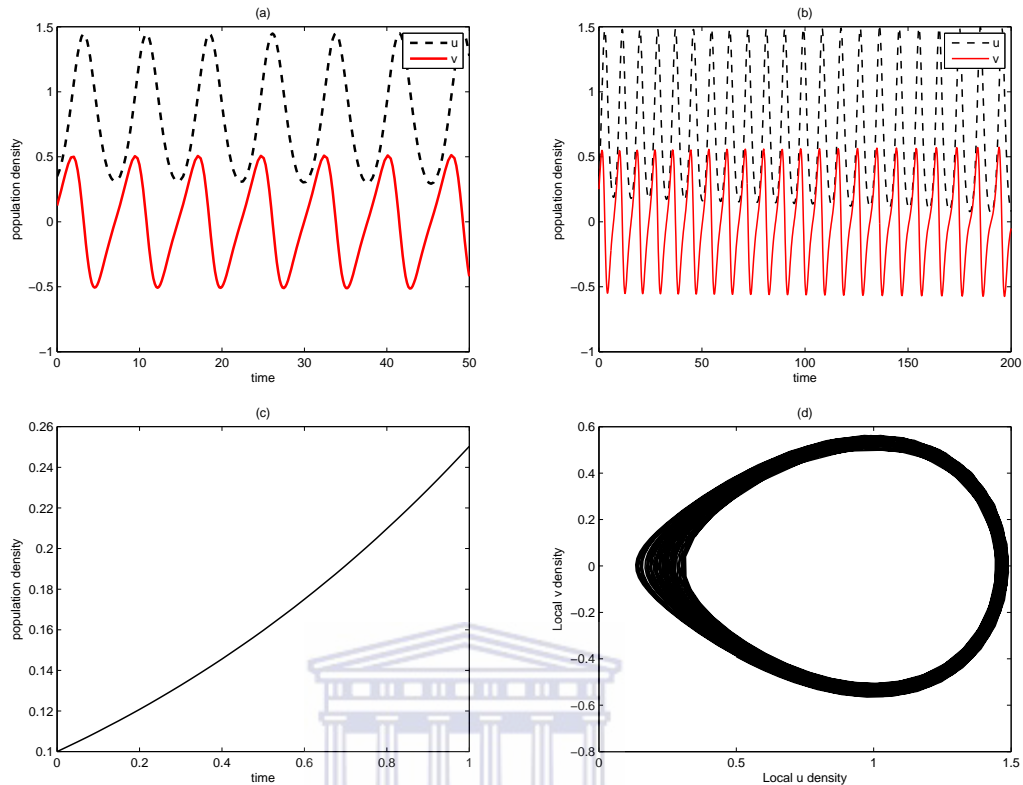


Figure 1.3.1: Time series solution of equation (1.3.4): (a) obtained at $t = 50$ and (b) obtained at $t = 200$. Plot (c) represents the logistic population growth (1.2.13): at $t = 1$, $\tau = 0.9$, $K = 2$. Plot (d) is the phase plane limit circle obtained at $t = 400$, with ratio $\frac{\tau}{D} = 1$.

Traveling wave solution:

To discuss the traveling wave like solutions for reaction-diffusion models, we consider the famous Fisher equation of the form

$$u_t = Du_{xx} + \beta u(1 - u), \quad (1.3.6)$$

where β , κ and D are all positive parameters. The travelling wave solutions of this equation have been studied extensively, see for example, [50], Britton [23], Kot [102] and Murray [136, 139, 140]. The discovery, investigation and analysis of traveling waves of (1.3.6) was earlier reported by Luther [117] in 1906 for the modeling of chemical reaction. In his work, he obtained the waves speed in terms of the parameters associated with the reactions he was studying. The first explicit analytic form of a cline solution

for the Fisher equation were obtained by Albowitz and Zeppetella in making use of the Painlevé analysis [2]. The work of Murray [139] has shown that the analytical form of (1.3.6) is the same as that found by Kolmogoroff et al. [100] and Fisher [51].

To discuss some of these aspects briefly here, we rescale the variables in (1.3.6) by applying $\hat{u} \equiv u/K$, $\hat{t} \equiv \beta t$, $\hat{x} \equiv \sqrt{\beta/D}x$. This, after dropping the hats, gives

$$u_t = u_{xx} + u(1 - u). \quad (1.3.7)$$

We had previously considered the steady-state solutions but in the context of biology, we need to study the spread of population dynamics, it is obvious that we can not keep a particular species say an animal in a particular spot or position without exhibiting a kind of movement. The best way to tackle this is by introducing another new variable, say $\xi = x - ct$ [102, 119, 139]. We equally consider the positive movement since it is unrealistic to have negative speed, the moving wave is let to be $u(x, t) = u(x - ct) = u(\xi)$, then $u(x, t)$ is a traveling wave, and it moves at constant speed c in the positive x -direction. Obviously, if $x - ct$ is constant, so also is u . This also implies that the coordinate of the system moves with speed c . Our interest is to determine the wave-speed c . The dependent variable ξ is called sometimes the wave variable. To be physically realistic [139], $u(\xi)$ has to be bounded for all ξ and nonnegative with the quantities with which we are concerned, such as chemicals and populations.

With this information in place, it is convenient to reduce the partial differential equation (1.3.7) to an equivalent system of ordinary differential equations

$$\frac{\partial u}{\partial t} = \frac{\partial u}{\partial \xi} \frac{\partial \xi}{\partial t} = -cu', \quad (1.3.8)$$

$$\frac{\partial u}{\partial x} = \frac{\partial u}{\partial \xi} \frac{\partial \xi}{\partial x} = u', \quad (1.3.9)$$

so that equation (1.3.7) reduces to $u'' + cu' + u(1 - u) = 0$, which we can write further

to give a first order system of equations

$$\begin{aligned} u' &= v, \\ v' &= -cv - u(1 - u). \end{aligned} \tag{1.3.10}$$

The pair of equation (1.3.10) possess two equilibria at $(1, 0)$ and $(0, 0)$, so that

$$\lim_{\xi \rightarrow -\infty} (u, v) \rightarrow (1, 0) \text{ and } \lim_{\xi \rightarrow +\infty} (u, v) \rightarrow (0, 0).$$

Next, we need to find the heteroclinic connection between the two equilibria points.

First, we start with the determination of the nature of the two phase-plane equilibria.

At point $(1, 0)$, the Jacobian becomes

$$J = \begin{pmatrix} 0 & 1 \\ -1 + 2u & -c \end{pmatrix}_{(1,0)} = \begin{pmatrix} 0 & 1 \\ 1 & -c \end{pmatrix}, \tag{1.3.11}$$

whose characteristic equation is $\lambda^2 + c\lambda - 1 = 0$. Obviously, the equilibrium here is a saddle point for $c > 0$. The stable and unstable saddle eigenvectors that are compatible with the heteroclinic connection can also be determined at this point. At the origin, the equilibrium points satisfy the characteristics equation $\lambda^2 + c\lambda + 1 = 0$, whose solutions yield

$$\lambda_{1,2} = -\frac{c}{2} \pm \frac{\sqrt{c^2 - 4}}{2}, \tag{1.3.12}$$

which implies by following the Routh-Hurwitz criterion [88] which gives the necessary and sufficient conditions for the roots of the characteristic equation (1.3.12) to be asymptotically stable at the origin. We can see that the origin is a stable focus for $0 < c < 2$, all orbits close to the origin in this range oscillate to mean that finding a nonnegative heteroclinic connection between the points $(1, 0)$ and $(0, 0)$ is becoming impossible. For $c \geq 2$, the origin is no longer a stable focus, it is now a stable node and a nonnegative heteroclinic connection may be possible. Therefore, $c \geq 2$ is the necessary condition of a traveling wave.

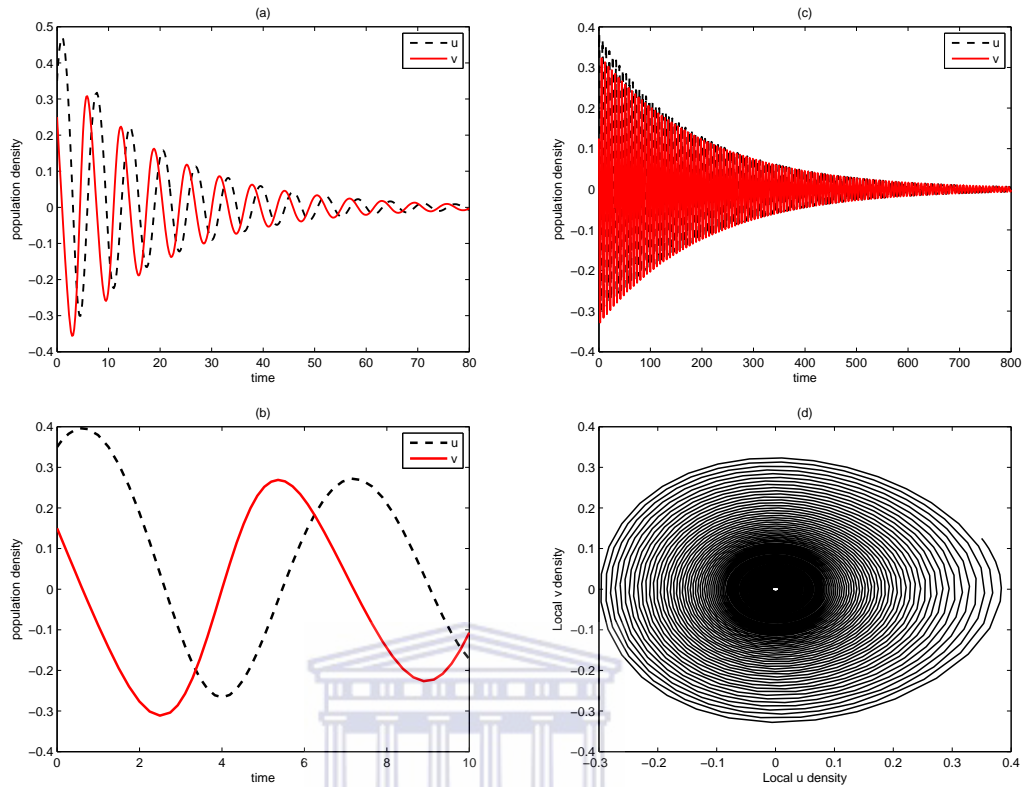


Figure 1.3.2: Time series solutions and phase plane trajectory of (1.3.10).

1.4 Literature review

Mathematical modeling of real-life problems usually results into a reaction-diffusion equations which naturally exist in the form of differential equations. Reaction-diffusion and a wide variety of physical phenomena involving functions of several variables, such as the propagation of heat or sound, fluid flow, elasticity, electrostatics and electrodynamics, exist in the form of partial differential equations (PDEs). Reaction-diffusion equations are regarded as a special class of parabolic time-dependent partial differential equations.

Nonlinear phenomena occurs in various fields of science and engineering. In fact, in biology and medicine there is a wide spectrum of examples which exhibit collective behavior, such as formation of patterns and clustering. This may happen at any scale, from the cellular scale of embryonic tissue formation, wound healing or tumor growth, and vasculogenesis, the microscopic scale of life cycles of bacteria or social amoebae, to the larger scale of animal grouping, indeed animals may form swarms, characterized

by a cohesive but unorganized aggregation (such as midges), or schools with a cohesive and synchronized organization (for example, in fish schooling, individuals are oriented so that distances are uniform), or shoals (for instance, fish) and flocks (as in birds) in which animals are gathered together for social aims, in a synchronized or asynchronized way, or herds, congregation, and so on [137]. Much attention has been devoted recently to the search for better and more efficient way of determining a solution, approximate or exact, analytical or numerical, to nonlinear models.

The major way of solving the class of these equations is through discretization. A well-known approach to solve time-dependent partial differential equation, whose solutions vary both in time and space, is the *method of lines* [10, 174, 183, 186]. Application of this method requires to first construct a semi-discrete approximation to the problem by setting up a regular grid in space, this is achieved by discretising the spatial independent variables with boundary constraints. Hence, a couple system of ordinary differential equations are generated in time, which is associated with the initial value. Once that is done, we numerically approximate the solutions to the original time-dependent partial differential equation by marching forward in time on this grid. Conveniently, we can now apply any existing, and generally well established, time-stepping numerical methods such as the implicit-explicit (IMEX) schemes, Runge-Kutta methods or exponential time differencing (ETD) schemes among many others.

In this work, for the spatial discretisation, we are primarily concerned with the use of higher-order finite difference method. The finite difference methods have gained its dominance in the various fields of computational science since its inception as the major method of choice back to 1960s. Other methods such as finite element and boundary element methods enjoyed recent popularity, finite difference methods are still well utilized for a wide array of computational engineering and science problems. Readers are referred to [52, 53] and the references therein, where schematic illustration of how to generate the weights of higher order centered and one-side finite differences formulas for approximating derivatives up to fourth-order equi-spaced grids with order of accuracy up to eighth can be found. In all, the discrete approximation to the derivatives will be converted into Toeplitz matrices. Our time integration approach

uses mostly the ETD schemes, other time-stepping methods include but not limited to the fourth-order Runge-Kutta (RK4) method and the family of IMEX schemes.

Numerous time stepping methods have been designed to integrate the dynamical systems arising from spatially discretized time-dependent partial differential equations, reference shall be made to those that are of practical use in this thesis. One example is the family of Implicit-Explicit (IMEX) schemes. These schemes have been rediscovered several times in various forms and under various names [10, 11, 30, 66, 86, 112, 167] have been often used, especially in conjunction with spectral methods [186, 187]. This type of schemes are specifically designed to suite the semi-linear problems. In particular the reaction-diffusion problems which can be split into linear and nonlinear parts. IMEX schemes consist of using an explicit multi-step formula, for example, the second order Adams-Bashforth formula, to advance the nonlinear part which varies slowly than the linear part, and an implicit scheme, for instance, the second order Adams-Moulton formula, to advance the linear part which contain the stiffest part of the dynamics of the problem.

Other kinds of formulations also exist, for development based on Runge-Kutta rather than Adams-Bashforth formulae. It is worth mentioning among the most recent implicit-explicit Runge-Kutta schemes developed, for instance, Ascher et al. [11] developed a family of L-stable two-, three-stages diagonally implicit Runge-Kutta (DIRK) and four-stage, third-order combination schemes whose constructions were based on implicit-explicit Runge-Kutta methods for integration of convection-diffusion equation. In another development, Kennedy and Carpenter [95] construct a family of higher-order, L-stable explicit and singly diagonally implicit Runge-Kutta using IMEX schemes for addressing one-dimensional convection-diffusion-reaction equations. More recently, Koto [103] constructs IMEX Runge-Kutta schemes for reaction-diffusion equations with an established convergence and stability. An explicit Runge-Kutta (ERK) method is used to solve the non-stiff part and a diagonally implicit Runge-Kutta (DIRK) method is employed to solve the stiff part of the problem to overcome the severe stability restriction inherent in the explicit method.

Another family of time stepping method is the well known Runge-Kutta methods.

In Butcher [28, 29], the centenary history of Runge-Kutta methods contains an appreciation of the early work of Runge [165], Heun [71], Kutta [106], and Nyström [143] and a survey of some significant developments of these methods over the last hundred years was presented. Runge-Kutta methods have been adapted to the solution of more general problem classes each of which has been the subject of specialized research in recent years. In addition to the use of Runge-Kutta methods in their traditional role of differential equation solvers, related types of initial value problems have been found to be amenable to solution by Runge-Kutta methods suitably adapted to the more general problem class. Examples of these wider classes of problems are PDE's, Volterra integral equations, delay differential equations, differential-algebraic equations and stochastic differential equations.

The method of integrating factor is a technique by which both sides of a differential equation is multiplied by some integrating factor and then make some relevant changes. This approach is peculiar to the theory of ordinary differential equations. The change of variable idea permits us to solve the linear part exactly, and then use a numerical scheme of our interest to solve the transformed nonlinear equation. This technique has been used for partial differential equations by Kassam and Trefethen [92], Cox and Matthews [36], Trefethen [187], Berland and Skaflestad [16].

Recently, there has been a great deal of interest in the construction of exponential integrators. Even though the theory of numerical methods for time integration is well established for a general class of problems, recently due to improvements in the efficient computation of the exponential function, exponential integrators for the time integration of semi-linear problems have emerged as a viable alternative. The history and emergence of exponential integrator as reported in [128] could be traced to the first paper to construct what are now known as exponential integrators [33].

Down the memory lane, in 1998 the term "Exponential Integrators" was proposed by Hochbruck et al. [74]. As a result of their work one of the first efficient implementations of an Exponential Integrator was developed. The code uses Rosenbrock-type methods, adaptive time stepping and Krylov sub-sampling for the exponential functions. A completely different class of methods, the so called RKMK methods, were

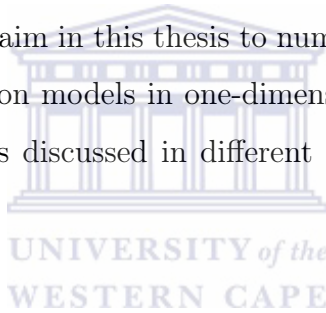
developed in [132] in which the equation is transformed in such a way that it evolves on a Lie algebra. He used the affine action on the algebra to construct integrators that solve semi-linear problems. These methods lead to the Generalized Integration Factor (GIF) methods introduced by Krogstad [104].

The major focus of this thesis is the use of Exponential Time Differencing (ETD) schemes to solve some reaction-diffusion equations arising from biology. Numerical experiments were performed on certain stiff PDEs in [92] using the IF, ETD, linearly implicit methods and splitting methods. It was concluded that the ETD methods consistently outperformed all other methods. This class of schemes is especially suited to semi-linear problems which can be split into the linear and nonlinear parts. These schemes have been rediscovered several times in various forms and under various names, for instance, [31, 33, 74, 83, 104, 142]. A given example is the exact linear part (ELP) schemes that were derived by Beylkin et al. [18] for arbitrary order. In [18], a variety of explicit and implicit exponential integrators based on multi-step methods are constructed. Although the methods are derived for arbitrary systems of ODEs they give special attention to those arising from the discretization of advection-diffusion equations. They give the coefficients of the method based on the third order Adams-Bashforth formula, the coefficients of the method based on the fourth order Adams-bashforth formula are implicit in the presentations [18, 36], explicitly stated in [128]. These third and fourth order methods are selected as classical examples of multi-step based exponential integrators termed ETDAB3 and ETDAB4 in [66]. It was noted in [12] that the authors did not give explicit formulas for the method's coefficients.

The most and first comprehensive treatment, and in particular the exponential time differencing fourth order formula was derived in the paper by Cox and Matthews [36] where the explicit derivation of the explicit ELP methods for arbitrary order s , with explicit formulas for the methods' coefficients is presented and referred to these methods as the Exponential Time Differencing (ETD) schemes. Cox and Matthews argued that ETD schemes outperforms IMEX schemes because they treat transient solutions (where the linear term dominates) better, and also outperform integrating factor schemes because they treat non-transient solutions (where the nonlinear term

dominates) better. In addition, the authors of [36] further developed some explicit time differencing Runge-Kutta (ETDRK) schemes of order up to four.

The coefficients of the ETD methods are the exponential and related functions of the linear operators. These coefficients can be evaluated once before the integration begins if a constant time step is used throughout the integration. The convergence analysis for the explicit s -step exponential schemes was carried out in [16, 31, 128] for solving semi-linear equations. The analysis showed that the schemes achieve order of accuracy s , for appropriate starting values at the n th and previous time steps. In addition, the authors of [74, 75, 76] analyzed the convergence behavior of the explicit exponential Runge-Kutta methods for integrating semi-linear parabolic problems. They gave a new derivation of the classical order conditions and showed convergence for these methods up to order four. It is our aim in this thesis to numerically explore one, two, and three systems of reaction-diffusion models in one-dimension. Other relevant works pertaining to individual problems discussed in different chapters are reviewed in respective chapters.



1.5 Outline of the thesis

The rest of this thesis is organized as follows.

In Chapter 2, we present in detail, the algorithmic formulation of the fourth-order exponential time differencing Runge-Kutta and that of Adams-type which we denoted for brevity as ETDRK4 and ETDADAMS schemes, respectively, by following the approach introduced in [36, 92]. We in addition, examine the stability analysis of these schemes. This chapter marks the beginning of our numerical experiments on real application problems.

Chapter 3 marks the beginning of our study of systems of time-dependent reaction-diffusion equations which allow for much more complex behaviour than a scalar reaction-diffusion equation that describe pulse splitting processes and self-replicating patterns.

Some ecological species dynamics involving the predator-prey, competitive, and mutualism models are considered in chapter 4. The results of the numerical experiments

presented grant a deep understanding to what each of the models stand for.

In Chapter 5, we demonstrate the use of higher order methods to solve some time-dependent system of reaction-diffusion problems. We extend in this chapter, the compatibility of fourth-order finite difference scheme (in space) coupled with fourth-order time-stepping methods; such as IMEXLM4, IMEXPC4, IMEXRK4 and ETDRK4 (in time); for direct integration of reaction-diffusion equations. Some interesting numerical anomaly phenomenons associated with steady state solutions of the examples chosen from the literature are well presented to address points and queries that may occur. Our findings have lead to the understanding of pattern formation such as spiral waves and patchy structures as well as some spatiotemporal dynamical structures.

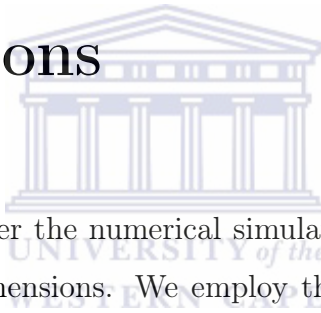
The links between the Fisher and Burgers equations are demonstrated through some numerical experiments by considering a class of Burgers-Fishers equation in Chapter 6. In this chapter, we mainly use the first and second order methods among the families of implicit-explicit linear multi-step (IMEXLM1,2) and implicit-explicit predictor-corrector (IMEXPC1,2) schemes. Note that these family of methods are restricted from having an order higher than two if A-stability is required.

Finally, in Chapter 7, the most important ideas presented in this thesis are highlighted with the biological relevance of our results. Furthermore, we list a number of possible extensions to this work.

Before we move on to the rest of the thesis, it is worth mentioning here that simulation results presented in this work are performed by using MATLAB.

Chapter 2

Numerical simulation of some scalar reaction-diffusion models in one and two dimensions



In this chapter, we consider the numerical simulations of nonlinear form of the KISS model in one and two-dimensions. We employ the popular fourth-order exponential time differencing Runge-Kutta (ETDRK4) schemes proposed by Cox and Matthew [36], that was modified by Kassam and Trefethen [92], for the time integration of spatially discretized partial differential equations. We demonstrate the supremacy of ETDRK4 over the existing exponential time differencing integrators that are of standard approaches and provide timings and error comparison. Numerical results obtained in this chapter have granted further insight to the question '*What is the minimal size of the spatial domain so that the population persists?*' posed by Kierstead and Slobodkin [97], with a conclusive remark that the population size increases with the size of the domain. In attempt to examine the biological wave phenomena of the solutions, we present the numerical results in both one- and two-dimensional space, which have interesting ecological implications. Initial data and parameter values were chosen to correspond to some existing patterns.

2.1 Introduction

Reaction-diffusion models are mathematical equations that describe the way the concentration of substances is being distributed in space, under the influence of two important terms or processes called the reaction and diffusion. The reaction term deals with the way two or more substances are transformed into each other, and the diffusion term which is responsible for the substances to spread out in space. Most reaction-diffusion systems exist in form of semi-linear parabolic partial differential equations which interact mainly in a nonlinear manner. They are widely encountered in various fields of science and engineering, in particular, the application areas of mathematical biology and ecology. Reaction-diffusion equations can be written in the general form

$$\partial_t u = D\nabla^2 u + N(u), \quad (2.1.1)$$

where $u(x, t)$ is termed the concentration of a substance or the density of a particular specie, D is the diffusion coefficients, and the term $N(u)$ accounts for the local reactions which either exists in linear or nonlinear forms, and ∇^2 denotes the laplace operator in one-dimensional space.

The solution of reaction-diffusion equations has over decades generated a lot of attentions and displayed a wide range of behaviours such as the wave-like phenomena as well as other self-organized patterns like stripes, hexagons or more intricate structure like dissipative solitons. If the reaction term vanishes, then the equation represents a pure diffusion or heat equation. The study of nonlinear reaction-diffusion equation of the form

$$\frac{\partial u}{\partial t} = D\nabla^2 u + f(u), \quad (2.1.2)$$

has a long-standing history in mathematical modeling of propagation phenomena that mostly occurs in distributed dissipative dynamics. Most realistic physical problems such as Allen-Chan, Burgers, Cahn-Hilliard, Fisher-KPP, Nagumo, Gray-Scott (or cubic autocatalytic), Kierstead, Slobodkin and Skellam (KISS), Kuramoto-Sivashinsky and host of others, naturally exist in form of higher-order partial differential equations. In [80], PDEs of the class (2.1.2) have shown to provide a natural framework

for investigating the influence of patch size and geometry on the population dynamics of organisms living within an habitat. Many researchers have used equations of the form (2.1.2) in different forms especially in relation to three applications that model the behaviour of biological systems in a spatial setting. The three major and popular applications of reaction-diffusion models relate to critical patch size [97], spread of advantageous genes [51], and pattern formation [189]. For instance, if the reaction or interaction term $f(u)$ is replaced by $\kappa u(1 - u)$, where κ and D are positive parameters regarded as the carrying capacity and diffusion respectively in the context of biology, then (2.1.2) becomes the classic simplest case of a nonlinear reaction-diffusion equation popularly referred to as Fisher equation [51] with history dated back to 1937, which has since becomes one of the most well-studied reaction-diffusion models in population biology to describe the spread of an advantageous allele.

In this work, numerical solution of an exponential growth model of the form (2.1.2), where the reaction term $f(u)$ is given as τu^α , so that equation (2.1.2) becomes


$$\frac{\partial u}{\partial t} = D \nabla^2 u + \tau u^\alpha, \quad (2.1.3)$$

where the diffusion coefficient D , the growth rate τ and the critical exponent constant α , are all positive parameters. This equation is the critical patch model popularly known as the KISS model named after Skellam [181] and Kierstead and Slobodkin [97] which was originally developed to describe the spread of red tide outbreaks. Red tide is a name given to the discolored waters caused by the aggregation or blooming of microscopic organisms. A model for growth and spread of a population is used to determine the minimal size of the spatial domain needed for population to survive and this minimal size is referred to as the critical patch size [7].

In the classical paper [97], the critical patch size was determined for a simple reaction-diffusion equation with exponential growth, their model was applied to study phytoplankton plants living in the ocean. Determination of patch size of one-dimensional form of (2.1.3) have been considered [7, 97, 102, 137, 145] on the spatial domain $[0, l]$ via separation of variables method. In one-dimension with the choice $\alpha = 1$, we have

the KISS model

$$\frac{\partial u}{\partial t} = D \frac{\partial^2 u}{\partial x^2} + \tau u, \quad 0 \leq x \leq l, \quad t > 0, \quad (2.1.4)$$

subject to initial and homogeneous Dirichlet boundary conditions

$$u(x, 0) = u_0(x), \quad 0 \leq x \leq l, \quad (2.1.5)$$

$$u(0, t) = u(l, t) = 0, \quad t > 0, \quad (2.1.6)$$

where $D > 0$ and $\tau > 0$. The solution is given as

$$u(x, t) = \sum_{n=1}^{\infty} a_n \sin\left(\frac{n\pi x}{l}\right) \exp\left[\tau - \frac{n^2\pi^2}{l^2}\right] t, \quad (2.1.7)$$

with

$$a_n = \frac{2}{l} \int_0^L u_0(x) \sin\left(\frac{n\pi x}{l}\right) dx. \quad (2.1.8)$$

By examining the solution reveals the condition that supports population growth and extinction. For instance, if

$$l < \pi \sqrt{\frac{D}{\tau}},$$

then $u(x, t)$ will approach zero as time progresses, while if

$$l > \pi \sqrt{\frac{D}{\tau}},$$

$u(x, t)$ will increase indefinitely with time, thus leading to the bloom of the plankton.

In attempt to have a better understanding of how the solution of the reaction-diffusion equation (2.1.3) behaves, we let $\tau = 0$. Hence, equation (2.1.3) reduces to diffusion equation. We can now find the solution of the general initial value problem of solving (2.1.3) in spatial variable x , subject to

$$u(x, 0) = u_0(x), \quad \text{for } -l \leq x \leq l, \quad (2.1.9)$$

with the aid of the Fourier transforms, as

$$u(x, t) = \frac{1}{\sqrt{4\pi Dt}} \int_{-l}^l u_0(X) \exp \left\{ \frac{(x - X)^2}{4Dt} \right\} dX. \quad (2.1.10)$$

On using the initial condition as the localized source of the spread of species population, $u_0(x) = \delta(x)$, then, (2.1.10) becomes

$$u(x, t) = \frac{e^{-x^2/4Dt}}{\sqrt{4\pi Dt}}. \quad (2.1.11)$$

As time increases the solution spreads out, having a typical width of $O(\sqrt{4\pi Dt})$ and a maximum height of $1/\sqrt{4\pi Dt}$. It is also noticeable that the diffusion transports the species within the interval of integration $[-l, l]$, since $u(x, t) > 0$ for all x when $t > 0$. For $|x| \gg 1$ and $t \ll 1$, the corresponding species concentration are very small. If $u_0(x) = G(-x)$, then the solution takes the form

$$u(x, t) = \frac{1}{\sqrt{\pi}} \int_{x/\sqrt{4Dt}}^l e^{-\xi^2} d\xi. \quad (2.1.12)$$

Despite the considerable progress made so far in the field of population dynamics, there are still many open problems. In particular, the numerical exploration of (2.1.3) for $\alpha > 1$ has received little or no attention when the domain of interaction is considered wide enough to contain the population spread. Put together all these findings, we are motivated to seek for an appropriate and efficient numerical solution of (2.1.3) in one and two dimensional space which we consider on an infinite domain truncated at some large, but finite value of l .

The rest of this chapter is organized as follows. In Section 2.2, we discuss numerical methods where finite difference and spectral methods are considered for spatial discretisation. Construction of an exponential time differencing schemes are also considered. In Section 2.3, we examined the stability analysis of the numerical methods. Numerical results of KISS model in one and two dimensions, Fisher equation and Nagumo equation are presented in Section 2.4. The chapter ends with summary and discussions in Section 2.5.

2.2 Numerical methods

We discuss briefly the spatial discretisation methods used in this thesis. The method of lines (MoL) [173, 174] is an important technique that is widely used for solving partial differential equations (PDEs) in which all but one dimension is discretized. The MoL provides standard, general-purpose methods and software, developed for the numerical integration of ODEs, to be used. The method of lines most often refers to the construction or analysis of numerical methods for PDEs that proceeds by first discretizing the spatial derivatives only and leaving the time variable continuous. This leads to a system of ordinary differential equations to which a numerical method for initial value ordinary equations can be applied.

Virtually, most realistic mathematical biology models such as, Fisher, Gray-Scott and Auto-catalysis equations exist in nonlinear form. They do not have closed form solutions, thus numerical methods have an important role to play in examining the behaviour of their solutions. Many researchers have used finite-difference technique as a way of approximating the reaction-diffusion equations (see for example, [72, 131]). However there are comparatively few studies [126, 149, 162] that give stability and convergence results. Recently, Garvie [57, 59] presented two stable finite difference methods for the numerical solution of predator-prey interaction that was previously studied by Garvie and Trenchea [58].

When a time-dependent partial differential equation is discretized in space especially with either a finite difference or spectral approximations, it results to system of coupled ordinary differential equations in time, the resulting ODEs coming from the notion of method of lines (MoL) is stiff, such a system requires the use of higher-order approximation scheme in both space and time since naturally some of these time-dependent problems are found of combining lower-order nonlinear terms with higher-order linear terms. In one-dimension, we consider the semi-linear partial differential equation

$$\left. \begin{aligned} \frac{\partial u}{\partial t} &= D \frac{\partial^2 u}{\partial x^2} + \tau u^\alpha, & -l \leq x \leq l, & \quad t > 0, \\ u(x, 0) &= u_0(x), & -l \leq x \leq l, \\ u(0, t) &= u(l, t) = 0, & \quad t > 0, \end{aligned} \right\} \quad (2.2.1)$$

with $D > 0$, $\tau > 0$ and $\alpha > 0$. We discretize in space with step-size $h = x/(N - 1)$ and approximate the second-order spatial derivative by the fourth order central difference operator. We then obtain a system of nonlinear ordinary differential equations

$$\frac{du_{i,j}}{dt} = D \left[\frac{-u_{i+2,j} + 16u_{i+1,j} - 30u_{i,j} + 16u_{i-1,j} - u_{i-2,j}}{12h^2} \right] + \tau(u_{i,j})^\alpha, \quad (2.2.2)$$

with $u = [u_1, u_2, \dots, u_l]^T$, for $1 \leq i, j \leq l$.

Now, the two-dimensional form of system (2.1.3) can be written as

$$\left. \begin{aligned} \frac{\partial u}{\partial t} &= D \left(\frac{\partial^2 u}{\partial x^2} + \frac{\partial^2 u}{\partial y^2} \right) + \tau u^\alpha, & (x, y) \in \Omega = (l_1 \leq x, y \leq l_2), & \quad t > 0, \\ u(x, y, 0) &= u_0(x, y), & l_1 \leq x, y \leq l_2, \\ u(0, t) &= u(l_2, t) = 0, & \quad t > 0, \end{aligned} \right\} \quad (2.2.3)$$

now, we discretize the spatial domain by mesh $(x_i, y_j) = (l_1 + i \times h_x, l_1 + j \times h_y)$ where $h_x = (l_2 - l_1)/(N_x + 1)$, $h_y = (l_2 - l_1)/(N_y + 1)$ and $0 \leq i \leq N_x + 1$ and $0 \leq j \leq N_y + 1$. Using fourth order central difference discretization on the linear term, we obtain a system of nonlinear ODEs of the form

$$\frac{du_{i,j}}{dt} = \frac{D}{12} \left[\frac{-u_{i+2,j} + 16u_{i+1,j} - 30u_{i,j} + 16u_{i-1,j} - u_{i-2,j}}{h_x^2} \right] + \frac{D}{12} \left[\frac{-u_{i,j+2} + 16u_{i,j+1} - 30u_{i,j} + 16u_{i,j-1} - u_{i,j-2}}{h_y^2} \right] + \tau(u_{i,j})^\alpha, \quad (2.2.4)$$

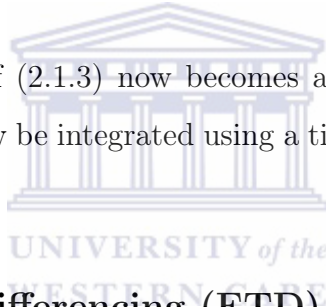
where

$$u = \begin{pmatrix} u_{1,1} & u_{1,2} & \dots & u_{1,N_y} & u_{1,N_y+1} \\ u_{2,1} & u_{2,2} & \dots & u_{2,N_y} & u_{2,N_y+1} \\ \vdots & \vdots & \vdots & \vdots & \vdots \\ u_{N_x,1} & u_{N_x,2} & \dots & u_{N_x,N_y} & u_{N_x,N_y+1} \end{pmatrix}_{N_x \times (N_y+1)}. \quad (2.2.5)$$

Spatial discretisation of equation (2.1.3) can also be done using Fourier spectral method with periodic boundary conditions [37, 83, 92, 187]. We adapt the Fourier spectral method from [187] and applied it to (2.1.3). Leaving all the time stepping in Fourier space gives the following system of ordinary differential equations

$$\widehat{u}_t = -Dk^2\widehat{u} + \widehat{\tau(u)^\alpha}, \quad (2.2.6)$$

so that the linear term of (2.1.3) now becomes a diagonal matrix. Systems (2.2.2), (2.2.4) and (2.2.6) will now be integrated using a time integration method as explained in the following section.



Exponential time differencing (ETD) schemes:

Numerous time discretization methods that are designed to handle stiff systems have been developed in the past. Among which are split-step (SS) methods which seems to have originated in the late 1950s, see for example, Barrinovskii and Godunov [14]. It was later discussed in revised forms by Ruth [166], Sanz-Serna and Calvo [169] and Schatzman [172]. Another example is the family of methods called implicit-explicit schemes (IMEX) whose usage is based on using the explicit method to advance the nonlinear part of the problem and the implicit scheme for the linear part, a notable example is the fourth-order Adams (Bashforth-Moulton) method (AB4BD4) discussed in Kassam and Trefethen [92] or called SBDF4 in Ascher et al. [10]. Other time-stepping methods include the integrating factor the sliders and finally, the exponential time-differencing (ETD) schemes.

The ETD schemes are time integration methods that can be effectively combined with spatial approximations to provide accurate smooth solutions for stiff or highly

oscillatory semi-linear PDEs. The work reported here gives the derivation of the explicit ETD schemes for arbitrary order following the approach used in [37, 83, 92], and present the explicit fourth-order (ETD) versions of these schemes constructed by Cox and Matthews [36]. In this thesis, our major focus shall be on the fourth-order exponential time-differencing Runge-Kutta (ETDRK4) scheme. This class of schemes is especially suited to semi-linear problems which can be split into a linear part, which is highly stiff and a nonlinear part, that we expect to vary more slowly than the linear part. These schemes have been rediscovered several times in various forms and under various names, see for example, [36, 37, 92, 155] to mention a few.

Construction of general ETD schemes:

We begin our formulation by considering the semi-linear partial differential equations (PDEs) of the form

$$\frac{\partial u(x, t)}{\partial t} = f(u(x, t)) = DLu(x, t) + N(u(x, t), t), \quad (2.2.7)$$

where x and t denote the spatial coordinate and time respectively. L is the linear operator that contains higher-order spatial derivatives and N typifies the nonlinear operators with spatial derivatives lower than the linear term [92]. Clearly from equation (2.2.7), semi-linear PDEs can be split into a linear part, which contains the stiffest part of the dynamics of the problem, and a nonlinear (non-stiff or mildly stiff) part, which varies more slowly than the linear part. Once we discretize the spatial part of PDE (2.2.7) by adopting the method of lines procedure discussed in the previous chapter, the resulting system of ODEs obtained in time takes the form

$$\frac{du(t)}{dt} = \mathbf{L}u(t) + \mathbf{N}(u(t), t). \quad (2.2.8)$$

Generally, for semi-linear problems, the difficult part (stiff or oscillatory nature) of the differential equation is in the linear part of the problem. By treating the linear part of the problem exactly, using the exponential and related functions, the remaining part

of the integrator can be explicit. The tradeoff here is that the exponential and related functions are computed, rather than using an implicit integrator. When a constant step-size is used throughout the integration, the exponential and related functions can be evaluated before the integration begins, given that storing such information is feasible [36, 92]. These functions can be a significant overhead depending on the dimensionality of the differential equation and the structure of the matrix \mathbf{L} . Therefore, exponential integrators are likely to be most competitive when the matrix \mathbf{L} is diagonal or cheaply diagonalizable. We require that the nonlinear term \mathbf{N} be handled explicitly, since fully implicit methods have been demonstrated [36] to be too costly for large-scale PDE simulations.

To derive the time discretization methods, for simplicity and by following mostly both the notation and the approach used in [36, 46], we consider the model ODE

$$\frac{du(t)}{dt} = \mathbf{L}u(t) + \mathbf{N}(u(t), t), \quad (2.2.9)$$

where \mathbf{L} is classified as the stiffness parameter considered to be large, negative and real, or large and imaginary, or complex with large, negative real part and $\mathbf{N}(u(t), t)$ stands for nonlinear and forcing term. The derivation of the s -step ETD schemes is taken from [12, 18, 36, 128, 142]), we begin by multiplying (2.2.9) through by the integrating factor $e^{-\mathbf{L}t}$, then integrating the equation over a single time step from $t = t_n$ and $t = t_{n+1} = t_n + \Delta t$ to give

$$u(t_{n+1}) = u(t_n)e^{\mathbf{L}\Delta t} + e^{\mathbf{L}\Delta t} \int_0^{\Delta t} e^{-\mathbf{L}\tau} \mathbf{N}(u(t_n + \tau), t_n + \tau) d\tau. \quad (2.2.10)$$

Various ETD schemes come from the approximations to the integral in (2.2.10). This formula is regarded as the *exact* [36], and the next step is to derive approximations to the integral. The issue of an unwanted fast time scale in the solution is well circumvented in this procedure and the schemes can be generalized to arbitrary order.

On applying the Newton backward difference formula [12, 25], using information about $\mathbf{N}(u(t), t)$ at the n th and previous time steps, the polynomial approximation to

$\mathbf{N}(u(t_n + \tau), t_n + \tau)$ is given in the form

$$\mathbf{N}(u(t_n + \tau), t_n + \tau) \approx G_n(t_n + \tau) = \sum_{j=0}^{s-1} (-1)^j \binom{-\tau/\Delta t}{j} \nabla^j G_n(t_n), \quad (2.2.11)$$

where ∇ is the backward difference operator defined as

$$\begin{aligned} \nabla^j G_n(t_n) &= \sum_{k=0}^j (-1)^k \binom{j}{k} G_{n-k}(t_{n-k}), \\ &\approx \sum_{k=0}^j (-1)^k \binom{j}{k} \mathbf{N}(u(t_{n-k}), t_{n-k}), \end{aligned} \quad (2.2.12)$$

and

$$j! \binom{-\Phi}{j} = (-\Phi - 1) \cdots (\Phi - j + 1), \quad \text{for } j = 1, \dots, s - 1,$$

where

$$\Phi = \tau/\Delta t.$$

If we substitute the approximation (2.2.11) into integrand (2.2.10), bear in mind that $(0! \binom{-\Phi}{0} = 1)$, we have

$$u(t_{n+1}) - u(t_n)e^{\mathbf{L}\Delta t} \approx \Delta t \sum_{j=0}^{s-1} (-1)^j \int_0^1 e^{\mathbf{L}\Delta t(1-\Phi)} \binom{-\Phi}{j} d\Phi \nabla^j G_n(t_n). \quad (2.2.13)$$

At this point, by following the work reported in [12, 36], we are pleased to indicate the integral in (2.2.13) by

$$\mathbf{g}_j = (-1)^j \int_0^1 e^{\mathbf{L}\Delta t(1-\Phi)} d\Phi, \quad (2.2.14)$$

by bringing in the generating function, we can calculate the \mathbf{g}_j . For $z \in \mathbb{R}, |z| < 1$, thus, this is easily accomplished by introducing the generating function defined by

$$\Gamma(z) = \sum_{j=0}^{\infty} \mathbf{g}_j z^j, \quad (2.2.15)$$

which is readily found to be

$$\begin{aligned}
 \Gamma(z) &= \int_0^1 e^{\mathbf{L}\Delta t(1-\Phi)} \sum_{j=0}^{\infty} \binom{-\Phi}{j} (-z)^j d\Phi, \\
 &= \int_0^1 e^{\mathbf{L}\Delta t(1-\Phi)} (1-z)^{-\Phi} d\Phi, \\
 &= \frac{e^{\mathbf{L}\Delta t}(1-z - e^{-\mathbf{L}\Delta t})}{(1-z)(\mathbf{L}\Delta t + \log(1-z))}.
 \end{aligned} \tag{2.2.16}$$

Next, we rearrange (2.2.16) in the form

$$(\mathbf{L}\Delta t + \log(1-z))\Gamma(z) = e^{\mathbf{L}\Delta t} - \frac{1}{1-z},$$

and then find the expansion in powers of z

$$\left(\mathbf{L}\Delta t - z - \frac{z^2}{2} - \frac{z^3}{3} - \dots \right) (g_0 + g_1 z + g_2 z^2 + \dots) = e^{\mathbf{L}\Delta t} - 1 - z - z^2 - z^3 - \dots,$$

for $j \geq 0$, we can obtain a recurrence relation for g_j in such a way that

$$\mathbf{L}\Delta t g_0 = e^{\mathbf{L}\Delta t} - 1, \tag{2.2.17}$$

$$\mathbf{L}\Delta t g_{j+1} + 1 = g_j + \frac{1}{2}g_{j-1} + \frac{1}{3}g_{j-2} + \dots + \frac{1}{j+1}g_0 = \sum_{k=0}^j \frac{1}{j+1-k} g_k.$$

On substituting equations (2.2.12) and (2.2.14) into (2.2.13), the general ETD schemes [12, 36] of order s is given as explicit generating formula of the form

$$u_{n+1} = u_n e^{\mathbf{L}\Delta t} + \Delta t \sum_{j=0}^{s-1} g_j \sum_{k=0}^j (-1)^k \binom{j}{k} \mathbf{N}_{n-k}, \tag{2.2.18}$$

where u_n and \mathbf{N} are the respective numerical approximation to $u(t_n)$ and $\mathbf{N}(u(t_n), t_n)$.

Exponential time differencing Adams (ETDADAMS4) scheme:

By setting $s = 4$ in formula (2.2.18), we obtain the fourth-order exponential time differencing method of Adams-type [12, 18, 31, 36, 130]. We denote this scheme for

brevity as ETDADAMS4:

$$u_{n+1} = u_n e^{\mathbf{L}\Delta t} + (\Theta_1 \mathbf{N}_n - \Theta_2 \mathbf{N}_{n-1} + \Theta_3 \mathbf{N}_{n-2} - \Theta_4 \mathbf{N}_{n-3}) / (6\mathbf{L}^4 \Delta t^3), \quad (2.2.19)$$

where

$$\Theta_1 = (6\mathbf{L}^3 \Delta t^3 + 11\mathbf{L}^2 \Delta t^2 + 12\mathbf{L} \Delta t + 6) e^{\mathbf{L}\Delta t} - 24\mathbf{L}^3 \Delta t^3 - 26\mathbf{L}^2 \Delta t^2 - 18\mathbf{L} \Delta t - 6,$$

$$\Theta_2 = (18\mathbf{L}^2 \Delta t^2 + 30\mathbf{L} \Delta t + 18) e^{\mathbf{L}\Delta t} - 36\mathbf{L}^3 \Delta t^3 - 57\mathbf{L}^2 \Delta t^2 - 48\mathbf{L} \Delta t - 18,$$

$$\Theta_3 = (6\mathbf{L}^2 \Delta t^2 + 24\mathbf{L} \Delta t + 18) e^{\mathbf{L}\Delta t} - 24\mathbf{L}^3 \Delta t^3 - 42\mathbf{L}^2 \Delta t^2 - 42\mathbf{L} \Delta t - 18,$$

$$\Theta_4 = (2\mathbf{L}^2 \Delta t^2 + 6\mathbf{L} \Delta t + 6) e^{\mathbf{L}\Delta t} - 6\mathbf{L}^3 \Delta t^3 - 11\mathbf{L}^2 \Delta t^2 - 12\mathbf{L} \Delta t - 6.$$

It is noticeable that the ETDADAMS4 will reduce to the corresponding order of the Adams-Bashforth method as $\mathbf{L} \rightarrow 0$.

Exponential time differencing Runge-Kutta (ETDRK4) scheme:

The description and formulation of ETD schemes described earlier are based on multi-step idea. Hence, their usage requiring s previous evaluations of the nonlinear term $\mathbf{N}(u(t), t)$ which makes them inconvenient to use because of their requirement of starting values. This problem actually prone Cox and Matthew [36] to look for a way to circumvent this particular challenge, they suggested that this problem can be avoided with the use of Runge-Kutta methods that are already available with all the information required to start the integration. In addition, they also have the advantages of smaller error constants and larger stability regions than multi-step methods. It would therefore be of good interest to design ETD schemes that are based on Runge-Kutta's approach.

Direct extension of the standard fourth-order Runge-Kutta method with further introduction of some parameters based on the formulation of the methods in [36, 55], gives birth to the well-known Cox and Matthews [36] fourth-order exponential time

differencing Runge-Kutta scheme, which we denoted in this thesis as ETDRK4:

$$\begin{aligned}
 u_{n+1} = & u_n e^{\mathbf{L}\Delta t} + \mathbf{N}_n [-4 - \mathbf{L}\Delta t + e^{\mathbf{L}\Delta t} (4 - 3\mathbf{L}\Delta t + \mathbf{L}^2 \Delta t^2)] \\
 & + 2(\mathbf{N}(a_n, t_n + \Delta t/2) + \mathbf{N}(b_n, t_n + \Delta t/2)) [2 + \mathbf{L}\Delta t + e^{\mathbf{L}\Delta t} (-2 + \mathbf{L}\Delta t)] \\
 & + \mathbf{N}(c_n, t_n + \Delta t) [-4 - 3\mathbf{L}\Delta t - \mathbf{L}^2 \Delta t^2 + e^{\mathbf{L}\Delta t} (4 - \mathbf{L}\Delta t)] / \mathbf{L}^3 \Delta t^2, \quad (2.2.20)
 \end{aligned}$$

where

$$\begin{aligned}
 a_n &= u_n e^{\mathbf{L}\Delta t/2} + (e^{\mathbf{L}\Delta t/2} - \mathbf{I}) \mathbf{N}_n / \mathbf{L}, \\
 b_n &= u_n e^{\mathbf{L}\Delta t/2} + (e^{\mathbf{L}\Delta t/2} - \mathbf{I}) \mathbf{N}(a_n, t_n + \Delta t/2) / \mathbf{L}, \\
 c_n &= u_n e^{\mathbf{L}\Delta t/2} + (e^{\mathbf{L}\Delta t/2} - \mathbf{I}) (2\mathbf{N}(b_n, t_n + \Delta t/2) - \mathbf{N}_n) / \mathbf{L}.
 \end{aligned}$$

The terms a_n and b_n approximate the values of u at $t_n + \Delta t/2$ while the term c_n approximates the value of u at $t_n + \Delta$. The formula (2.2.20) is the quadrature formula for (2.2.10) derived from quadratic interpolation through the points t_n , $t_n + \Delta t/2$ and $t_n + \Delta t$, when an average value of \mathbf{N} is used at a_n and b_n .

The major computational task in the implementation of the exponential time differencing methods could be the need of fast and stable evaluations of exponential and related φ -functions [184]

$$\varphi(z) = \frac{1}{(j-1)!} \int_0^1 e^{(1-\theta)z} \theta^{j-1} d\theta, \quad j \geq 0, \quad (2.2.21)$$

that is, functions of the form $(e^z - 1)/z$. The computation of these functions depend significantly on the structure and the range of the eigenvalues of their linear operators and the dimensionality of the semi-discretized PDE. Krylov method was introduced in [73, 168] to compute the φ -functions. Years later, authors in [92] used the Cauchy integral representation on a circle for the stable computation of the φ -functions. Our evaluation of the exponential and the related φ -matrix functions follow the idea of

[175]. The φ -functions can be computed explicitly by using a recursive formula

$$\left. \begin{aligned} \varphi_0(z) &= e^z, \\ \varphi_j(z) &= \frac{\varphi_{j-1}(z) - \varphi_{j-1}(0)}{z}, \quad j \geq 1. \end{aligned} \right\} \quad (2.2.22)$$

Another way of computing the functions φ_j is to use the Taylor series representation. Thus, for the complex numbers z , we have

$$\varphi_j(z) = \sum_{k=j}^{\infty} \frac{1}{k!} z^{k-j}, \quad (2.2.23)$$

it is known that the computation of these functions in their explicit or Taylor series form suffers from computational inaccuracy for the matrices whose eigenvalues are equal to or approaching zero. In order to circumvent the numerical difficulties posed in the computation of (2.2.22) and (2.2.23), a different method of attack for evaluating the function was suggested in [92]. The main idea is to approximate the matrices and scalars functions by means of contour integrals in the complex plane

$$\begin{aligned} \varphi_j(z) &= \frac{1}{2\pi i} \int_{\Gamma} \frac{\varphi_j(s)}{(s-z)} ds \\ &= \frac{1}{M} \sum_{\ell=j}^M \varphi_j(z + e^{i\theta_{\ell}}), \quad \text{for } \theta_{\ell} = \frac{2\pi\ell}{M}. \end{aligned} \quad (2.2.24)$$

If the size of the matrix \mathbf{L} is large, it is more advantageous to compute the product of the functions $\varphi_j(z)$ and the vectors b rather than to compute $\varphi_j(z)$ explicitly. We have

$$\varphi_j(A)b = \frac{1}{2\pi i} \int_{\Gamma} \varphi_j(s)(s\mathbf{I} - \mathbf{L})^{-1} b ds \approx \sum_{\ell=1}^n c_{\ell}(s_{\ell}\mathbf{I} - \mathbf{L})^{-1} b, \quad (2.2.25)$$

where s_{ℓ} and c_{ℓ} represent the poles and the residues respectively. The sum in (2.2.25) is evaluated by solving at most n shifted linear systems. For the computation of the poles and the residues, see Carathéodory-Fejér method [175, 184] for details.

2.3 Analysis of the numerical methods

In mathematics, stability theory addresses the stability of solutions of differential equations and of trajectories of dynamical systems under small perturbations of initial conditions. A crucial question in the step-by-step solution of such problems is whether the method will behave stably or not. Here we use the term stability to designate that any numerical errors, introduced at some stage of the calculations, are propagated in a mild fashion, that is, they do not blow up in the subsequent steps of the method.

Widely accepted tools to assess the stability a priori, in the numerical solution of partial differential equations, include Fourier transformation and the corresponding famous Von Neumann condition for stability [183]. Further tools of recognized merit for assessing stability, in the solution of ordinary differential equations, comprise so-called stability regions in the complex plane. Since the mid sixties these stability regions have been studied extensively; numerous papers have appeared dealing with the shape and various peculiarities of these regions.

However, the above tools are based on the behaviour that the numerical method would have when applied to quite simple test problems. Accordingly, in the case of partial differential equations Fourier transformation provides a straightforward and reliable stability criterion primarily only for certain numerical methods applied to pure initial value problems in linear differential equations with constant coefficients. In many cases of practical interest, Fourier transformation is not relevant to analysing stability: e.g. for pseudo-spectral methods [186] applied to initial-boundary value problems, for finite difference or finite element methods related to highly irregular grids, and for methods applied to equations with strongly varying coefficients. Similarly, in the case of ordinary differential equations, stability regions are primarily relevant only to numerical methods when applied to the scalar linear model equation

$$\frac{du(t)}{dt} = \lambda u(t) \quad \text{for } t \geq 0,$$

with given complex constant λ .

Generally speaking, the stability analysis of time discretization methods is valid for

a linear autonomous system of ordinary differential equations, linearized about a fixed point. This analysis only provides an indication to how stable a numerical method is. It cannot be applied directly to solutions of nonlinear time-dependent partial differential equations with large amplitude since convergence and stability are solution-dependent matters.

The stability approach was developed in [18, 36, 46] for the analysis of (composite) schemes that use different methods for both linear and nonlinear parts of the equation of the form (2.2.8), to compute the boundaries of the stability regions for a general test problem. Stability of the family of explicit and implicit exact linear part (EPL) schemes have been reported in [18] with a view that the schemes have shown significantly better stability properties. Also, various stability regions of some ETD methods have been analyzed in [12, 36, 104].

Owing to the general idea as suggested and used in [12, 18, 36, 46, 83], we investigate the stability of the ETD schemes by linearizing the nonlinear autonomous ODEs

$$\frac{du(t)}{dt} = \mathbf{L}u(t) + \mathbf{N}(u(t)), \quad (2.3.1)$$

with $\mathbf{N}(u(t))$ the nonlinear part, we suppose that there exist a fixed point u_0 in such that $\mathbf{L}u_0 + \mathbf{N}(u_0) = 0$. Linearizing about this fixed point, we obtain

$$\frac{du(t)}{dt} = Lu(t) + \lambda u(t), \quad (2.3.2)$$

where $u(t)$ is now the perturbation of u_0 and $\lambda = \mathbf{N}'(u_0)$ is a diagonal or a block diagonal matrix containing the eigenvalue of \mathbf{N} . In attempt to keep the fixed point u_0 stable, we require that $Re(L + \lambda) < 0$, for all λ . It is naturally important for a numerical method to satisfy this property with respect to capturing as much as the dynamics of the system is possible. The stability region is four-dimension if both L and λ are complex [12], otherwise the stability region is two-dimensional if both L and λ are purely imaginary or purely real, or if λ is complex and L is fixed and real, see [18, 36] for details.

Stability of ETDADAMS4 scheme:

When applying ETDADAMS4 (2.2.19) to the linearized problem (2.3.2), a polynomial equation of the order-four in r is obtained in the form

$$u_4 r^4 + u_3 r^3 + u_2 r^2 + u_1 r + u_0 = 0, \quad (2.3.3)$$

where

$$\begin{aligned} u_4 &= 6y^4, \\ u_3 &= -6y^6 e^y + [(-6y^3 - 11y^2 - 12y - 6)e^y + 24y^3 + 26y^2 - 18y + 6]x, \\ u_2 &= [(18y^2 + 30y + 12)e^y - 36y^3 - 57y^2 - 48y - 18]x, \\ u_1 &= [(-9y^2 - 24y - 18)e^y + 24y^3 + 42y^2 + 42y + 18]x, \\ u_0 &= [(2y^2 + 6y + 6)e^y - 6y^3 - 11y^2 - 12y - 6]x. \end{aligned}$$

In the real (x, y) plane, the right-hand boundary for ETDADAMS4 scheme corresponds to substituting $r = 1$ in equations (2.3.3) is the line $x + y = 0$. For $r = -1$, the left-hand boundaries for (2.3.3) is given by the curve

$$x = -\frac{3y^4(e^y + 1)}{(3y^3 + 20y^2 + 36y + 24)e^y - 45y^3 - 68y^2 - 60y - 24}, \quad (2.3.4)$$

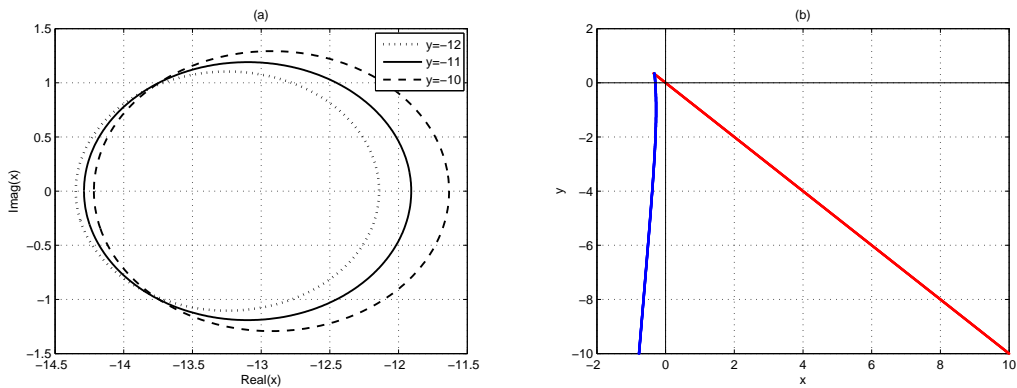


Figure 2.3.1: Stability regions of the ETDADAMS4 scheme (2.2.19) in (a) the complex x plane and (b) the real (x, y) plane.

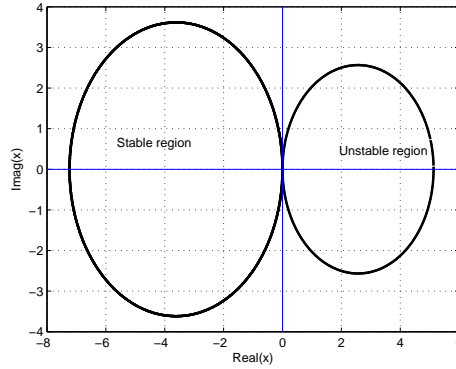


Figure 2.3.2: Stable and unstable regions of the ETDADAMS4 scheme in the real (x, y) plane at $y = \pm 1$.

Stability of ETDRK4 scheme:

The application of ETDRK4 method (2.2.20) to (2.3.2) leads to a recurrence relation

$$r = \frac{u_{n+1}}{u_n} = L_0 + L_1x + L_2x^2 + L_3x^3 + L_4x^4, \quad (2.3.5)$$

where

$$\begin{aligned} L_0 &= e^y, \\ L_1 &= -\frac{4}{y^3} + \frac{8e^{y/2}}{y^3} - \frac{8e^{3y/2}}{y^3} + \frac{4e^{2y}}{y^3} - \frac{1}{y^2} + \frac{4e^{y/2}}{y^2} - \frac{6e^y}{y^2} + \frac{4e^{3y/2}}{y^2} - \frac{e^{2y}}{y^2}, \\ L_2 &= -\frac{8}{y^4} + \frac{16e^{y/2}}{y^4} - \frac{16e^{3y/2}}{y^4} + \frac{8e^{2y}}{y^4} - \frac{5}{y^3} + \frac{12e^{y/2}}{y^3} - \frac{10e^y}{y^3} + \frac{4e^{3y/2}}{y^3} \\ &\quad - \frac{e^{2y}}{y^3} - \frac{1}{y^2} + \frac{4e^{y/2}}{y^2} - \frac{e^{y/2}}{y^2}, \\ L_3 &= \frac{4}{y^5} - \frac{16e^{y/2}}{y^5} + \frac{16e^y}{y^5} + \frac{8e^{3y/2}}{y^5} - \frac{20e^{2y}}{y^5} + \frac{8e^{5y/2}}{y^5} + \frac{2}{y^4} - \frac{10e^{y/2}}{y^4} \\ &\quad + \frac{16e^y}{y^4} - \frac{12e^{3y/2}}{y^4} + \frac{6e^{2y}}{y^4} - \frac{2e^{5y/2}}{y^4} - \frac{2e^{y/2}}{y^3} + \frac{4e^y}{y^3} - \frac{2e^{3y/2}}{y^3}, \\ L_4 &= \frac{8}{y^6} - \frac{24e^{y/2}}{y^6} + \frac{16e^y}{y^6} + \frac{16e^{3y/2}}{y^6} - \frac{24e^{2y}}{y^6} + \frac{8e^{5y/2}}{y^6} + \frac{6}{y^5} - \frac{18e^{y/2}}{y^5} \\ &\quad + \frac{20e^y}{y^5} - \frac{12e^{3y/2}}{y^5} + \frac{6e^{2y}}{y^5} - \frac{2e^{5y/2}}{y^5} + \frac{4}{y^4} - \frac{6e^{y/2}}{y^4} + \frac{6e^y}{y^4} - \frac{2e^{3y/2}}{y^4}, \end{aligned}$$

with $x = \lambda h$, $y = Lh$ (since the problem we are considering is in one dimension). It is noticeable that the computation of L_1 , L_2 , L_3 and L_4 suffers from computational in-

stability for values of y equal to or approaching zero. For that reason, their asymptotic expansions are sought. This leads to

$$\left. \begin{aligned} L_1 &= 1 + y + \frac{y^2}{2} + \frac{y^3}{6} + \frac{13y^4}{320} + \frac{7y^5}{960} + \mathcal{O}(y^6), \\ L_2 &= \frac{1}{2} + \frac{y}{2} + \frac{y^2}{4} + \frac{247y^3}{2880} + \frac{131y^4}{5760} + \frac{479y^5}{96768} + \mathcal{O}(y^6), \\ L_3 &= \frac{1}{6} + \frac{y}{6} + \frac{61y^2}{720} + \frac{y^3}{36} + \frac{1441y^4}{241920} + \frac{67y^5}{120960} + \mathcal{O}(y^6), \\ L_4 &= \frac{1}{24} + \frac{y}{32} + \frac{7y^2}{640} + \frac{19y^3}{11520} + \frac{25y^4}{64512} + \frac{311y^5}{860160} + \mathcal{O}(y^6). \end{aligned} \right\} \quad (2.3.6)$$

We can define the amplification factor for ETDRK4, $r(x, y)$ for $y > 0$. If $y = 0$, the amplification factor becomes $1 - x + \frac{x^2}{2} - \frac{x^6}{6} + \frac{x^4}{24}$. At this point, we can see that the stability curve of ETDRK4 at $y = 0$ coincides with that of corresponding fourth-order Runge-Kutta method. Using (2.3.5) and (2.3.6), we see that

$$\lim_{y \rightarrow 0} r(x, y) = 1 - x + \frac{x^2}{2} - \frac{x^6}{6} + \frac{x^4}{24}.$$

Also, $\lim_{x, y \rightarrow 0} \partial_y r(x, y) = -1$, $\lim_{x, y \rightarrow 0} \partial_x r(x, y) = -1$, and the absolute value of the amplification factor is given as $|r(x, y)| \leq 1$. The boundary of the stability region is determined by setting $r = e^{i\theta}$, for $\theta \in [0, 2\pi]$. We plot the stability region in the complex x -plane, see Figure 2.3.3, where the horizontal and vertical axes represent the real and imaginary parts of x , respectively. Convincingly, we can deduce from Figure 2.3.3 that the stability of ETDRK4 method grows larger as $y \rightarrow -\infty$. The curve (a) indicates the case $y = 0$, it is convincing that the stability region of the ETDRK4 scheme coincides with that of the corresponding order of the fourth-order Runge-Kutta (RK4) method, and (b) shows the curve of ETDRK4 at some negative values of $y = -15, -10, -5$, from outer to the inner curves. The inner curve is the stability region obtained when $y = 0$.

Our major goal in this thesis is to use ETDRK4 scheme as our time-stepping method, but for the purpose of comparisons, higher-order time stepping schemes such as exponential time differencing multi-step (ETDM4, ETDM5, ETDM6), implicit-explicit linear multi-step (IMEXLM1,2,4), implicit-explicit predictor-corrector (IMEXPC1,2,4), implicit-explicit Runge-Kutta (IMEXRK4), and the classical fourth-order

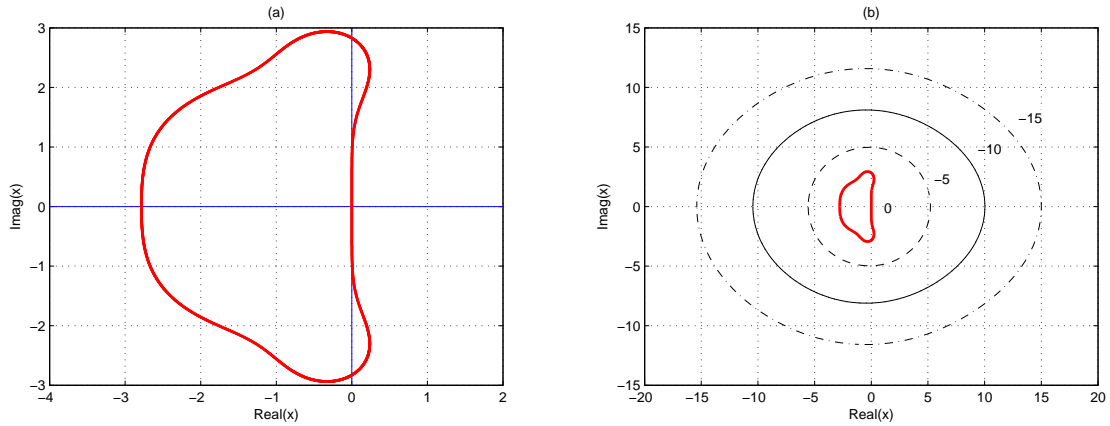


Figure 2.3.3: Boundary of stability regions in the complex x plane for the ETDRK4 scheme (2.2.20).

Runge-Kutta (RK4) methods are considered.

2.4 Numerical results

To examine the efficiency and accuracy of our approach for ETD methods, we consider the numerical simulations of system (2.1.3) in one and two dimensions. We further justify the supremacy of ETDRK4 in comparison with the existing standard schemes of higher-orders by reporting the relative infinity and root mean square norm errors of the solution defined by

$$\|L\|_{\infty} = \frac{\max_{1 \leq j \leq N} |e_j - c_j|}{\max_{1 \leq j \leq N} |e_j|}, \quad (2.4.1)$$

and

$$\|L_2\| = \sqrt{\frac{\sum_{j=1}^n (e_j - c_j)^2}{\sum_{j=1}^n (e_j)^2}}, \quad (2.4.2)$$

respectively, where e_j and c_j are the exact and computed values of the solution u at point j , and n is the number of interior points. As test examples, we consider the following problems.

One-dimensional KISS model:

In one-dimension, we consider the KISS model of [97, 181].

$$\left. \begin{aligned} \frac{\partial u}{\partial t} &= D \frac{\partial^2 u}{\partial x^2} + \tau u^\alpha, & -l \leq x \leq l, & \quad t > 0, \\ u(x, 0) &= \sin(2\pi x), & -l \leq x \leq l, \\ u(0, t) &= u(l, t) = 0, & \quad t > 0, \end{aligned} \right\} \quad (2.4.3)$$

where $u(x, t)$ is the density of the organisms at spatial domain x and time t , τ and α are both positive parameters, and D is the diffusion coefficient that measures the rate of dispersal. The particular choice of boundary conditions indicates that the organisms cannot boom or live beyond the domain. This assumption is taken to ensure that the experiment is not influenced by any external factor. Results are presented in figures 2.4.1 and 2.4.2.

The successive profile in Figure (a) is obtained at $T = 0.01$ to 0.05 in the step 0.005 . Panel (b) and the contour plots (d) are obtained for $[0, 20]$, $T = 0.05$. Surface plot (c) is obtained at $T = 0.05$, in the interval $[-2, 2]$. Panels (e) is obtained at $T = 0.1$ in the interval $[0, 1]$ whereas (f) is obtained at final time $T = 0.05$ on domain $[-1, 1]$. The results presented here have shown various patterns that could evolved when the patch size of KISS model is varied in spatial domain. For all simulations, we took $N = 200$.

The plots in Figure 2.4.2 indicate the results from initial time (t_0) to final time T showing the density profiles $u(x, t)$ versus position x on a closed interval $-l \leq x \leq l$ for the choice of the growth rate $\tau = 0.5$ and critical exponent $\alpha = 2$. The successive profile in (a) is obtained at $T = 0.01$ with $D = 0.5$ on $[-1, 1]$; (b) large $D = 2$, $T = 0.05$ on $[0, 3]$; (c) $D = 0.1$, $T = 0.01$ on $[0, 1]$; (d) is obtained on $[-4, 4]$, $T = 0.02$ for large diffusion coefficient $D = 1.5$; (e) is obtained on the spatial domain $[0, 5]$ with $T = 0.1$ and $D = 0.05$. Contour plot (f) is obtained with parameter values $D = 0.2$, $T = 0.1$ on domain of size $[0, 4]$. The results presented here have equally revealed some of the dispersal-driven patterns that arise as a result of diffusion. For all simulations, we took $N = 200$.

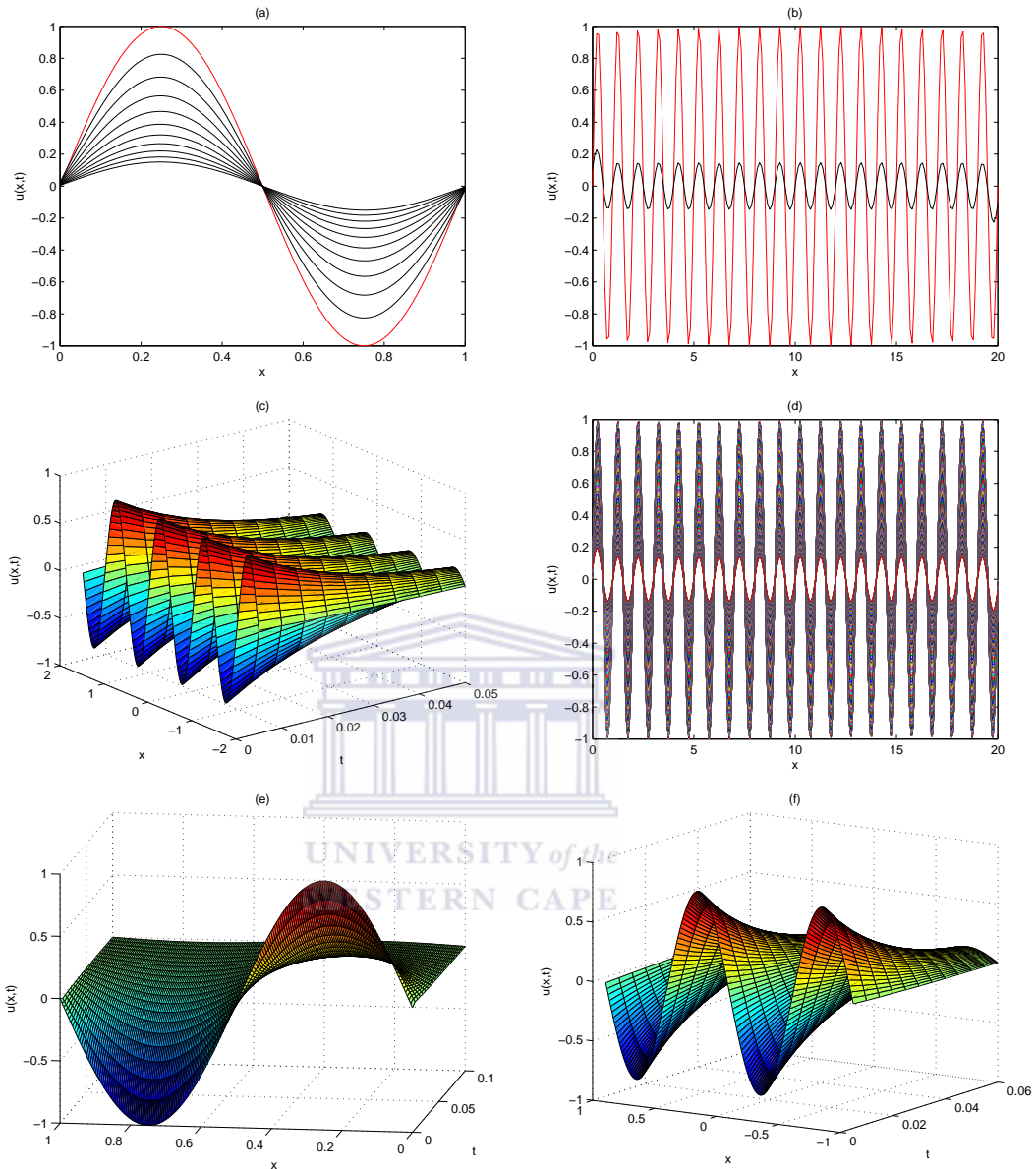


Figure 2.4.1: Numerical solutions of one-dimensional KISS model (2.4.3): Time dependent density profiles $u(x, t)$ versus position x on interval $-l \leq x \leq l$ for $D = \tau = \alpha = 1$.

Two-dimensional KISS model:

Our major aim in this section is to examine the behavior of system (2.1.3) numerically in two-dimensional space, that is, when the Laplacian operator $\nabla^2 \equiv \partial^2/\partial x^2 + \partial^2/\partial y^2$. One-dimensional form of KISS equations are relatively simple to undertake using method of lines coupled with spatial adaptive schemes. In-fact, solutions of the form (2.1.3) have been sought theoretically [7, 102, 145]. Unfortunately, in two space di-

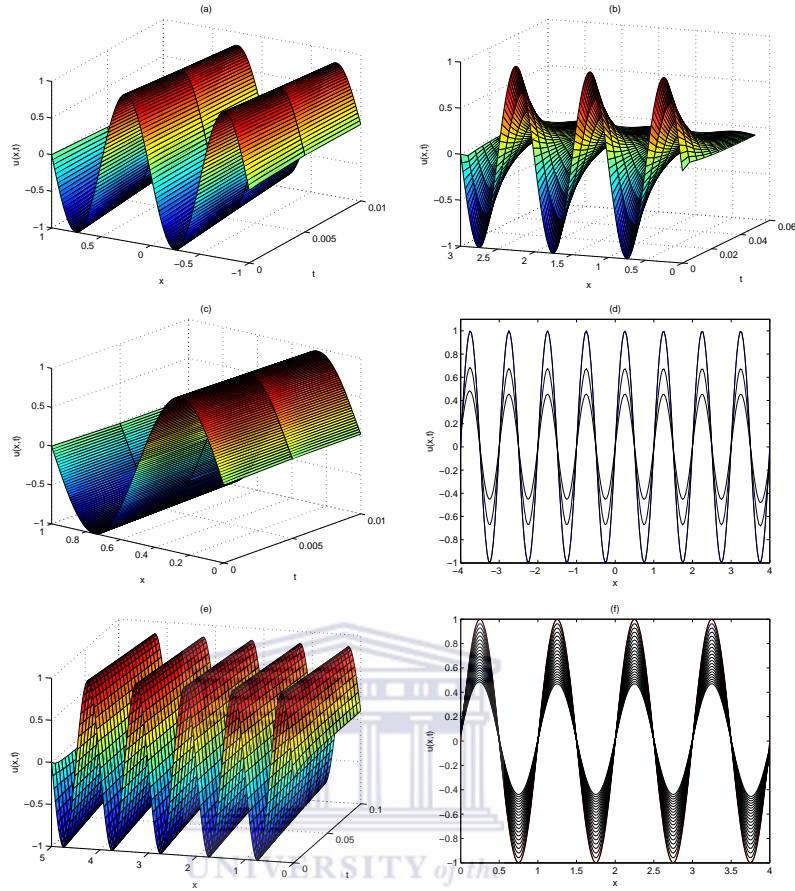


Figure 2.4.2: Diffusion-driven spatial pattern in one-dimensional KISS model (2.4.3) as it changes with both spatial domain x with varying time t .

mensions, numerical solutions of KISS model (2.2.3) still requires some attention, since simulations based upon the more conventional ideas become more time consuming. We therefore consider its two-dimensional case:

$$\left. \begin{aligned} \frac{\partial u}{\partial t} &= D \left(\frac{\partial^2 u}{\partial x^2} + \frac{\partial^2 u}{\partial y^2} \right) + \tau u^\alpha, \quad (x, y) \in \Omega = (l_1 \leq x, y \leq l_2), \quad t > 0, \\ u(x, y, 0) &= u_0(x, y), \quad l_1 \leq x, y \leq l_2, \\ u(0, t) &= u(l_2, t) = 0, \quad t > 0, \end{aligned} \right\} \quad (2.4.4)$$

where $u(x, y, t)$ is the density of organisms at spatial coordinates x, y and time t . $D > 0$ remains the diffusion coefficient, while $\tau > 0$ and $\alpha \geq 1$ are the respective growth rate and critical exponent.

The initial data and parameter values were carefully chosen to make the figures (2.4.3), (2.4.4) and (2.4.5) replicate some of the existing patterns. In all cases, the

space step h was kept equal to l , that is, $h_x = h_y = l$ in the spatial domain $-l \leq x, y \leq l$. It is clear from the result presented in Figure 2.4.6, that ETDRK4 has the best convergence when compared to other exponential time differencing schemes, such as ETDM4, ETDM5, ETDM6 and ETDADAMS4 methods. In Table 2.4.1, we illustrate the tradeoff between the computational [CPU (s)] time and the accuracy as time step k is refined for each of the methods.

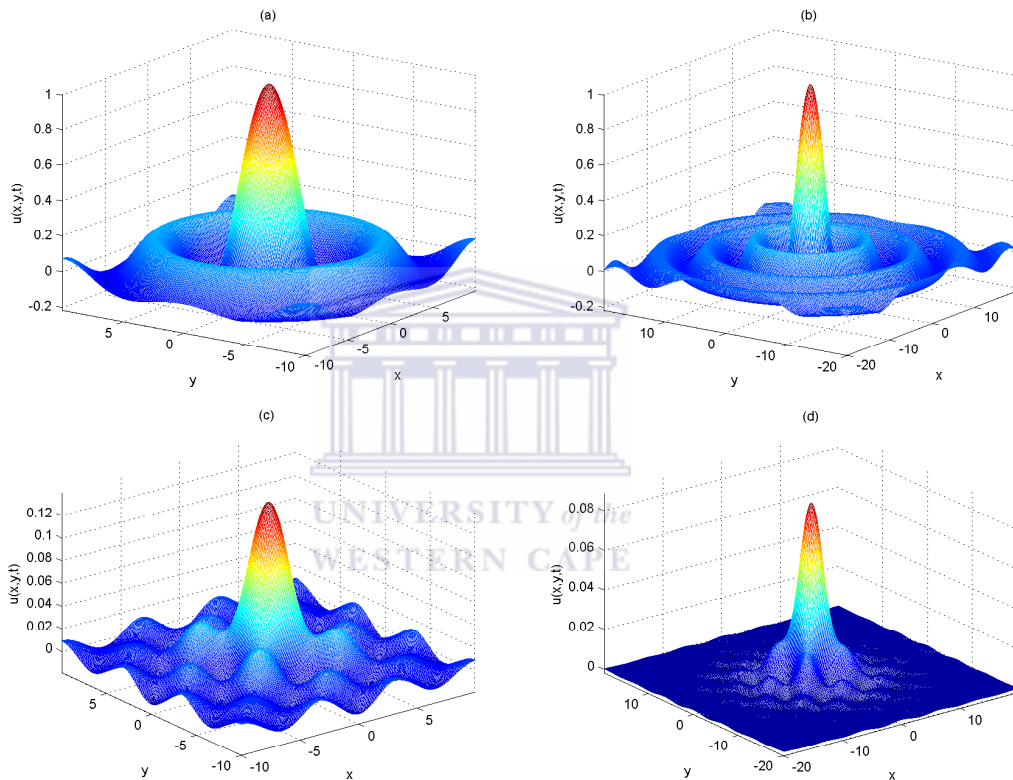


Figure 2.4.3: Solutions of two-dimensional KISS model (2.4.4) on different spatial domain.

In Figure 2.4.3, the initial data is $u_0(x, y) = \text{sinc}(\sqrt{(x/\pi)^2 + (y/\pi)^2})$. Other parameter values are $D = 1$, $\tau = 0.01$, $T = 0.5$ and $\alpha = 2$ for (a) $l = 10$ and (b) $l = 20$. Plots (c) $T = 1.2$, $l = 10$ and (d) $T = 2$, $l = 20$ are obtained with the initial data $u_0(x, y) = \cos(x) \cos(y) \exp(-\sqrt{x^2 + y^2}/4)$.

Table 2.4.1: Error norm L_2 at some selected time steps for solving KISS equation (2.4.3). Parameter values are $T = 1$, $D = 0.5$, $\tau = 0.5$ and $\alpha = 2$ on interval $[-1,1]$ for $N = 200$. We present CPU times for each of the schemes to check competitiveness of the methods.

Method	Time step (k)	L_2 -error	CPU time (in seconds)
ETDM4	1/32	0.2150	1.5086
	1/64	0.0301	1.5467
	1/256	3.3910e-004	1.7189
	1/1024	3.4784e-006	3.8817
ETDM5	1/32	0.2170	1.9896
	1/64	0.0195	2.0277
	1/256	1.7793e-005	2.3538
	1/1024	1.7923e-006	4.6010
ETDM6	1/32	0.0664	2.0405
	1/64	8.5299e-004	2.0515
	1/256	4.2840e-004	2.2500
	1/1024	1.8248e-007	8.2387
ETDADAMS4	1/32	0.0050	1.485
	1/64	0.0029	1.5511
	1/256	1.3334e-004	1.8339
	1/1024	2.3963e-006	4.4020
ETDRK4	1/32	7.2013e-004	1.1146
	1/64	5.0921e-005	1.0236
	1/256	3.5038e-007	1.3198
	1/1024	4.4086e-009	3.8726

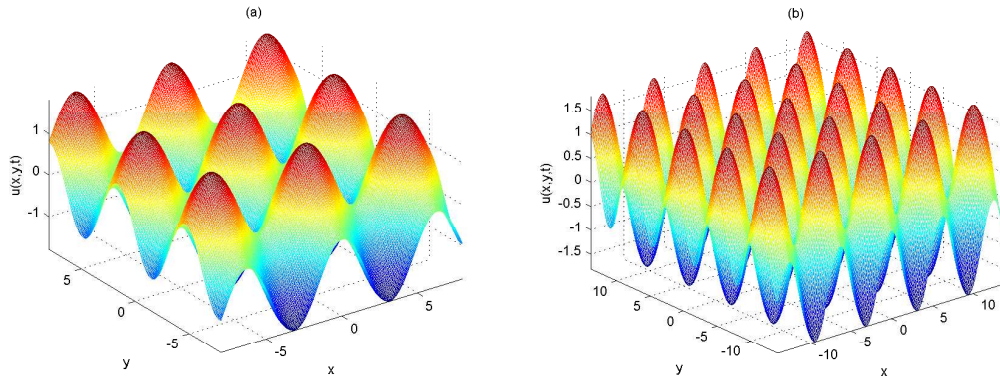


Figure 2.4.4: Solutions of two-dimensional KISS model (2.4.4) on different spatial domain. The initial data is $u_0(x, y) = \exp(1/10)(\cos x + \sin y)$. Other parameters are $T = 0.05$, $D = 1$, $\tau = 0.01$ and $\alpha = 2$ on (a) $l = 8$ and (b) $l = 14$.

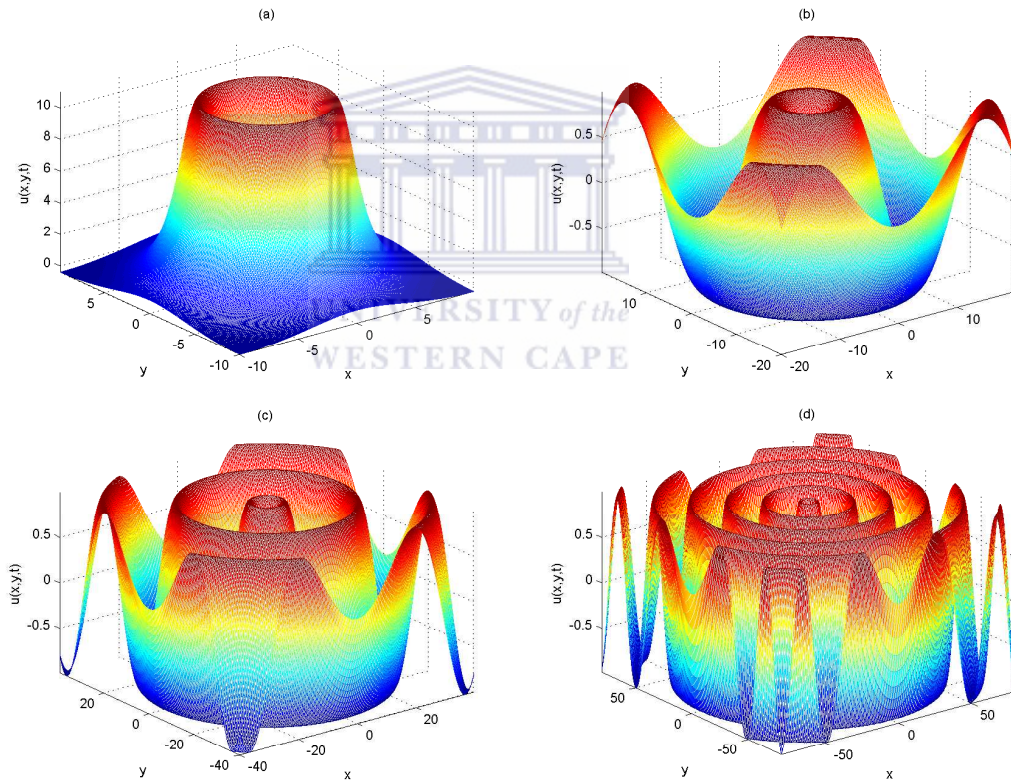


Figure 2.4.5: Solutions of two-dimensional KISS model (2.4.4) on different spatial domain. The initial data is $u_0(x, y) = \sin(\sqrt{(x/\pi)^2 + (y/\pi)^2})$. Other parameters are $D = 1$, $\tau = 0.01$ and $\alpha = 2$ on (a) $l = 10$, $T = 1$; (b) $l = 20$, $T = 0.05$; (c) $l = 40$, $T = 0.05$, and (d) $l = 80$, $T = 0.05$.

Fisher’s equation with simple population density:

Our first example evolves a simple population density $u(x, t)$ on setting $D = \tau = \kappa = 1$ in (2.4.13) (see also, [4], [37]):

$$u_t = u_{xx} + u(1 - u), \quad |x| < L \tag{2.4.5}$$

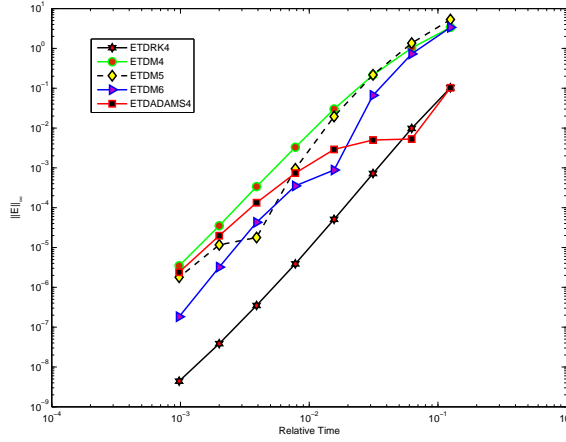


Figure 2.4.6: Performance of ETDRK4, ETDM4, ETDM5, ETDM6 and ETADAMS4 methods for solving the KISS equation (2.4.3) with parameter values $T = 1$, $D = 0.5$, $\tau = 0.5$ and $\alpha = 2$ on interval $[-1,1]$ for $N = 200$.

on the domain of interval $-\infty \leq L \leq \infty$, using a periodic boundary conditions with the initial condition

$$u(x, 0) = \frac{1}{2 \cosh \delta x} \quad (2.4.6)$$

that has exponential decay $\exp(-\delta |x|)$ as $|x| \rightarrow \infty$. The solution to (2.4.5) depends on the initial data, $u_0(x)$. Kolmogorov et al. [100] proved that if $u_0(x)$ is monotonic and continuous with $u_0(x) = 1$ for $x < a$ and $u_0(x) = 0$ for $x > b$, where $-\infty < a < b < \infty$, the solution evolves into a traveling wave with the speed $c = 2$ for $\delta > 1$ and $c = \delta + 1/\delta$ if otherwise.

Analysis of traveling wave solutions of (2.4.5) could be traced back to [100], where it was shown that the solutions that are functions of $x - ct$ exists for $c \geq 2$, and that the traveling wave with minimum speed 2 possesses the long time limit for any initial conditions satisfying

$$u(x, t) = \xi(x \pm ct) \equiv \xi(\omega),$$

where ξ is increasing

$$\lim_{\omega \rightarrow -\infty} \xi(\omega) = 1, \quad \lim_{\omega \rightarrow \infty} \xi(\omega) = 0.$$

This implies that, the solution switches between two equilibrium positions $u = 0$ and

$u = 1$. The travelling wave solution of Fisher's equation is given as

$$\xi(\omega) = \left(1 + ce^{\frac{\pm \omega}{\sqrt{6}}}\right)^{-2}, \quad (2.4.7)$$

for all $c > 0$.

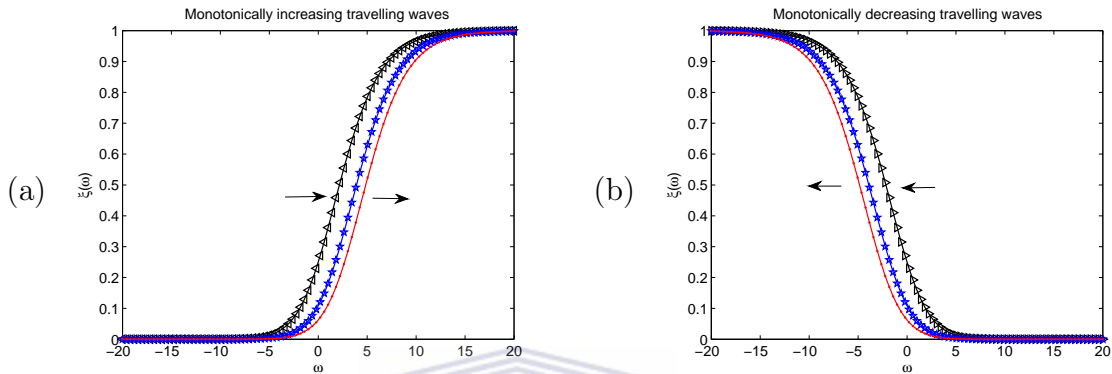


Figure 2.4.7: Monotonically increasing (a) and decreasing (b) travelling wave solutions of Fisher-KPP equation that switches between two equilibrium points 0 and 1 on $-\infty < x < \infty$.

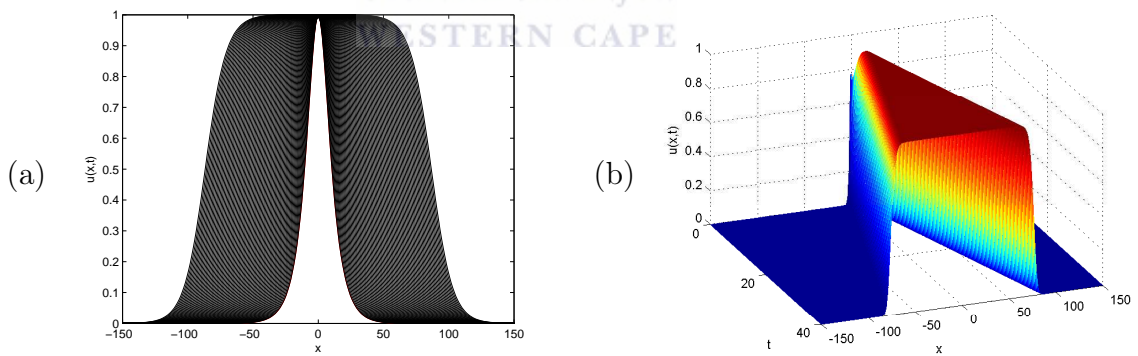


Figure 2.4.8: Fisher's equation (2.4.5): solution is obtained on interval $-L \leq x \leq L$, for $L = 150$; simulation runs for $N = 250$. Parameter values: Panels (a) at $\delta = 1/8$, $T = 12$ and surface plot (b) is obtained at $T = 40$ when $\delta = 1$, notice the variation at the peaks of (a) and (b).

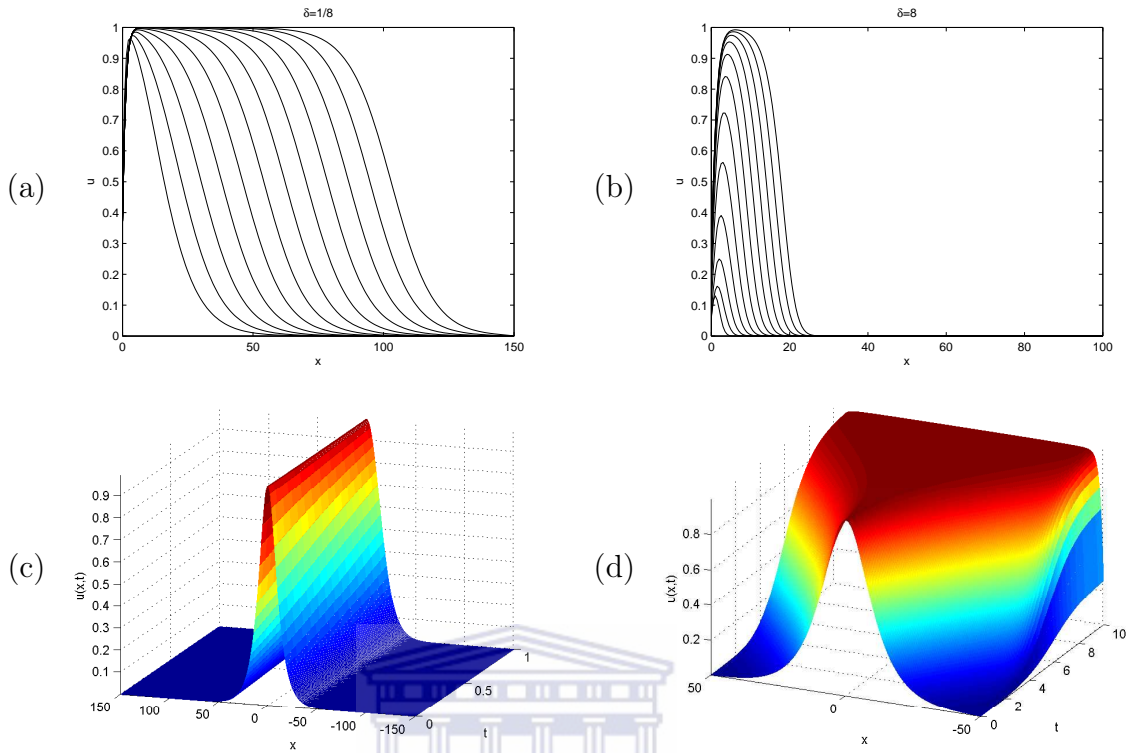


Figure 2.4.9: Fisher's equation (2.4.5): Panels (a) and (b) show the profiles of $u(x, t)$ at unit time intervals $T = 1(1)12$ for $\delta = 1/8$ and $\delta = 8$ respectively. Surface plot C is obtained at parameter values $\delta = 1/8$ with final time $T = 1$. D is the solution at $T = 10$ for $\delta = 1/8$. We took $N = 200$.

Fisher's population dynamics problem:

We consider the Fisher population dynamic problem [4] with three kinds of local waves

$$u_t(x, t) = \beta u_{xx}(x, t) + \phi u \left(1 - \frac{u}{k} \right), \quad -L \leq x \leq L, t > 0 \quad (2.4.8)$$

$$\lim_{|x| \rightarrow L} u(x, t) = 0. \quad (2.4.9)$$

The first one is

$$g_1(x) = \text{sech}^2(7x) \quad (2.4.10)$$

with a sharp peak in the middle, and the second one is

$$g_2(x) = \left. \begin{array}{l} \exp[7(x + 1)], \quad x < -1, \\ \exp[-7(x - 1)], \quad x > 1, \end{array} \right\}, \quad (2.4.11)$$

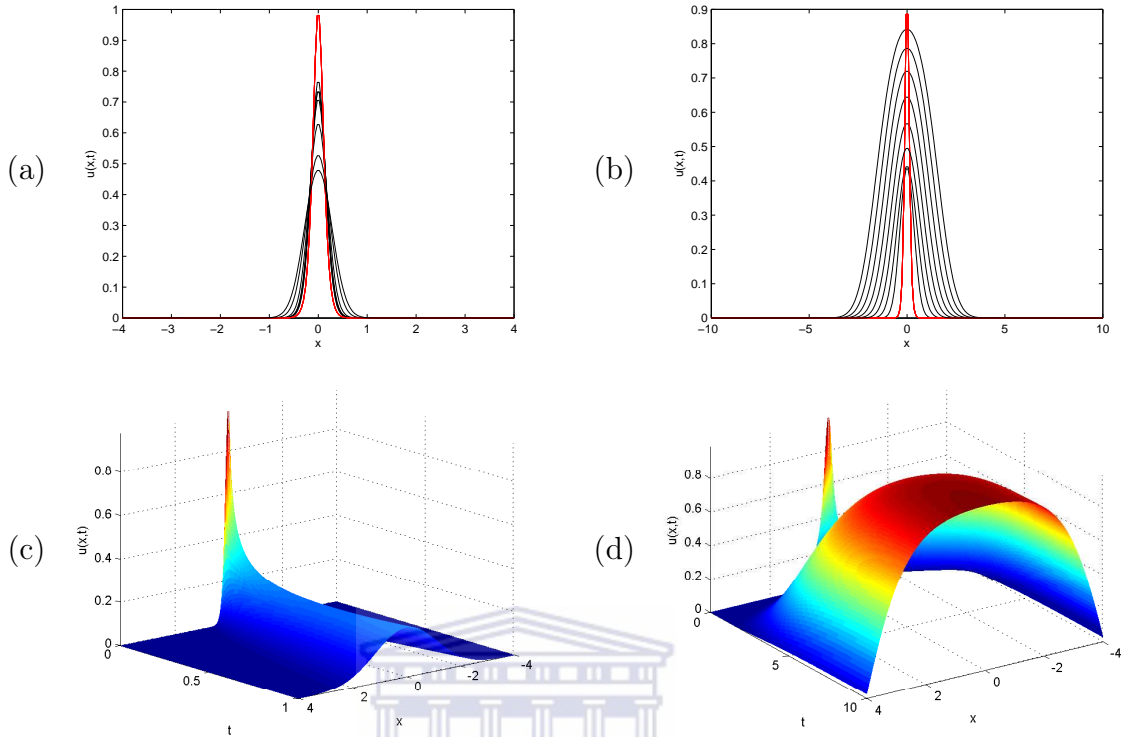


Figure 2.4.10: Plots of $u(x, t)$ for the first kind in problem (2.4.8) on $-L \leq x \leq L$.

with sinusoidal (smooth peak pattern), where $\phi > 0$ is the growth rate and $\kappa > 0$ is the carrying capacity. If u is small, the linear growth term ϕu results in rapid population growth, but as u become large, the competing term $-\phi u/\kappa$ slow down the growth rate. For large time T , the population experience an equilibrium growth, that is, $\phi = \kappa$. Also, we consider a situation where the reaction term $u(1 - u)$ is small which allows diffusion to gain dominance effect over the reaction. Clearly we can see that the peak in the second kind gets flatter quickly, this is achieved by introducing the third condition

$$g_3(x) = \left. \begin{array}{l} \exp[7(x + 1)], \quad x < -1, \\ \operatorname{sech}^2(7x), \quad -1 \leq x \leq 1, \\ \exp[-7(x - 1)], \quad x > 1, \end{array} \right\}, \quad (2.4.12)$$

for further details, the readers are referred to [4].

In Figure 2.4.10, the parameter values used are: (a) $N = 100$, $T = 0.5$, $L = 4$, $\beta = 0.1$, $\phi = k = 1$; (b) $N = 150$, $T = 0.05$, $L = 10$, $\beta = 0.5$, $\phi = k = 1$; mesh

solutions (c) is obtained at $T = 1$, $L = 4$, $\beta = 0.6$, $\phi = k = 1$, and (d) is obtained with $T = 10$, $L = 4$, $\beta = 0.9$, $N = 200$, $\phi = 1$ and $k = 2$.

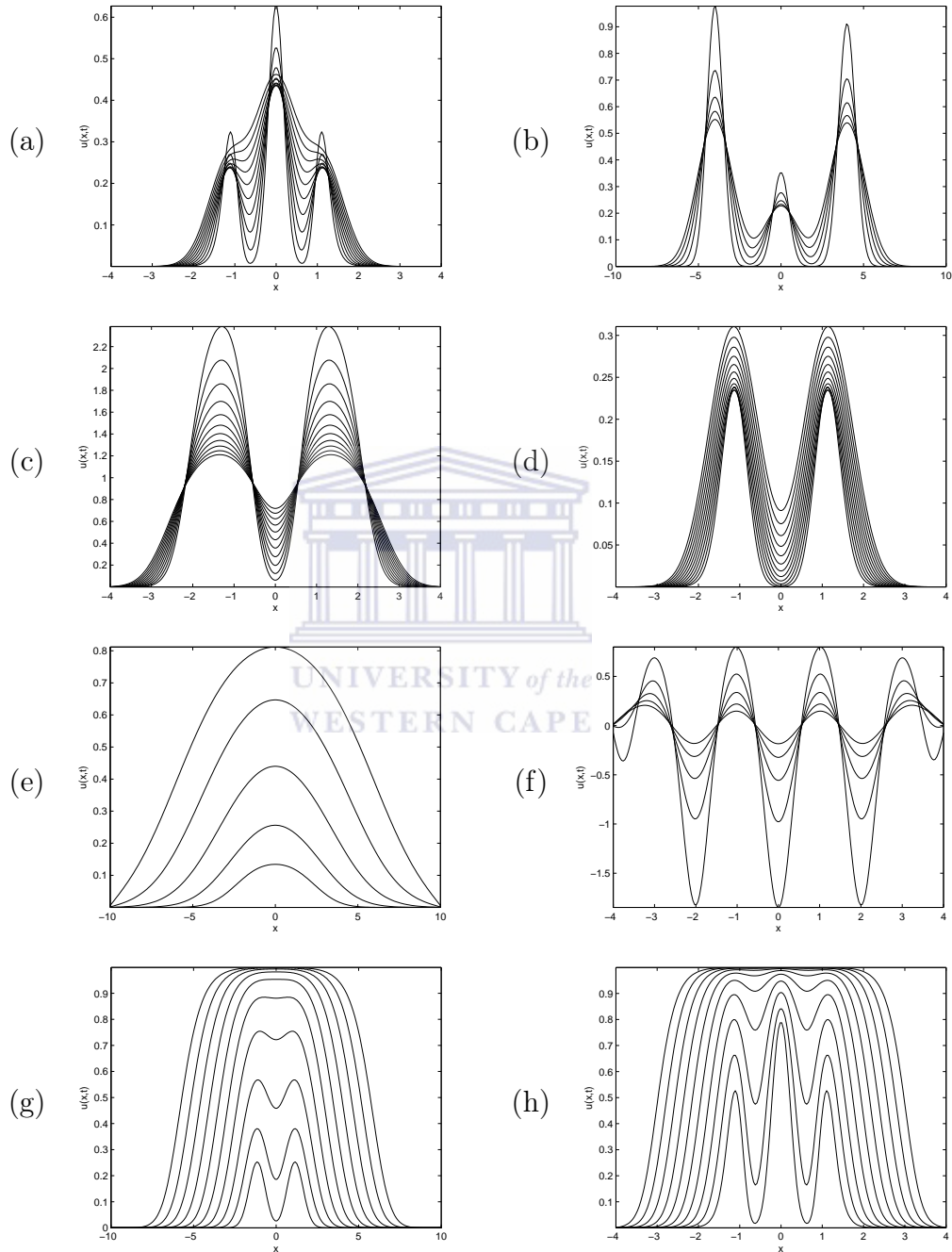


Figure 2.4.11: Various behavioural patterns of traveling waves emanating as a result of the perturbation of the second (2.4.11) and third (2.4.12) kinds of waves for problem (2.4.8).

The space L is adjusted in Figure 2.4.11 to ensure that there is enough space for

waves to propagate. The solutions of problem (2.4.8) exhibit various interesting diverse chaotic and periodic population oscillations arising from the three kinds of local waves considered. We have seen the local waves (2.4.10) with sharp peak in (2.4.10). The results of second (2.4.11) and the third (2.4.12) kinds local waves are presented in Figure 2.4.11, ranging from the sharp peak contour to the flat roof contour as a result of diffusion effects in the interval of space L . Readers are to take note of the difference in shape at the peaks as well as amplitudes of these solutions.

Fisher's equation with a specific logistic term:

Various choices of the reaction terms lead to different models, for instance, the choice $N(u) = u(1 - u)$ yields Fisher's equation that was originally used to describe the spreading of biological populations. The Fisher-Kolmogorov, Petrovskii, and Piskunov (KPP) equation is one of the simplest examples of a nonlinear reaction-diffusion equation. The equation dates to two independent publications in [100], they began with an equation in two-dimension with general reaction term, the report of their work laid the foundation for rigorous analytical study of the reaction-diffusion models. Fisher's equation is one-dimensional and had a specific *logistic* reaction term:

$$u_t = Du_{xx} + \tau u \left[1 - \frac{u}{\kappa} \right]. \quad (2.4.13)$$

Fisher proposed this equation as a model of diffusion of species in a one-dimensional habitat; D is the diffusion constant, τ is the growth rate of the species, and κ is the carrying capacity. Conveniently, we can re-scale the variables in (2.4.13), so that

$$\hat{u} \equiv \frac{u}{\kappa}, \quad \hat{t} \equiv \tau t, \quad \hat{x} \equiv \sqrt{\frac{\tau}{D}} x, \quad (2.4.14)$$

and therefore equation (2.4.13) implies

$$\hat{u}_t = \hat{u}_{xx} + \hat{u}(1 - \hat{u}). \quad (2.4.15)$$

After dropping the hats, equation (2.4.15) becomes

$$u_t = u_{\xi\xi} + \eta u_{\xi} + u(1 - u) \quad (2.4.16)$$

in terms of $\xi = \gamma - \eta t$. The perturbation effect to a traveling wave solution can be observed by introducing

$$u(\xi, t) = u_{\gamma}(\xi) + \delta(\xi, t),$$

where $\delta(\xi, t)$ denotes the small perturbation. Following the idea in [20] with a view of determining whether δ grows (if it grows, the solution is unstable) or decays (if it decays, the solution is linearly stable) as t increases, we discuss the linear partial differential equation

$$\delta_t = \delta_{\xi\xi} + \eta\delta_{\xi} + (\Phi)\delta, \quad (2.4.17)$$

for $\Phi = 1 - 2u_{\eta}(\xi)$, with a leading order for $|\delta| \ll 1$ is solved, subject to the initial condition

$$\delta(\xi, t=0) = \delta_{t=0}(\xi),$$

and $\delta_{t=0} \rightarrow 0$ as $\xi \rightarrow \pm\infty$. By introducing another variable, say $\sigma(\xi, t)$, through

$$\delta(\xi, t) = e^{-\lambda\xi}\sigma(\xi, t),$$

which in terms of σ , equation (2.4.17) now becomes

$$\sigma_t = \sigma_{\xi\xi} + \left(\sqrt{\eta^2 - 4}\right)\sigma_{\xi} - 2u_{\eta}(\xi)\sigma, \quad (2.4.18)$$

subject to

$$\sigma(\xi, 0) - \sigma_0(\xi) = e^{\lambda\xi}\sigma_0(y).$$

Equation (2.4.18) models an advective-diffusive process with a term $-2u_{\eta}(\xi)\sigma$, that typifies the consumption of σ , see [23, 102, 139] for details. Further analysis of equation (2.4.18) is beyond the scope of this thesis, we shall rather focus our attentions on reaction-diffusion problems.

Since 1937, equation (2.4.15) has been widely used to study flame propagation and nuclear reactors as well as population dynamics and genetics. Many researchers have studied this model. For instance, Al-Khaled [4] examined equation (2.4.15) with the aid of sinc collocation method where it was established that initial disturbance can propagate with a constant limiting speed when time becomes sufficiently large. Abdullaev [1] studies the stability of symmetric traveling waves in the Cauchy problem for more general case than equation (2.4.15). In [114], this problem was studied by using a perturbation method to find an approximate solution through expansion of the terms in power series.

Using the theory of finite difference approximations and Richardson's extrapolation, equation (2.4.13) can be approximated as

$$\left(\frac{\partial u}{\partial t}\right)_{i,j} = D \left[\frac{-u_{i+2,j} + 16u_{i+1,j} - 30u_{i,j} + 16u_{i-1,j} - u_{i-2,j}}{12h^2} \right] + \tau u_{i,j} \left[1 - \frac{u_{i,j}}{K} \right], \quad (2.4.19)$$

and $u = [u_1, u_2, \dots, u_l]^T$, for $1 \leq i, j \leq l$. $u_0 = u(x, 0)$ and $u_l = u(x, l)$ are the given boundary conditions. The system (2.4.19) will now be integrated using a time integration method as explained in the previous section.

The performance of our approach in this chapter is further tested on some reaction-diffusion problems in one-dimension. To show the efficiency of the present method, we report the relative errors defined by

$$\text{Relative Error} = \frac{\max |\bar{u}_j - u_j|}{\max |\bar{u}|}, \quad (2.4.20)$$

where \bar{u}_j and u_j are the exact and numerical values of u at point j in the collocation interval of points

$$\{x_1 = a, \dots, x_i = a + (i - 1)h, \dots, x_N = b\}, \text{ for } h = \frac{|b - a|}{N - 1}. \quad (2.4.21)$$

We investigate here numerically the varying effects of the diffusion coefficient D ,

growth rate τ and carrying capacity κ in (2.4.13).

$$u_t = Du_{xx} + \tau u \left[1 - \frac{u}{\kappa} \right], \quad (2.4.22)$$

subject to initial condition (2.4.6) for various parameter value of D , τ and K . This equation was earlier introduced by Fisher [51] as a model for the spread of an advantageous allele. It has also been used as an ecological model to describe the spread of a population enjoying logistic growth and simple Fickian diffusion.

In Figure 2.4.12, numerical results for problem 2.4.22 are presented at different parameter values. For Panel (a), parameter values are $D = 1$, $\tau = \kappa = 1$ at time $t = 1$, we noticed a slight change in the amplitude of the computed value in (b), as a result of diffusive effect when $D = 10$. A steady plot in (c) is obtained for $D = 1$, $t = 1$ when $\tau = 1, 2, \dots, 5$. In (d), $t = 1$, $D = 5$ and $\kappa = 1$ for $\tau = 0, 1, 2, 3$ from inner to the outer curve, the effect of diffusion dominates over the effect of reaction, so the peak goes down rapidly and gets flatter. Plot (e) is obtained with parameter values $t = 1$, $D = 2$, $\tau = 1$ for $\kappa = 2, 5$. In a similar way, we got panel (f) with $\tau = 1$, $D = 4$, $\kappa = 2, 5, 7, 9$ at $t = 5$. For plot (g), $D = 0.01$, $\tau = 5$, $\kappa = 1$ at $t = 0.001$, and (h) is obtained with $\kappa = 10$, $D = 2$, $\tau = 50$ for $t = 10$, are the sharp and flat surface plots showing the evolution from some initial perturbation to steady types.

Density dependent Nagumo equation:

Finally, we consider the density dependent diffusion Nagumo equation

$$u_t = Du_{xx} + f(u), \quad x \in \mathbb{R}, t \in [0, T) \quad T > 0, \quad (2.4.23)$$

where t is time in the spatial coordinate, D is the diffusion coefficient, and f is the nonlinear reaction term considered as

$$f(u) = \alpha u - \beta u^3, \quad (2.4.24)$$

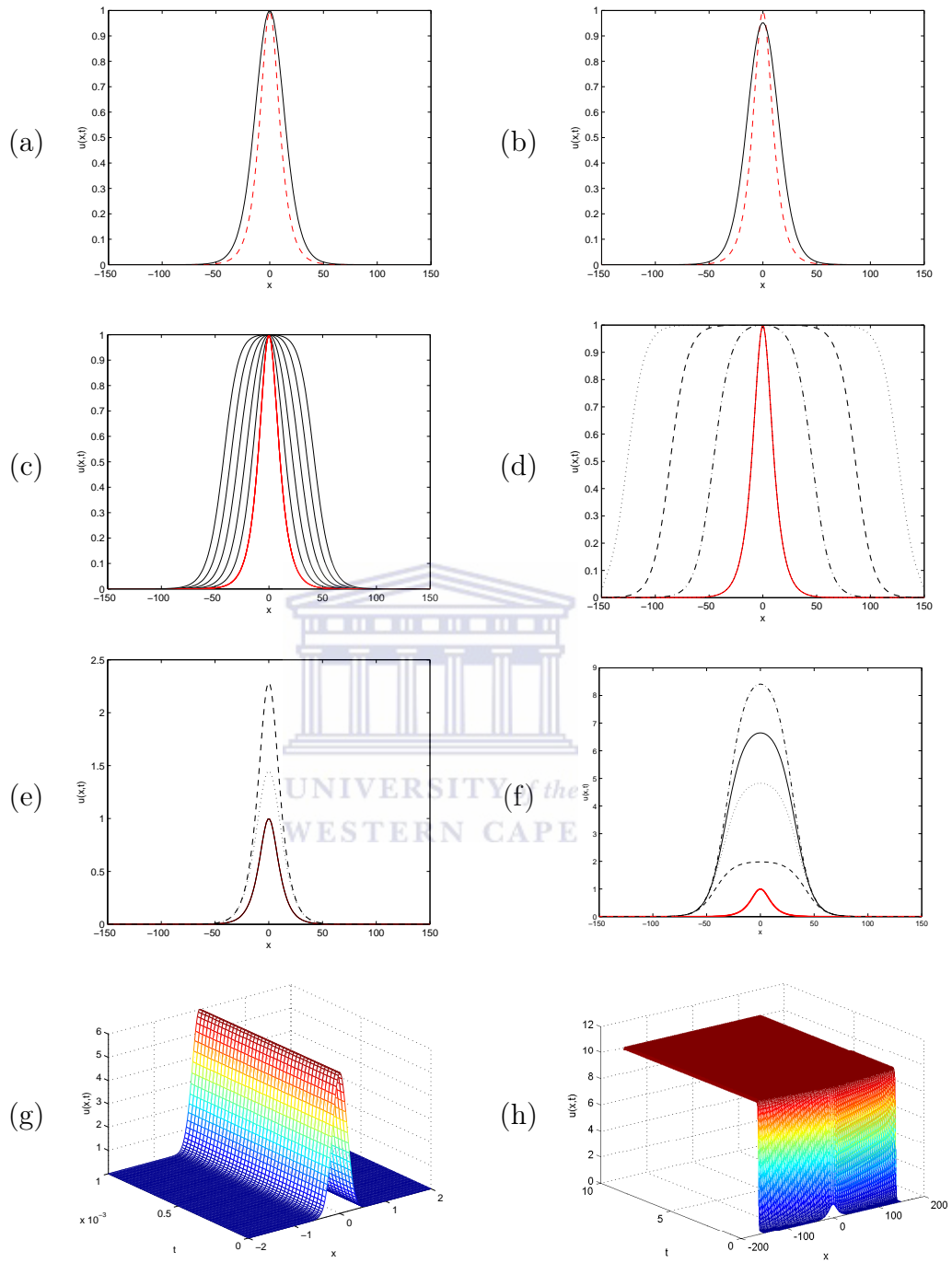


Figure 2.4.12: Numerical solutions of equation (2.4.13) for different parameters values of diffusion coefficient D , carrying capacity κ , growth rate τ and time t for initial condition (2.4.6) with $\delta = 1/8$.

subject to initial condition

$$u(x, 0) = 3 \exp(-20(x + 4)^2) + 2.05 \exp(-10(x - 4)^2) + \exp(-20(x)^2). \quad (2.4.25)$$

The boundary conditions are taken as

$$\left(\frac{\partial u}{\partial x}\right)_{x=0} = \left(\frac{\partial u}{\partial x}\right)_{x=l} = 0. \quad (2.4.26)$$

Equation (2.4.23) has many applications in real life. It is used to describe the model for the spread of genetic traits, and also for the propagation of nerve pulses in a nerve axon [121, 141, 156, 203].

Clearly, when $D = 0$, it is not difficult to see that the equilibrium points are at $u_1 = 0$, $u_2 = +\sqrt{\frac{\alpha}{\beta}}$ and $u_3 = -\sqrt{\frac{\alpha}{\beta}}$, $\beta \neq 0$. Moreover, equation (2.4.23) has infinitely many stable waves lying in $\left(-\sqrt{\frac{\alpha}{\beta}}, \sqrt{\frac{\alpha}{\beta}}\right)$.

The linearized form of density dependent Nagumo equation was solved in [156] with assumptions that $D = \alpha = \beta = 1$. In the present context, equation (2.4.23) is solved to investigate the varying effects of these parameter values. Panels (a)-(h), have revealed the steady structures (types in Turing patterns) [32, 137, 171]. At $D = \alpha = 1$, $\beta = 0.1, 0.2, 0.4, 0.5, 0.8$, we obtain (a) for $t = 1$. Effect of α is shown in (b) with parameter values $\alpha = 1, 4, 8$, $\beta = 0.05$, $D = 1$, $t = 1$. Cases (a)-(d) are similar in pattern obtained with different parameters. Solutions of plots (e), (f) and (h) blew up into three points that oscillate in phase to form steady structures. Parameter values are: $t = 0.1$, $D = 0.01$, $\beta = 0.5$, $\alpha = 0.1$ for (c). Figure 2.4.13 (d) corresponds in a unique way (at equilibrium point $\bar{u} = 0$) to Figure 2.4.12 (g). Notice the different scales on their vertical axes. Plot (g) is obtained at $\beta = \alpha = 10$, $D = 0.01$, at time step $t = 10$. At time step $t = 0.5$, $\alpha = 8$, $\beta = 0.5$ and $D = 0.8$, surface plot (h) is produced.

Table 2.4.2: Maximum relative error for Fisher's equation (2.4.5) at various step-sizes for $\delta = 1/8$, final time $T = 1$, $N = 250$ and $x \in [-150, 150]$.

Time step	ETDM4	ETDADAMS4	ETDM5	ETDM6	ETDRK4
1	0.4649	0.4649	0.6386	0.7654	5.1659e-004
1/2	0.1257	0.1257	0.2469	0.3616	3.0577e-005
1/4	9.5006e-005	2.8320e-005	4.2117e-006	0.0630	2.2117e-006
1/8	1.5550e-005	8.9104e-006	1.0327e-005	3.1063e-006	1.4920e-007
1/16	1.7100e-006	1.4519e-006	1.5496e-006	2.9810e-007	9.6955e-009

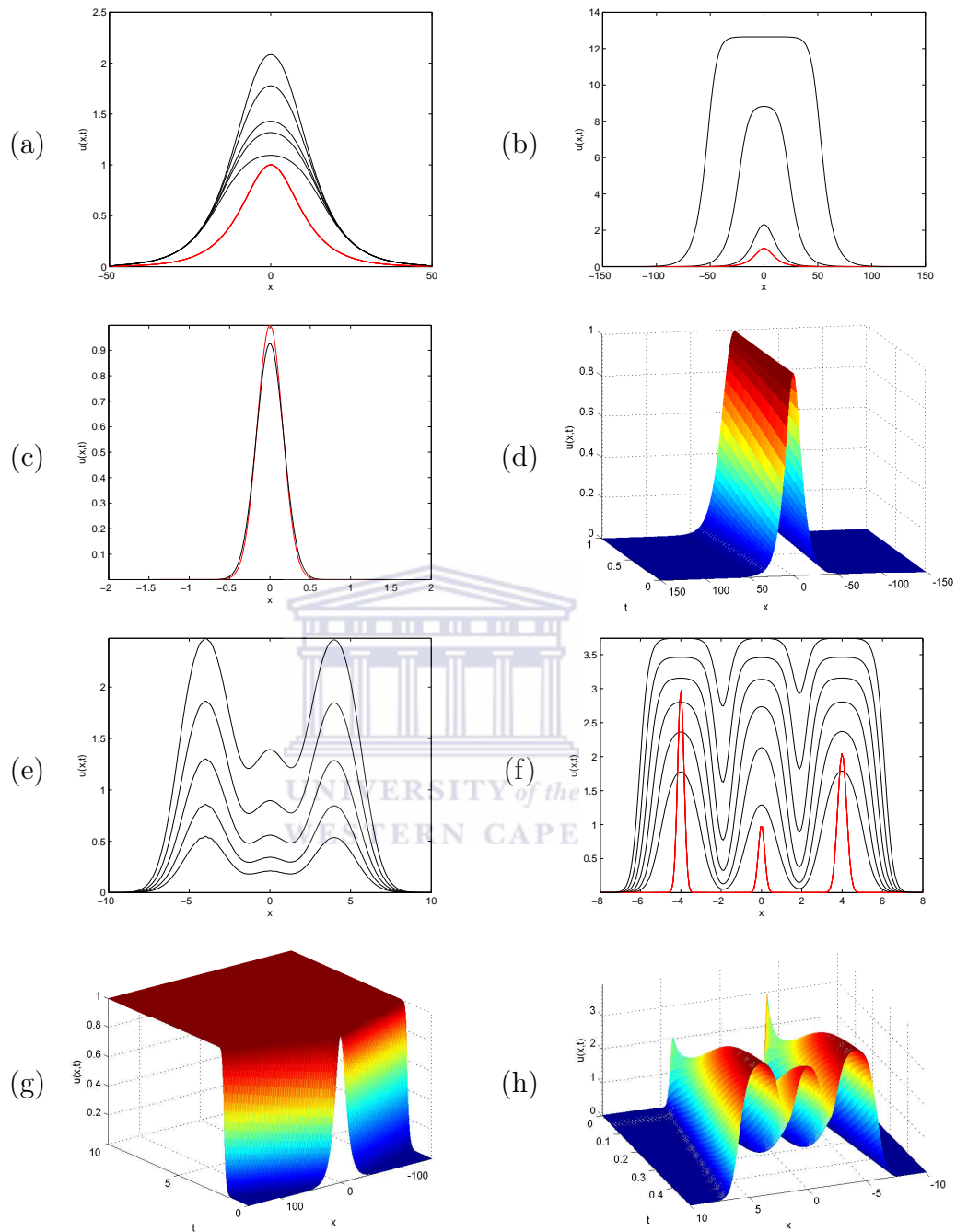


Figure 2.4.13: Numerical solutions of Nagumo equation (2.4.23) for different parameter values of D , α , β and time t .

The numerical experiments as indicated in Table 2.4.2 and Figure 2.4.14 are enough to grant sweeping statements that the ETDRK4 method is better than its competitors when used in conjunction with finite difference schemes. This assertion is evident in the results presented. It is worth noting that at $k = 1/4$, all other schemes including

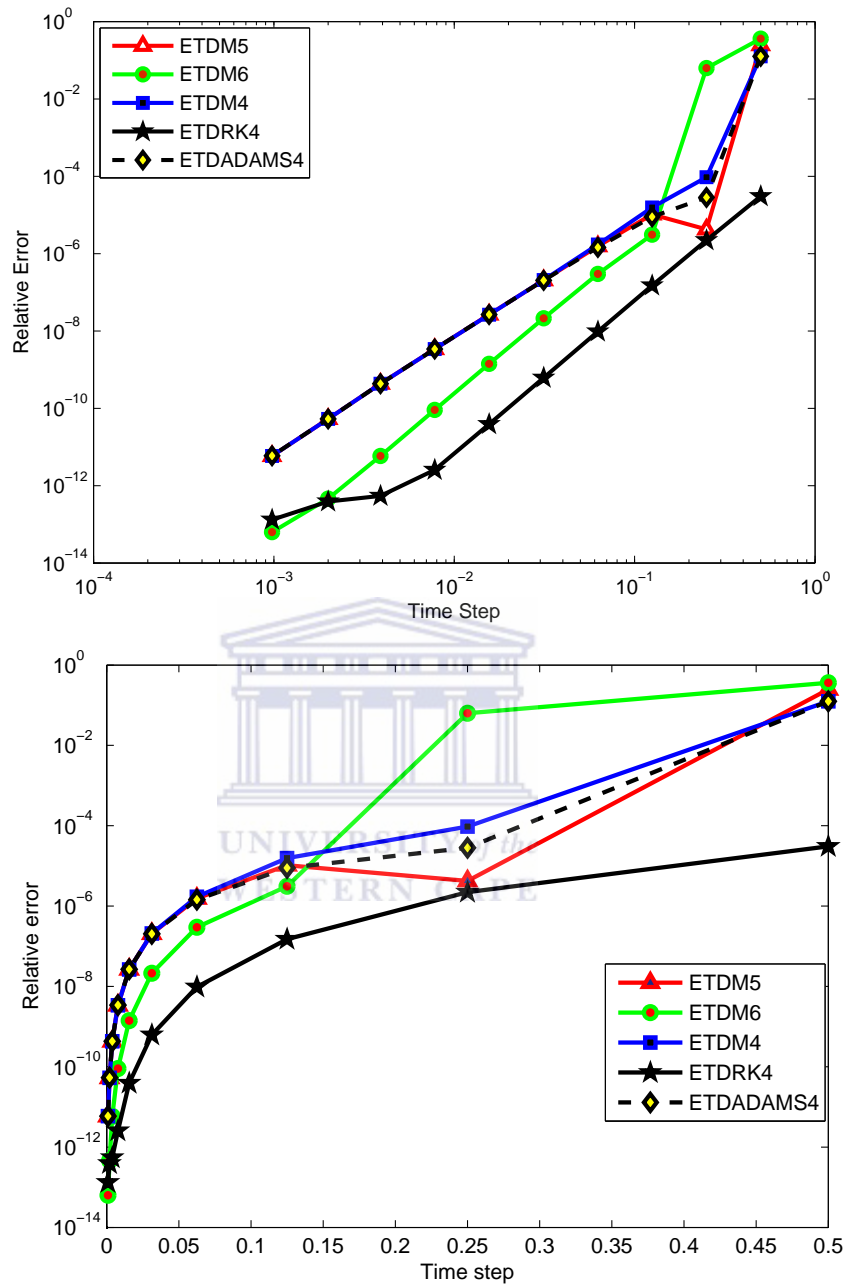


Figure 2.4.14: The top and lower panels show the relative errors as a function of time-step k for various higher-order time stepping methods for Fisher equation (2.4.5). The parameter values are: $\delta = 1/8$, $T=1$, $N = 250$ and $x \in [-150, 150]$

the fifth-order ETDM5 and sixth-order ETDM6 methods were both experienced a kind of shock, whereas, ETDRK4 provides a smooth, accurate and stable result in the same region even with large step size as shown in Table 2.4.2.

2.5 Summary and discussions

Exponential time differencing methods are time-stepping formulas that separate the linear term involving $\mathbf{L}u(x, t)$, which is solved exactly by a matrix exponential, from the nonlinear term $N(u(x, t), t)$. We have justified the assertion made by Kassam and Trefethen [92] on the efficiency and suitability of ETDRK4 schemes in conjunction with spatial discretisation methods by comparing it with exponential time differencing method (ETDADAMS4) of Adams type and exponential time differencing multi-step (ETDM4, ETDM5, ETDM6) methods, all are of the higher orders. This approach was first tested with the reaction-diffusion equation, a nonlinear form of KISS model that was named after Kierstead and Slobodkin [97] and Skellam [181], which was originally developed to investigate the size of nutrient patches needed to sustain phytoplankton blooms. We carried out numerical simulations in both one- and two-dimensional space on spatial domain $x \in [-l, l]$, that are chosen large enough to support the boom. Our numerical results revealed that the population size increases if the domain size l also increased. Some initial data and parameter values are chosen to mimic some existing patterns.

We have also studied both Fisher and Nagumo equations in ecological context to examine the rate of diffusivity, logistic growth and speed selection process. We believe also that the work done in this chapter could grant an insight to the understanding of pattern formation in one-dimensional reaction-diffusion systems. In comparison with other existing numerical methods that solve Fisher's equation, our approach compared favourably well for all the examples taken from the literature and the references therein. The ETDRK4 method demonstrates its superiority over some of the existing ETD counterparts as seen in Table 2.4.2 and Figure 2.4.14. The most amazing factor is the fact that it is much more accurate than fifth and sixth order ETD schemes. Biologically, the result presented in this chapter for the cases considered are interesting and seen as means of displaying the complexities that nonlinearity has introduced into the simplest equations of population biology, this assertion is evident in the displayed figures. Numerical simulations of all the examples considered are carried out on an

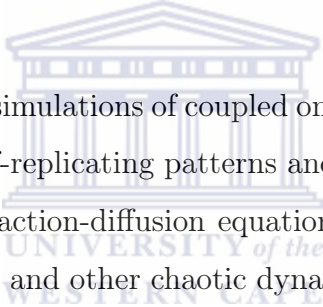
adjustable space scale defined by L with a view to ensure that there is sufficient space for waves to propagate.

In the next chapter, we shall extend our approach to solve systems of reaction-diffusion problems.



Chapter 3

Numerical solution of systems of reaction-diffusion models



In this chapter, numerical simulations of coupled one-dimensional Gray-Scott model for pulse splitting process, self-replicating patterns and unsteady oscillatory fronts associated with autocatalytic reaction-diffusion equations as well as homoclinic stripe patterns, self replicating pulse and other chaotic dynamics in Gierer-Meinhardt equations [45] are investigated. Our major approach is to use the exponential time differencing schemes of Cox and Matthews [36], which was later presented as a result of instability in a modified form by Krogstad [104], to solve stiff semi-linear problems. The semi-linear problems under consideration in this context are split into linear, which harbors the stiffest part of the dynamical system and nonlinear part that varies slowly than the linear part. For the spatial discretization, we employ higher-order symmetric finite difference scheme and solve the resulting system of ODEs with higher-order ETD methods. We refer readers to chapter two for the derivation and stability of ETD schemes. Numerical examples are given to illustrate the accuracy and implementation of the methods, results and error comparisons with other standard schemes are well presented.

3.1 Introduction

In the last decades, efficient and accurate simulation of reaction-diffusion systems has attracted the attention of many researchers in various fields, especially in science and engineering. Their interest was based on a number of phenomena ranging from the formation of spatial and temporal patterns in Turing systems [150, 171, 189], travelling waves in Fisher's equation [4, 51], nonlinear and spiral waves [144, 190].

In 1952, the British mathematician Alan Turing [189] first introduced a simple reaction-diffusion system describing chemical reaction and diffusion to account for morphogenesis, i.e. the development of patterns in biological systems. In paper [189], Turing employed linear analysis idea to find the threshold for the instability of spatially homogeneous equilibrium solutions of general two-system reaction-diffusion models. Turing in his work proved that a chemical state can attain a stable state against some perturbations in the absence of diffusion, and it may become unstable to perturbations in the presence of diffusion. Diffusion-driven instability or Turing instability is mostly initiated by arbitrary random deviations of the equilibrium state and results in equilibrium spatially periodic variations in the chemical concentration, that is, chemical patterns.

The choice of parameters determine that the system will evolve, e.g., towards stripes of a fixed width instead of spots, but the random initial conditions together with the effects of the boundaries and the domain geometry determine the exact positions and the alignment of the stripes (the phase) [139]. This idea becomes evident by considering the fact that all tigers have stripes, but the stripe pattern is not exactly similar in all individual tigers.

Experiments on Turing patterns were first seen in the late 1990s. In addition to experiments, previous studies of Turing systems have employed analytical mathematical tools and numerical computer simulations in studies of different models exhibiting Turing instability. Apart from physicists, also mathematical biologists have been interested in the Turing systems, which have been shown to be able to at least qualitatively imitate many biological patterns such as the stripes of a zebra or spots of a chee-

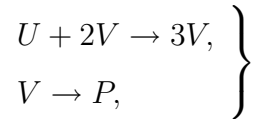
tah [43, 44, 139, 140] and even more irregular patterns such as those on leopards and giraffes, not to talk about the patterns on exotic fish, butterflies or beetles.

In 1993, Pearson [150] observed that for parameter values far from the Turing instability regime, the Gray-Scott model in a two-dimensional spatial domain can exhibit a rich variety of spatio-temporal patterns including, stationary spots, traveling spots, spot self-replication, spot-annihilation, growing stripes, labyrinthian patterns, stripe filaments, and spatial-temporal chaos, etc. The common feature in all of these patterns is that each consists of two distinct states of solutions: some localized regions where the chemical concentrations are very large, and a background ambient spatially homogeneous state. As time evolves, the localized regions of elevated chemical concentrations can remain stable, or develop very complicated structures through drifting, splitting, breaking, etc., driven by intricate and unknown mechanisms that depend on the range of parameters in the reaction-diffusion model.

Self-replicating patterns have been observed numerically in a reaction diffusion system [198] as well as in laboratories [111]. A prototypical model is the irreversible Gray-Scott (GS) model that exhibits a variety of new patterns including spots that self replicate and develop into a variety of asymptotic states in two dimensions [150] as well as pulses that self replicate in one dimension [159]. Several interesting analytical works have also appeared: for instance, formulation of single-spot solution to the Gray-Scott model and its stability has been done by Reynolds et al. [160] with the aid of formal matched asymptotic analysis, which is closely related to the splitting phenomenon; a tedious analysis regarding the existence and stability of steady single pulse as well as nonexistence of traveling pulses has been studied by [42, 43]. Their works are highly suggestive, there are lot to be understood about the mechanism that drives the replication dynamics itself.

A detailed mathematical study of these localized structures could have significant applications in controlling chemical reactions for certain purposes, and in understanding and classifying patterns in biological systems. One example is the self-organized formation of either labyrinths, spots, or stripe patterns. Very complicated patterns were described in a paper by Pearson [150], for a parabolic system called the Gray-

Scott system developed in 1980s at the university of Leeds by P. Gray and S. K. Scott. Since then the model has been an important benchmark for the description autocatalytic reaction as an isothermal system with chemical feedback in a continuous flow stirred tank reactor. The initial GS model describes the two irreversible chemical reactions



where U and V are the reacting chemicals and P is an inert product (see [42, 62, 63, 64]). Since V appears on both side of (3.1.1), it acts as catalyst for its own production. In biological context, we could also describe model equation (3.1.1) as predator-prey model to illustrate the predominance of one specie over the other. In GS model, it was assumed that the chemical U is in contact with a reservoir and chemical V is removed from the system at constant rate F . Using the law of mass action, the resulting pair of coupled reaction-diffusion equations in dimensionless units is

$$\left. \begin{aligned} \frac{\partial u}{\partial t} &= D_u \nabla^2 u - uv^2 + F(1 - u), \\ \frac{\partial v}{\partial t} &= D_v \nabla^2 v - uv^2 - (F + k)v, \end{aligned} \right\} \quad (3.1.1)$$

where D_u and D_v are the respective diffusion coefficients in u and v components, F is the dimensionless flow rate and k is decay constant of the activator, V . Gray-Scott equations (3.1.1) have been studied in one- and two-dimensions, for example, pulse splitting was observed in one-dimension [42, 159], when $(D_u, D_v) = (1, 0)$, $u = u(x, t)$ and $v = v(x, t)$, ($x \in \mathbb{R}$ and $\nabla^2 \equiv \partial^2/\partial x^2$). By contrast, original study in two-dimensions, [37, 134, 135] involved fixed diffusion coefficients where the diffusion ratio is taken as 2, that is, $D_u = 2 \times 10^{-5}$ and $D_v = 10^{-5}$, $u = u(x, y, t)$ and $v = v(x, y, t)$, ($x, y \in \mathbb{R}^2$ and $\nabla^2 \equiv \partial^2/\partial x^2 + \partial^2/\partial y^2$), with F and k being the control parameters.

This system of Turing pattern has a stable steady state with respect to homogeneous temporal oscillations which becomes unstable towards state-periodic perturbations of the diffusion. We further investigate the equilibria and stability of system (3.1.1) by

setting the diffusion terms to zero, it reduces to system of ordinary differential equations

$$\left. \begin{aligned} u_t &= -uv^2 + F(1 - u) = 0, \\ v_t &= +uv^2 - (F + k)v = 0, \end{aligned} \right\} \quad (3.1.2)$$

this implies that

$$\left. \begin{aligned} -uv^2 + F(1 - u) &= 0, \\ uv^2 - (F + k)v &= 0, \end{aligned} \right\} \quad (3.1.3)$$

which on addition, yields

$$v = \frac{F}{F + k}(1 - u). \quad (3.1.4)$$

Further substitution and simplification arrives to

$$(u^2 - u + F\psi^2)(1 - u) = 0, \quad \psi = \frac{F + k}{F}. \quad (3.1.5)$$

The linear analysis shows the existence of a trivial homogeneous steady state red stage $u_R = 1$ and $v_R = 0$, that occurs as a result of continuous supply of stable substrate for the pair of (F, k) . Clearly, the roots of cubic equation (3.1.5) are the equilibrium solutions. For $u_0 = 1$, it follows from (3.1.4) that $v_0 = 0$. The remaining two steady states are obtained from $u^2 - u + F\psi^2$ as

$$\left. \begin{aligned} u_{a,b} &= \frac{1}{2} \left(1 \pm \sqrt{1 - 4\psi^2 F} \right), \\ v_{a,b} &= \frac{1}{2\psi} \left(1 \pm \sqrt{1 - 4\psi^2 F} \right), \end{aligned} \right\} \quad (3.1.6)$$

the trivial solution $(u_0, v_0) = (1, 0)$ exists for any value of pair (F, k) , but the other two steady states exist only when the discriminant $1 - 4\psi^2 \geq 0$, this implies that $(F + k)^2 \leq \frac{F}{4}$. The saddle node-bifurcation point in the (F, k) parameter space in Turing structures that describe when the stable equilibrium state of the system becomes

unstable (stability to instability) occurs when

$$\left. \begin{aligned} (F + k)^2 &= \frac{F}{4}, \\ 4F^2 + (8k - 1)F + 4k^2 &= 0, \end{aligned} \right\} \quad (3.1.7)$$

following the way, we obtain

$$F_{a,b} = \frac{-(8k - 1) \pm \sqrt{1 - 16k}}{8}. \quad (3.1.8)$$

We analyse further the stability of the above system by letting u_η and v_η be the steady-state solutions of (3.1.1), on perturbation [163], we set $u = u_\eta + \delta\hat{u}$ and $v = v_\eta + \delta\hat{v}$, and neglect the second order term to yield

$$\left. \begin{aligned} \frac{\partial\hat{u}}{\partial t} &= \mathbf{D}_u \nabla^2 \hat{u} - (v_\eta^2 + F)\hat{u} - 2u_\eta v_\eta \hat{v} + O(\delta) \\ \frac{\partial\hat{v}}{\partial t} &= \mathbf{D}_v \nabla^2 \hat{v} - (F + k - 2u_\eta v_\eta)\hat{v} + v_\eta^2 \hat{u} + O(\delta). \end{aligned} \right\} \quad (3.1.9)$$

The point (1,0) is always stable, the stability of the other two rest-points are given by setting $\hat{u} = u_\alpha \eta^{\lambda t - ikx}$ and $\hat{v} = v_\alpha \eta^{\lambda t - ikx}$, (u_α and v_α are the amplitudes of the perturbation, k is the wave number in the direction of x), to yield the eigenvalues of the following matrix

$$M = \begin{pmatrix} D_u k^2 + v_\eta^2 + F + \lambda & -2u_\eta v_\eta \\ v_\eta^2 & D_v k^2 + F + k - 2u_\eta v_\eta + \lambda \end{pmatrix} = 0. \quad (3.1.10)$$

The negative eigenvalues for the trivial steady state when $u_\eta = 1$ and $v_\eta = 0$ are $\lambda_1 = D_u k^2 - F$, $\lambda_2 = D_v k^2 - F - k$, further indicates the stability of the system for all values of parameters pair (F,k). The system undergoes Hopf bifurcation when

$$F_H = \frac{1}{2} \left[\sqrt{k} - 2k - \sqrt{(2k - \sqrt{k})^2 - 4k^2} \right]. \quad (3.1.11)$$

The point at which the saddle-node and the Hopf bifurcation intersect is known as Bogdanov-Takens (BT-point), see Figure 3.1.1. The Hopf line lies and intersect the steady state bifurcation line at (0,0) and the turning (BT)-point (1/16, 1/16) in the

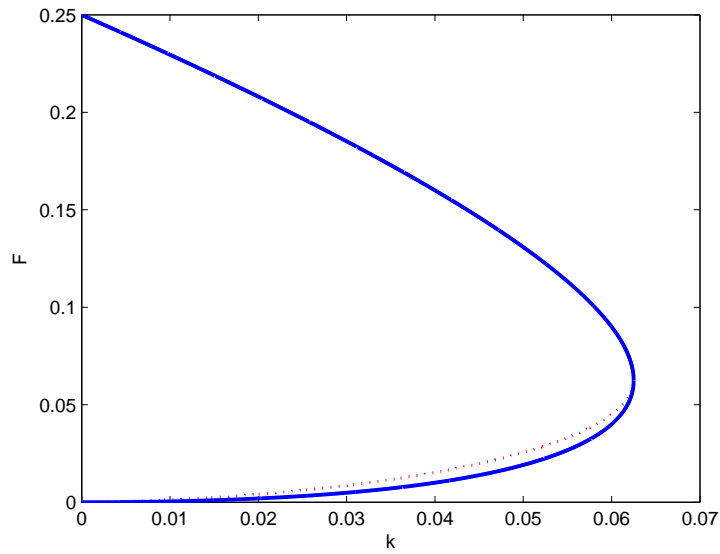


Figure 3.1.1: Bifurcation curves showing the saddle-node (*solid line*) and the Hopf bifurcation curve (*dotted line*). The area enclosed to the left and right of the bifurcation curves described the stable and unstable regions.

parameter space (F, k) . Readers are referred to ([37, 42, 133]), for further analysis.

The rest of this chapter is structured as follows. In Section 3.2, we discuss the model problems. A brief account of the numerical method is presented in Section 3.3. Section 3.4 accounts for the numerical results of Gray-Scott, autocatalytic and Gierer-Meinhardt models. Finally, we summarize in Section 3.5.

3.2 Model problems

We arrived at the coupled reaction-diffusion equations considered in this report by setting $F = A$ and $F + 1 = B$, then equation (3.1.1) discussed above becomes

$$\left. \begin{aligned} \frac{\partial u}{\partial t} &= \mathbf{D}_u \nabla^2 u - uv^2 + A(1 - u), \\ \frac{\partial v}{\partial t} &= \mathbf{D}_v \nabla^2 v - uv^2 - Bv, \end{aligned} \right\} \quad (3.2.1)$$

where $u = u(x, t)$ and $v = v(x, t)$ remain the concentrations of the two chemical species the inhibitor u and the activator v . The operator $\nabla^2 \equiv \partial^2/\partial x^2$ in one space dimension is the Laplacian operator with respect to $x \in \mathbb{R}$, the terms Du and Dv

are the diffusivities. The parameter A describes the rate at which the inhibitor u is fed from the reservoir into the reactor, and B is the overall rate of decay of v due to draining. Equation (3.2.1) was proposed by [62, 63] and has since been studied in various forms [37, 42, 43].

In order to study the pair of coupled reaction-diffusion equations in (3.2.1) for pulse dynamics and self replicating patterns, we need to analyze its steady state, that is when the system is independent of time and also the stationary solution which is also independent of the spatial variable x , this could only be achieved by letting

$$\frac{\partial u}{\partial t} = \frac{\partial v}{\partial t} = u_{xx} = v_{xx} = 0.$$

Hence, equation (3.2.1) reduces to

$$\left. \begin{aligned} 0 &= -uv^2 + A(1 - u), \\ 0 &= uv^2 - Bv, \end{aligned} \right\} \quad (3.2.2)$$

following the analysis discussed in section 1, it is not difficult to see that the point $(u, v) = (1, 0)$ is the solution of equations in (3.2.2), keeping in mind that $4B^2 < A$ and that

$$u_{\alpha,\beta} = \frac{1}{2} \left[1 \pm \sqrt{1 - \frac{4B^2}{A}} \right], \quad (3.2.3)$$

$$v_{\alpha,\beta} = \frac{A}{2B} \left[1 \pm \sqrt{1 - \frac{4B^2}{A}} \right], \quad (3.2.4)$$

as the remaining two steady states solution.

To determine the stability of the stationary states, we need to consider first the model equation (3.2.1) without the diffusion terms. So, setting the diffusion terms to zero, we have

$$\left. \begin{aligned} \frac{\partial u}{\partial t} &= -uv^2 + A(1 - u), \\ \frac{\partial v}{\partial t} &= uv^2 - Bv. \end{aligned} \right\} \quad (3.2.5)$$

Conveniently, we present the Jacobian in the form

$$Df(u, v) = \begin{pmatrix} -v^2 - A & -2uv \\ v^2 & 2uv - B \end{pmatrix}. \quad (3.2.6)$$

Thus, we have

$$Df(1, 0) = \begin{pmatrix} -A & 0 \\ 0 & -B \end{pmatrix}, \quad (3.2.7)$$

for the stationary state $(u, v) = (1, 0)$. The presence of the two negative eigenvalues is an indication that the model equation is stable, though without diffusion. We also study here the rescaled version of $A = \epsilon a$, $B = \epsilon^{\frac{2}{3}} b$ by following the analysis discussed in [42, 43] closely for single pulse and spatially periodic stationary patterns.

3.3 Numerical method

Attempt to find an accurate and efficient simulation of equation of the form (3.1.1), is handled in two ways. Since the coupled partial differential system (3.1.1) contains both linear and nonlinear parts, we introduce a sixth-order finite difference scheme for the spatial approximations. Finite difference approximation technique is a numerical procedure which solves a partial differential equation (PDE) [173] of the form (3.1.1) by discretizing the spatial physical domain into a discrete finite difference grid, and then approximating the individual exact partial derivatives in the PDE by algebraic finite difference approximations (FDAs), substituting the FDAs into the PDE to obtain an algebraic finite difference equation (FDE), and solving the resulting algebraic finite difference equations for the dependent variable.

Spatial approximations of the individual derivatives appearing in the partial differential equations (3.2.1), must be represented, this task is achieved through Taylor series expansions. Suppose we have a function $u(x)$, which is assumed to be continuous and differentiable over the range of interest. We assumed at this point that the value $u(x_0)$ and all the derivatives at $x = x_0$ are known. In this part, following our description above, we will show how to discretize system (3.2.1) and transform it into

a matrix problem. It is clear that the state variable x in (3.2.1) is unbounded, we need to first truncate the infinite x -domain \mathbb{R} to a finite domain $[x_{\min}, x_{\max}]$. Once the spatial domain is truncated, we consider a computational grid defined by

$$x_j : x_i = x_{\min} + i\Delta_x, i = 1, 2, \dots, n, \Delta_x = \frac{x_{\max} - x_{\min}}{n + 1}.$$

We then approximate the spatial derivatives in (3.2.1) by the sixth-order central difference scheme where $u_i(t)$ and $v_i(t)$ are denoted by $u(x_i, t)$ and $v(x_i, t)$ respectively, for $i = 1, 2, \dots, n$. Therefore, (3.2.1) results to system of ODEs in time which is an $n \times n$ Toeplitz matrix with entries

$$\left. \begin{aligned} \frac{du_i}{dt} &= [2u_{i-3,t} - 27u_{i-2,t} + 270u_{i-1,t} - 490u_{i,t} + 270u_{i+1,t} - 27u_{i+2,t} \\ &+ 2u_{i+3,t}]/[180h^2] - u_{i,t}(v_{i,t})^2 + A(1 - u_{i,t}), \\ \frac{dv_i}{dt} &= [2v_{i-3,t} - 27v_{i-2,t} + 270v_{i-1,t} - 490v_{i,t} + 270v_{i+1,t} - 27v_{i+2,t} \\ &+ 2v_{i+3,t}]/[180h^2]u_{i,t}(v_{i,t})^2 + Bv_{i,t}, \end{aligned} \right\} \quad (3.3.1)$$

for $i = 1, 2, \dots, n$ and $u_{i,t} = [u_{1,t}, u_{2,t}, \dots, u_{n,t}]^T$. Now, equation (3.3.1) is ready to be advanced with a time differentiation methods as discussed in chapter two. We can see that the nonlinear part now becomes a function of $u(t)$ and $v(t)$, so the need for the improvement of ETDRK4 (2.2.20) [92, 104], is required to make it suitable for system of coupled equations. We present the new fourth-order ETDRK4 scheme as

$$\begin{aligned} u_{n+1} &= u_n e^{\mathbf{L}h} + h[4\varphi_2(\mathbf{L}h) - 3\varphi_1(\mathbf{L}h) + \varphi_0(\mathbf{L}h)]\mathbf{N}(u_n, v_n, t_n) \\ &+ 2h[\varphi_1(\mathbf{L}h) - 2\varphi_2(\mathbf{L}h)]\mathbf{N}(a_n, t_n + h/2) \\ &+ 2h[\varphi_1(\mathbf{L}h) - 2\varphi_2(\mathbf{L}h)]\mathbf{N}(b_n, t_n + h/2) \\ &+ h[\varphi_2(\mathbf{L}h) - 2\varphi_1(\mathbf{L}h)]\mathbf{N}(c_n, t_n + h), \end{aligned} \quad (3.3.2)$$

where

$$\begin{aligned}
 a_n &= u_n e^{\mathbf{L}h/2} + (\mathbf{L}h/2)\varphi_0(\mathbf{L}h/2)\mathbf{N}(u_n, v_n, t_n), \\
 b_n &= u_n e^{\mathbf{L}h/2} + (\mathbf{L}h/2)[\varphi_0(\mathbf{L}h/2) - 2\varphi_1(\mathbf{L}h/2)]\mathbf{N}(u_n, v_n, t_n) \\
 &\quad + h\varphi_1(\mathbf{L}h/2)\mathbf{N}(a_n, t_n + h/2), \\
 c_n &= u_n e^{\mathbf{L}h} + h[(\varphi_0(\mathbf{L}h) - 2\varphi_1(\mathbf{L}h))\mathbf{N}(u_n, v_n, t_n) + 2h\varphi_1(\mathbf{L}h)\mathbf{N}(c_n, t_n + h)].
 \end{aligned}
 \tag{3.3.3}$$

The stability analysis of the ETDRK4 method has been discussed in Chapter 1.

3.4 Numerical results

In this section, we test the approach we discussed above on some reaction-diffusion problems in one-dimension.



Gray-Scott equation:

We study in this context the popular Gray-Scott equation in one-dimension. For example, the pulse splitting process that was observed in [37, 42, 43]. Pulse splitting or shedding is an interesting phenomenon that has widely generated a lot of attentions in the current field of research. It illustrates a meaningful interaction between two chemical species u and v in a gel reactor, such interaction is govern by a pair of coupled reaction-diffusion equations

$$\left. \begin{aligned}
 \frac{\partial u}{\partial t} &= D_u \nabla^2 u - uv^2 + A(1 - u), \\
 \frac{\partial v}{\partial t} &= D_v \nabla^2 v + uv^2 - Bv,
 \end{aligned} \right\}
 \tag{3.4.1}$$

with initial conditions

$$\left. \begin{aligned}
 u(x, t = 0) &= 1 - \frac{1}{2} \sin^{100}(\pi(x - L)/2L) \\
 v(x, t = 0) &= \frac{1}{4} \sin^{100}(\pi(x - L)/2L),
 \end{aligned} \right\}
 \tag{3.4.2}$$

where $D_u = 1 = D_v$, are the diffusion parameters of the two chemical species v and u called activator and inhibitor in [63], with assumptions that the diffusivities are equal and nearly equal ($D_u = 1, D_v = \epsilon$). The variables $u = u(x, t)$ and $v = v(x, t)$ denote the concentrations of the inhibitor U and the activator V , ∇^2 denotes the Laplacian with respect to $x \in \mathbb{R}$, the parameters A and B are small, usually $\ll 1$. The boundary conditions are of Dirichlet type

$$u(x = 0, t) = u(x = 1, t) = 1, \quad v(x = 0, t) = v(x = 1, t) = 0, \quad (3.4.3)$$

it was observed that even when Neumann conditions were used, noticeable enough, the inner solutions were not influenced. In Figure 3.4.1 (a) and (b), the parameter values are: $A=0.02, B=0.079, \epsilon=0.01$ for both u and v . Plot (c) is obtained with $A=0.021, B=0.069, \epsilon=0.01$; (d) $A=0.022, B=0.059, \epsilon=0.01$. In (e) and (f), we re-scale parameters $A = \epsilon a, B = \epsilon^{\alpha/3} b, \alpha = 1$ in the interval of length $L = \pm 50$ with $a = 9, b = 0.4, \epsilon = 0.01$.

In Figure 3.4.2, the rescaled parameters values are: $A = a\epsilon$ and $B = \epsilon^{1/3}b$ when (a) $a = 2, b = 0.4, \epsilon = 0.01, L = 20$. (b) $a = 3, b = 0.4, \epsilon = 0.01, L = 20$. (c) $a = 4, b = 0.4, \epsilon = 0.01, L = 20$. (d) $a = 4, b = 0.4, \epsilon = 0.01, L = 30$. Panels (e) and (f) are obtained at $A = 0.021, B = 0.069, L = 50$. Also, we obtained the pair (g) and (h) at $A = 0.02, B = 0.0863, L = 50$. Notice the difference between figures 3.4.1 and 3.4.2.

All the simulations presented have been repeated several times on intervals of different lengths, we show simulations on large intervals since enlarging the intervals have no influence on the behaviour of the dynamic system (3.4.1), regardless of the boundary conditions. We equally used three parameters in (3.4.1), where A and B are re-scaled into $A = \epsilon a$ and $B = \epsilon^{\alpha/3} b$, with the choice $\alpha = 1$, magnitude of B is measured by α . Parameter B was studied in [42], as $B = b\delta^{2\alpha/3}$ which we as well considered. Since the best values of a are known to have contained in the interval $2 \leq a \leq 9$, conveniently, we have the choice of varying $\epsilon \in [0.003, 0.01]$ for self-replicating pulse patterns.

Numerical simulation of (3.4.1) have revealed some chaotic and periodic behaviour patterns that evolve from the interaction of two species u and v in a domain defined

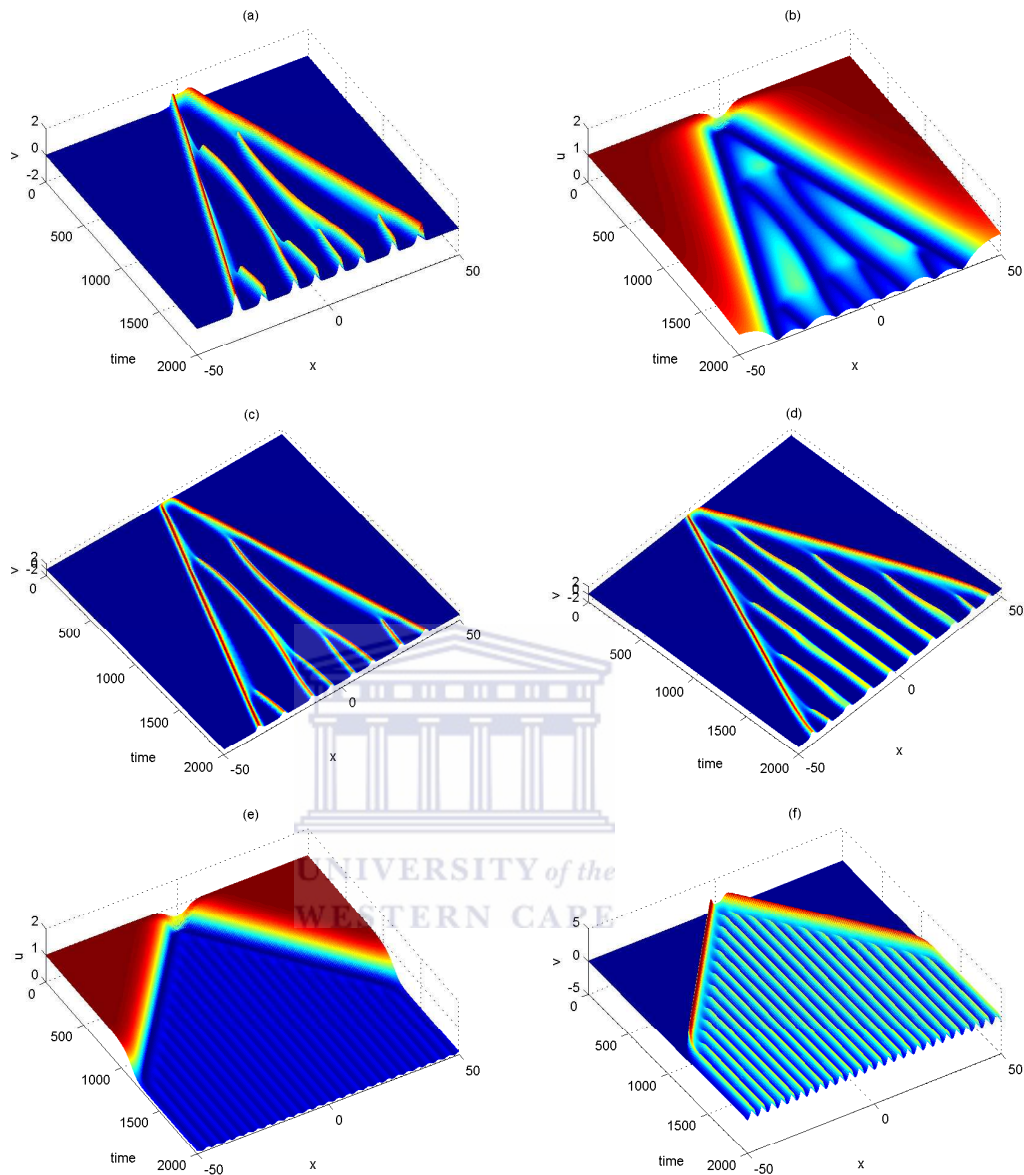


Figure 3.4.1: Surface plots of $u(x, t)$ and $v(x, t)$, propagation of pulses and shedding phenomena are observed in the numerical simulation of (3.4.1) at $t = 2000$.

as L . The results presented in Figure 3.4.4 are obtained with parameter values $a = 9$, $b = 0.4$, $A = \epsilon a$, $B = \epsilon^{\alpha/3} b$, $\alpha = 1$ defined in the interval $[0, L]$ for (a) $t = 1000$, $\epsilon = 0.001$, $N = 100$, $L=300$; (b) $t = 100$, $\epsilon = 0.01$, $N = 230$, $L=400$; (c) $t = 100$, $\epsilon = 0.01$, $N = 190$, $L=400$; (d) $t = 100$, $\epsilon = 0.01$, $N = 160$, $L=400$; (e) $t = 100$, $\epsilon = 0.01$, $N = 250$, $L=400$; (f) $t = 1000$, $\epsilon = 0.001$, $N = 250$, $L=400$; (g) $t = 1000$, $\epsilon = 0.001$, $N = 200$, $L=400$; (h) $t = 1000$, $\epsilon = 0.001$, $N = 200$. Oscillatory and more pronounced type are seen in (d), (e) and (f).

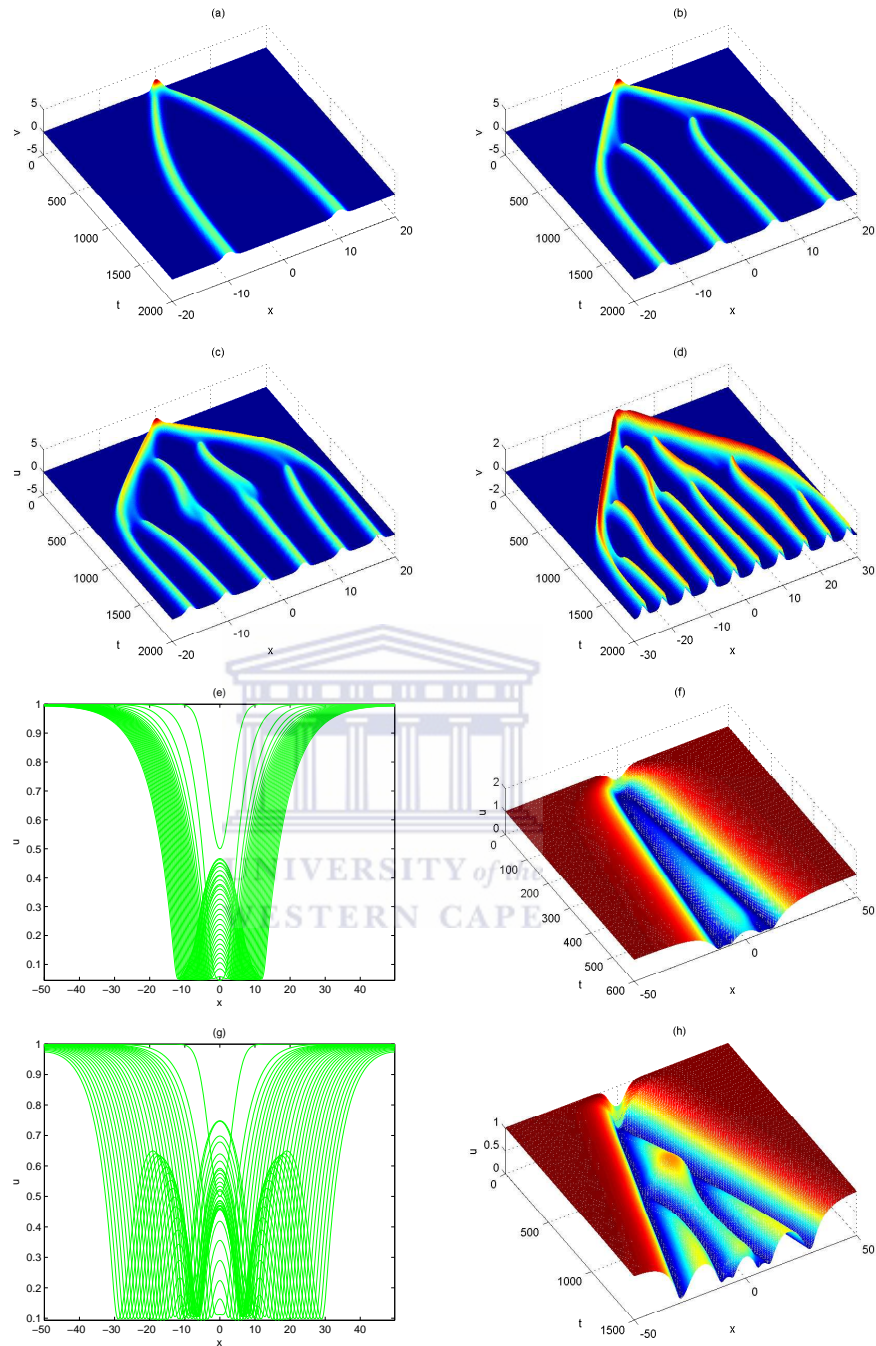


Figure 3.4.2: Propagation of pulses and shedding phenomena of problem (3.4.1) at re-scaled values for $A = \epsilon a$ and $B = \epsilon^{1/3} b$.

Clearly, numerical simulation of system (3.4.1) have generated series of self-replicating pulses as shown in Figure 3.4.5, it is noticeable in panels (a)-(f) that the resulting pulses obtained from the concentrations of u and v are repelling each other. A periodic and stationary self-replicating patterns is obtained in Figure 3.4.5 (a)-(d) for the two

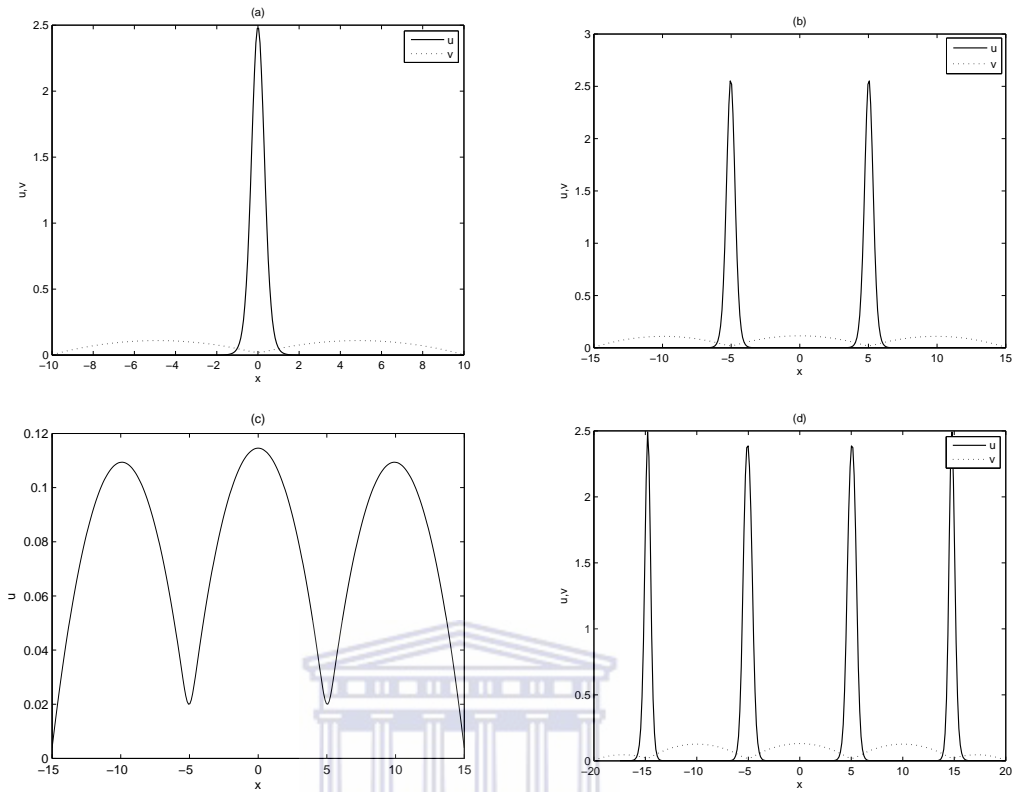


Figure 3.4.3: Plots (a)-(d) showing self-replicating patterns and pulse splitting procedures in (3.4.1) for the species u and v .

chemical species. Panels (e) and (f) show the result of unstable seven and three-pulse solutions. The amplitude of v is large when compared to u . The stable one- two- and three-pulse solutions is shown in Figure 3.4.3, we plot the results of a simulation with $a = 9$, $b = 0.4$ and $\epsilon = 0.01$ with assumptions that $A = \epsilon a$ and $B = \epsilon^{\alpha/3} b$, $\alpha = 1$ with period $L = \pm 10$, $L = \pm 15$ and $L = \pm 20$ respectively.

In each of the panels in Figure 3.4.5, the amplitudes of u remain small when compared to v in the regions in which the self-replicating process takes place. Panel (a) stable multiple pulse solution with concentrations v (black) and u (dotted-line) at $t = 1000$, $\epsilon = 0.001$, $N = 300$ and period $L = 400$. Panels (b) the eleven-pulse solution, $\epsilon = 0.01$, $t = 100$ for $N = 140$, $L = 400$ and (c) is a stable eight-pulse solution obtained at $\epsilon = 0.001$, $t = 1000$, $L = 400$ and $N = 100$. (d) is also a nine-pulse solution that is stable with parameters $\epsilon = 0.001$, $t = 1000$, $L = 300$ with $N = 100$. Panels (e) and (f) are unstable seven-and three-pulse solutions obtained when period $L = 100$

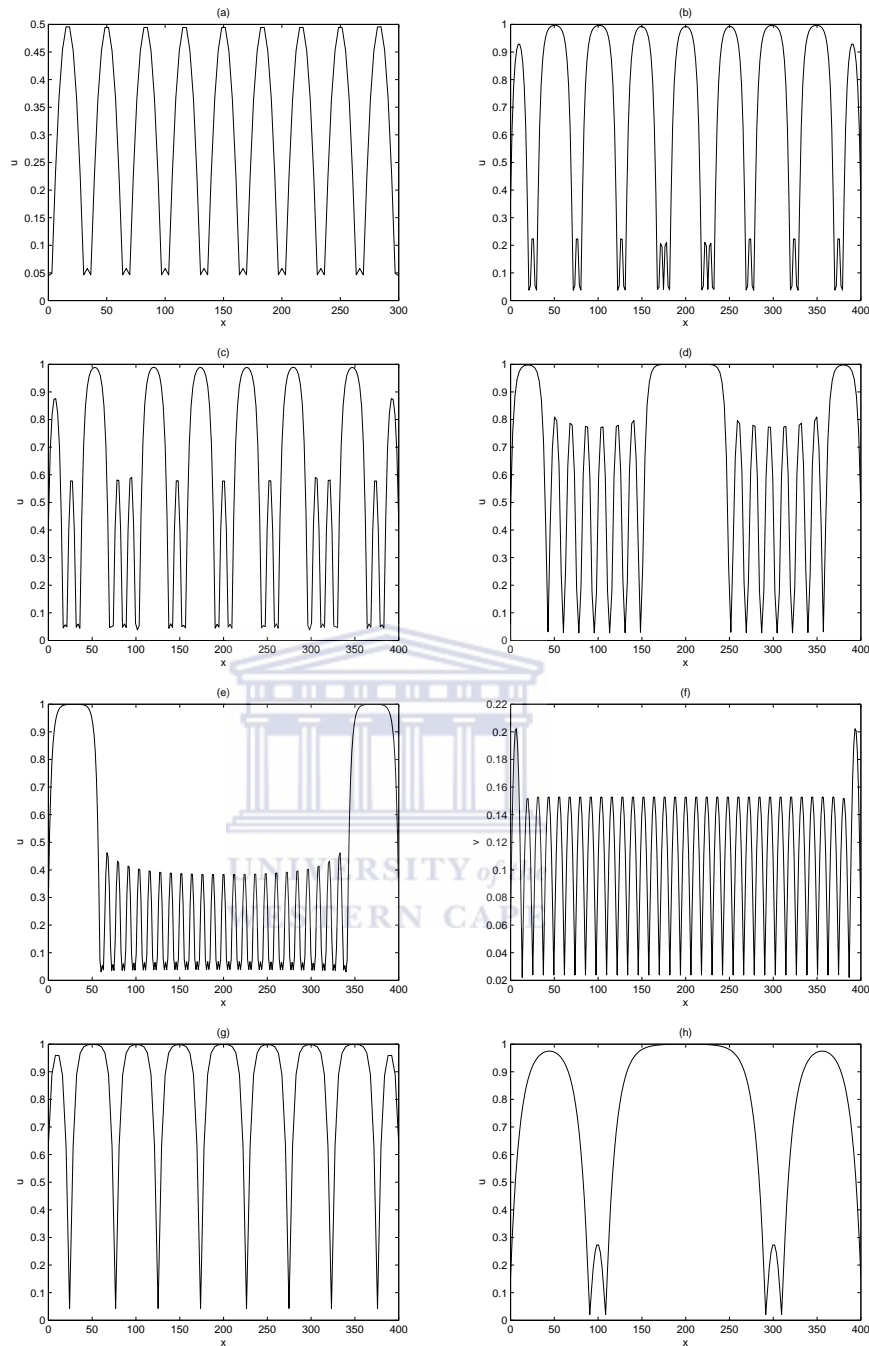


Figure 3.4.4: Spatially periodic stationary solutions of (3.4.1) observed basically in the positive quadrant. Numerical simulations are obtained with $A = \epsilon a$, $B = \epsilon^{1/\alpha} b$; where $a = 9$, $b = 0.4$ and $\alpha = 1$.

at a rescaled values $A = 0.021$, $B = 0.069$, $t = 1000$ and $a = 2$, $b = 0.4$, $\epsilon = 0.001$, $t = 500$ respectively. It was further observed that stationary splitting occurs but, v does not become exponentially small and u remains small in that region, see [42, 43]

for details.

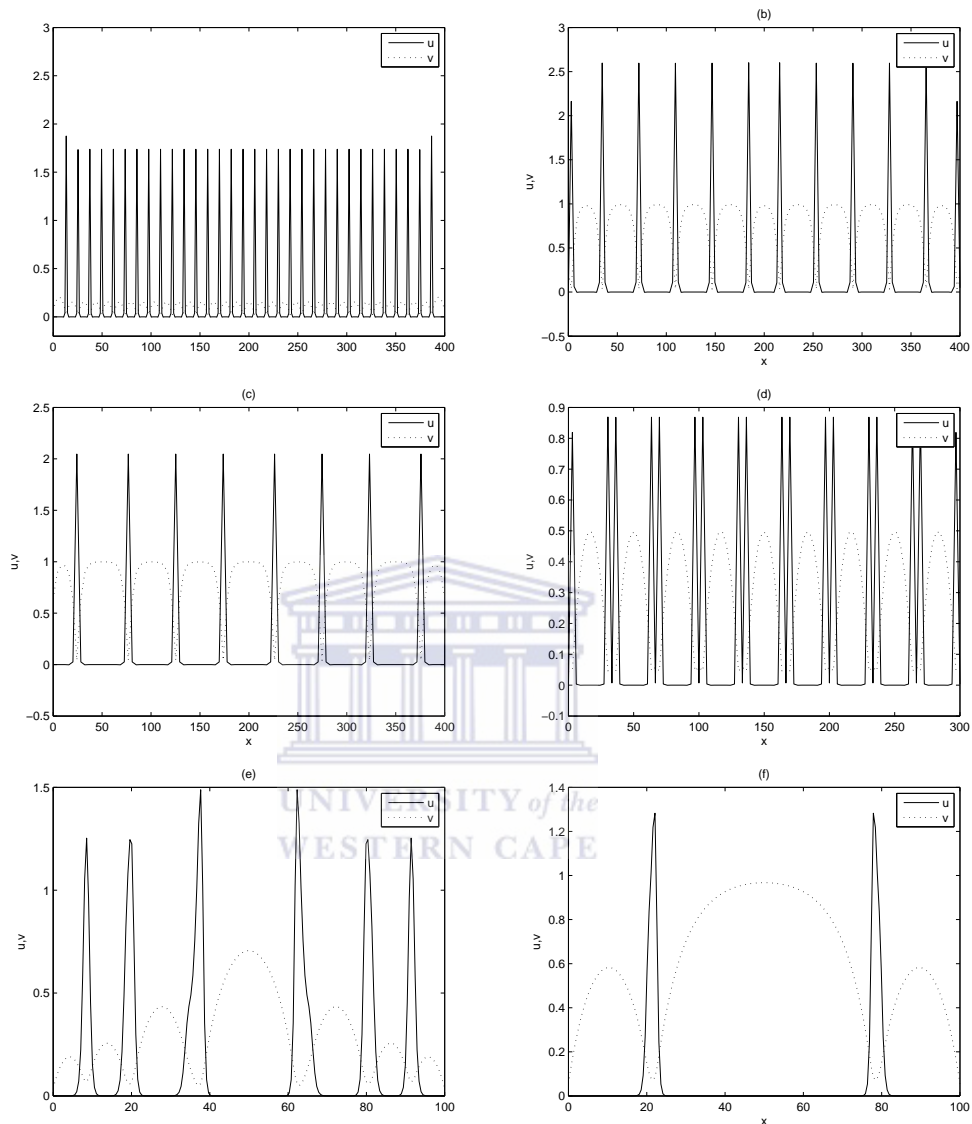


Figure 3.4.5: The dynamic of multiple pulse-splitting process, spatially periodic stationary states of (3.4.1) obtained with $a = 9$, $b = 0.4$, $A = \epsilon a$, $B = \epsilon^{\alpha/3} b$, $\alpha = 1$.

Autocatalytic equation:

Our interest here is on the oscillatory fronts dynamics of some particular autocatalytic reaction-diffusion equations which have some similarities with systems used in combustion theory. Specific example here is a non-dimensional coupled system of autocatalytic

reaction equations involving two diffusing chemical species in one spatial dimension

$$\left. \begin{aligned} \frac{\partial u}{\partial t} &= \frac{\partial^2 u}{\partial x^2} + v f(u), \\ \frac{\partial v}{\partial t} &= \epsilon \frac{\partial^2 v}{\partial x^2} - v f(u), \end{aligned} \right\} \quad (3.4.4)$$

with

$$f(u) = \begin{cases} u^m, & u \geq 0 \\ 0, & u < 0 \end{cases}, \quad (3.4.5)$$

and ϵ is given as the inverse of the Lewis number (that is, the ratio of diffusion rates). As mentioned in [125] and later suggested by Balmforth et al. [15], the advancing fronts of the autocatalysis, $u(x, t)$, lose its stability and begin to eat into reactant, $v(x, t)$. It was opined in their numerical results that reaction terms are of the form $\pm u^m$, where m is regarded as the largest possible orders for $u(x, t)$ and $v(x, t)$ respectively. The simulations of equations (3.4.4) is sought for $\epsilon > 0$, in the range $0 < \epsilon < 1$ with $m \geq 2$.

Moving coordinate frame, $\xi = x - ct$, is introduced in [15] to compute steadily propagating fronts equilibria by setting $u(x, t) = U(\xi)$ and $v(x, t) = V(\xi)$ in (3.4.4)

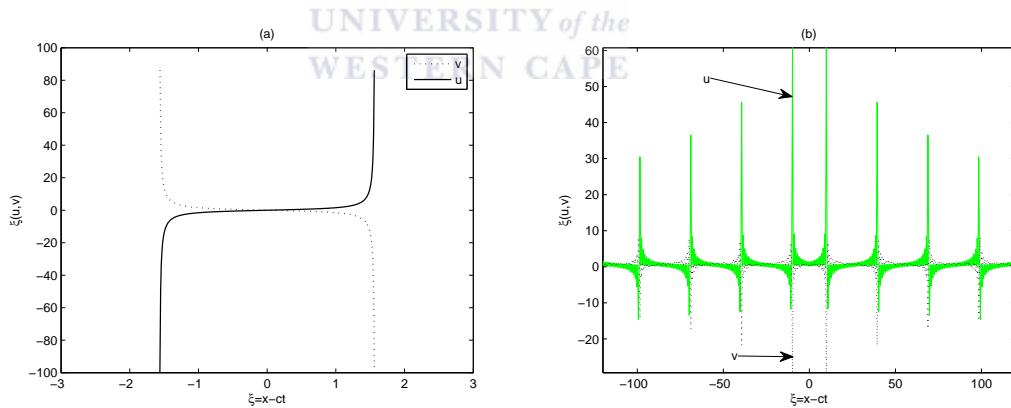


Figure 3.4.6: Front solutions showing amplitudes of u and v at $\epsilon = 0.1$. In panels (a) and (b): The solid curves show $U(\xi) = U(x - ct)$ and the dotted curves show $V(\xi) = V(x - ct)$ at different time.

In Figure 3.4.6 (a), we consider the only case where the travelling speed $c > 0$, for $\xi = x - ct$ as $\xi \rightarrow \infty$ since it is unrealistic to have a negative speed. At the neighborhood of the origin, where ξ is very close to zero ($\xi \rightarrow 0$), both $U(x - ct)$ and $V(x - ct)$ repelled one another as shown in panel (b) of figure 3.4.6, the two turnings fronts are at equilibrium. An unstable eigenfunction for $\epsilon = 0.1$ and $m = 9$ is shown

in Figure 3.4.7.

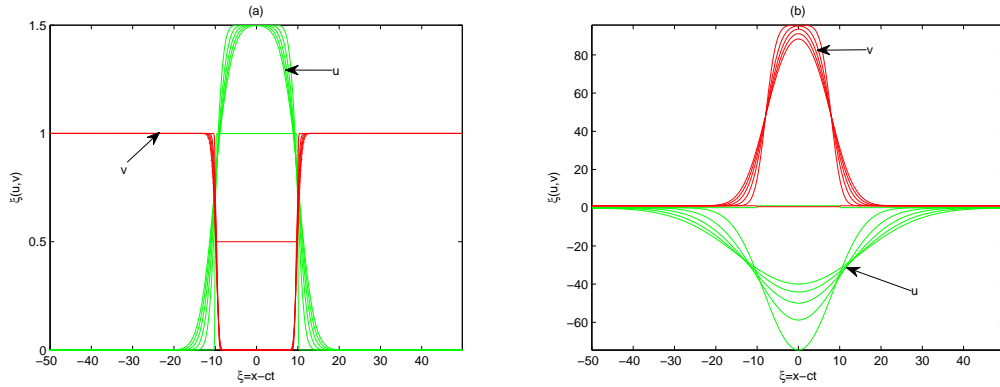


Figure 3.4.7: Contour plots showing an unstable eigenfunction of the perturbation $\xi(u, v)$ for $\epsilon = 0.1$, $m = 9$ and the eigenvalue $\lambda = (0.01, 0.2)$.

When eigenvalue is becoming large say, $\lambda \geq 0.1$, the system becomes very unstable, clearly the travelling fronts behaviour is chaotic. We further our study by following conditions initiated in [15, 37]:

$$\left. \begin{aligned} u(x, t = 0) &= \frac{1}{2} (1 + \tanh(10(10 - |x|))), \\ v(x, t = 0) &= 1 - \frac{1}{4} (1 + \tanh(10(10 - |x|))). \end{aligned} \right\} \quad (3.4.6)$$

Equation (3.4.4) is solved on an infinite domain that was used for the construction of the travelling fronts. This is achieved by applying conditions, $u(x, t) \rightarrow 1$, $v(x, t) \rightarrow 0$, as $x \rightarrow -\infty$ and $u(x, t) \rightarrow 0$, $v(x, t) \rightarrow 1$, as $x \rightarrow \infty$, we replace the infinite domain by a long finite domain and impose the left- and right-hand boundary conditions at $x = \pm L$. We present numerical simulations of equations (3.4.4), subject to initial conditions (3.4.6) for the reaction order, $m \geq 2$ and $\epsilon < 1$.

A close observation of the results obtained in Figure 3.4.8: (a) and (b) have granted a deep understanding to the behaviours of the chemical species whenever ϵ and m are slightly altered in the domain of length L . This assertion is evident in panels (c) and (d) at parameter values $m = 9$, $\epsilon = 0$ while panels (a), (b), (e) and (f) are obtained with parameter values $\epsilon = 0.1$, $m = 9$ on different domain sizes. Clearly, $(u(x, t))$ enjoys complete dominance over $(v(x, t))$ throughout the entire localized domain. The

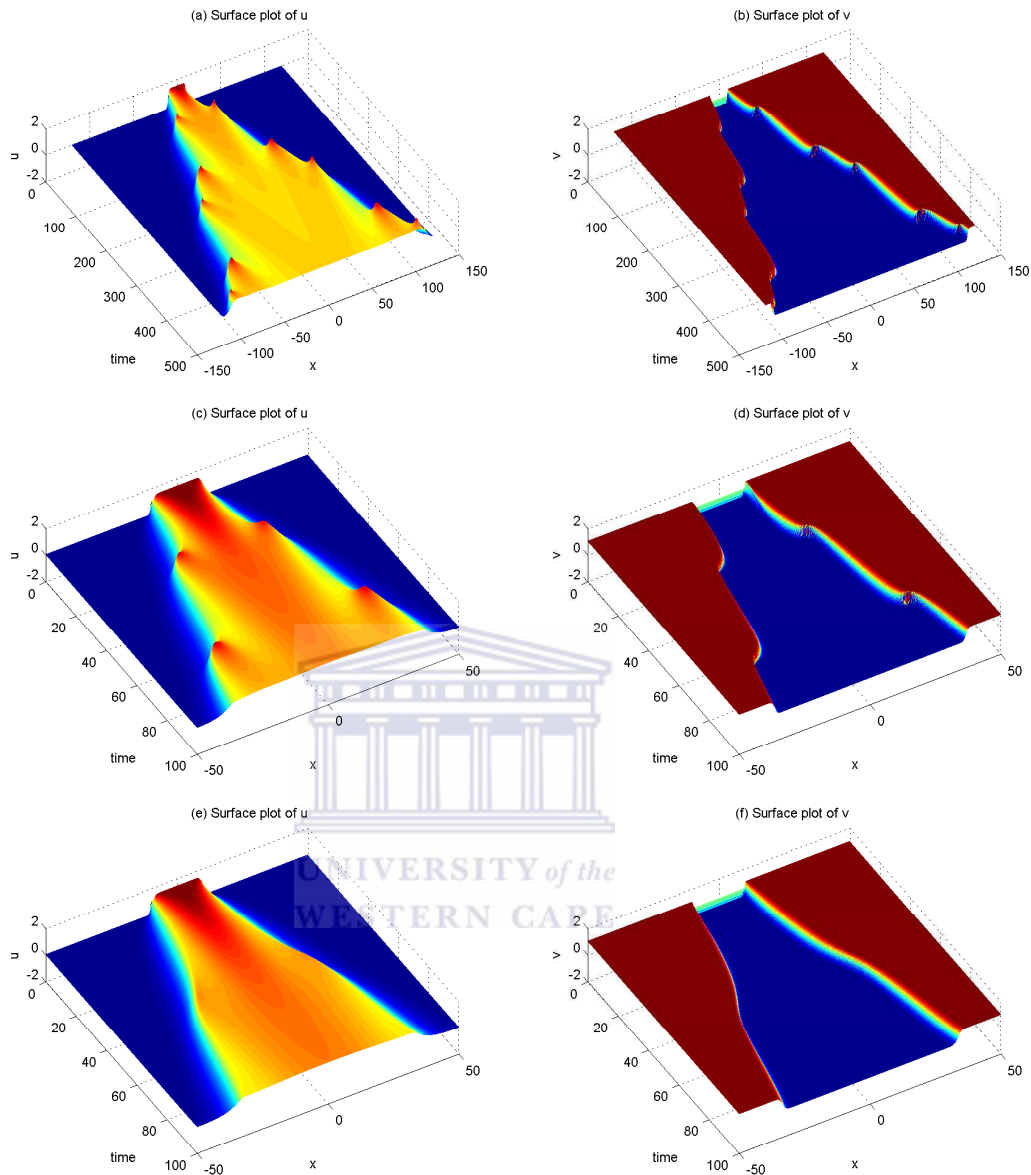


Figure 3.4.8: Results for the autocatalytic model (3.4.4) with $\epsilon = 0.1$, $m = 9$ at $t = 500$ in panels (a, b) and $m = 9$, $\epsilon = 0$ at time $t = 100$ in panels (c) and (d) for the chemical species u and v . Panels (e) and (f) represent respective surface plots that illustrate the extent at which autocatalytic specie $u(x, t)$ eats into the reactant $v(x, t)$. The parameters chosen here are $\epsilon = 0.1$, $m = 9$ at time $t = 100$.

catalyst and reactant mentioned here could be interpreted to the standard of predator-prey system which was developed to give detail understanding of the mechanism of Turing instability.

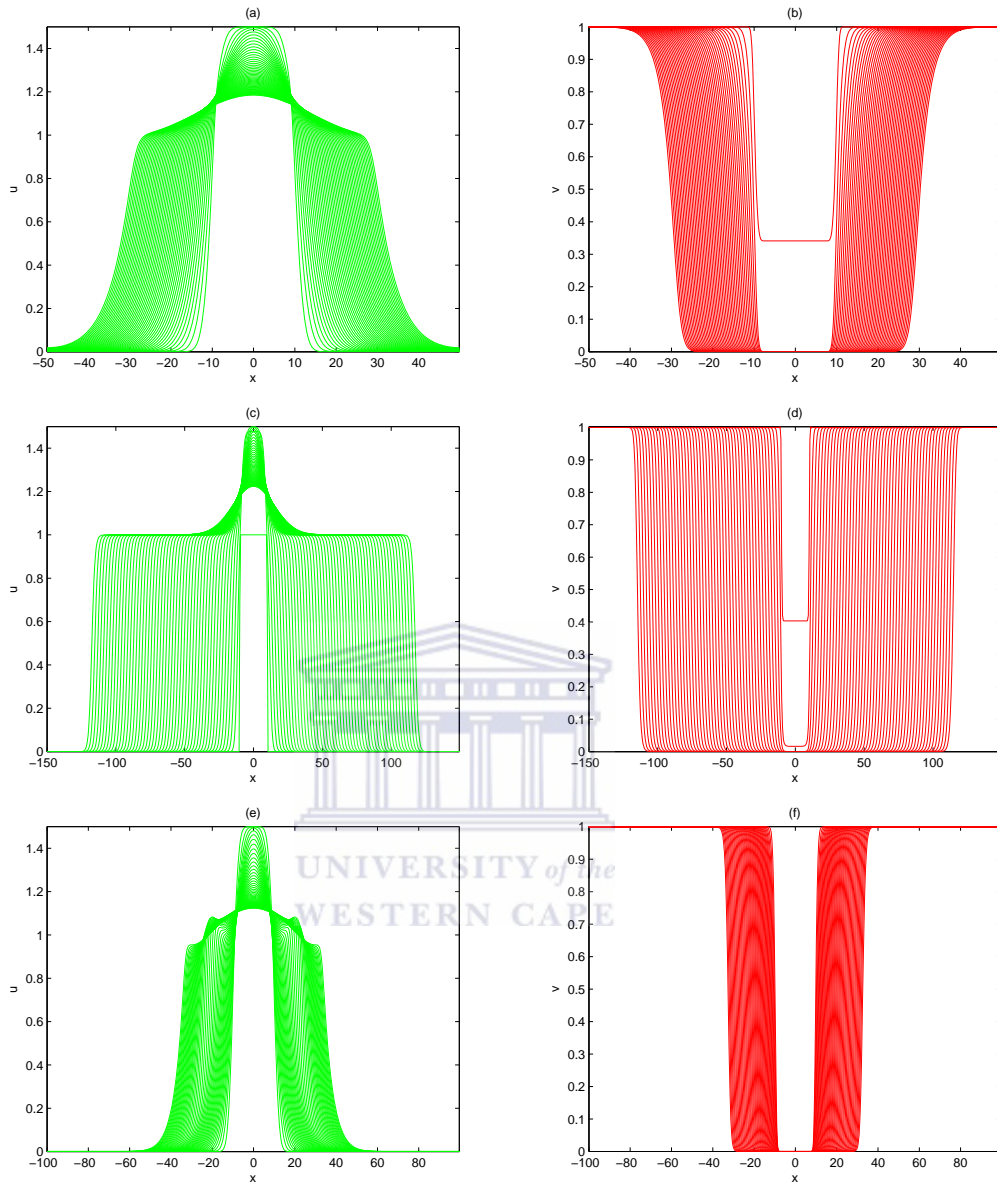


Figure 3.4.9: Contour plots (3.4.4) indicating the spatial behavior of the travelling fronts of the two species. The parameter values are: For panels (a) and (b): $\epsilon = 0.5$, $m = 9$, $L = 50$. Panel (c) and (d): $\epsilon = 0.01$, $m = 9$, $L = 150$; for (e): $\epsilon = 0.1$, $m = 9$, $L = 100$, and for (f): $\epsilon = 0.2$, $m = 9$, $L = 100$.

Gierer-Meinhardt equations:

We finally consider here the Gierer-Meinhardt reaction kinetics that represents a phenomenological model as suggested by Gierer and Meinhardt [60], the term containing the reaction kinetics are stated in such a way that one of the two (chemicals) species named activator, activates the production of the other specie called the inhibitor which,

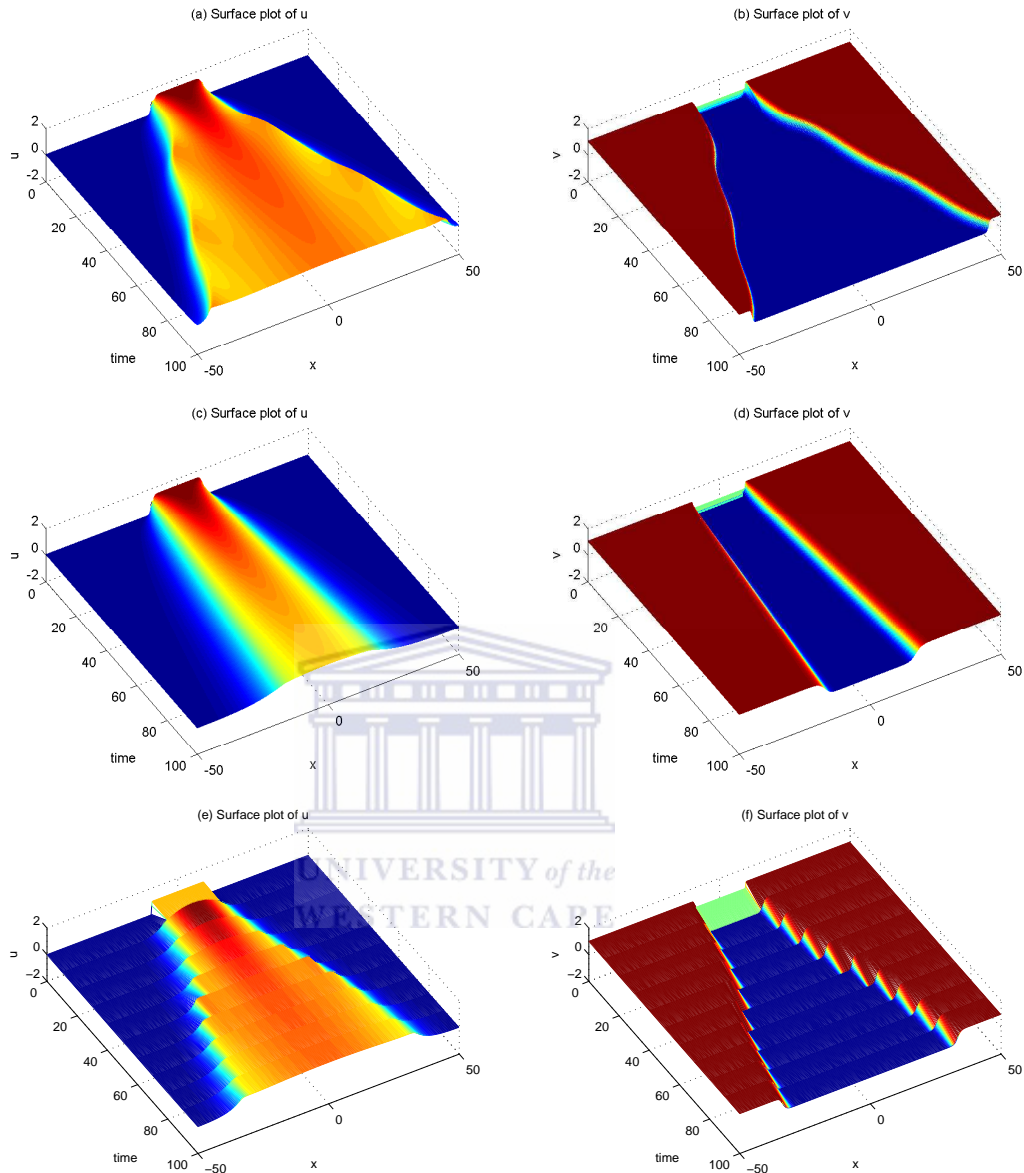


Figure 3.4.10: Panels (a) and (b): Show typical result of autocatalytic model (3.4.4), at $t = 100$, $\epsilon = 0$ and $m = 7.649$. In (c, d), clearly, the rate at which $u(x, t)$ gains dominance over $v(x, t)$ has been reduced for choosing the parameters $m = 13$, $\epsilon = 0.5$. Panels (c) and (d) describe how u eats into v for $m = 9$, $\epsilon = 0.001$.

in turn, slows down the production rate of the activator on the bounded spatial one-dimensional space $\pm L$. Activator-inhibitor systems have been studied extensively in the mathematical theory of biological pattern formation [123, 124]. Among them is the Gierer-Meinhardt system that falls within the frame work of a theory proposed by Turing [189], and since has been the object of extensive mathematical treatment in the

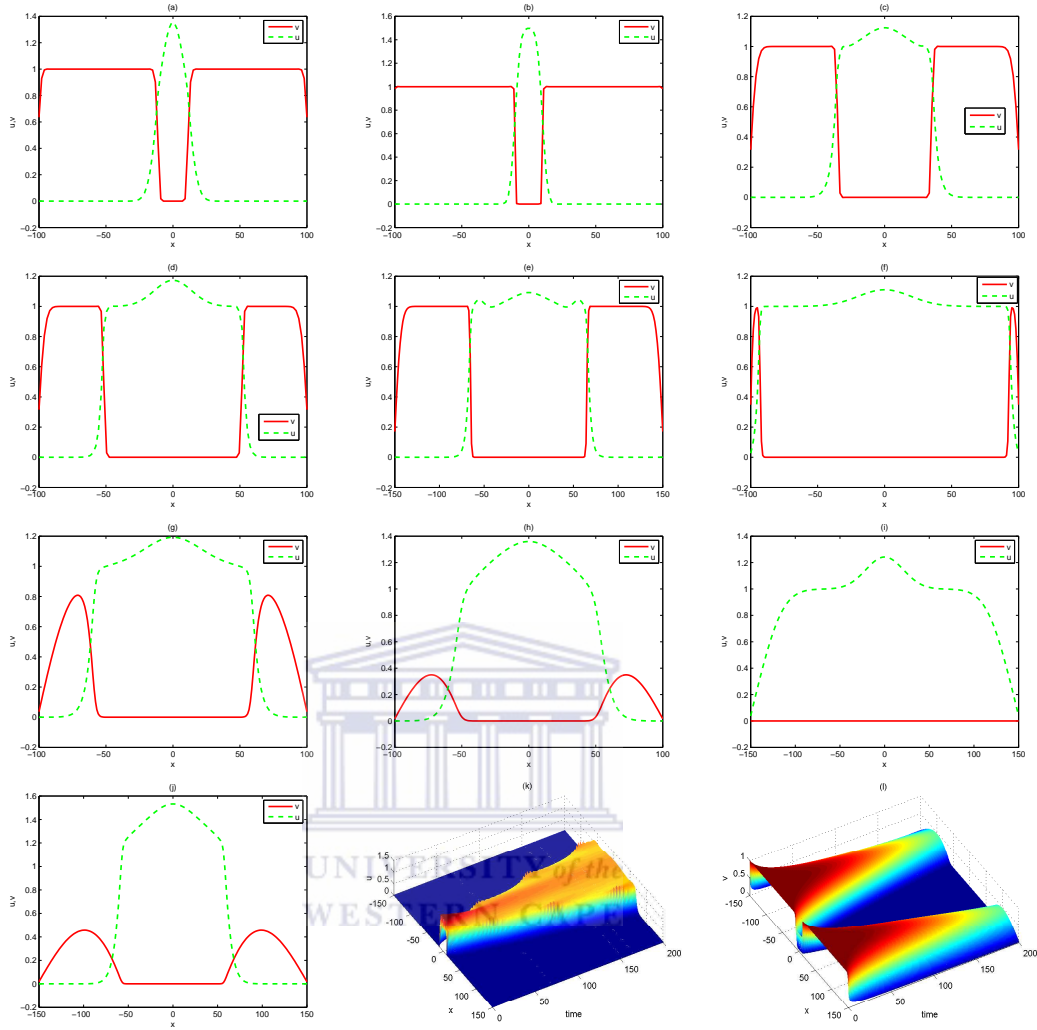


Figure 3.4.11: Plots indicating the behavioural patterns of the two species u and v in equation (3.4.4) during the process of their interactions in space. Different parameter values of $m > 0$ and $\epsilon > 0$ are used in a specified domain $-L \leq x \leq L$.

past few decades.

$$\left. \begin{aligned} \frac{\partial u}{\partial t} &= d_u \nabla_u + f(u, v), \\ \frac{\partial v}{\partial t} &= d_v \nabla_v + g(u, v), \end{aligned} \right\} \quad (3.4.7)$$

where d_u and d_v are diffusion constants of activator and inhibitor of the chemicals u and v respectively, ∇ is the laplace operator with $u, v : \mathbb{R} \times \mathbb{R} \rightarrow \mathbb{R}$, and $0 < d_u, d_v \ll 1$. The nonlinear reaction terms $f, g : \mathbb{R}^2 \rightarrow \mathbb{R}$ are assumed and expected to satisfy $f(\hat{u}, \hat{v})=g(\hat{u}, \hat{v})=0$ for certain (\hat{u}, \hat{v}) , such that trivial background state $(u, v) \equiv f(\hat{u}, \hat{v})$

is stable.

We first investigate the homoclinic stripe patterns in one-dimensional Gierer-Meinhardt equation

$$\left. \begin{aligned} \epsilon^2 u_t &= u_{xx} - \epsilon^2 \mu u + u^{\alpha_1} v^{\beta_1}, \\ v_t &= \epsilon^2 v_{xx} - v + u^{\alpha_2} v^{\beta_2}, \end{aligned} \right\} \quad (3.4.8)$$

where $-L \leq x \leq L$ for some fixed L . The boundary conditions are taken as

$$u(x = -L, t) = u(x = L, t) = 0, \quad (3.4.9)$$

with analogous relation for the chemical specie v . The initial conditions (3.4.2), are taken with some parameter perturbations. Letting $u = u(x, t)$ and $v = v(x, t)$ denote the concentrations of the two species u and v , the special case $\alpha_1 = 0$, $\alpha_2 = -1$, $\beta_1 = 2$ and $\beta_2 = 2$.

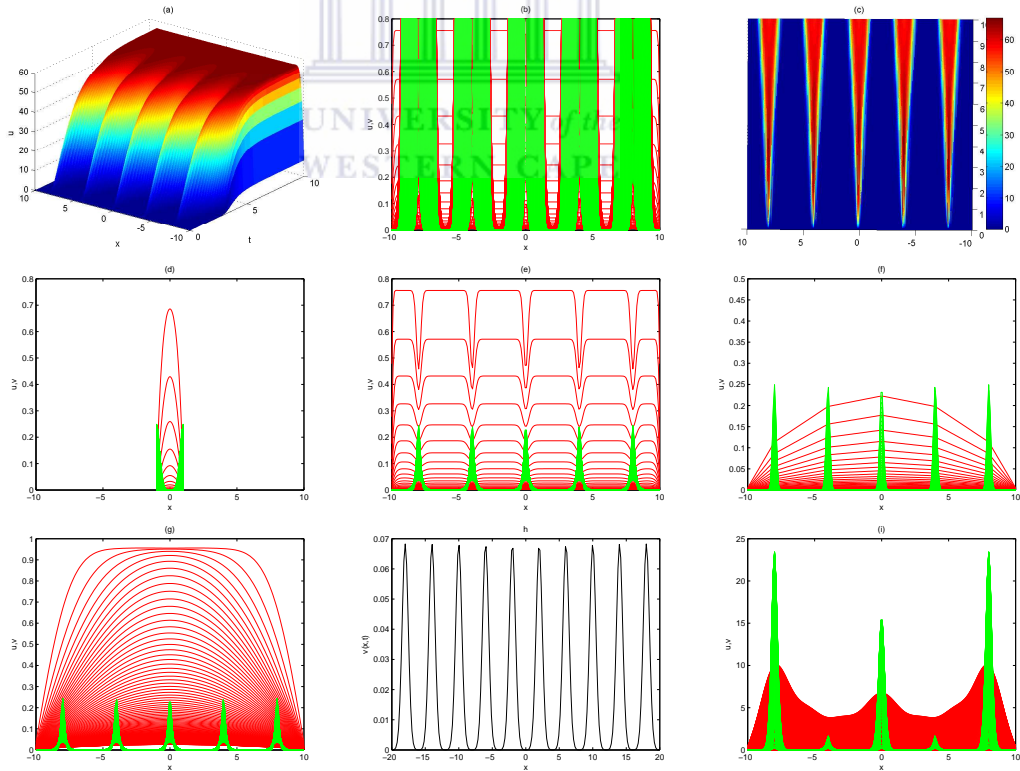


Figure 3.4.12: Results for Gierer-Meinhardt equation (3.4.8) at various parameter values.

The results presented here in Figure 3.4.12 establish the existence of homoclinic

stripe patterns in (3.4.8) where we vary the half domain length L . This decision is taken to replicate some figures in literature. Notably, the simulations differ as the boundary conditions here at $\pm L$ are periodic and eventually a steady spatially periodic state emerges. Parameter values are: (a) $\alpha_1 = 0, \alpha_2 = -1, \beta_1 = \beta_2 = 2, \epsilon^2 = 0.05, \mu = 56, L = 10, T = 10$; (b) $\alpha_1 = 0, \alpha_2 = -1, \beta_1 = \beta_2 = 2, \epsilon^2 = 0.01, \mu = 56, L = 10, T = 10$; (c) parameter values are the same as in (b); (d) $\alpha_1 = 0, \alpha_2 = -1, \beta_1 = \beta_2 = 2, \epsilon^2 = 0.01, \mu = 56, L = 1, T = 0.5$; (e) $\alpha_1 = -1, \alpha_2 = 0, \beta_1 = \beta_2 = 2, \epsilon^2 = 0.01, \mu = 56, L = 10, T = 1$; (f) $\alpha_1 = -1, \alpha_2 = 0, \beta_1 = \beta_2 = 2, \epsilon^2 = 0.001, \mu = 1, L = 10, T = 10$; (g) $\alpha_1 = 0, \alpha_2 = -1, \beta_1 = \beta_2 = 2, \epsilon^2 = 0.05, \mu = 56, L = 10, T = 1$; (h) $\alpha_1 = 0, \alpha_2 = -1, \beta_1 = \beta_2 = 2, \epsilon^2 = 20, \mu = 56, L = 20, T = 20$ and panel (i) at $\alpha_1 = 0, \alpha_2 = -1, \beta_1 = \beta_2 = 2, \epsilon^2 = 0.05, \mu = 56, L = 10, T = 2$.

We further the experiment with four important cases taken across literature:

Case I: We consider, a non-dimensionalized form of equation (3.4.7) given by

$$\left. \begin{aligned} \frac{\partial u}{\partial t} &= d_u \nabla_u^2 + \tau \left[\alpha - \beta u + \frac{u^2}{v(1+\kappa u^2)} \right], \\ \frac{\partial v}{\partial t} &= d_v \nabla_v^2 + \tau(u^2 - v), \end{aligned} \right\} \quad (3.4.10)$$

where $u(x, t)$ describes the concentration of the activator, $v(x, t)$ the inhibitor concentration, t is the time and ∇^2 remains the laplace operator defined in one-dimension. Parameters α, β, τ, d_u and d_v are all positive and κ determines the rate of concentration. From the biological point of view, the term $\frac{u^2}{v(1+\kappa u^2)}$ is described to imply the autocatalysis in u with saturation at high concentration values of u , and inhibition of u through the production of v , meaning that u is produced at a constant rate $\tau\alpha$ and is degraded linearly at rate $\tau\beta$.

Figure 3.4.13 shows the interactions between species u and v for case I of the Gierer-Meinhardt kinetics (3.4.10). The parameters used are: (a) $\alpha = 0.35, \beta = 0.065, \kappa = 2, \tau = 0.1, d_u = d_v = 0.1$; (b) $\alpha = 0.035, \beta = 0.065, \kappa = 2, \tau = 0.01, d_u = d_v = 0.01$; (c) $\alpha = 0.35, \beta = 0.065, \kappa = 1, \tau = 0.1, d_u = d_v = 0.01$; (d) $\alpha = 0.035, \beta = 0.065, \kappa = 8, \tau = 0.1, d_u = d_v = 0.1$; (e) and (f) $\alpha = 0.035, \beta = 0.065, \kappa = 2, \tau = 0.1, d_u = d_v = 1$.

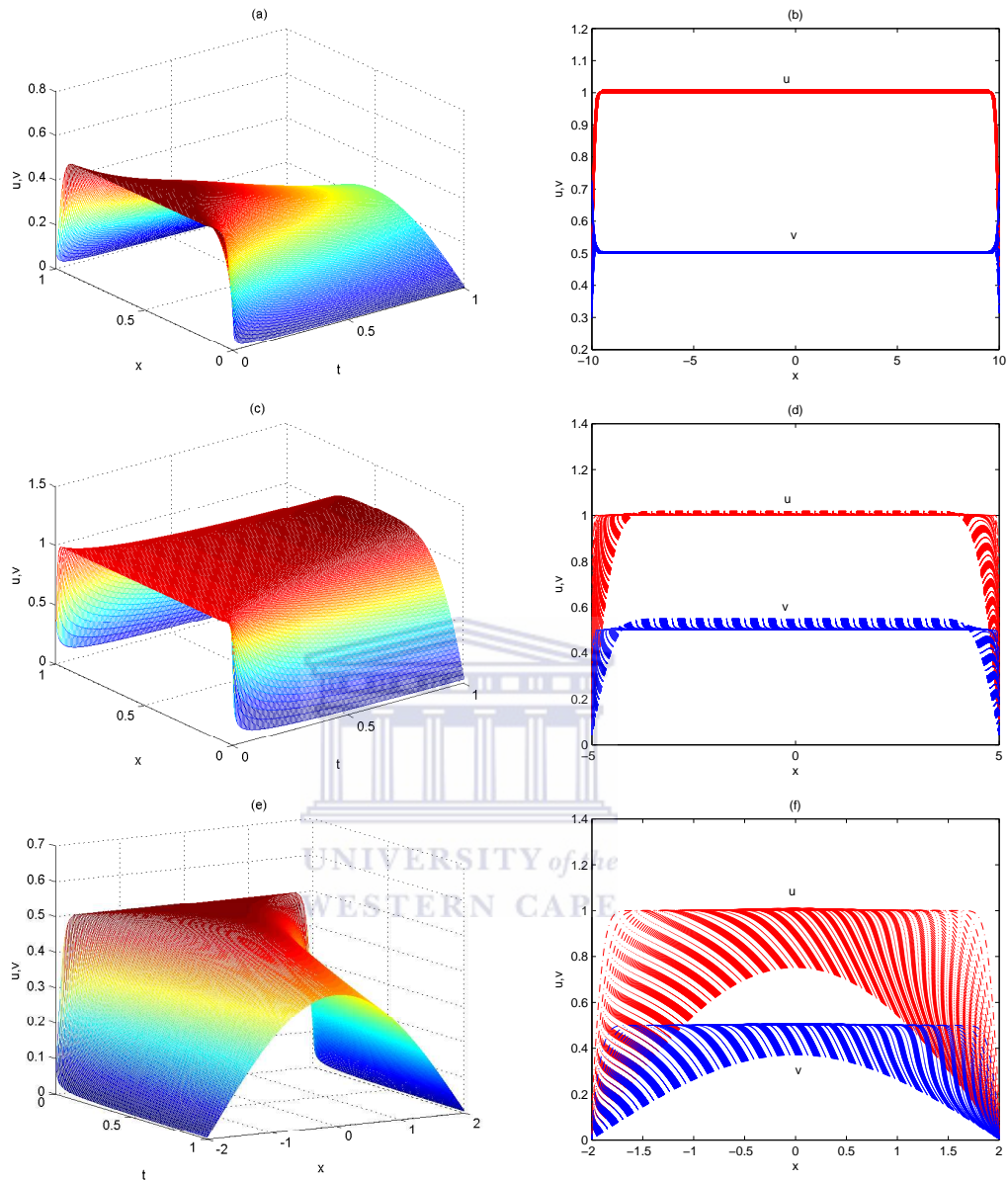


Figure 3.4.13: Concentration profiles for *Case I* of the Gierer-Meinhardt reaction kinetics (3.4.10) describing the interaction between the activator $u(x, t)$ and inhibitor $v(x, t)$.

Case II: We consider, in another form the Gierer-Meinhardt system

$$\left. \begin{aligned} u_t &= \epsilon^2 u_{xx} - u + \frac{u^p}{v^q} && \in \Omega, \\ v_t &= D v_{xx} - v + \frac{u^m}{v^s} && \in \Omega, \end{aligned} \right\} \quad (3.4.11)$$

where the exponents (p, q, m, s) satisfy the conditions

$$p > 1, \quad q > 0, \quad m > 1, \quad s \geq 0, \quad \frac{qm}{(p-1)(1+s)} > 1, \quad (3.4.12)$$

ϵ and D are also positive parameters defined in $\Omega = \mathbb{R}^2$. Problem (3.4.11) have been shown to exhibit single or multiple bump solutions in one-two dimensions [40, 45].

The parameters used in Figure 3.4.14 for the case II of the Gierer-Meinhardt (3.4.11) are: (a) $(p, q, m, s) = (2, 1, 2, 0)$, $T = 5$, $\epsilon = 0.02$, $D = 0.1$; (b) $(p, q, m, s) = (2, 1, 2, 1)$, $T = 2$, $\epsilon = 0.01$, $D = 0.01$; (c) $(p, q, m, s) = (2, 1, 2, 0)$, $T = 5$, $\epsilon = 0.01$, $D = 0.1$; (d) $(p, q, m, s) = (2, 1, 2, 1)$, $T = 1$, $\epsilon = 0.01$, $D = 1$; (e) $(p, q, m, s) = (2, 1, 2, 2)$, $T = 0.5$, $\epsilon = 0.01$, $D = 0.1$; (f) $(p, q, m, s) = (2, 1, 2, 0)$, $T = 1$, $\epsilon = 0.01$, $D = 0.1$ on the interval $\pm L$ and $N = 200$. Note the variation in amplitudes with respect to space and final time T .

Case III: We consider the classical Gierer-Meinhardt equation

$$\left. \begin{aligned} u_t &= u_{xx} - \alpha u + \delta v^2 \\ v_t &= \epsilon v_{xx} - v + \frac{v^2}{u}, \end{aligned} \right\} \quad (3.4.13)$$

in which $\alpha > 0$ is the main bifurcation parameter and $\delta > 0$ is most often scaled to 1. The model in case III differs from the one earlier considered in case II in the sense of some parameters.

In Figure 3.4.15, the parameters used are: (a) solution of u with $\alpha = 0.2$, $\delta = 0.1$, $\epsilon = 0.002$ final time $T = 5$ on $L = \pm 10$; (b) $\alpha = 0.2$, $\delta = 0.1$, $\epsilon = 0.002$ final time $T = 10$ on $L = \pm 5$; (c) $\alpha = 0.2$, $\delta = 2$, $\epsilon = 0.002$ final time $T = 5$ on $L = \pm 4$; (d) $\alpha = 0.2$, $\delta = 0.1$, $\epsilon = 0.002$ final time $T = 2$ on $L = \pm 5$; (e) is the solution of v obtained with the same parameters as in (a); (f) solution of u with the same parameters as in (d); (g) $\alpha = 0.02$, $\delta = 2$, $\epsilon = 0.002$ final time $T = 5$ on $L = \pm 1$; (h) $\alpha = 0.2$, $\delta = 0.01$, $\epsilon = 0.002$ final time $T = 1$ on $L = \pm 10$ and (i) parameters are same as in (h) except that the final time is $T = 5$.

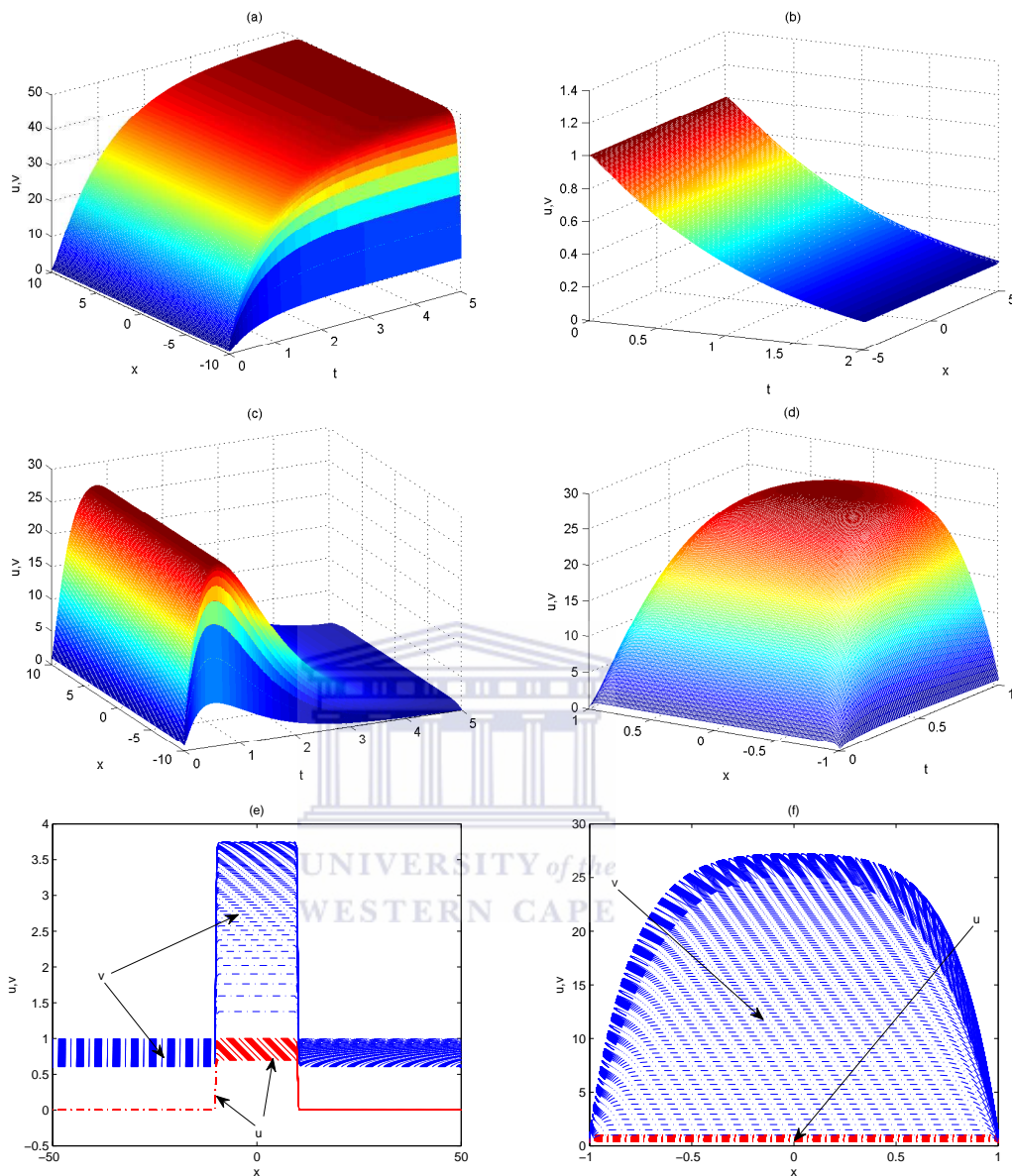


Figure 3.4.14: Concentration profiles for *Case II* of the Gierer-Meinhardt (3.4.11) reaction kinetics describing the interaction between the activator $u(x, t)$ and inhibitor $v(x, t)$.

Case IV: Here, study the Gierer-Meinhardt equation (3.4.13) for slowly nonlinearized version, we scale u and v as well as x and ϵ in the form

$$u \rightarrow \frac{u}{\epsilon}, \quad v \rightarrow \frac{v}{\epsilon}, \quad x \rightarrow \sqrt{\epsilon}x, \quad \epsilon \rightarrow \epsilon^2, \quad (3.4.14)$$

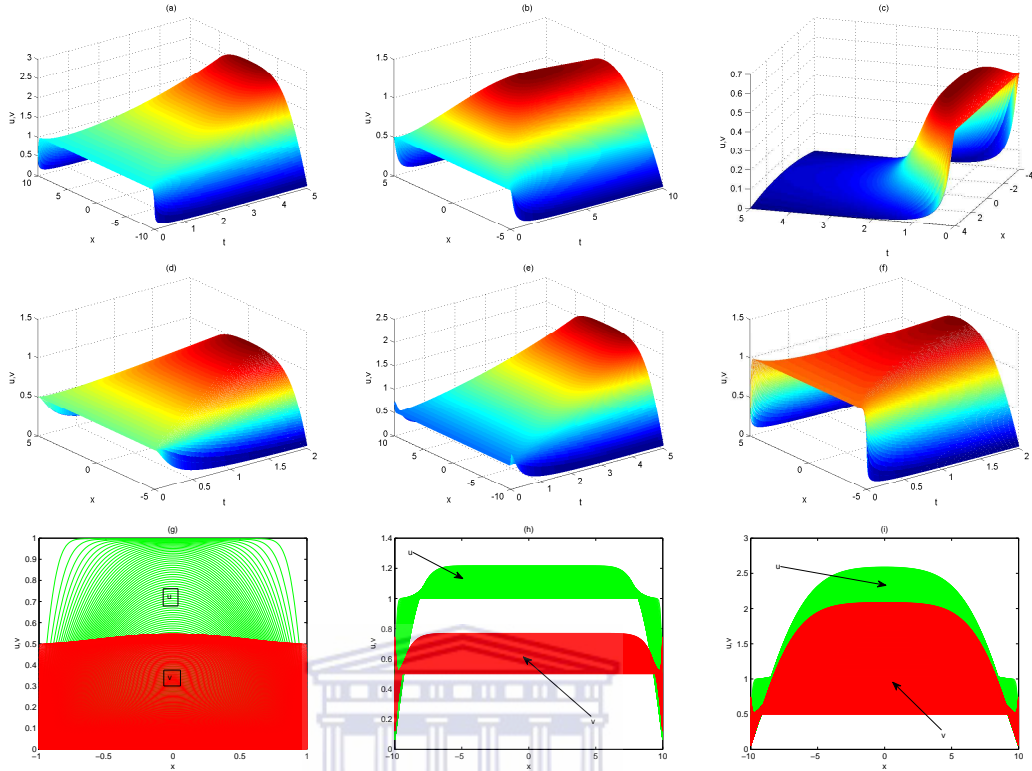


Figure 3.4.15: Solution for *Case III* of the Gierer-Meinhardt equation (3.4.13) indicating reaction kinetics between two competing species with concentrations $u(x,t)$ as the activator and $v(x,t)$ that stands for the inhibitor.

to obtain

$$\left. \begin{aligned} \epsilon^2 u_t &= u_{xx} - \epsilon^2 \alpha u + \delta v^2, \\ v_t &= \epsilon v_{xx} - v + \frac{v^2}{u}, \end{aligned} \right\} \quad (3.4.15)$$

which is in normal form of (3.4.13). We present the slowly nonlinearized form by adding a very simple term to its slow u -equation in (3.4.15) to yield

$$\left. \begin{aligned} \epsilon^2 u_t &= u_{xx} - \epsilon^2 (\alpha u - \beta u^d) + \delta v^2, \\ v_t &= \epsilon v_{xx} - v + \frac{v^2}{u}, \end{aligned} \right\} \quad (3.4.16)$$

with parameters $\beta \geq 0$, $d > 1$, $\epsilon > 0$ and $\delta \in \mathbb{R}$. Readers are referred to [110, 195] for further analysis.

The parameters used for case IV of the Gierer-Meinhardt equation (3.4.16) are: (a) u at $\alpha = 90.6$, $\beta = 30$, $\delta = 5$, $d = 5$, $\epsilon = 1$, $L = 10$ and $T = 0.01$; (b) $\alpha = 90.6$, $\beta = 30$, $\delta = 5$, $d = 5$, $\epsilon = 1$, $L = 0.5\epsilon^{-1}$ and $T = 10$; (c) $\alpha = 90.6$,

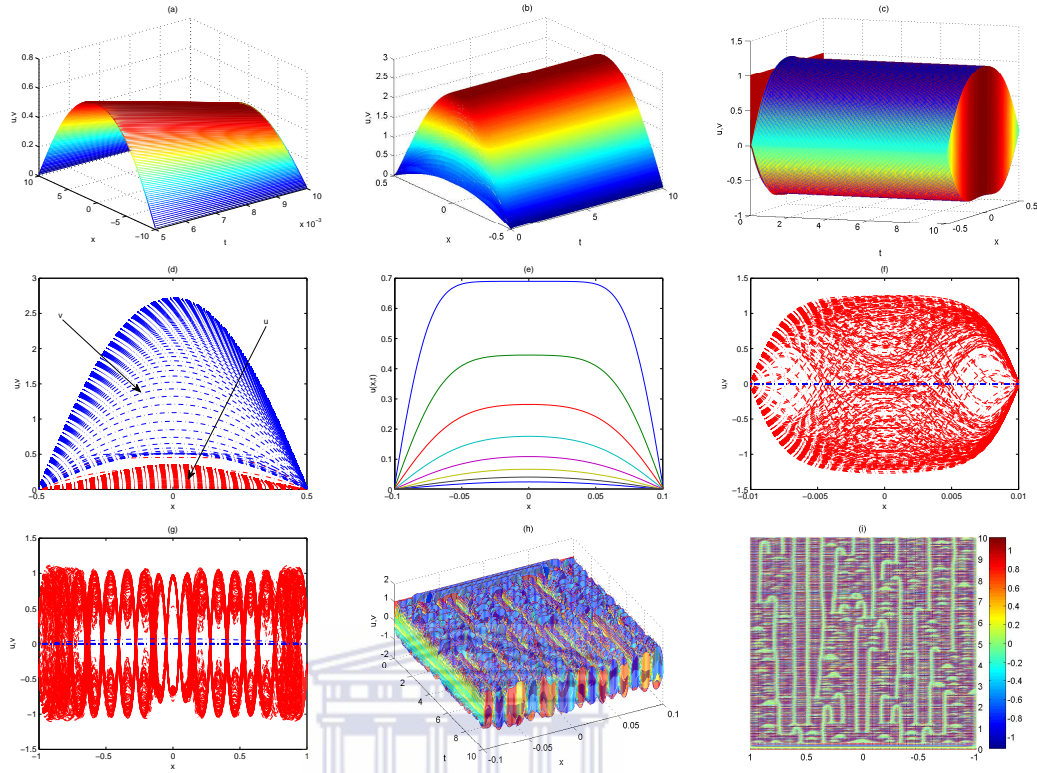


Figure 3.4.16: Solution of Gierer-Meinhardt equation (3.4.16) for *Case IV* that describes the effect of slowly and mild nonlinear term introduced to the reaction kinetics between two competing chemicals with concentrations $u(x, t)$ as the activator and $v(x, t)$ that stands for the inhibitor.

$\beta = 60$, $\delta = 5$, $d = 5$, $\epsilon = 1$, $L = 0.5\epsilon^{-1}$ and $T = 10$; (d) solution showing the concentration of both species in phase with parameters $\alpha = 90.6$, $\beta = 30$, $\delta = 5$, $d = 5$, $\epsilon = 1$, $L = 0.5\epsilon^{-1}$ and $T = 10$; (e) plot of u at $\alpha = 90.6$, $\beta = 30$, $\delta = 5$, $d = 5$, $\epsilon = 5$, $L = 0.1$ and $T = 20$; (f) plot $u, v(x, t)$ at $x \in [-\epsilon^{-1}, \epsilon^{-1}]$ $\alpha = 90.6$, $\delta = 2$, $\epsilon = 200$, $\beta = 5$, $d = 5$ final time $T = 20$ on $L = 0.01$; (g) ring-like solution of $u, v(x, t)$ at $x \in [-10\epsilon^{-1}, 10\epsilon^{-1}]$ $\alpha = 90.6$, $\delta = 2$, $\epsilon = 200$, $\beta = 5$, $d = 5$ final time $T = 10$ on $L = 0.01$; (h) surface plot using the same parameters as in (g); (i) the dynamics of the maximum of the u -pulse as a function of time in a simulation, traces of some long standing stripes are noticeable with $\alpha = 90.6$, $\beta = 5$, $\delta = 2$, $d = 5$, $\epsilon = 10$ on interval $L = 10\epsilon^{-1}$ at final time $T = 10$.

We solve the problems with higher order finite difference discretization in space and ETDRK4 as a time-stepping method. Variations in accuracy depend on the na-

ture of the particular problem solved due to some complexities in the behavior of the equations, most of these problems exhibit chaotic solutions. The convergence of the three methods (ETDRK4, ABM4 and RK4) are examined by considering the Gray-Scott, Autocatalysis and Gierer-Meinhardt equations. Since analytical solutions for these equations are not available, we design a reference solution which we referred to as our exact solution (\hat{U}_j) by using an extremely fine discretization (say, $\Delta t = 1/2000$), a much finer than that used for the actual computation. Error measure estimate in the component U is defined as

$$\text{Relative Error} = \frac{\max |\hat{U}_j - U_j|}{\max |\hat{U}_j|}, \quad 0 \leq j \leq N,$$

where U_j is the actual solution at point j . Hence, numerical observation has clearly indicated in Table 3.4.1 demonstrates the supremacy of ETDRK4 over its fourth-order counterparts such as ABM4 and the RK4 methods. The scheme ETDRK4 works perfectly with any step-size whereas both ABM4 and RK4 failed at $t > 1/128$, their functionality requires a small time-step. The dash signs are the points where ABM4 and RK4 produced no result.

Table 3.4.1: Absolute relative error for autocatalysis equation (3.4.4) for parameter values $\epsilon = 0.1$, $m = 9$, final time $T = 1$, $L = 50$, $N = 100$.

Time-step	ABM4	RK4	ETDRK4
1/2	-	-	1.2922
1/4	-	-	0.8684
1/8	-	-	0.0334
1/16	-	-	5.7513e-05
1/32	-	-	1.4296e-06
1/64	-	-	7.8257e-08
1/128	8.0242e-02	8.0151e-02	4.6683e-09
1/256	3.9167e-02	3.9120e-02	2.8693e-10
1/512	1.7114e-02	1.7093e-02	1.8426e-11
1/1024	5.6812e-03	5.6742e-03	1.3454e-12

The results obtained in Table 3.4.1 and Figure 3.4.17 have shown that the ETDRK4 method provides a better accuracy over the ABM4 and RK4 methods. Hence to ascertain further justification of our approach, we sought for some exponential multi-step

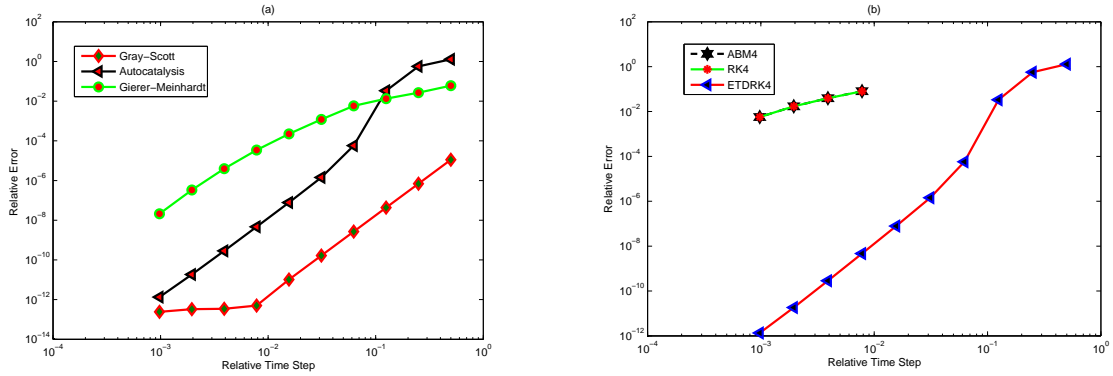


Figure 3.4.17: (a) Results for Gray-Scott (3.4.1), autocatalytic (3.4.4) and Gierer-Meinhardt (3.4.11) equations obtained by ETDRK4 scheme at $T = 2$ (b) Comparative results for autocatalytic equation (3.4.4) obtained by ETDRK4, ABM4 and RK4 schemes at $T = 1$.

schemes of order-four (ETDM4), order-five (ETDM5) and order-six (ETDM6) with fourth-order Adams type (ETDADAMS4). For the purpose of comparison, it would go far beyond the scope of this article to introduce the family exponential multi-step methods, fourth-order Adams-Bashforth-Moulton (ABM4) and the classical Runge-Kutta method of order four (RK4) in details. Instead, we have decided to pick some of the typical but rather distinctive members of the huge family of exponential time differencing methods.

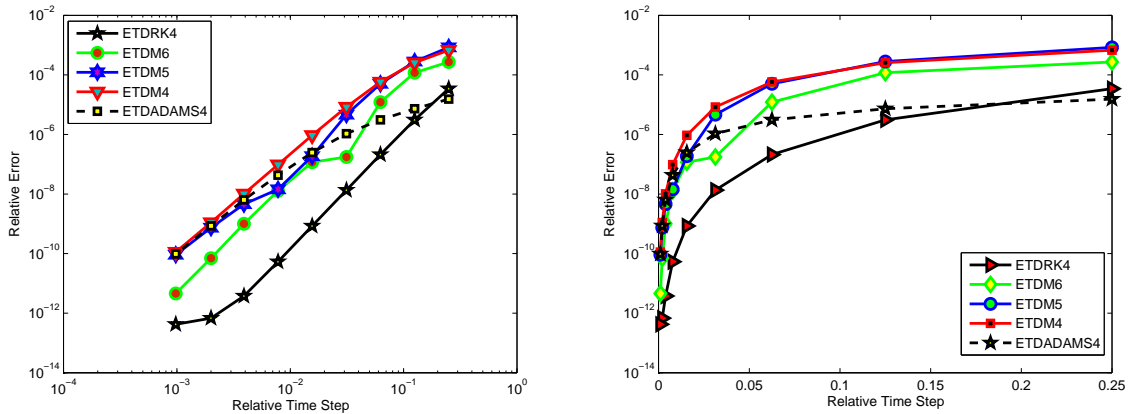


Figure 3.4.18: Comparative results for Gray-Scott equation (3.4.1) obtained by ETDRK4, ETDM4, ETDM5, ETDM6 and ETDADAMS4 schemes at $T = 2$, $L = 50$, $A = 9\epsilon$, $B = 2\epsilon^{1/3}$, $\epsilon = 0.001$, $N = 200$, $x \in [0, 100]$.

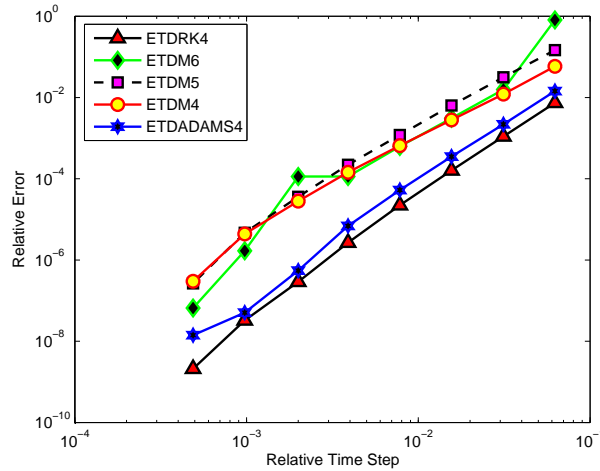


Figure 3.4.19: Comparative results for Gierer-Meinhardt equation (3.4.11) obtained by ETDRK4, ETDM4, ETDM5, ETDM6 and ETDADAMS4 schemes at $T = 1$, $D = 1$, $\epsilon = 0.01$, $p = 2$, $q = 1$, $m = 2$, $s = 1$ and $N = 250$ for $x \in [-1, 1]$.

3.5 Summary and discussions

In this chapter, we considered equations that lead to some interesting phenomena, such as, pattern formation far from equilibrium, pulse splitting and shedding processes, reactions and competitions in excitable mediums, nonlinear waves and spatiotemporal chaos. We have equal urge to study numerically in this thesis, the simulations of one-dimensional Gray-Scott-like models (Gray-Scott, Autocatalysis and Gierer-Meinhardt equations) to unveil pulse splitting process and self-replicating patterns in such dynamical systems. We attain this feat by combining the fourth-order exponential time differencing Runge-Kutta method (in time) with higher-order finite difference scheme (in space), we obtain a good result with accuracy of over 10^{-12} . It is also clear from the numerical analysis of the result presented here that the parameters A and B determine which physical process are more dominant as the system evolves. The two chemical species u and v are studied in this paper for different diffusivities in the limit when the ratio of diffusion rates $\epsilon < 1$.

Our results have sparked renewed interest in reaction-diffusion models for biological pattern formation and, in particular, the roles that domain growth and diffusion coefficient played in the mechanisms of pattern formation. A particular feature of reaction-diffusion patterns on increasing or extending domains is the tendency for stripe-like

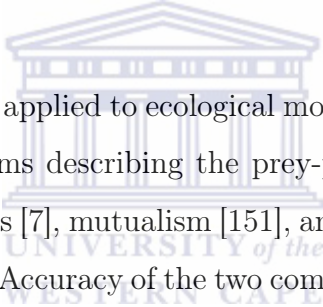
patterns to double in the number of stripes each time the domain doubles in length or the system is slightly perturbed. This appears to be a general result for a wide variety of reaction-diffusion models with different reaction kinetics. Findings in this paper have also revealed that some patterns generated are synonymous to the features found in the river course, in particular, the lower course. The landmark results presented in Table 3.4.1 and figures 3.4.17, 3.4.18 and 3.4.19, grant a further justification on the issue of applicability and accuracy of ETDRK4 method when applied to reaction-diffusion problems.

In the next chapter, we shall extend our method of solution to some ecological problems consisting of two and three species interactions.



Chapter 4

Numerical simulations of reaction-diffusion models in ecology



Using local analysis theory applied to ecological modeling in this chapter, we study four important ecological systems describing the prey-predator dynamics [59], interaction between competitive species [7], mutualism [151], and a three species competition model of May and Leonard [120]. Accuracy of the two competing exponential time differencing (ETD) Runge-Kutta and Adams-type methods that are of order-four, are used as the major time stepping methods. We justify the supremacy of these two schemes when applied to the mentioned dynamical systems and compared with other existing multi-step exponential integrators of orders four, five and six.

4.1 Introduction

In this chapter, we consider the numerical study of reaction-diffusion systems involving two or more species. We address the interaction between two species in terms of predator-prey systems and the biological system displaying the formation of chaotic spatiotemporal patterns arising from a community of three competitive species [7, 57, 59, 102, 139, 140, 151, 153, 190, 199]. The most popular and well-known predator-prey model is named after the two scientists, Alfred Lotka (1880-1949) and Vito Volterra (1860-1940). The duo earlier combined to study and apply the model to

address the interacting population systems called predator-prey. Our numerical study in this chapter shall be based mainly to reflect the types of interactions which we describe as predation (a process where one specie of organisms called predator depends solely on the other called the prey, for survival. In other words, if the growth rate of one population is decreased and the other is increased the populations are in a predator-prey situation), competition (a situation whereby two or more different species of organisms compete for the available resources, definitely we expect the growth rate of each population to decrease) and lastly, the mutualism or symbiosis (organisms coexist without affecting each other, hence, species growth rate is increased).

A large amount of research has been devoted to the study of population dynamics and ecological interactions over the past few decades, such study includes the predator-prey system that describes the situation in which the existence of the specie called the predator depends solely on the other specie called the prey. The predator-prey system has received a tremendous attraction over years but represented mainly in terms of ordinary differential equations, which modelled the spatial distribution of species. The Dynamics of the Lotka-Volterra predator-prey model are quite interesting, unfortunately, this model is structurally unstable since a small perturbation of the equations often results to a drastic change in the dynamical system. For this reason, the presence of diffusion mechanism however changes the behavior of the whole model to coupled partial differential equations which we termed as reaction-diffusion system. With the introduction of diffusion, its analysis remain tactical [193, 194], hence, numerical simulations are sought.

Predator-prey systems have been studied by many researchers in various forms, for instance, in bacteria ecology, computer simulations of complex spatiotemporal patterns [13, 57, 129] of *Bacillus subtilis* based on stochastic models [93] and deterministic models [127], Allee effect of patchy invasion on predator-prey dynamics [5, 8, 17, 41, 67, 153]. The diffusive predator-prey system have been studied extensively by [57, 80, 118, 122, 129, 137, 152, 190]. Wang et al. [193] investigate the spatial pattern formation of a predator-prey system with prey-dependent functional response of Ivlev type and reaction-diffusion. Analysis of predator-prey systems showing the Holling

type II functional response is examined in Garvie and Trenchea [59].

Another type of inter-species interaction is given by competition. Competitive species models or community models further describe a situation where consumers share some resources that can affect their rate of production. Many ecologists, however, put greater weight on competition which was thought to have played a predominant role over the years in structuring ecological communities. There is a classical model of competition model due to Lotka [115, 116] and Volterra [191, 192].

The Lotka-Volterra competition model is an interference model where two species are assumed to diminish each other's per capita growth rate by direct interference. It is assumed here that each species has a different population of different sizes that grow logistically in absence of each other and that each has a per capita growth rate that decreased linearly with the population size with their own intrinsic growth rate and carrying capacity [151]. Mathematically, the simplest and instructive case is described by a system of just two coupled-reaction diffusion equations. The system of two competing species has won a lot of attentions, and has been almost completely investigated. We however considered in addition in this chapter a general case of n competing species that is less studied and still poorly understood for case $n > 2$. Among few handful work done when $n > 2$ include [151, 171, 190].

In mutualistic systems, organisms are found to evolve together. The existence of one has no negative effect on the other, each is part of the other's environment, so as they adapt to their environment, they make use of each other in such a way that both organisms are benefited. Mutualism has rarely gained the attention of predation and competition. Further classification of mutualism is beyond the scope of this thesis. However, interested readers are referred to [89, 102] for thorough review of the natural history of mutualism. Community invasion models have an issue of significant importance in the contemporary study of biological and ecological systems which have drawn the attention of both theorists and ecologists since the foundation work of Holt [81]. In [56, 70, 199] details and full understanding of competition models are given to study the effects of alien species invasion on native ecosystem. Some of the evolution processes here are characterized owing to the fact that certain moments of time they

experience a sudden change of state.

Despite the considerable achievement recorded in the field of population dynamics modeling the interaction of a multi-species community, so many challenging problems are still open to better estimate ecological importance of the results, an extension has to be granted for the case of a multi-species community which has received little attention in the literature. We therefore consider in this chapter as well, the model of a dynamic consisting of three competitive species. We equally demonstrate numerically for a class of biological system that lead to the evolution of travelling waves and formation of chaotic spatiotemporal patterns [151, 154, 171, 199].

The structure of rest of this chapter is as follows. In Section 4.2, we describe the model problems of spatiotemporal dynamics of multiple species. A brief description of the numerical method is considered in Section 4.3. Numerical results for each of the problems are presented in Section 4.4 to justify the performances of the methods. Finally, we summarize our conclusion in Section 4.5.

4.2 Model problems

Owing to a widely accepted approach, we describe the spatiotemporal dynamics of a system of n interacting biological [78, 102, 137, 154, 171] species by the following equations

$$\frac{\partial u_i(\tau)}{\partial t} = D_i \Delta u_i(\tau) + f_i(u_1, \dots, u_n), \quad x \in \mathbb{R}, \quad t \in [0, T], \quad T > 0, \quad (4.2.1)$$

the corresponding initial conditions are given by the functions

$$u_i(\tau, 0) = u_{i0}(\tau), \quad i = 1, 2, \dots, n, \quad (4.2.2)$$

with an assumption that there is no external input imposed from the outside. Since the initial densities of the above systems are nonnegative, hence, the boundary conditions can be taken as

$$\left(\frac{\partial u_i}{\partial t} \right)_{x=0} = \left(\frac{\partial u_i}{\partial t} \right)_{x=l} \quad (4.2.3)$$

where u_i is considered as the density of the i th species, Δ is the usual Laplacian operator, R is a subset of $(-\infty, \infty)$, $\tau = (U, V, W)$ stands for the position in space, f_i , for $i = 1, \dots, n$ represent the local kinetics or reaction term of the system that depends on quite number of parameters in the context of biology, such as the growth and death rates of the various species, Positive parameter D_i is the diffusion coefficient describing the spread and mixing strength of the species within a give spatial domain and t is the time.

Analysis of the system (4.2.1) still remain tactical, we apply the stability analysis to (4.2.1) with absence of diffusion. We need to examine under what conditions the system (4.2.1) obeys Turing instability. This could only be achieved by taken an assumption that the right hand side of (4.2.1) is zero and that equations (4.2.1) and (4.2.2) together with the boundary conditions (4.2.3) admit a solution, say steady state $u_i = \hat{u}_i$ for $\hat{u}_i > 0, i = 1, \dots, n$, that is spatially and temporarily uniform. The solution $u_i = \hat{u}_i$ is said to be Turing unstable if it is locally stable as a solution of the system (4.2.1) without diffusion term D_i , therefore

$$\frac{du_i(t)}{dt} = f_i(u_i), \quad i = 1, \dots, n. \quad (4.2.4)$$

At steady state, we expect all the eigenvalue to have a negative real parts at the neighbourhood of \hat{u}_i . If we let $u_i(t) - \hat{u}_i = \mu(t)$, we have

$$\frac{d\mu_i(t)}{dt} = a_{i,j} = A, \quad i, j = 1, \dots, n, \quad (4.2.5)$$

where

$$a_{i,j} = \frac{\partial f_i(\hat{u}_i)}{\partial u_j}, \quad (4.2.6)$$

are the elements of the Jacobi matrix at steady state with associated eigenvalues λ_i for $i = 1, \dots, n$ defined by the equation $\det(A - \lambda I) = 0$, I is the identity matrix. Further analysis of our kinetic systems shall be determined on individual basis henceforth.

Two-species predator-prey system:

It is clear from our introduction that predator-prey models are much more similar in description to both parasite and parasitoid models. Here, the predator does not live on the host unlike the cases of mutualism and competitive species models. Setting $n = 2$, $i = 1, 2$ in (4.2.1), we have dynamics of one dimensional two-species prey-predator reaction-diffusion system which takes the form

$$\left. \begin{aligned} \frac{\partial U}{\partial T} &= D_1 \frac{\partial^2 U}{\partial X^2} + F(U, V), \\ \frac{\partial V}{\partial T} &= D_2 \frac{\partial^2 V}{\partial X^2} + G(U, V), \end{aligned} \right\} \quad (4.2.7)$$

where U and V are the respective densities of the prey and predator, $F(U, V)$, $G(U, v)$ are also their respective reaction terms at position X and time T , D_1 and D_2 are diffusion constants for the prey and predator.

We consider as an example here the reaction-diffusion system (4.2.7) by choosing the appropriate parameters in line with the general form (Holmes et al. [80], Murray [137, 138] and Sherratt [180]), so $F(U, V)$ and $G(U, V)$ are specified to have

$$\left. \begin{aligned} \frac{\partial U}{\partial T} &= D_1 \frac{\partial^2 U}{\partial X^2} + U \left[\alpha \left(1 - \frac{U}{K} \right) - \frac{\gamma V}{U + \delta} \right], \\ \frac{\partial V}{\partial T} &= D_2 \frac{\partial^2 V}{\partial X^2} + V \left[\beta \left(1 - \frac{hV}{U} \right) \right], \end{aligned} \right\} \quad (4.2.8)$$

where $D_1, D_2, \alpha, \beta, \gamma, \delta, h$ and K are positive parameters. $U(X, T)$ and $V(X, T)$ remain the population densities of prey and predator. The term $\alpha U(1 - U/K)$ represents the logistic growth, α is the intrinsic growth rate, and K the carrying capacity. The term γV is the per capital prey reduction due to consumption by the predator, β describes the intensity of predation.

Since analysis of (4.2.8) still remains tactical with the presence of diffusion, we then nondimensionalize by re-scaling with variables

$$u(t) = \frac{U(T)}{K}, \quad v(t) = \frac{hV(T)}{K}, \quad t = \alpha T, \quad \mu = \frac{\gamma}{h\alpha}, \quad \psi = \frac{\beta}{\alpha}, \quad \phi = \frac{\delta}{K}, \quad D = \frac{D_2}{D_1} \quad (4.2.9)$$

then on substitution, system (4.2.8) becomes

$$\left. \begin{aligned} \frac{\partial u}{\partial t} &= \frac{\partial^2 u}{\partial x^2} + u(1-u) - \frac{\mu u}{u+\phi} v = f(u, v), \\ \frac{\partial v}{\partial t} &= D \frac{\partial^2 v}{\partial x^2} + \psi v - \frac{\psi v^2}{u} = g(u, v). \end{aligned} \right\} \quad (4.2.10)$$

To study Turing instability, we have to analyze the stability criteria of the non-diffusive system. The spatial model (4.2.10) has the corresponding non-diffusion model

$$\left. \begin{aligned} \frac{du}{dt} &= u(1-u) - \frac{\mu u}{u+\phi} v = f(u, v), \\ \frac{dv}{dt} &= \psi v - \frac{\psi v^2}{u} = g(u, v). \end{aligned} \right\} \quad (4.2.11)$$

The three parameters μ , ψ and ϕ are now in dimensionless form and that they are strictly positive. There are other choices for the change of variables to put the system in dimensionless form, but we made a good choice that suit our purposes since the dimensionless groupings used here give relative measures of the effect of dimensional parameters. For instance, ϕ now becomes the ratio of the linear growth rate of the predator to that of the prey, for $\psi < 1$. Based on the fact established in [139], naturally we expect the prey to reproduce faster than the predator otherwise the system will go into extinction.

At equilibrium, we have

$$f(\hat{u}, \hat{v}) = g(\hat{u}, \hat{v}) = 0$$

since the steady state populations \hat{u} and \hat{v} are solutions of $du/dt = dv/dt = 0$, so that

$$\left. \begin{aligned} \hat{u}(1-\hat{u}) - \frac{\mu \hat{u}}{\hat{u}+\phi} \hat{v} &= 0 \\ \psi \hat{v} - \frac{\psi \hat{v}^2}{\hat{u}} &= 0. \end{aligned} \right\} \quad (4.2.12)$$

Naturally, for the dynamical system under consideration to be biologically meaningful, $u \geq 0$, $v \geq 0$ for all time. Clearly, equation (4.2.10) has three positive steady states (\hat{u}, \hat{v}) , the two trivial states or saddle points are at point $(0, 0)$ which describes complete extinction of both prey and predator and point $(1, 0)$, which shows that the predator is absent leading to unbounded logistic growth of the prey species. The stationary point (\hat{u}, \hat{v}) corresponding to the existence of prey and predator bearing in mind that the

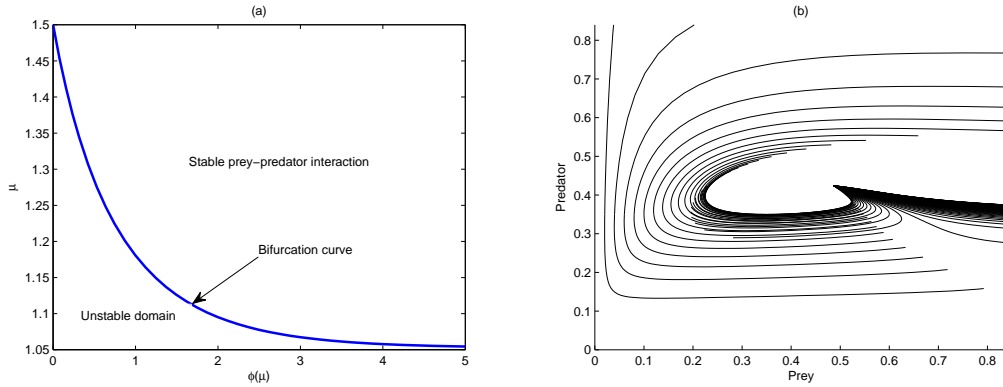


Figure 4.2.1: (a) Bifurcation diagram for $\mu > 0$ and $\phi > 0$, for $\phi = \sqrt{\mu^2 + 4\mu} + \mu - 1$. (b) Phase plane trajectory for prey-predator system (4.2.10) for parameter value $\mu = 1.025$, $\phi = 0.3$ and $\psi = 0.05$

parameters must be strictly restricted to the positive quadrants, we have

$$\hat{v} = \hat{u}, \quad \frac{(1 - \mu - \phi) + [(1 - \mu - \phi)^2 + 4\phi]^{1/2}}{2}, \quad (4.2.13)$$

the stability of the steady or equilibrium states are the singular points in the phase plane of (4.2.10). We let

$$A = \begin{pmatrix} \hat{u} \left[\frac{\mu \hat{u}}{(\hat{u} + \phi)^2} - 1 \right] & \frac{-\mu \hat{u}}{\hat{u} + \phi} \\ \psi & -\psi \end{pmatrix}. \quad (4.2.14)$$

where A is regarded as the community matrix with eigenvalues given by

$$|A - \lambda I| = 0 \Rightarrow \lambda^2 - (tr A)\lambda + det A = 0, \quad (4.2.15)$$

for stability, we require that $Re(\lambda) < 0$. The necessary and sufficient conditions for linear stability become

$$\begin{aligned} tr A < 0 &\Rightarrow \hat{u} \left[\frac{\mu \hat{u} - (\hat{u} + \phi)^2}{(\hat{u} + \phi)^2} \right] < \psi \\ det A > 0 &\Rightarrow \frac{(\hat{u} + \phi)^2 + \mu(\hat{u} + \phi) - \mu \hat{u}}{(\hat{u} + \phi)^2} > 0. \end{aligned} \quad (4.2.16)$$

On substituting \hat{u} in equation (4.2.13) provides the stability conditions in terms of the positive parameters μ , ψ and ϕ .

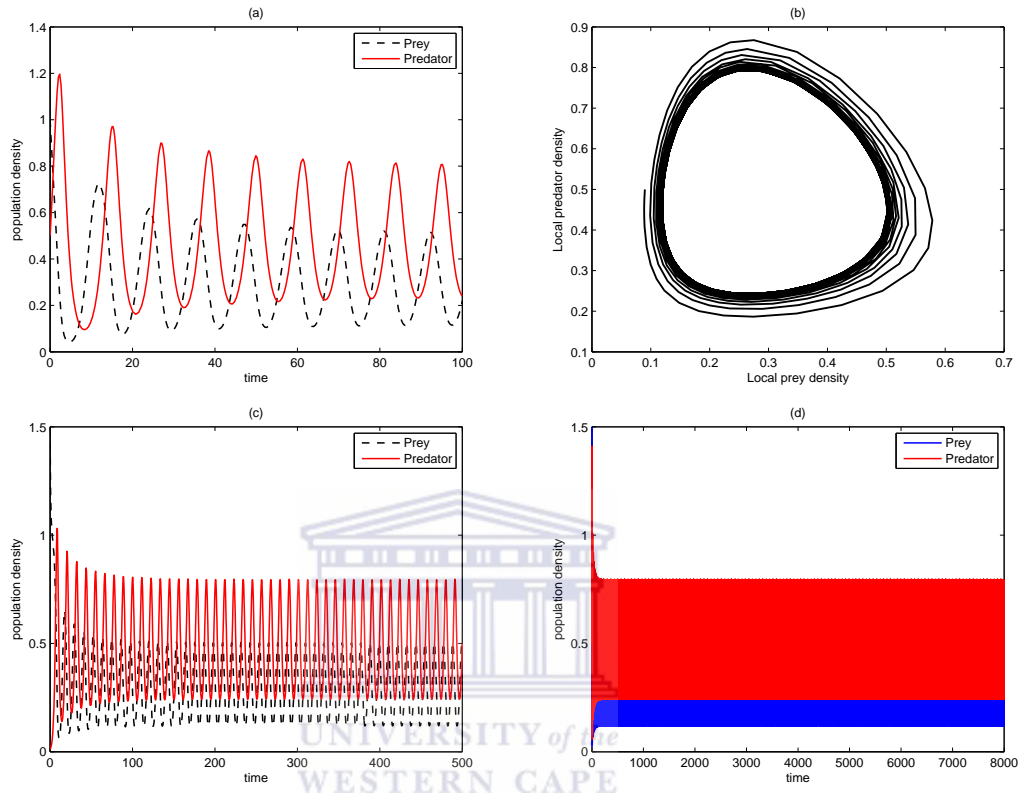


Figure 4.2.2: Typical phase trajectories for (b) the unrealistic prey-predator system (4.2.8). Plots (a), (c), (d) are the various periodic behaviour of the prey u and predator v populations. Parameter values: $\mu = 0.8$, $\psi = 2$, $\phi = 0.4$, which give a steady state at $\hat{u} = 1.5$, $\hat{v} = 0.1$ for (a) at $t = 100$, (b) $t=8000$, (c) $t=500$ and (d) $t=8000$.

Figures 4.2.2 and 4.2.3 represent the unrealistic and realistic population dynamics of a prey-predator systems. The system with a kinetics of first type as described in Garvie [57] is quite unrealistic due to the choices of parameters used in transforming the system into a dimensionless form. This shortcoming actually motivate us to choose some appropriate parameters since it is always helpful to write the system in nondimensional form. Nondimensionalisation plays an important role when carefully considered because it reduces the number of parameters by grouping them in a more meaningful manner, this is obvious when relations in (4.2.9) relates equations (4.2.7) and (4.2.8) without losing our focus in biological context. In Figure 4.2.2, we expect to see that the prey produces more faster than the predator but the case here is oth-

erwise. So, the system described in Figure 4.2.2 is totally unrealistic as its prone to danger of extinction of the prey species that would in turn results to total break down of the ecosystem since all the predators will die out in absence of food.

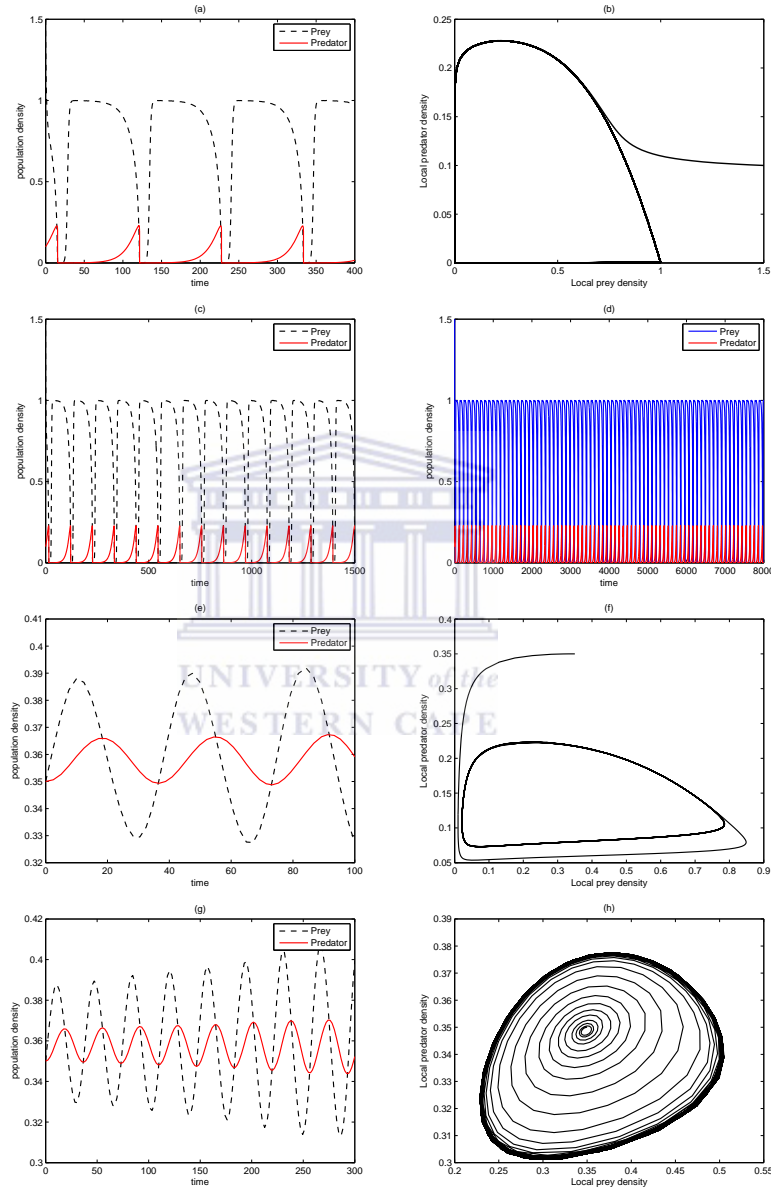


Figure 4.2.3: Typical phase trajectories for (b), (f) and (h) for the realistic prey-predator system (4.2.8). Plots (a), (c), (d), (e) and (g) are the various periodic behaviour of the prey u and predator v populations. Parameter values: $\mu = 1.5$, $\psi = 0.08$, $\phi = 0.01$, which give a steady state at $\hat{u} = 1.5$, $\hat{v} = 0.1$ for (a) at $t = 400$, (b) $t = 7000$, (c) $t = 1500$ and (d) $t = 8000$. By taking $\hat{u} = \hat{v} = 0.35$, $\mu = 1$, $\psi = 0.05$, $\phi = 0.2$, we obtain (e) for $t = 100$, (f) for $t = 1000$ and (g) for $t = 300$. For (h), $\mu = 1.025$, $t = 8000$

Two and three-species competitive system:

Competition model describes a situation in which two or three species compete for the same insufficient resources like food, territory or in some way inhibit their rate of growth. For simplicity and following the approach we used above, we consider here a two-species Lotka-Volterra competition model

$$\left. \begin{aligned} \frac{\partial U}{\partial T} &= \delta_1 \frac{\partial^2 U}{\partial X^2} + \alpha_1 U \left(1 - \frac{U}{K_1} - \beta_1 \frac{V}{K_1} \right), \\ \frac{\partial V}{\partial T} &= \delta_2 \frac{\partial^2 V}{\partial X^2} + \alpha_2 V \left(1 - \frac{V}{K_2} - \beta_2 \frac{U}{K_2} \right), \end{aligned} \right\} \quad (4.2.17)$$

with species U and V having logistic growth at the absence of the other. The parameters α_1 and α_2 represent their linear birth rates, β_1 and β_2 measure the competitive effect of V on U and vice versa, δ_1 and δ_2 stand for the diffusion coefficients of species U and V . K_1 and K_2 are their respective carrying capacities.

Again, we nondimensionalize (4.2.17) by introducing a set of dimensionless variables

$$u(t) = \frac{U(T)}{K_1}, \quad v(t) = \frac{V(T)}{K_2}, \quad t = \alpha_1 T, \quad \mu = \frac{\alpha_2}{\alpha_1}, \quad \phi = \beta_2 \frac{K_2}{K_1}, \quad \psi = \beta_1 \frac{K_1}{K_2}, \quad \delta = \frac{\delta_2}{\delta_1}. \quad (4.2.18)$$

As suggested by Medvinsky et al. [122] and Garvie [57], that the local stability analysis will always grant a deep understanding that will provide important information on the choice of parameters for numerical integration, we henceforth continue with the local stability analysis with absence of diffusion for simplicity. Hence, using (4.2.18) in (4.2.17), we obtain

$$\left. \begin{aligned} \frac{\partial u}{\partial t} &= \frac{\partial^2 u}{\partial x^2} + (u - u^2 - \phi uv) = f(u, v), \\ \frac{\partial v}{\partial t} &= \delta \frac{\partial^2 v}{\partial x^2} + \mu(v - v^2 - \psi uv) = g(u, v). \end{aligned} \right\} \quad (4.2.19)$$

For Turing instability, we consider the case of spatially homogeneous solutions, in which the spatial model (4.2.19) is equivalent to

$$\left. \begin{aligned} \frac{du}{dt} &= (u - u^2 - \phi uv) = f(u, v), \\ \frac{dv}{dt} &= \mu(v - v^2 - \psi uv) = g(u, v). \end{aligned} \right\} \quad (4.2.20)$$

Here, we regard the steady states and phase plane singularities, \hat{u} and \hat{v} as the solutions of $f(u, v) = g(u, v) = 0$ with the possibilities of four positive equilibrium states,

$$\left. \begin{aligned} (\hat{u}, \hat{v}) &= (0, 0), \quad (\hat{u}, \hat{v}) = (1, 0), \quad (\hat{u}, \hat{v}) = (0, 1), \\ (\hat{u}, \hat{v}) &= \left(\frac{1-\phi}{1-\phi\psi}, \frac{1-\psi}{1-\phi\psi} \right), \end{aligned} \right\} \quad (4.2.21)$$

the first three states are trivial and the last is non-trivial. The state $(0, 0)$ corresponds to total extinction of the two species population, the second $(1, 0)$ typifies the existence and extinction of species u and v respectively and the third trivial state $(0, 1)$ indicate that only species v exist. We can see clearly that non of the three trivial states could give a meaningful interpretation about the competition model, therefore we need to explore further the non-trivial equilibrium state (\hat{u}, \hat{v}) . The points $(0,0)$, $(1,0)$ and $(0,1)$ are all unstable. $(0,0)$ is an unstable node, $(1,0)$ and $(0,1)$ are saddle point equilibria.

From (4.2.20), for $f = g = 0$, we have that $(u - u^2 - \phi uv) = 0$, it follows that either $u = 0$ or $1 - u - \phi v = 0$ and also from the second equation, $\mu(v - v^2 - \psi uv) = 0$, this implies, $\mu v = 0$ and $1 - v - \psi u = 0$. On differentiating (4.2.20) partially with respect to (u, v) at steady states (\hat{u}, \hat{v}) , we assume that this equilibrium point is asymptotically stable, with all of the eigenvalues of the Jacobian or community matrix

$$A = \begin{pmatrix} 1 - 2u - \phi v & -\phi u \\ -\mu\psi v & \mu(1 - 2v - \psi u) \end{pmatrix}_{(\hat{u}, \hat{v})}. \quad (4.2.22)$$

In Figure 4.2.4, the populations converge on the intersection of the isoclines regardless of the initial population densities. The intersection point of the two lines gives the positive steady state as in (a) where the point $(1.4, 1.4)$ corresponds to $(\frac{1}{\phi}, \frac{1}{\psi})$. The locations of the isoclines in (b) dictate that species u out-competes species v , the point

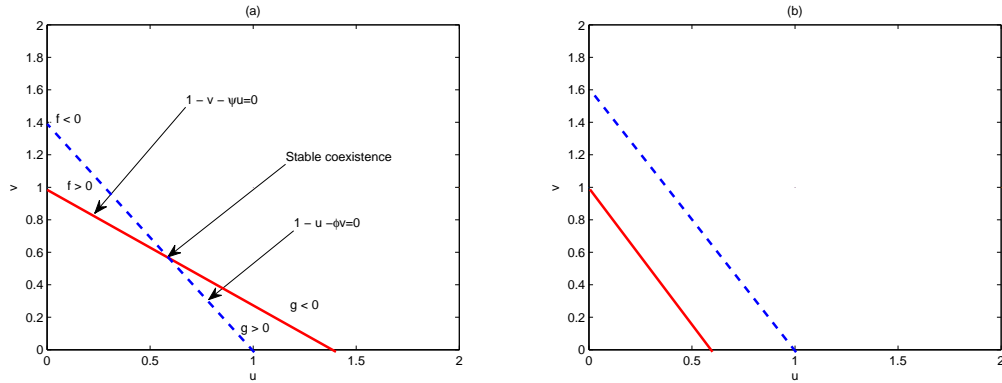


Figure 4.2.4: A graph depicting stable equilibrium between two competing species of system (4.2.20).

$(\frac{1}{\phi}, \frac{1}{\psi})$ corresponds to the value (1.6, 0.6) of species u and v respectively.

The point (0, 0), is unstable since the eigenvalues λ can be written in the form

$$|A - \lambda I| = \begin{vmatrix} 1 - \lambda & 0 \\ 0 & \mu - \lambda \end{vmatrix} = 0,$$

which implies that $\lambda_{1,2}=(1, \mu)$. At (1, 0), community matrix A becomes

$$|A - \lambda I| = \begin{vmatrix} 1 - \lambda & -\phi \\ 0 & \mu(1 - \psi) - \lambda \end{vmatrix} = 0,$$

which means $\lambda_{1,2}=(-1, \mu(1 - \psi))$, so we can say that the steady state $(\hat{u}, \hat{v}) = (1, 0)$ is stable if $\psi > 1$ and unstable if otherwise. In the same manner, the steady states (0, 1) has the eigenvalues λ when substituted to the community matrix A , we have

$$|A - \lambda I| = \begin{vmatrix} (1 - \phi) - \lambda & 0 \\ \mu\phi & -\mu - \lambda \end{vmatrix} = 0,$$

therefore, $\lambda_{1,2} = (-\mu, (1 - \phi))$. This means that the steady $(\hat{u}, \hat{v}) = (0, 1)$ is stable if $\phi > 1$ and unstable if $\phi < 1$.

On substituting the fourth steady state into the main community matrix, we have

$$|A - \lambda I| = \begin{vmatrix} \left[1 - 2\left(\frac{1-\phi}{1-\phi\psi}\right) - \phi\left(\frac{1-\psi}{1-\phi\psi}\right)\right] - \lambda & -\phi\frac{1-\phi}{1-\phi\psi} \\ -\mu\frac{1-\psi}{1-\phi\psi} & -\mu\left[1 - 2\left(\frac{1-\psi}{1-\phi\psi}\right) - \psi\left(\frac{1-\phi}{1-\phi\psi}\right)\right] - \lambda \end{vmatrix} = 0.$$

Further simplification leads to

$$\begin{aligned} \lambda_1 &= \xi + \sqrt{D(\phi, \mu, \psi)}/\chi, \\ \lambda_2 &= \xi - \sqrt{D(\phi, \mu, \psi)}/\chi, \end{aligned} \quad (4.2.23)$$

where $\xi = (\phi - 1) + \mu(\psi - 1)$, $D(\phi, \mu, \psi) = [(\phi - 1) + \mu(\phi - 1)]^2 - 4\mu(1 - \phi\psi)(\phi - 1)(\phi - 1)$ and $\chi = 2(1 - \phi\psi)$.

The good thing is that all the four steady states exist in the positive quadrant which make the whole process meaningful in the biological and ecological contexts. Clearly, the stability of the steady state depends on the size of the positive parameters μ , ϕ and ψ subject to various cases such as; $(\phi > 1, \psi > 1)$, $(\phi > 1, \psi < 1)$, $(\phi < 1, \psi > 1)$ or $(\phi < 1, \psi < 1)$. A biological interpretation of Figure 4.2.4(b) suggests that because the carrying capacity of species u is so high, this species is not limited by this resource to the extent to which species v seems to be. Maybe species u can use other resources not utilized by species v , so on losing some of this resources to species v , it has little or no effect.

Stable coexistence occurs when the isoclines are arranged as in 4.2.4(a) for $K_1 < K_2/\psi$ and $K_2 < K_1/\phi$. Clearly, on rearranging, we can see that $\psi < K_2/K_1$ and $\phi < K_1/K_2$, and these competition coefficients must be made as small as possible relative to the ratio of its carrying capacity to that of other species. This conditions must hold for both species simultaneously, and this is possible only if the carrying capacities of the two species are similar in such a way that their ratio is close to one regardless of which is the numerator. As the resources declined, the two species shown in Figure 4.2.5 compete for the limited resources, this is mostly evident in (b).

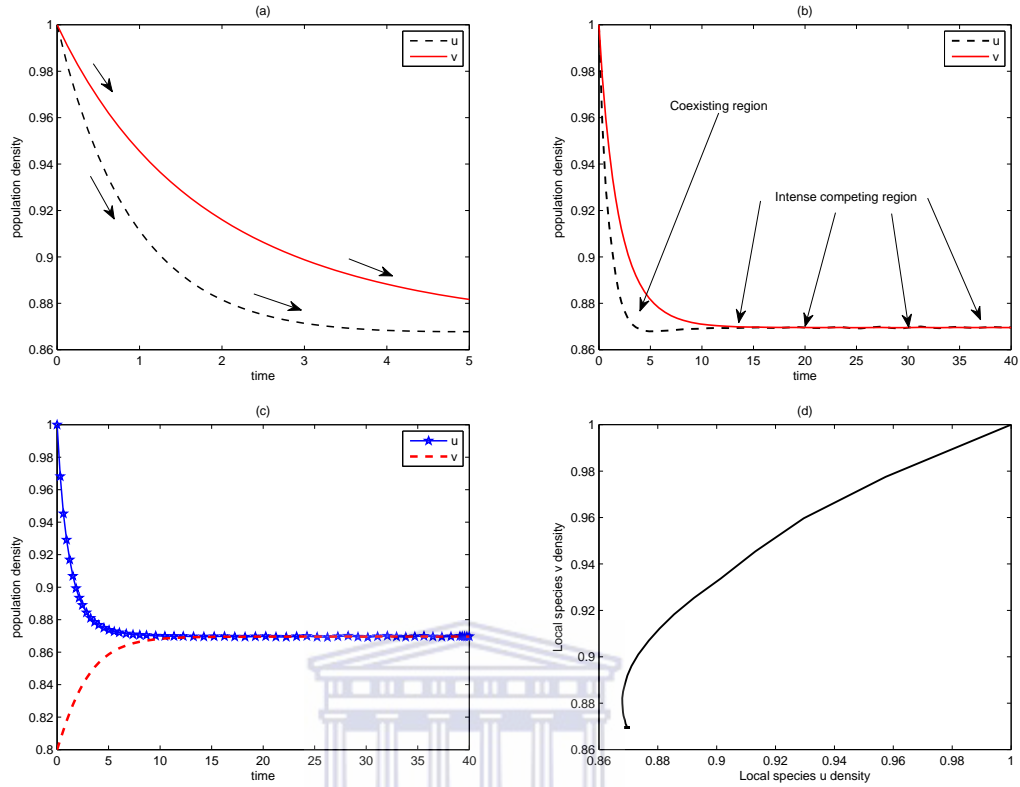


Figure 4.2.5: A decline population density associated with the competitive system (4.2.19). Parameter values: (a) $\hat{u} = \hat{v} = 1$, $\mu = 0.5$, $\phi = 0.5$, $\psi = 0.5$ at $t = 5$ and (b) $\hat{u} = \hat{v} = 1$, $\mu = 0.5$, $\phi = 0.15$, $\psi = 0.15$ at $t = 40$. Other parameters are as in (b) except at $\hat{v} = 0.8$, $t = 40$ for (c) and $t = 20000$ for (d).

The three species system of consideration is of the form

$$\frac{\partial U_i}{\partial T} = \delta_i \frac{\partial^2 U_i}{\partial X^2} + \xi_i U_i \left(1 - \sum_{j=1}^n \alpha_{ij} U_j \right), \quad T > 0. \quad (4.2.24)$$

This is in line with three-species Lotka-Volterra competition model where $\xi_i > 0$, $i = 1, 2, 3$ give the intrinsic growth rates of the species for the case $n = 3$, $i, j = 1, 2, 3$. $U_i > 0$ gives the density of each of the species population at corresponding time t for position $X \in \mathbb{R}$ in space [120]. The term $\alpha_{ij} > 0$ for $i, j = 1, 2, 3$ describes both intra-species competition for $i = j$ and inter-species competition for $i \neq j$. The intensity of spatial mixing due to self-motion is given by the term $\delta_i > 0$, for $i = 1, 2, 3$.

Three-species competition model displays more interesting and diverse phenomena than two-species competition. It is possible for one- or two-species extinction, or global

stability of a positive three-species equilibrium. The analogous behavioural solutions of this type of system have been shown in periodic form [79, 201] and also in the form of heteroclinic orbit as indicated in [120]. In [7], it was suggested that the competitive outcome depends solely on the relationship between pairwise interactions.

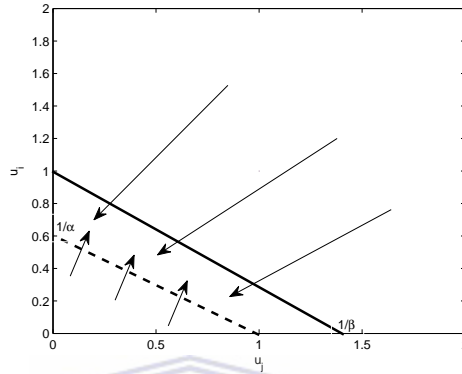


Figure 4.2.6: Phase plane trajectory that represents a nontransitive interactions between three-species in the May-Leonard competition model. The $u_i - u_j$ phase plane for $i \neq j$, indicates that species u_i eliminates u_j and that, there are no two-species positive equilibria. The solutions tend to equilibrium at points $u_i = 1$ and $u_j = 0$.

Thus, for three competitors, $n = 3$, $i, j = 1, 2, 3$; we have

$$\left. \begin{aligned} \frac{\partial U_1}{\partial t} &= \delta_1 \frac{\partial^2 U_1}{\partial X^2} + \xi_1 U_1 (1 - \alpha_{11} U_1 - \alpha_{12} U_2 - \alpha_{13} U_3), \\ \frac{\partial U_2}{\partial t} &= \delta_2 \frac{\partial^2 U_2}{\partial X^2} + \xi_2 U_2 (1 - \alpha_{21} U_1 - \alpha_{22} U_2 - \alpha_{23} U_3), \\ \frac{\partial U_3}{\partial t} &= \delta_3 \frac{\partial^2 U_3}{\partial X^2} + \xi_3 U_3 (1 - \alpha_{31} U_1 - \alpha_{32} U_2 - \alpha_{33} U_3). \end{aligned} \right\} \quad (4.2.25)$$

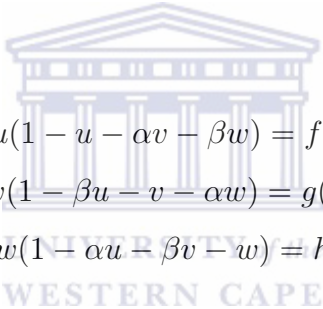
Following the approach used for the analysis of two-species model, here, we shall qualitatively describe the spatiotemporal dynamics of a community consisting of three competitive species. Equation (4.2.25) has so many parameters that could make local its analysis to be more cumbersome, hence, following the steps described earlier, we rescale the system (4.2.25) by letting

$$\left. \begin{aligned} \xi_1 &= \xi_2 = \xi_3 = \xi = \alpha_{11} = \alpha_{22} = \alpha_{33} = 1, \\ \zeta_1 &= \frac{\delta_2}{\delta_1}, \quad \zeta_2 = \frac{\delta_3}{\delta_1} \quad t = \xi t, \quad x = \sqrt{\frac{\xi_1}{\delta_1}} X, \\ u &= \alpha_{11} U_1, \quad v = \alpha_{22} U_2, \quad w = \alpha_{33} U_3, \\ \alpha &= \alpha_{12} = \alpha_{23} = \alpha_{31}, \quad \beta = \alpha_{13} = \alpha_{21} = \alpha_{32}, \end{aligned} \right\} \quad (4.2.26)$$

and obtain

$$\left. \begin{aligned} \frac{\partial u}{\partial t} &= \frac{\partial^2 u}{\partial x^2} + u(1 - u - \alpha v - \beta w), \\ \frac{\partial v}{\partial t} &= \zeta_1 \frac{\partial^2 v}{\partial x^2} + v(1 - \beta u - v - \alpha w), \\ \frac{\partial w}{\partial t} &= \zeta_2 \frac{\partial^2 w}{\partial x^2} + w(1 - \alpha u - \beta v - w), \end{aligned} \right\} \quad (4.2.27)$$

which has been reduced to only 4 dimensionless parameters α and β . We can see that nondimensionalisation reduces the number of parameters here from 9 to 4. The ODE system corresponding to (4.2.28) is sometimes called the May Leonard model [120] and has been used in many studies to fit both ecological and biological data. By Turing instability analysis, we only consider the equivalent non-diffusive system, hence, (4.2.28) is further reduced to



$$\left. \begin{aligned} \frac{du}{dt} &= u(1 - u - \alpha v - \beta w) = f(u, v, w), \\ \frac{dv}{dt} &= v(1 - \beta u - v - \alpha w) = g(u, v, w), \\ \frac{dw}{dt} &= w(1 - \alpha u - \beta v - w) = h(u, v, w), \end{aligned} \right\} \quad (4.2.28)$$

where $0 < \alpha < 1$, $\beta > 1$, $u > 0$, $v > 0$ and $w > 0$. The equilibrium or steady state populations \hat{u} , \hat{v} and \hat{w} are solutions of

$$\frac{du}{dt} = 0, \quad \frac{dv}{dt} = 0, \quad \frac{dw}{dt} = 0,$$

in such that

$$f(\hat{u}, \hat{v}, \hat{w}) = 0, \quad g(\hat{u}, \hat{v}, \hat{w}) = 0, \quad h(\hat{u}, \hat{v}, \hat{w}) = 0$$

which, from the last equations implies that

$$\left. \begin{aligned} \hat{u} - \hat{u}^2 - \alpha \hat{v} \hat{v} - \beta \hat{u} \hat{w} &= 0, \\ \hat{v} - \beta \hat{u} \hat{v} - \hat{v}^2 - \alpha \hat{v} \hat{w} &= 0, \\ \hat{w} - \alpha \hat{u} \hat{w} - \beta \hat{v} \hat{w} - \hat{w}^2 &= 0. \end{aligned} \right\} \quad (4.2.29)$$

It is obvious that system (4.2.29) possesses five stationary states that are located in

the positive quadrant, they are points $(0, 0, 0)$, $(1, 0, 0)$, $(0, 1, 0)$, $(0, 0, 1)$ and $(1, 1, 1)/(1 + \alpha + \beta)$. The point $(0, 0, 0)$ is called unstable node, it corresponds to the trivial state that indicates the total extinction of the three-species population. The points $(1, 0, 0)$, $(0, 1, 0)$, $(0, 0, 1)$ are the three semi-trivial states where only one species exist while the other two dies out, they are in fact the saddle points. The trivial steady-state correspond to the point $(1, 1, 1)/(1 + \alpha + \beta)$ whose community matrix is given as

$$\begin{aligned}
 D &= \begin{pmatrix} \frac{\partial f}{\partial u} & \frac{\partial f}{\partial v} & \frac{\partial f}{\partial w} \\ \frac{\partial g}{\partial u} & \frac{\partial g}{\partial v} & \frac{\partial g}{\partial w} \\ \frac{\partial h}{\partial u} & \frac{\partial h}{\partial v} & \frac{\partial h}{\partial w} \end{pmatrix}_{(\hat{u}, \hat{v}, \hat{w})} \\
 &= \begin{pmatrix} 1 - 2u - \beta v - \alpha w & -\alpha v & -\beta w \\ -\beta u & 1 - \beta u - 2v - \alpha w & -\alpha v \\ -\alpha w & -\beta w & 1 - \alpha u - \beta v - 2w \end{pmatrix}_{(\hat{u}, \hat{v}, \hat{w})} \quad (4.2.30)
 \end{aligned}$$

We can see that the eigenvalues $(\lambda_1, \lambda_2, \lambda_3)$ of community matrix D at the origin are all positive, i.e, when $(\hat{u}, \hat{v}, \hat{w}) = (0, 0, 0)$, then the diagonal of (4.2.30) gives $(\lambda_1 = \lambda_2 = \lambda_3) = 1$, hence the trivial state is unstable. Again, we also consider the semi-trivial case of the single-species equilibria, the eigenvalues of the community matrix are given as $\lambda_1 = -1$, $\lambda_2 = 1 - \beta$ and $\lambda_3 = 1 - \alpha$, so, the semi-trivial state is also unstable since $\alpha\beta < 1$. We finally evaluate the community matrix at non-trivial steady state, i.e. at

$$(\hat{u}, \hat{v}, \hat{w}) = \frac{(1, 1, 1)}{(1 + \alpha + \beta)}.$$

It is known [7, 120, 151] that the three species equilibrium is stable if and only if all the eigenvalues of the community matrix

$$M = \left(-(1 + \alpha + \beta)^{-1} \right) \begin{pmatrix} 1 & \alpha & \beta \\ \beta & 1 & \alpha \\ \alpha & \beta & 1 \end{pmatrix}_{(\hat{u}, \hat{v}, \hat{w})} \quad (4.2.31)$$

have positive real parts. The eigenvalues of M are given by

$$\begin{aligned}\lambda_1 &= 1 + \alpha + \beta, \\ \lambda_2 &= 1 - \frac{(\alpha + \beta)}{2} + i(\alpha - \beta) \left(\frac{\sqrt{3}}{2} \right), \\ \lambda_3 &= 1 - \frac{(\alpha + \beta)}{2} - i(\alpha - \beta) \left(\frac{\sqrt{3}}{2} \right).\end{aligned}$$

The three-species positive equilibrium is conditionally stable if $\alpha + \beta < 2$ for $\alpha > 0$ and $\beta > 0$.

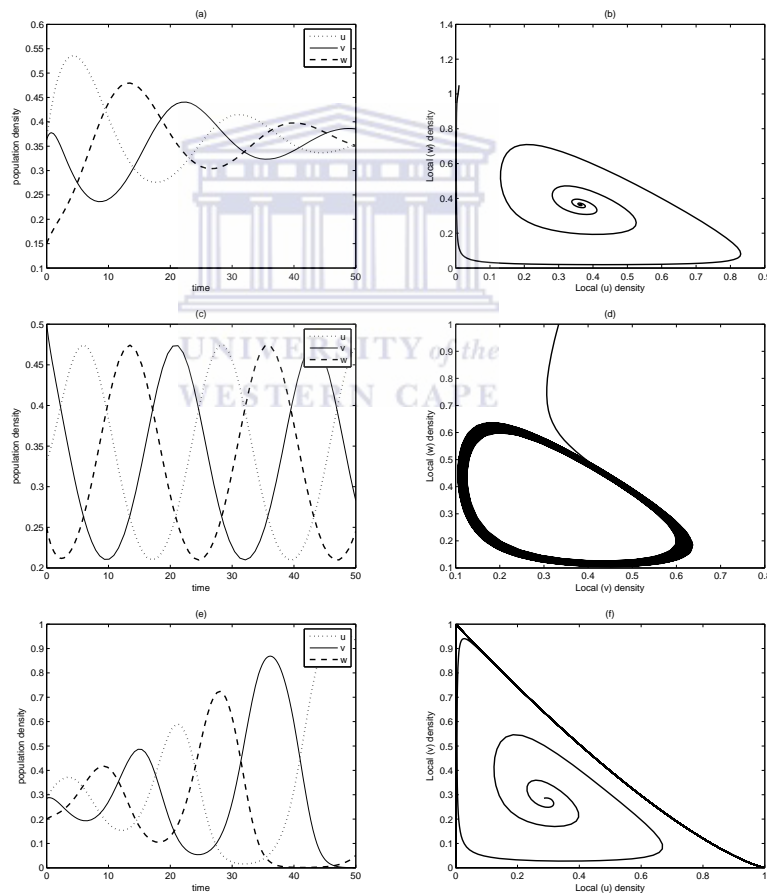


Figure 4.2.7: Typical phase trajectory limit circle solutions (a), (d) and (f) for the May-Leonard three-species competition system (4.2.28). Plots (a), (c), (e), (g) and (h) show some of the local chaotic behaviours of the three competing species u , v and w population densities.

In Figure 4.2.8, three important cases are considered for positive equilibrium $(\hat{u}, \hat{v}, \hat{w})$ are the locally asymptotically stable for $\alpha + \beta < 2$, neutrally stable for $\alpha + \beta = 2$ and

the unstable case when $\alpha + \beta > 2$. Take note of variation in their amplitudes.

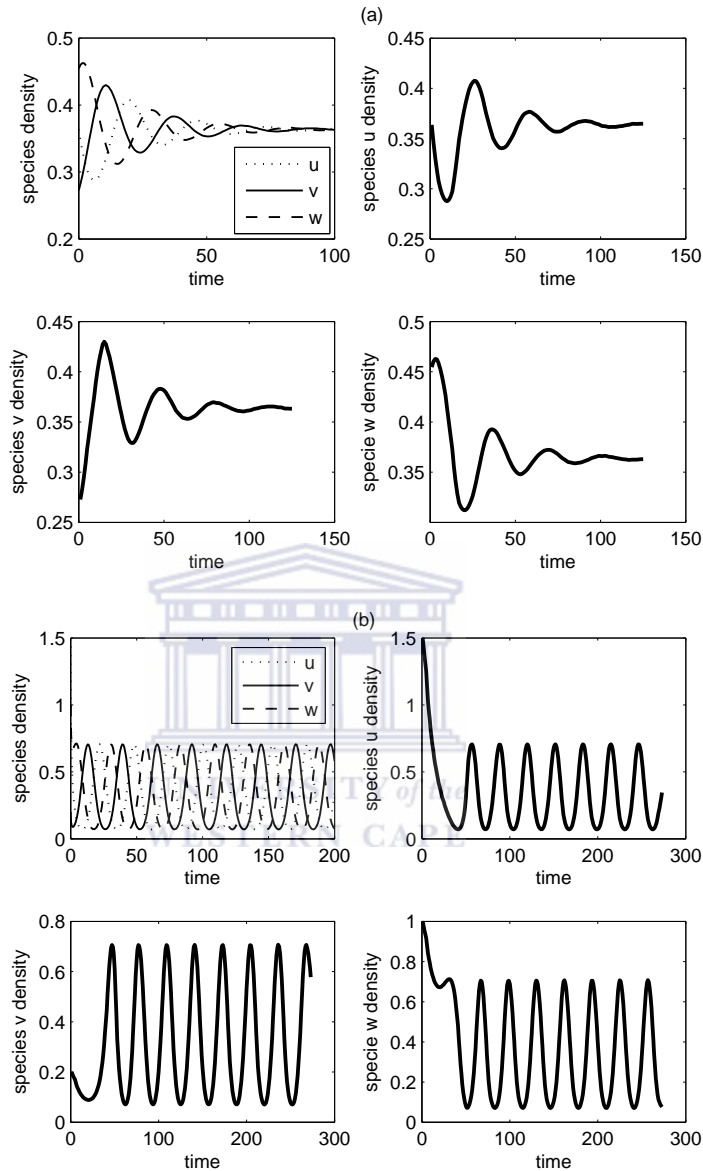


Figure 4.2.8: Plots describing individual (chaotic) behaviours in the May-Leonard three-species competition system (4.2.28).

Two-species mutualism system:

This is a type of association in theoretical ecology in which the existence of one species has no negative influence on the other. This type of model receives little attention and has not been studied as others even though its importance is comparable to that of

prey-predator and competition models. We shall analyze briefly the two-species model

$$\left. \begin{aligned} \frac{\partial U}{\partial T} &= \sigma_1 \frac{\partial^2 U}{\partial X^2} + F(U, V), \\ \frac{\partial V}{\partial T} &= \sigma_2 \frac{\partial^2 V}{\partial X^2} + G(U, V), \end{aligned} \right\} \quad (4.2.32)$$

where

$$F(U, V) = \alpha_1 U \left(1 - \frac{U}{K_1} + \beta_1 \frac{V}{K_1} \right) \quad \text{and} \quad G(U, V) = \alpha_2 V \left(1 - \frac{V}{K_2} + \beta_2 \frac{U}{K_2} \right)$$

are the nonlinear reaction terms for the two species U and V respectively, $\sigma_1, \sigma_2, \alpha_1, \alpha_2, \beta_1, \beta_2, K_1$ and K_2 are all positive parameters. This system has a similar look with equation (4.2.17), with exception that the β 's are treated positive in the present case.

We then nondimensionalize using the same parameters

$$u(t) = \frac{U(T)}{K_1}, \quad v(t) = \frac{V(T)}{K_2}, \quad t = \alpha_1 T, \quad \mu = \frac{\alpha_2}{\alpha_1}, \quad \phi = \beta_2 \frac{K_2}{K_1}, \quad \psi = \beta_1 \frac{K_1}{K_2}, \quad \sigma = \frac{\sigma_2}{\sigma_1}. \quad (4.2.33)$$

which on substitution to (4.2.32) yields

$$\left. \begin{aligned} \frac{\partial u}{\partial t} &= \frac{\partial^2 u}{\partial x^2} + (u - u^2 + \phi uv) = f(u, v), \\ \frac{\partial v}{\partial t} &= \sigma \frac{\partial^2 v}{\partial x^2} + \mu(v - v^2 + \psi uv) = g(u, v). \end{aligned} \right\} \quad (4.2.34)$$

Again, by following analysis of turing instability, we analyze the stability criteria of the non-diffusive system. We present the corresponding non-diffusion model as

$$\left. \begin{aligned} \frac{du}{dt} &= (u - u^2 + \phi uv) = f(u, v), \\ \frac{dv}{dt} &= \mu(v - v^2 + \psi uv) = g(u, v). \end{aligned} \right\} \quad (4.2.35)$$

It is not difficult to see that the steady states (\hat{u}, \hat{v}) are

$$\left. \begin{aligned} (\hat{u}, \hat{v}) &= (0, 0), \quad (\hat{u}, \hat{v}) = (1, 0), \quad (\hat{u}, \hat{v}) = (0, 1), \\ (\hat{u}, \hat{v}) &= \left(\frac{1+\phi}{1-\phi\psi}, \frac{1+\psi}{1-\phi\psi} \right). \end{aligned} \right\} \quad (4.2.36)$$

We also assume that the steady state is asymptotically stable, with all of the eigenvalues of the community matrix being negative.

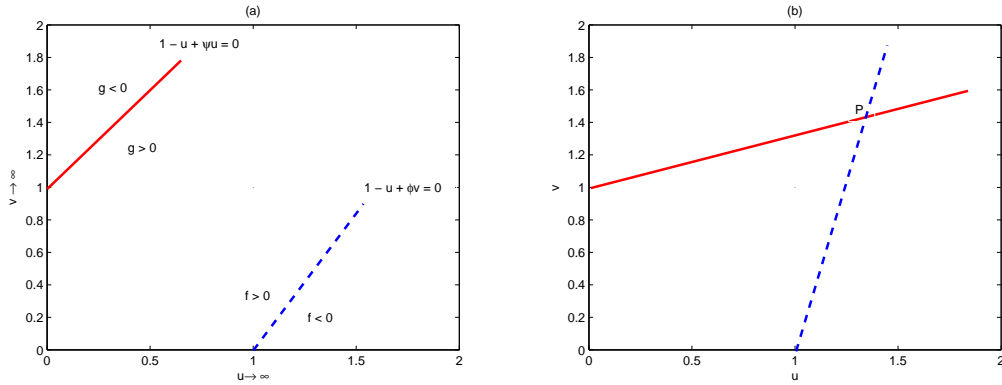


Figure 4.2.9: Phase trajectories of the two-species mutualism model (4.2.35) with limited carrying capacities. (a) With $\phi\psi > 1$, the system experience an unbounded growth as $u \rightarrow \infty$ and $v \rightarrow \infty$. (b) With $\phi\psi < 1$, all trajectories tend to a positive steady state P with $\hat{u} > 1$ and $\hat{v} > 1$.

$$B = \begin{pmatrix} \frac{\partial f}{\partial u} & \frac{\partial f}{\partial v} \\ \frac{\partial g}{\partial u} & \frac{\partial g}{\partial v} \end{pmatrix}_{(\hat{u}, \hat{v})} = \begin{pmatrix} 1 - 2\hat{u} - \phi\hat{v} & -\phi\hat{u} \\ -\mu\psi\hat{v} & \mu(1 - 2\hat{v} - \psi\hat{u}) \end{pmatrix}_{(\hat{u}, \hat{v})}. \quad (4.2.37)$$

Repeating the process of calculating the community matrix denoted by B , we can easily show that the points $(0, 0)$, $(1, 0)$ and $(0, 1)$ are all unstable, the point $(0, 0)$ is unstable node while $(1, 0)$ and $(0, 1)$ are the saddle point equilibria. Evaluation of the eigenvalues of the community matrix B for the fourth steady state for $1 - \phi\psi > 0$ (located in the positive quadrant) is an indication of stable equilibrium.

4.3 Numerical method

Nonlinear time dependent reaction-diffusion problems (for example, prey-predator, competitive and mutualism systems) often arise in the field of computational biology and intrigue lots of researchers in computational implementation and to solve numerically, the systems of partial differential equations of the general form (4.2.1), where x and t denote the time and spatial coordinate respectively. We discretize in space

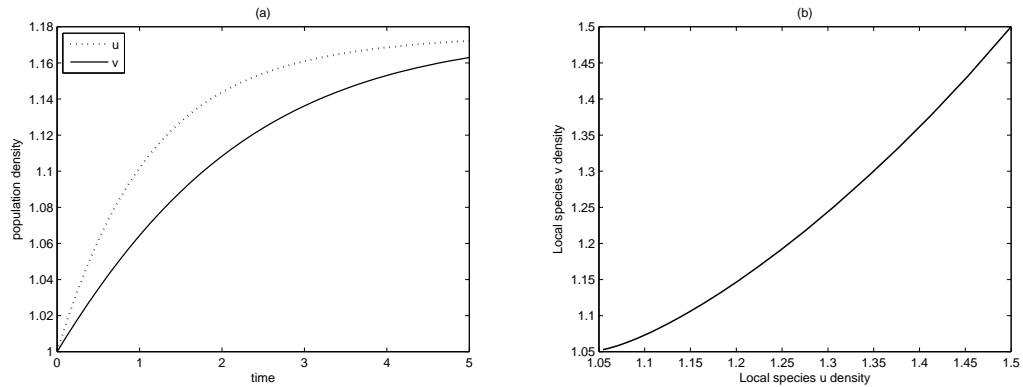


Figure 4.2.10: Phase plane trajectory for mutualism system (4.2.35). (a) Linear behaviour of species u and v . Each species experienced an unbounded population growth since the existence of one has no effect on the other and their relationship is linear as in (b). Parameter values are; $u_0 = v_0 = 1$, $\mu = 1/2$, $\phi = \psi = 0.15$ at $t = 5$.

as usual with stepsize $h = T/(N - 1)$ and approximate the spatial derivative by the fourth-order central difference formula to obtain a system of ordinary differential equations (ODEs). The resulting stiff ODEs are then solved with the various time-stepping integrators proposed in earlier chapters.

UNIVERSITY of the
WESTERN CAPE

4.4 Numerical results

In order to justify the suitability of the accuracy of ETDADAMS4 and ETDRK4 schemes. We carried out numerical experiments on the four major problems discussed and analyzed in Section 2, that is, the prey-predator system (4.2.10), competitive system (4.2.20), the mutualism or symbiosis system (4.2.34) and finally the three species system (4.2.28). The performance of ETDRK4 and ETDADAMS4 are investigated and compared with the family of exponential time differencing multi-steps schemes of order four, five and six which we denoted in this thesis as ETDM4, ETDM5 and ETDM6 respectively. The maximum absolute errors of the solution is calculated as discussed in earlier chapters

It is obvious from the results presented in figures 4.4.1 and 4.4.2 that the ETDRK4 has a better convergence as compared to other exponential time differencing methods for each of the problems considered in this chapter. Due to the similarity and the

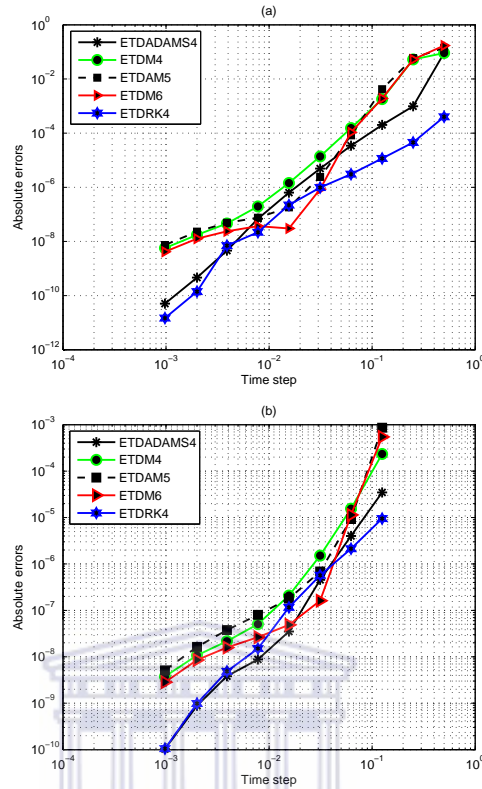


Figure 4.4.1: Absolute errors obtained by the computational methods ETDRK4, ETDM4, ETDADAMS4, ETDM4, ETDM5 and ETDM6 at various time steps, Panel (a): when applied to the prey-predator system (4.2.10) at parameter values $t = 1$, $\mu = 0.1$, $\psi = 0.08$, $\phi = 0.01$, $\delta = 0.01$, $N = 200$ and $x \in [-5, 5]$. Panel (b): when applied to the competitive system (4.2.20) with $t = 1$, $\mu = 0.5$, $\psi = 0.15$, $\phi = 0.15$, $\delta = 0.5$, $N = 200$ and $x \in [-5, 5]$.

choices of parameters used in the simulations of the competitive and the mutualism systems, one observes that the schemes behave in almost similar manner. The difference can only be seen in the amplitudes of figures 4.4.1 (b) and 4.4.2 (a). ETDADAMS4 competes very well with ETDRK4 when applied to the competitive system (4.2.20) as shown in Figure 4.4.1 (b). In all, the ETDRK4 out-shines all other schemes used.

4.5 Summary and discussions

In this chapter, we studied the dynamic complexities of the ecological models consisting of prey-predator, competitive, mutualism and competing three species dynamics are firstly studied by considering their local stability analysis in the absence of diffusion,

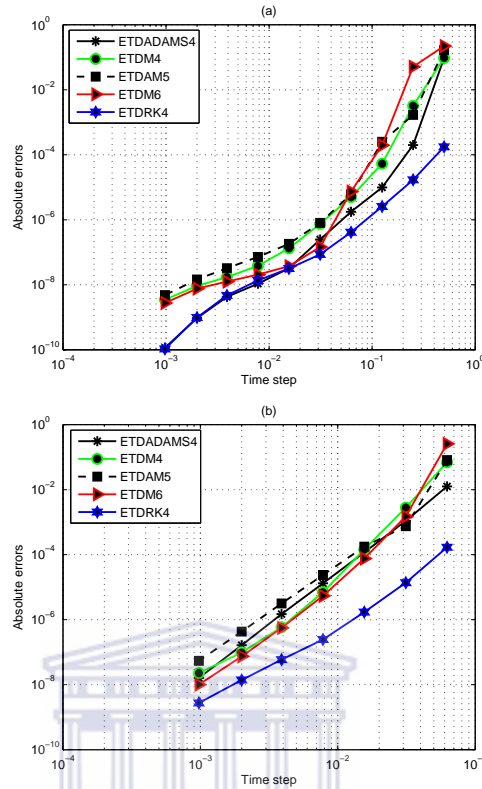


Figure 4.4.2: Absolute errors obtained by the computational methods ETDRK4, ETDM4, ETDADAMS4, ETDM4, ETDM5 and ETDM6 at various time steps. Panel (a): when applied to the mutualism system (4.2.34) at parameter values $t = 1$, $\mu = 0.5$, $\psi = 0.5$, $\phi = 0.5$, $\delta = 0.1$, $N = 200$ and $x \in [-1, 1]$. Panel (b): when applied to the competing three species system (4.2.28) with $t = 1$, $\alpha = 0.1$, $\beta = 0.5$, $\zeta_1 = 0.05$, $\zeta_2 = 0.015$, $N = 200$ and $x \in [0, 1]$.

and secondly by the numerical approach with the presence of diffusion. We discretize the problems in space using the fourth-order central finite difference scheme and integrate the resulting ODEs with the aid of exponential time differencing schemes based on the Runge-Kutta and multi-step methods of Adams-type. We compared the results obtained with both ETDADAMS4 and ETDRK4 for each of the dynamics, with their exponential fourth, fifth and sixth-orders counterparts denoted as ETDM4, ETDM5 and ETDM6 respectively. We can see the efficiency and accuracy of ETDRK4 (as compared to other methods) in figures 4.4.1 and 4.4.2. We observe that ETDRK4 is a very reliable numerical method and is computationally promising when applied to the reaction-diffusion problems.

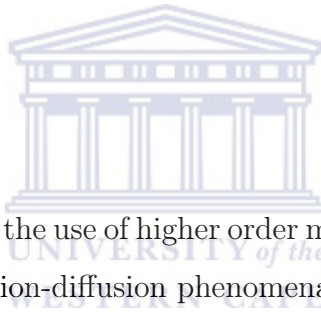
In the next chapter, we are introducing the family of fourth-order IMEX schemes

to solve three systems of reaction-diffusion problems.



Chapter 5

Higher-order numerical methods for time-dependent reaction-diffusion equations



This chapter demonstrates the use of higher order methods to solve some time-dependent stiff PDEs modelling reaction-diffusion phenomena. In the past, the most popular numerical methods for solving system of reaction-diffusion equations was based on the combination of low order finite difference method with low order time-stepping method. We extend in this report the compatibility of fourth-order finite difference scheme (in space) coupled with fourth-order time-stepping methods such as IMEXLM4, IMEXPC4, IMEXRK4 and ETDRK4 (in time), for direct integration of reaction-diffusion equations in one space dimension. Some interesting numerical anomaly phenomenons associated with steady state solutions of the examples chosen from the literature are well presented to address the naturally arise points and queries. Our findings have lead to the understanding of pattern formation such as spiral waves and patchy structures as well as some spatio-temporal dynamical structures.

5.1 Introduction

Over the last few years, numerical approximations of many time-dependent reaction-diffusion problems which occur largely in form of higher-order partial differential equations (PDEs) are addressed mainly by lower-order methods in time as a result of stiffness adhere to such a system. In recent times, many researchers have developed various higher-order methods to counter this challenge, among which are the implicit-explicit (IMEX), [10, 11, 38, 86, 112, 167]), methods and exponential time-differencing (ETD, [36, 37, 92]) methods. Other competing methods include the split step (SS, [169]), integrating factor (IF, [36, 187]) and sliders (SL, [52]) and implicit Runge-Kutta (IMRK, [30, 66]) methods among many others.

Naturally, majority of time-dependent equations such as Allen-Cahn, Brusselator, Burgers, Burger's-Fisher, Cahn-Hilliard, Fisher-Kolmogorov-Petrovsky-Piscounov (Fisher-KPP), Fitzhugh-Nagumo, Gray-Scott (GS), Kuramoto-Sivashinsky (KS), Robertson, Schnakenberg and Schrödinger equations exist in form of PDEs that combine lower- and higher-orders for their linear and nonlinear terms respectively. The efficient and accurate simulation of these type of equations become the major challenge because of the stiff diffusion term coupled with the nonlinear reaction term. We consider a general one dimensional reaction-diffusion equation of the form

$$\left. \begin{aligned} u_t &= \delta \Delta u + N(u(x, t)), & (x, t) &\in [0, T] \times [0, \infty), \\ u(x, 0) &= u_0(x), & u(0, t) &= \alpha(t), & u(T, t) &= \beta(t), \\ u &= u_i, & i &= 1, 2, 3, \end{aligned} \right\} \quad (5.1.1)$$

where $\Delta u = \partial^2 u / \partial x^2$, t and x denote the time and spatial coordinates respectively, $u_0(x)$, $\alpha(t)$ and $\beta(t)$ are the given initial and boundary conditions, $\delta > 0$ is the diffusion coefficient and N represents the (lower-order) nonlinear reaction operator that account for the reaction.

We discretize in space with step-size $h = T/N$ and approximate the second-order

spatial derivative by the fourth-order central difference operator

$$\frac{\partial^2 u}{\partial x^2} = \frac{-u_{i-2,j} + 16u_{i-1,j} - 30u_{i,j} + 16u_{i+1,j} - u_{i+2,j}}{12h^2},$$

where $u_{i,j}$ is defined as the numerical approximation to $u(x_i, t_j)$. Extension is given to $v(x_i, t_j)$ and $w(x_i, t_j)$. Spatial discretization of (5.1.1) using a well-known approach, called method of lines, in the numerical solution of evolutionary problems of PDEs in space leads to a large system of nonlinear ODEs in time, compactly written in the form

$$u_t = \delta \mathbf{L}u + \mathbf{N}(u, t), \quad u(0) = u_0(t), \quad (5.1.2)$$

where

$$\mathbf{L} = \begin{pmatrix} l_0 & l_1 & l_2 & \cdots & \cdots \\ l_{-1} & l_0 & l_1 & \ddots & \vdots \\ l_{-2} & l_{-1} & l_0 & \ddots & l_2 \\ \vdots & \ddots & \ddots & \ddots & \vdots \\ \cdots & \cdots & l_{-2} & l_{-1} & l_0 \end{pmatrix}_{(N-1) \times (N-1)}, \quad (5.1.3)$$

and $u = [u_1, u_2, \dots, u_n]^T$. The operator \mathbf{L} is the linear pentadiagonal matrix operator that represents a stiff part of the equation and \mathbf{N} is the nonlinear operator that stands for a non-stiff or mildly stiff part, and $\delta \gg 0$ is a matrix of diffusion coefficients. The function $u = e^{ikx + \lambda t} \xi$ is a solution of (5.1.2) if $(N - k^2 D - \lambda I)\xi = 0$. Thus \mathbf{N} must be strongly stable in order for the equilibrium to be asymptotically stable for all $\delta \gg 0$.

The rest of this chapter is organized as follows. A review of linear stability analysis is briefly discussed in Section 5.2. In Section 5.3, we introduced a fourth-order family of IMEX methods. Numerical results are presented in Section 5.4 to demonstrate the efficiency of the methods. We test the methods discussed in Section 5.3 with some numerical examples based on multi-species competitive community models, and finally summarize our findings in Section 5.5.

5.2 Qualitative analysis of model problems

We describe briefly in this section the behaviour of a coupled system of n interacting species, where $n \geq 1$ around the steady state through stability principle. Let us rewrite the evolution equation (5.1.2) for the case when $n = 1$, that is, the case of only one variable system.

$$\frac{dU}{dt} = f(U) \quad (5.2.1)$$

where $f(U)$ is the term containing both the linear and nonlinear part of (5.1.2) after we have scaled the diffusion coefficient, $\delta = 1$. Equation (5.2.1) satisfies a steady state condition if

$$\frac{dU_s}{dt} = f(U_s) = 0. \quad (5.2.2)$$

With slight perturbation, say u , we have $U = U_s + u$, subscript s stands for steady state. Putting together all these facts, we obtain

$$\frac{dU}{dt} = \frac{dU_s}{dt} + \frac{du}{dt} = \frac{du}{dt} = f(U), \quad (5.2.3)$$

we proceed further by linearizing the non-linear function $f(U)$ by neglecting the higher order terms to have

$$f(U) = f(U_s) + \left(\frac{df}{dU} \right)_s u + \left(\frac{d^2 f}{dU^2} \right)_s u^2 + \dots = \left(\frac{df}{dU} \right)_s u. \quad (5.2.4)$$

The equation for the evolution of the perturbation of u , by using (5.2.1) becomes

$$\frac{du}{dt} = f(U) = \left(\frac{df}{dU} \right)_s u, \quad (5.2.5)$$

from (5.2.5), after further simplification, it implies that

$$u = \hat{u}e^{\lambda t}, \quad (5.2.6)$$

where $\lambda = (df/dU)_s$ and $\hat{u} = u(0)$. The parameter λ here typifies whether system (5.1.2) is steady or unstable, if $\lambda > 0$, u will increase and the system will leave its

steady state. On the other hand, if $\lambda < 0$, it follows that all the eigenvalues of \mathbf{L} have negative real part, the perturbation will damp in such a way that the system is steady.

Consequently, for the two-variable system ($n = 2$), we follow closely the steps above and describe the coupled equations as:

$$\left. \begin{aligned} \frac{dU}{dt} &= f(U, V), \\ \frac{dV}{dt} &= g(U, V), \end{aligned} \right\} \quad (5.2.7)$$

with associated steady state U_s, V_s that satisfies $dU_s/dt = f(U_s, V_s)$ and $dV_s/dt = g(U_s, V_s)$, we as usual obtain $U = U_s + u$ and $V = V_s + v$ after a little perturbation with $u \ll U_s$ and $v \ll V_s$ respectively to obtain

$$\left. \begin{aligned} f(U, V) &= f(U_s, V_s) + \left(\frac{df}{dU}\right)_s u + \left(\frac{df}{dV}\right)_s v + \cdots \left(\frac{df}{dU}\right)_s u + \left(\frac{df}{dV}\right)_s v, \\ g(U, V) &= g(U_s, V_s) + \left(\frac{dg}{dU}\right)_s u + \left(\frac{dg}{dV}\right)_s v + \cdots \left(\frac{dg}{dU}\right)_s u + \left(\frac{dg}{dV}\right)_s v, \end{aligned} \right\} \quad (5.2.8)$$

after dropping the higher order terms involved. From left hand side of (5.2.8), let the associated Jacobian matrix for the steady state U_s, V_s be

$$\mathbf{J} = \begin{pmatrix} p_{11} & p_{12} \\ p_{21} & p_{22} \end{pmatrix}. \quad (5.2.9)$$

Using the facts in (5.2.8), and by definition, $dU_s/dt = 0$ and $dV_s/dt = 0$, we obtain the system of equations

$$\left. \begin{aligned} \frac{du}{dt} &= p_{11}u + p_{12}v, \\ \frac{dv}{dt} &= p_{21}u + p_{22}v, \end{aligned} \right\} \quad (5.2.10)$$

whose solution can be written as $u = \hat{u}e^{\lambda t}$ and $v = \hat{v}e^{\lambda t}$. We obtain a non-trivial solution on substituting for u and v in (5.2.10), if the determinant

$$\begin{pmatrix} p_{11} - \lambda & p_{12} \\ p_{21} & p_{22} - \lambda \end{pmatrix} = 0, \quad (5.2.11)$$

which implies that

$$\lambda^2 - (p_{11} + p_{22})\lambda + (p_{11}p_{22} - p_{12}p_{21}) = 0. \quad (5.2.12)$$

On replacing $p_{11} + p_{22} = \xi$ and $p_{11}p_{22} - p_{12}p_{21} = \varphi$, we obtain the roots of (5.2.12) as

$$\lambda_{1,2} = \frac{-\xi \pm \sqrt{\xi^2 - 4\varphi}}{2}, \quad (5.2.13)$$

if φ is positive, the quantity under the square root is either smaller than ξ^2 , or it is negative. If φ is negative, the solutions are complex with real part $-\xi$, which is negative. Otherwise, the roots must be smaller in absolute value than ξ , so that the two eigenvalues must still be negative, in this regard, we can say that the steady state is stable since the real parts of both eigenvalues is negative.

Finally, we can write the solution of the system (5.2.10) as $u(t) = \hat{u}_1 e^{\lambda_+ t} + \hat{u}_2 e^{-\lambda_- t}$ and $v(t) = \hat{v}_1 e^{\lambda_+ t} + \hat{v}_2 e^{-\lambda_- t}$. If $\lambda_{\pm} < 0$, the perturbation will decrease with respect to time and the steady state is stable. If $\lambda_{\pm} > 0$, the perturbation is increased with time and the steady state is unstable, and finally, if $\lambda_+ > 0$ and $\lambda_- < 0$, perturbation in this regard is either increases or decreases and the steady state becomes unstable.

The two competing species systems described above is comparatively simple and has been the major focus of study in the past few decades. However, a general case of n competing species has received little attention and is still poorly examined with just few paper considering spatiotemporal dynamics of a competing system with case $n > 2$. Among the few work that has been reported are the combined efforts in [151, 154, 171]. It was pointed out in [190] that the phase space for the system of three-species may contain not only the equilibrium points but also the limit cycles, and apart from monotonous travelling fronts that interlink different equilibrium (steady) states of the system, there could also be an oscillating fronts showing the effects of the dynamical stabilization of an unstable equilibrium and spatiotemporal chaos.

We conclude with the analysis given above for the case $n > 2$, for system involving n variables where the characteristic equation is of degree n . This type of equation is expected to have n distinct roots whose eigenvalues form the Jacobian matrix of size

$N \times N$. The system at this point is stable if there is no eigenvalue λ_j , $j = 1, \dots, n$ has positive real part. For the sake of brevity, readers are referred to [119] for detail information on analysis of competition in a multi-species system.

5.3 Numerical methods

Generally, differential equations are solved by integration, but unfortunately, for many practical applications encountered in science and engineering, most systems of differential equations cannot be integrated to give an accurate analytical (exact) solution, but rather need to be solved numerically. Development of accurate numerical methods for integration of large scale time-dependent reaction-diffusion partial differential equations that are used to model physical problems have been the subject of activity since last decade. Numerical solutions of such equations are computationally demanding due to the need to achieve high accuracy in order to circumvent numerical instabilities and stiffness in such models [11, 49, 103, 147, 182, 190]. Our subject in this chapter is to consider the fourth-order time-stepping methods such as implicit-explicit linear multi-step (IMEXLM), implicit-explicit predictor-corrector (IMEXPC), implicit-explicit Runge-Kutta (IMEXRK), and exponential time-differencing Runge-Kutta (ETDRK) methods with fourth-order finite difference schemes to discretize in space. We shall briefly discuss each of these methods.

Implicit-explicit linear multi-step (IMEXLM) methods:

Implicit-explicit schemes whose constructions were based on the general linear multi-step methods

$$\frac{1}{k}u_{n+1} + \frac{1}{k} \sum_{j=0}^{s-1} a_j u_{n-j} = \sum_{j=0}^{s-1} b_j \mathbf{N}(u_{n-j}) + \sum_{j=-1}^{s-1} c_j \mathbf{L}(u_{n-j}), c_{-1} \neq 0, \quad (5.3.1)$$

have widely been used by many researchers [11, 38, 112, 167], as one of the methods proposed some years ago to integrate the dynamical systems arising as a result of spatially discretized time-dependent partial differential equations of the form (5.1.1)

that consists of linear $L(u)$ and nonlinear $N(u)$ parts. Recently, Hundsdorfer and Ruuth [86], develop some higher-order implicit-explicit linear multi-step methods to examine both monotonicity and boundedness properties for the linear test problems for advection, diffusion and reactions. The main idea of IMEX methods is to use explicit multi-step scheme to tackle the nonlinear part and an implicit method to advance the linear part of (5.1.2). We shall focus our attention on fourth-order schemes. Ascher et al. [10] develop a general fourth-order, four-step IMEX scheme based on linear multi-step methods (5.3.1), for use in convection-diffusion equation. We refer here to the scheme as IMEXLM4, the formula for this scheme requires the use of only one evaluation of the nonlinear term per time step. The method IMEXLM4 when applied to (5.1.2) is defined as follows

$$u_{n+1} = \left(\frac{25}{12} \mathbf{I} - k\mathbf{L} \right)^{-1} \left[4u_n - 3u_{n-1} + \frac{4}{3}u_{n-2} - \frac{1}{4}u_{n-3} + 4k\mathbf{N}(u_n) - 6k\mathbf{N}(u_{n-1}) + 4k\mathbf{N}(u_{n-2}) - k\mathbf{N}(u_{n-3}) \right], \quad (5.3.2)$$

where \mathbf{I} is the identity matrix, \mathbf{L} and \mathbf{N} form the linear and nonlinear part of (5.1.2), this scheme has been considered in a Navier-Stokes context in [91]. Derivations, stability properties and starting values used in the computation of (5.3.2) are taken from Ascher et al. [10].

Implicit-explicit predictor-corrector (IMEXPC) methods:

This is another family of linear multi-step methods that adopt IMEX schemes, the most popular among these are the explicit Adam-Bashforth and implicit Adams-Moulton methods that have been used in various forms by different authors [10, 11, 36, 86, 92] in the literature. A simple way to find $u_{n+1}^{(0)}$ is to make use explicit method. Thus, a predictor formula (explicit multi-step formula) is used to obtain a first estimate of the next value of the dependent variable and the corrector formula is applied iteratively until convergence is reached. This approach was earlier introduced by Ascher et al. [10] in a different fashion for time-dependent PDEs. The third- and fourth-order IMEXPC schemes that we use to perform the time integration in this chapter are taken

PC(3,3) [112] and STVBDF4 [66] which we re-write when applied to (5.1.2) as

predictor:

$$\begin{aligned}
 \bar{u}_{n+1} = & \left[\left(\frac{1}{2}\gamma^2 + \gamma + \frac{1}{3} + \eta \right) \mathbf{I} - \left(\frac{\gamma^2 + \gamma}{2} + c \right) k\mathbf{L} \right]^{-1} \\
 & \left\{ \left[\left(\frac{3}{2}\gamma^2 + 2\gamma - \frac{1}{2} + \eta \right) \mathbf{I} + \left(1 - \gamma^2 - 3c + \frac{23}{12}\eta \right) k\mathbf{L} \right] u_n \right. \\
 & + \left[\left(\frac{-3}{2}\gamma^2 - \gamma + 1 \right) \mathbf{I} + \left(\frac{\gamma^2 - \gamma}{2} + 3c - \frac{4}{3}\eta \right) \right] u_{n-1} \\
 & + \left[\left(\frac{1}{2}\gamma^2 - \frac{1}{6} \right) \mathbf{I} + \left(\frac{5}{12}\eta - c \right) k\mathbf{L} \right] u_{n-2} \\
 & + \left(\frac{\gamma^2 + 3\gamma}{2} + 1 + \frac{23}{12}\eta \right) k\mathbf{N}(u_n) \\
 & \left. - \left(\gamma^2 + 2\gamma + \frac{4}{3}\eta \right) k\mathbf{N}(u_{n-1}) + \left(\frac{\gamma^2 + \gamma}{2} + \frac{5}{12}\eta \right) k\mathbf{N}(u_{n-2}) \right\}, \quad (5.3.3)
 \end{aligned}$$

corrector:

$$\begin{aligned}
 u_{n+1} = & \left[\left(\frac{1}{2}\gamma^2 + \gamma + \frac{1}{3} + \eta \right) \mathbf{I} - \left(\frac{\gamma^2 + \gamma}{2} + c \right) k\mathbf{L} \right]^{-1} \\
 & \left\{ \left[\left(\frac{3}{2}\gamma^2 + 2\gamma - \frac{1}{2} + \eta \right) \mathbf{I} + \left(1 - \gamma^2 - 3c + \frac{23}{12}\eta \right) k\mathbf{L} \right] u_n \right. \\
 & + \left[\left(\frac{-3}{2}\gamma^2 - \gamma + 1 \right) \mathbf{I} + \left(\frac{\gamma^2 - \gamma}{2} + 3c - \frac{4}{3}\eta \right) \right] u_{n-1} \\
 & + \left[\left(\frac{1}{2}\gamma^2 - \frac{1}{6} \right) \mathbf{I} + \left(\frac{5}{12}\eta - c \right) k\mathbf{L} \right] u_{n-2} \\
 & + \left(\frac{\gamma^2 + \gamma}{2} + c \right) k\mathbf{N}(\bar{u}_{n+1}) \\
 & + \left(1 - \gamma^2 - 3c + \frac{23}{12}\eta \right) k\mathbf{N}(u_n) \\
 & \left. + \left(\frac{\gamma^2 - \gamma}{2} + 3c - \frac{4}{3}\eta \right) k\mathbf{N}(u_{n-1}) + \left(\frac{5}{12}\eta - c \right) k\mathbf{N}(u_{n-2}) \right\}, \quad (5.3.4)
 \end{aligned}$$

where (γ, η, c) are treated as free parameters that enable us to generate a family of third-order IMEX predictor-corrector schemes and $\mathbf{N}(u)$ is $\mathbf{N}(u, t)$. The rest of starting values for the IMEX predictor-corrector methods (5.3.3) and (5.3.4) used in the computational

experiments can be found in [112]).

The fourth-order IMEX predictor-corrector methods [66] are defined here in conformity with (5.1.2) as

predictor:

$$\begin{aligned} \bar{u}_{n+1} = & \left(\mathbf{I} - \frac{4207}{8192}k\mathbf{L} \right)^{-1} \\ & \left\{ \left(\frac{21531}{8192}u_n - \frac{22753}{8192}u_{n-1} + \frac{12245}{8192}u_{n-2} - \frac{2831}{8192} \right) \right. \\ & + \mathbf{L} \left(-\frac{3567}{8192}u_n + \frac{697}{24576}u_{n-1} + \frac{4315}{24576}u_{n-2} - \frac{41}{384}u_{n-3} \right) \\ & + k \left[\frac{13261}{8192}\mathbf{N}(u_n) - \frac{75029}{24576}\mathbf{N}(u_{n-1}) + \frac{54799}{24576}\mathbf{N}(u_{n-2}) \right. \\ & \left. \left. - \frac{15245}{24576}\mathbf{N}(u_{n-3}) \right] \right\}, \end{aligned} \quad (5.3.5)$$

corrector:

$$u_{n+1} = (25\mathbf{I} - 12k\mathbf{L})^{-1} [48u_n - 36u_{n-1} + 16u_{n-2} - 3u_{n-3} + 12k\mathbf{N}(\bar{u}_{n+1})], \quad (5.3.6)$$

where \mathbf{I} is the identity matrix, \mathbf{L} is the linear part and \mathbf{N} stands for the nonlinear part of (5.1.2).

Implicit-explicit Runge-Kutta (IMEXRK) methods:

Fourth-order implicit-explicit Runge-Kutta (IMEXRK4) schemes belong to the family of linear multi-step methods that have been used by various authors in different forms. The main idea of IMEX methods is to use explicit scheme to advance the nonlinear part and an implicit method to advance the linear part to circumvent some of the difficulties posed on solving nonlinear systems of the form (5.1.2). Recently, Ascher et al. [11] developed a family of L-stable two-,three-stages diagonally implicit Runge-Kutta (DIRK) and four-stage, third-order combination schemes whose constructions were based on implicit-explicit Runge-Kutta methods for integration of convection-diffusion equation. In another development, Kennedy and Carpenter [95] constructed a family of

higher-order, L-stable explicit and singly diagonally implicit Runge-Kutta using IMEX schemes for addressing one-dimensional convection-diffusion-reaction equations. More recently, Koto [103] constructed IMEX Runge-Kutta schemes for reaction-diffusion equations with an established convergence and stability. An explicit Runge-Kutta (ERK) method is used to solve the non-stiff part $\mathbf{N}(u)$ and a diagonally implicit Runge-Kutta (DIRK) method is engaged to attack the stiff part $\mathbf{L}(u)$ of problem (5.1.2) to circumvent the issue of stability restriction inherent in the explicit method. The linearly implicit and explicit Runge-Kutta methods [26, 27, 30] are specified by the Butcher tableaux:

Table 5.3.1: Butcher s -stage implicit-explicit Runge-Kutta tableau.

c_1	0				0					
c_2	0	η			\hat{a}_{21}	0				
c_3	0	a_{32}	η		\hat{a}_{31}	\hat{a}_{32}	0			
\vdots	\vdots	\vdots	\ddots	\ddots	\vdots	\vdots	\ddots	\ddots		
c_{s+1}	0	$a_{s+1,2}$	\cdots	$a_{s+1,s}$	η	$\hat{a}_{s+1,1}$	$\hat{a}_{s+1,2}$	\cdots	$\hat{a}_{s+1,s}$	0
	0	b_2	\cdots	b_s	η	\hat{b}_1	\hat{b}_2	\cdots	\hat{b}_s	\hat{b}_{s+1}

Therefore, from (5.1.2),

$$\left. \begin{aligned} u_1 &= u_n, \\ u_i &= u_n + h \left(\sum_{j=2}^k a_{k,j} \mathbf{L}u_j + \sum_{j=1}^{k-1} \hat{a}_{k,j} \mathbf{N}(u_j, t_n + hc_j) \right), \quad 2 \leq k \leq s+1, \\ u_{n+1} &= u_n + h \left(\sum_{k=2}^{s+1} b_k \mathbf{L}u_k + \sum_{k=1}^{s+1} \hat{b}_k \mathbf{N}(u_k, t_n + hc_k) \right), \end{aligned} \right\} (5.3.7)$$

as t_n tends to $t_{n+1} = t_{n+h}$, where h is the step size, \mathbf{L} is computed as a toeplitz matrix of size $N - 1 \times N - 1$.

Stability of linear multi-step methods

We follow the concept of Lax-stability [157, 158, 185] for method of lines (MoL) based on linear multi-step time integration methods to give an overview of the stability properties of various IMEX schemes (IMEXLM4, IMEXPC4 and IMEXRK4) discussed above. An s -step linear multi-step method (5.3.1) to the semi-discretization of an

Table 5.3.2: Fourth-order implicit (Table(6.5) of [69]) and explicit (Equation (14) of [30]) Runge-Kutta Methods.

0					0		0				
0	$\frac{1}{4}$				$\frac{1}{4}$		$\frac{1}{4}$	0			
0	$\frac{1}{2}$	$\frac{1}{4}$			$\frac{3}{4}$		$-\frac{1}{4}$	1	0		
0	$\frac{17}{50}$	$-\frac{1}{25}$	$\frac{1}{4}$		$\frac{11}{20}$		$-\frac{13}{100}$	$\frac{43}{75}$	$\frac{8}{75}$	0	
0	$\frac{371}{1360}$	$-\frac{137}{2720}$	$\frac{15}{544}$	$\frac{1}{4}$	$\frac{1}{2}$		$-\frac{6}{85}$	$\frac{42}{85}$	$\frac{179}{1360}$	$-\frac{15}{272}$	0
0	$\frac{25}{24}$	$-\frac{49}{48}$	$\frac{125}{16}$	$-\frac{85}{12}$	$\frac{1}{4}$		0	$\frac{79}{24}$	$-\frac{5}{8}$	$\frac{25}{2}$	$-\frac{85}{6}$ 0
0	$\frac{25}{24}$	$-\frac{49}{48}$	$\frac{125}{16}$	$-\frac{85}{12}$	$\frac{1}{4}$		0	$\frac{25}{24}$	$-\frac{49}{48}$	$\frac{125}{16}$	$-\frac{85}{12}$ $\frac{1}{4}$

autonomous linear evolution equation

$$u_t = Lu, \quad u(x, 0) = u_0(x), \quad t \in [0, T], \quad (5.3.8)$$

where L is regarded as a linear operator that is independent of time, and u is a vector or scalar function of t and of one or more variables x , and on approximating (5.3.8) with respect to the space variables by the central fourth order finite difference, as discussed above, on a discrete grid, we obtained a system of ODEs

$$\eta_t = \mathbf{L}\eta, \quad \eta(0) = \eta_\kappa, \quad (5.3.9)$$

where $\eta(t)$ is a vector of dimension (say, N) and \mathbf{L} remains the matrix operator, and the subscript κ is an arbitrary positive real parameter. The semidiscretization of (5.3.8) can be written in the form

$$\sum_{j=0}^s \alpha_j \eta^{n+j} - k \sum_{j=0}^s \beta_j \mathbf{L} \eta^{n+j} = 0, \quad (5.3.10)$$

which is governed by the first and second characteristic polynomials

$$\rho(z) = \sum_{j=0}^s \alpha_j z^j, \quad \sigma(z) = \sum_{j=0}^s \beta_j z^j, \quad \text{for } 0 \leq j \leq s-1,$$

where $\alpha_s = +1$, and that the sum of α_0 and β_0 are not both zero, that is, $|\alpha_0 + \beta_0| \neq 0$. Hence, the stability region \mathbf{S} of the linear multi-step method is the set of numbers $\nu \in \mathbb{C}$ for which all roots z of the stability polynomial $\pi_\nu(z) = \rho(z) - \nu\sigma(z)$ satisfy $|z_i| \leq 1$. For further details on this topic, readers are referred to [11, 30, 69].

For the fourth-order exponential time differencing Runge-kutta method, we present the extension of this scheme to suite the solution of three system of equations, (e.g., (5.4.1)) in the following way:

$$\begin{aligned} u_{n+1} = & u_n e^{\mathbf{L}h} + h[4\varphi_2(\mathbf{L}h) - 3\varphi_1(\mathbf{L}h) + \varphi_0(\mathbf{L}h)]\mathbf{N}(u_n, v_n, w_n, t_n) \\ & + 2h[\varphi_1(\mathbf{L}h) - 2\varphi_2(\mathbf{L}h)]\mathbf{N}(a_n, t_n + h/2) \\ & + 2h[\varphi_1(\mathbf{L}h) - 2\varphi_2(\mathbf{L}h)]\mathbf{N}(b_n, t_n + h/2) \\ & + h[\varphi_2(\mathbf{L}h) - 2\varphi_1(\mathbf{L}h)]\mathbf{N}(c_n, t_n + h), \end{aligned} \quad (5.3.11)$$

and

$$\begin{aligned} a_n &= u_n e^{\mathbf{L}h/2} + (\mathbf{L}h/2)\varphi_0(\mathbf{L}h/2)\mathbf{N}(u_n, v_n, w_n, t_n) \\ b_n &= u_n e^{\mathbf{L}h/2} + (\mathbf{L}h/2)[\varphi_0(\mathbf{L}h/2) - 2\varphi_1(\mathbf{L}h/2)]\mathbf{N}(u_n, v_n, w_n, t_n) \\ &\quad + h\varphi_1(\mathbf{L}h/2)\mathbf{N}(a_n, t_n + h/2), \\ c_n &= u_n e^{\mathbf{L}h} + h[(\varphi_0(\mathbf{L}h) - 2\varphi_1(\mathbf{L}h)]\mathbf{N}(u_n, v_n, w_n, t_n) + 2h\varphi_1(\mathbf{L}h)\mathbf{N}(c_n, t_n + h), \end{aligned}$$

where \mathbf{I} is the $N \times N$ identity matrix, \mathbf{L} and \mathbf{N} are the linear and nonlinear operators as previously defined.

5.4 Numerical results

In this section, we present some numerical results using the time-stepping methods discussed above. We choose a range of one-dimensional examples to study the dynamics of an ecological model consisting of three competing species with impulsive control strategy. The solution of the system under consideration are numerically obtained with some initial conditions that are biologically feasible in the range of chosen parametric values. The three reaction-diffusion problems considered are still of current and recurring interest. To justify the efficiency and applicability of the present method, we report the relative errors as defined in (2.4.20).

Nonlinear stiff reaction-diffusion system:

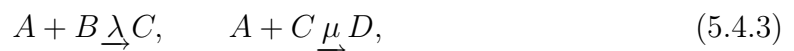
Spatiotemporal dynamics of a community of three competitive species [182] is described qualitatively by the following equations

$$\left. \begin{aligned} u_t &= \phi u_{xx} - \lambda_1 uv - uw, \\ v_t &= \varphi v_{xx} - \lambda_2 uv, \\ w_t &= \psi w_{xx} - \lambda_3 uv - uw, \end{aligned} \right\} x \in (0, 1), \quad (5.4.1)$$

with mixed Dirichlet and Neumann boundary conditions

$$\left. \begin{aligned} u &= \alpha > 0, & v_x &= 0, & w_x &= 0, & x &= 0, \\ u_x &= 0, & v &= \beta > 0, & w_x &= 0, & x &= 1, \end{aligned} \right\} \quad (5.4.2)$$

where $u(x, t), v(x, t), w(x, t)$, represent the densities of species A, B, C, respectively at time t for position x in space. Coefficients $\lambda_1, \lambda_2, \lambda_3$ give the intrinsic growth rate of the species. Diffusion coefficients ϕ, φ and ψ describe the intensity of the spatial mixing due to self-motion of species. The particular system discussed here mimics the chemical process



discussed in ([68, 176, 182]), where a reasonable hypotheses for the concentrations to be non-negative was made. We follow closely by taking our initial conditions to be

$$\left. \begin{aligned} u(x, t = 0) &= 27.3x^4 - 67x^3 + 53.7x^2 - 15.6x + 1.6, \\ v(x, t = 0) &= 9x^4 - 13.77x^3 + 5.5x^2, \\ w(x, t = 0) &= 0. \end{aligned} \right\} \quad (5.4.4)$$

In this example, we have considered a more general situation in which the species A and B are allowed to coexist everywhere in the given domain for $0 < \beta < \alpha < 1$. It was opined in [182], that due to the fast nature of the interaction between A and B, diffusion and slower reaction are expected to be negligible on comparison with intermediate C that was rapidly created until either of A or B is completely depleted.

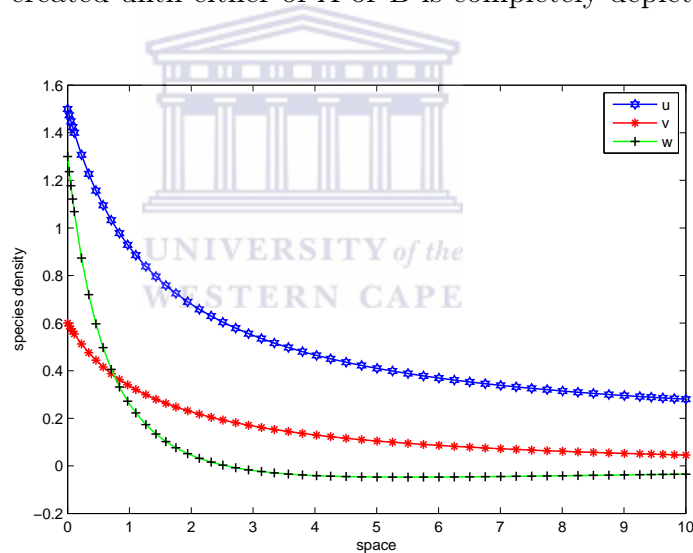


Figure 5.4.1: Geometric decay of the three species described in problem (5.4.1). Solution is obtained at $t = 20$ for parameter values $\phi = \varphi = \psi = 0$, $\lambda_1 = 0.1$, $\lambda_2 = 0.5$, $\lambda_3 = 0.5$ with initial size 1.5, 0.6, 1.3 for u , v and w respectively.

Figure 5.4.2 shows the solution explaining the coexistence of the two species u and v in the domain $\Omega = (0, 1)$, B is used up on interaction with A to produce C that do not coexist initially, see Figure 5.4.3. The simulation is performed here at different intervals within the domain under consideration. In Figure 5.4.3, the diffusivity ratio $\epsilon = 0.001$ at $t = 0.00007$ in the interval $0 \leq x \leq 1$, for (a). Panels (b) and (c) on $0 \leq x \leq 1$ at $t = 0.009$ and $t = 2$ respectively for $\epsilon = 1$, in panels (d)-(f), simulations

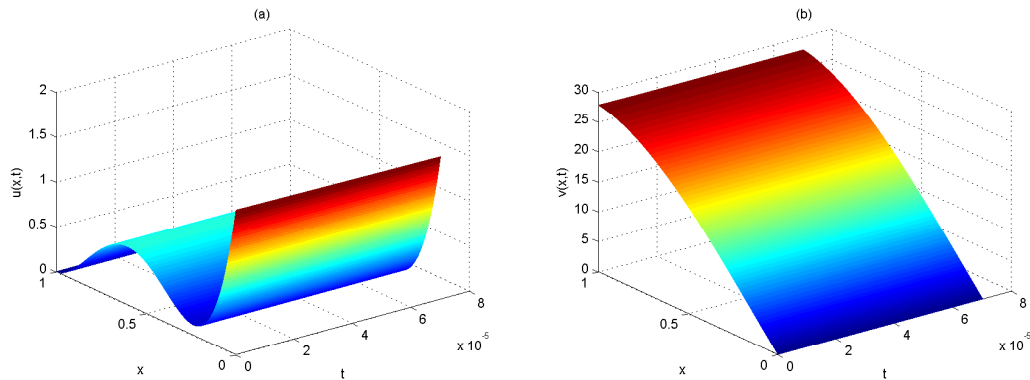


Figure 5.4.2: Surface plot of the solutions of (5.4.1) at $t = 0.00007$, for the case when the diffusion coefficients are treated to be equal and taken as $\epsilon = 0.001$.

are done with $\epsilon = 1$, at $t = 0.00007, 0.009, 1.086$ on $0 \leq x \leq 0.2$.

Finally, we obtain a steady-state solution for the reaction rate q , when the value of $\lambda = 0.5$ is fixed. This assertion was demonstrated in Figure 5.4.5, panels (a)-(c). Clearly, the solutions as $t \geq 0$, $k > 0$ has no influence on time, hence, a steady state is observed.

Results in Figure 5.4.5 (a)-(c) demonstrate the steady-state solution of the reaction rate $q = e^{\lambda uv}$, $\lambda = 0.5$, when changes in time $t \geq 0$ has no impact on the solutions obtained. Plots (d)-(f) show the overlapping phenomena in the reaction rate $q = \lambda uv$. Note the different scales on the vertical axes.

The result of the numerical experiment in Figure 5.4.6 shown that the ETDRK4 method provides more stable and reliable result with an accuracy of 10^{-13} when compared to the family of IMEX methods of the same orders. IMEXLM4 has accuracy of 10^{-7} followed by IMEXRK4 with 10^{-6} and IMEXPC4 with 10^{-5} at $t = 1/1024$.

Robertson's problem:

We present here the three-specie system which coincides at some parameter values with Robertson example [74, 161], (a reaction-diffusion equation with stiff chemistry), a one dimensional reaction-diffusion equations that describes an interaction between three

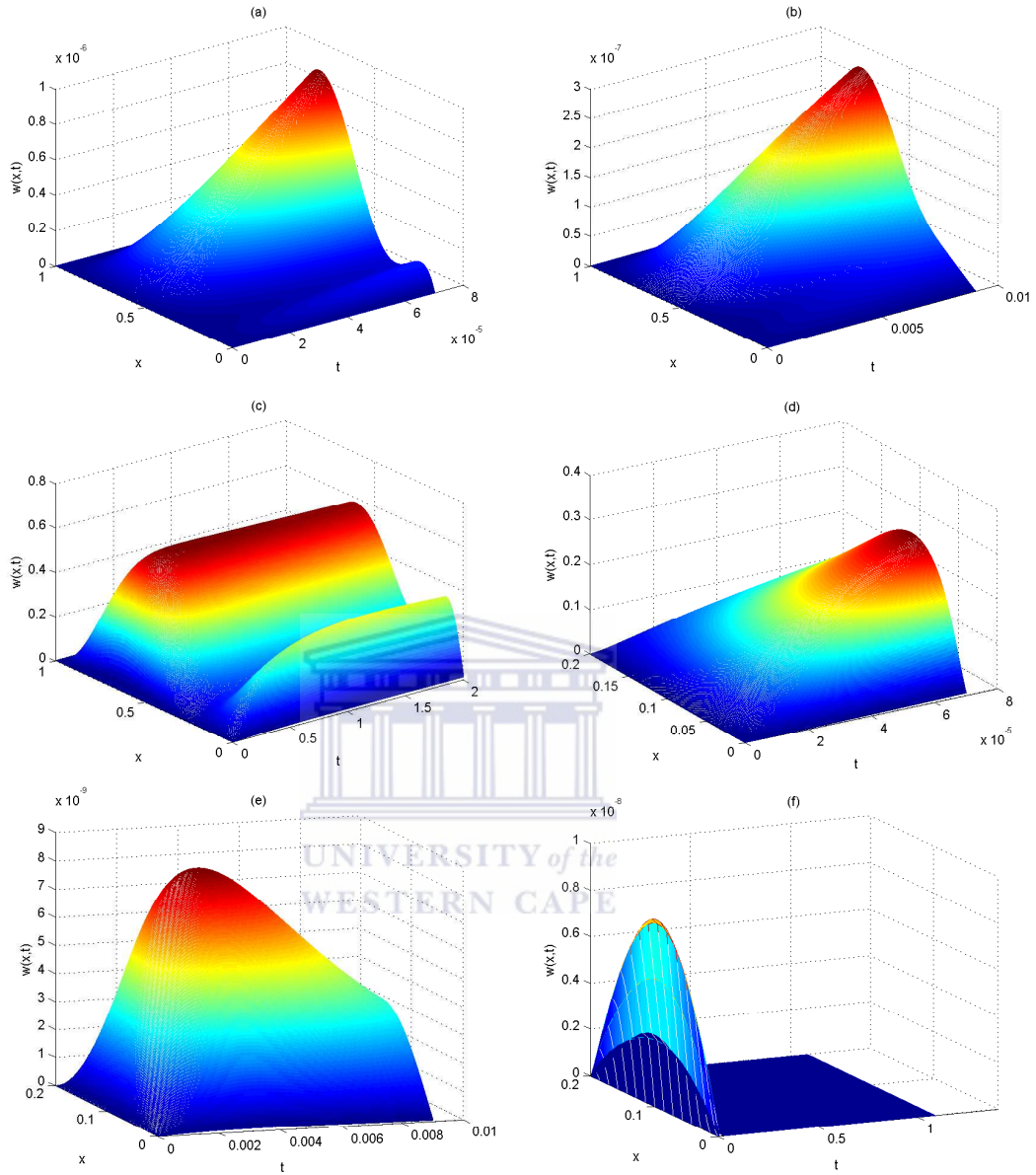


Figure 5.4.3: Surface plot of the solutions as a result of coexistence of species A and B to produce C at different time steps: (a) $t = 0.00007$, $\epsilon = 0.001$, $x \in [0, 1]$, (b) $t = 0.009$, $\epsilon = 1$, $x \in [0, 1]$, (c) $t = 2$, $\epsilon = 1$, $x \in [0, 1]$, (d) $t = 0.00007$, $\epsilon = 1$, $x \in [0, 0.2]$, (e) $t = 0.009$, $\epsilon = 1$, $x \in [0, 0.2]$ and (f) $t = 1.086$, $\epsilon = 1$, $x \in [0, 0.2]$, in (5.4.1), where ϵ is defined as diffusivity ratio and $k = 500$, the number of solutions attained between $t_{initial}$ and t_{final} .

species

$$\left. \begin{aligned} u_t &= \alpha u_{xx} - \tau_1 u + \tau_2 v w, \\ v_t &= \beta v_{xx} + \tau_3 u - \tau_4 v w - \tau_5 v^2, \\ w_t &= \gamma w_{xx} + \tau_6 v^2, \end{aligned} \right\} \quad (5.4.5)$$

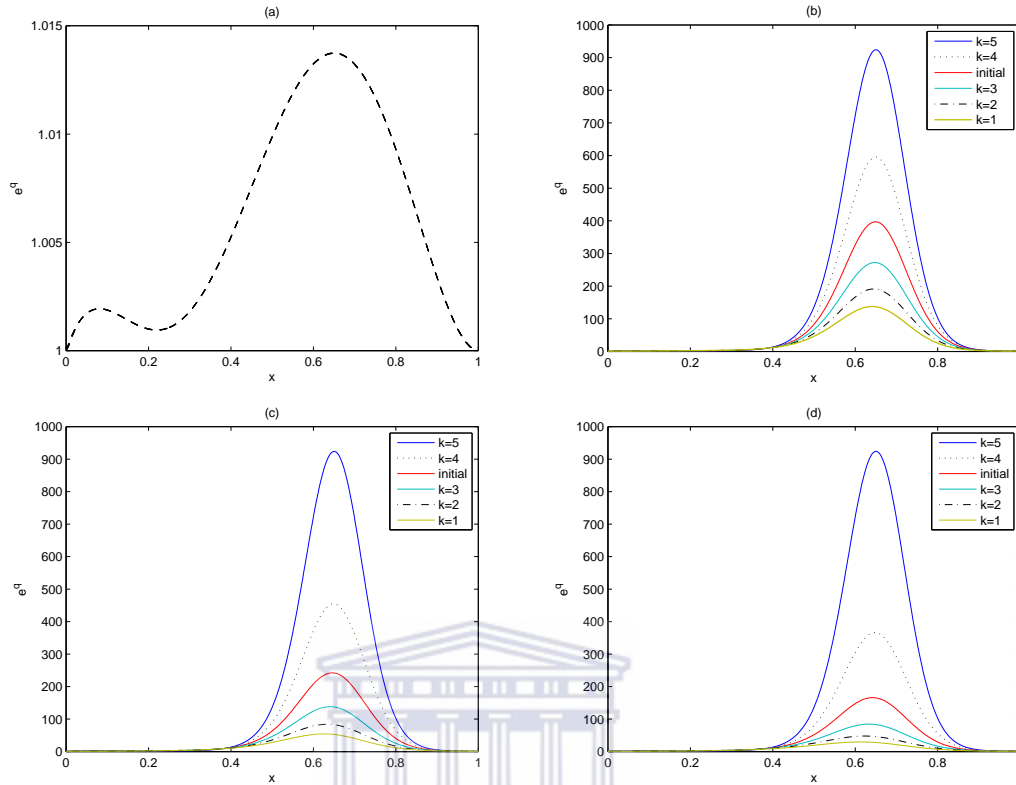


Figure 5.4.4: Plot of the reaction rate e^q , $q = \lambda uv$ in the interval $0 \leq x \leq 1$, $k = 5$, at different time steps: (a) $t = 0.00007$, $\lambda = 10^{-3}$, (b) $t = 0.009$, $\lambda = 0.5$, (c) $t = 0.015$, $\lambda = 0.5$, (d) $t = 0.02$, $\lambda = 0.5$ in problem (5.4.1), when the diffusion coefficients $\phi = \varphi = \psi = 1$.

in $\omega = (0, 1)$, for $0 < t \leq 1$ subject to boundary conditions

$$u(0, t) = u(1, t) = 1, \quad v(0, t) = v(1, t) = w(0, t) = w(1, t) = 0, \quad (5.4.6)$$

and initial values

$$u(x, t) = u_{ini}(x), \quad v(x, t) = v_{ini}(x), \quad w(x, t) = w_{ini}(x), \quad t = 0. \quad (5.4.7)$$

The patterning process of this type of system is greatly influenced by the choices of initial values $u_{ini}(x)$, $v_{ini}(x)$, $w_{ini}(x)$ that are chosen to satisfy the boundary conditions in the domain Ω . Due to the irrational and uneven behavior of this model, it has posed a lot of challenges to adequately present the numerical results arising from this particular system. The simulations for the time-dependent problem were carried out

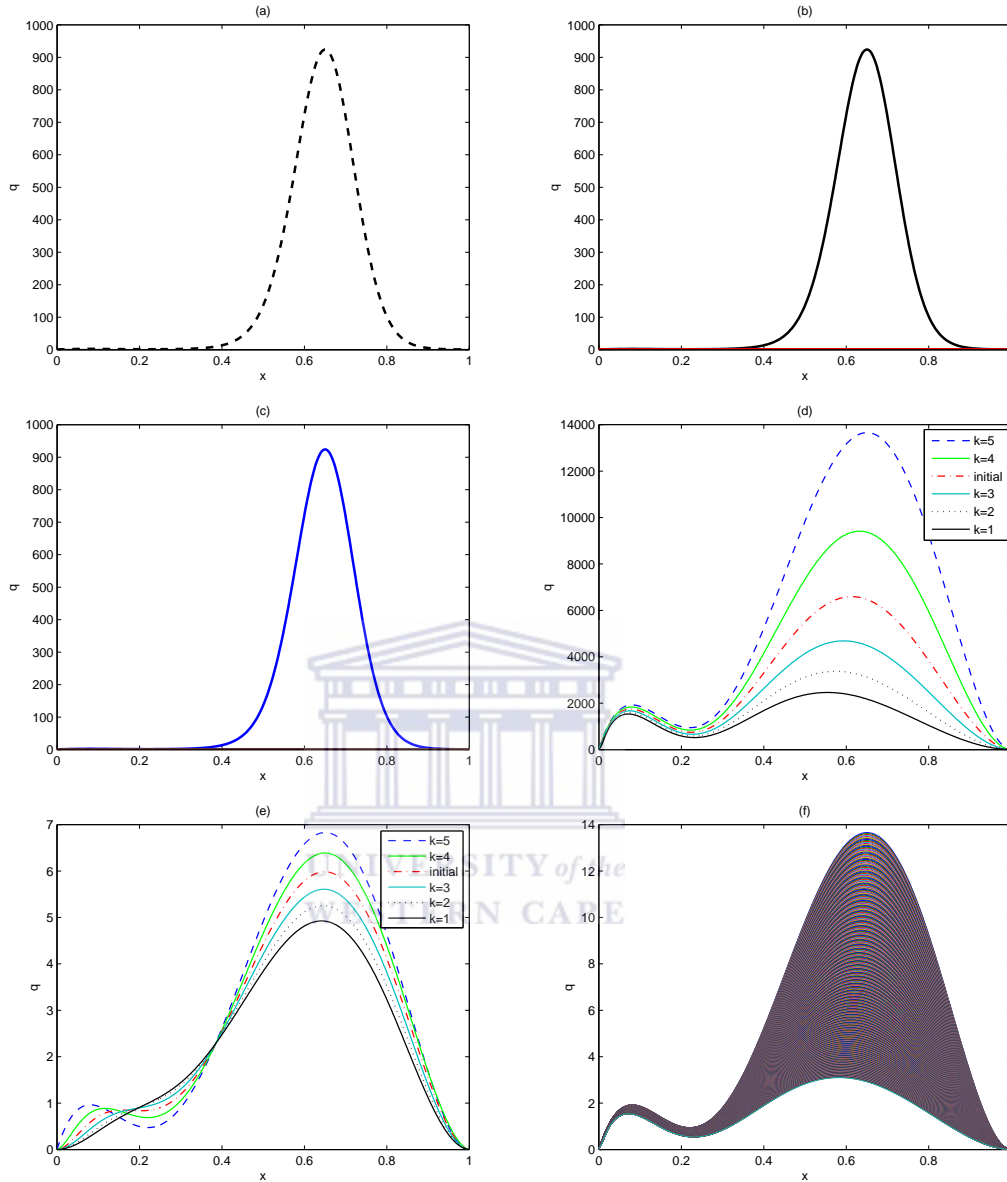


Figure 5.4.5: Plot of the reaction rate q at different time steps in the interval $0 \leq x \leq 1$ for (5.4.1). Panels (a) $t = 1, k = 1, \lambda = 0.5$ (b) $t = 50, k = 300, \lambda = 0.5$ and (c) $t = 100, k = 500, \lambda = 0.5$. Panels (d) $t = 0.00007, k = 5, \lambda = 10^3$, (e) $t = 0.009, k = 5, \lambda = 0.5$, and contour plot (f) $t = 0.00007, k = 500, \lambda = 10^3$.

with three distinct initial conditions of increasing complexity with varying diffusion coefficients.

Case (a):

$$u(x, 0) = 1 + \sin(2\pi x), \quad v(x, 0) = 0, \quad w(x, 0) = 0. \quad (5.4.8)$$

The first condition we consider here has been previously considered in [74] for

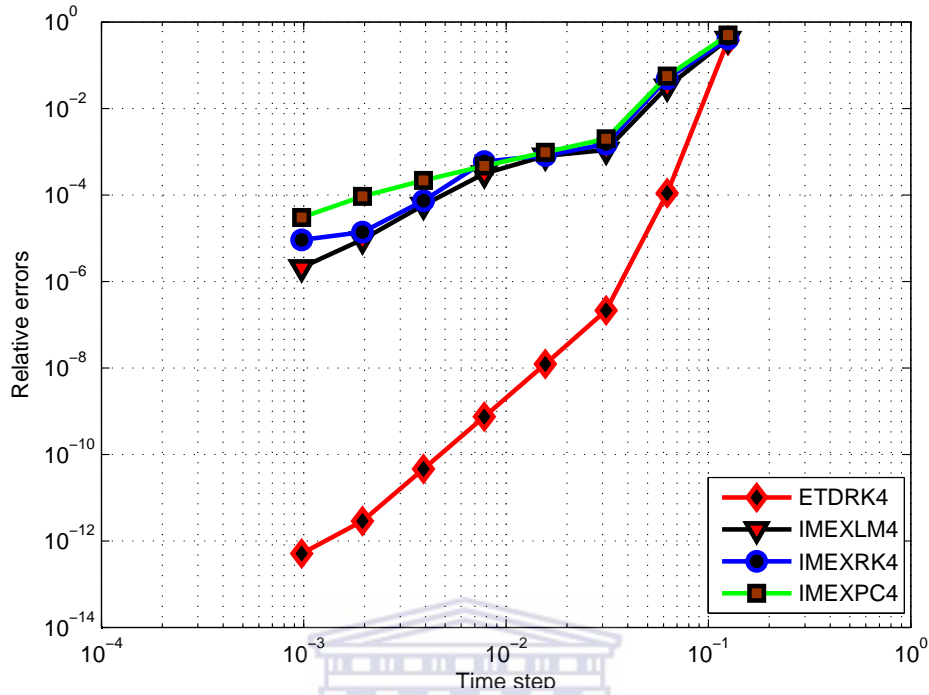


Figure 5.4.6: Comparative relative errors of ETDRK and various IMEX methods when applied to (5.4.1).

the performance evaluation of the numerical methods therein, we let the diffusion coefficients $\alpha = \beta = \gamma = 2.10^{-2}$.

It is noticeable that u -species has the highest amplitude in Figure 5.4.8 (a)-(e). Panels (a)-(c) are the concentration profiles for species u , v and w respectively at $t=0.01$. It is also apparent from the plots (d) and (e) that the amplitude of u is much higher than the other two, obviously in (e), the species v and w overlapped completely in the domain at $t = 0.1$.

Case (b): We present the second initial conditions as:

$$\left. \begin{aligned} u(x, 0) &= 0.53x + 0.47 \sin(-1.5\pi x), \\ v(x, 0) &= 1 + \sin(2\pi x), \\ w(x, 0) &= 0. \end{aligned} \right\} \quad (5.4.9)$$

We present in Figure (5.4.9) the behaviors of the interaction of the three species subject to the second case initial conditions. Species u and v interact in a pattern-like

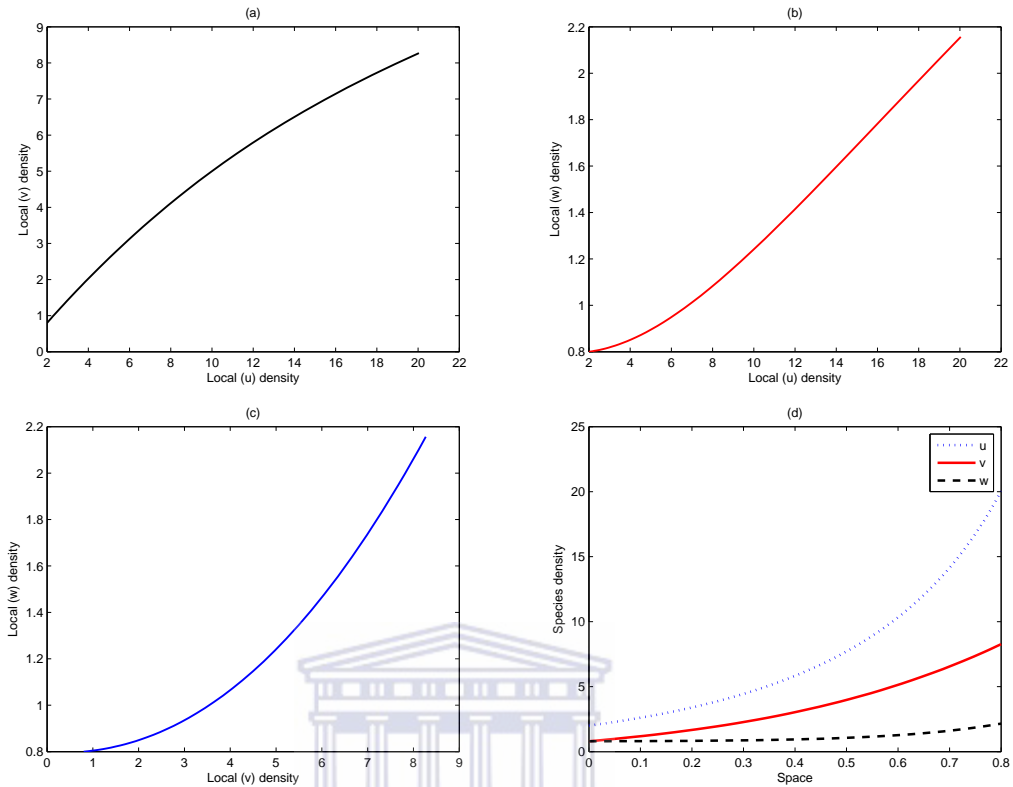


Figure 5.4.7: Local phase planes (a)-(d) for equation (5.4.5), showing spatial distribution of the species at parameter values $\alpha = \beta = \gamma = 0$, for $t = 0.8$, $u_0 = 2$, $v_0 = w_0 = 0.8$, $\tau_1 = \tau_3 = 2$, $\tau_2 = \tau_4 = 0.8$ and $\tau_5 = \tau_6 = 0.1$.

form that is well distinguished from w . Panels (a), (b), (c) and (e) are obtained by setting $v(x, 0) = w(x, 0) = 0$ in the domain at $t = 0.001$. It is clear from the contour plots in (e) that the concentration in u has been neutralized (reduced) by both v and w , this implies that the concentration of species u has been used up in (d) as a result of diffusion.

In figure 5.4.9, Panel (e) shows how the species u diffuses (spread) almost completely in the domain for problem (5.4.5). Concentration profiles in phase for the three species for case II taken at $v(x, 0) = w(x, 0) = 0$ are displayed in (a), (b) and (c) showing irregular oscillations with different types of traveling fronts propagating from the place of simultaneous introduction of the three species. Panel (d) is the contour plots for the species u , v and w . Notice the scales on the vertical axes for different amplitudes in the panels. Parameter values are: $t = 0.01$, $k = 1000$, $\alpha = \beta = \gamma = 2 \cdot 10^{-2}$, $\tau_1 = \tau_3 = 4 \cdot 10^{-2}$, $\tau_2 = \tau_4 = 10^4$, $\tau_5 = \tau_6 = 3 \cdot 10^7$.

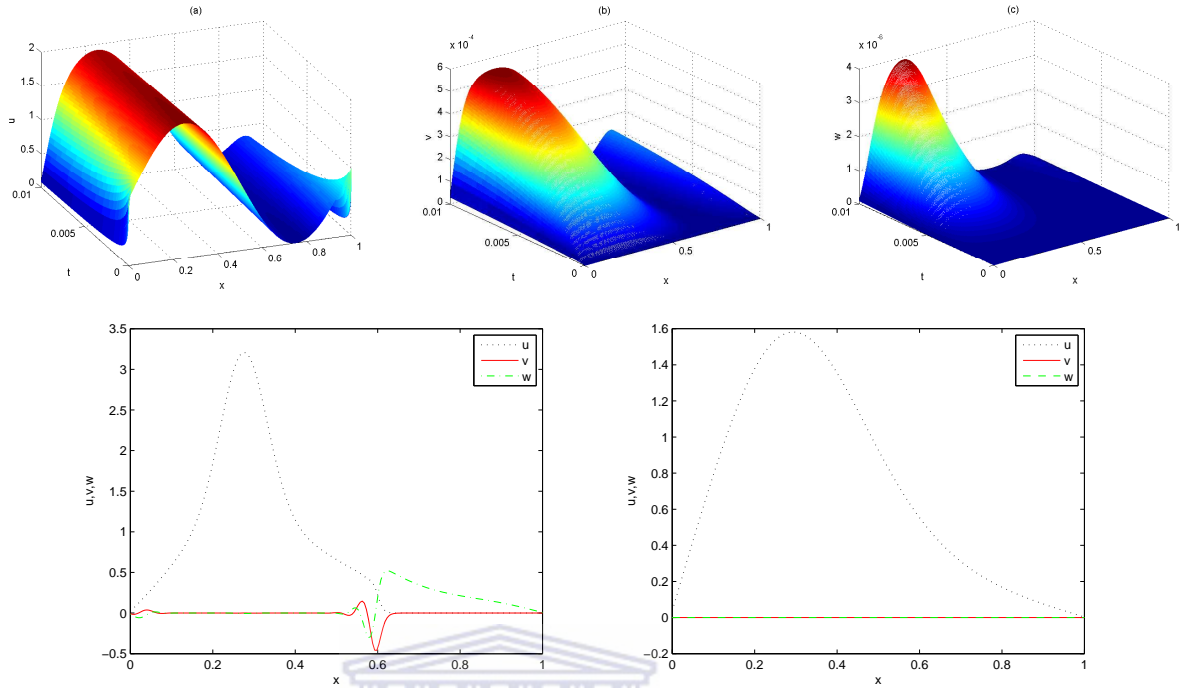


Figure 5.4.8: Concentration profiles of (5.4.5), obtained at $\tau_1 = \tau_3 = 4.10^{-2}$, $\tau_2 = \tau_4 = 10^4$, $\tau_5 = \tau_6 = 3.10^7$, $\alpha = \beta = \gamma = 1$ for the three species for case I initial condition at $t = 0.01$, $N = 200$, $k = 1000$ for panels (a)-(c). Panels (d) and (e) are obtained at time steps $t=0.05$ and $t=0.1$ respectively.

Further perturbation of the initial conditions in case II results to the three species to oscillate in phase, the concentration profiles indicating a steady structure has been established in Figure 5.4.7. The three species indicated in Figure 5.4.10 also oscillate in phase.

Stiff reaction-diffusion problem with spatiotemporal behaviour:

Finally, the following class of singularly perturbed reaction-diffusion equations was considered in [171] to illustrate spatio-temporal structures of three interacting species:

$$\left. \begin{aligned} u_t &= \alpha u_{xx} + \delta_{11}u + \delta_{12}v + \delta_{13}w + \tau_1 - \epsilon_1 u, \\ v_t &= \beta v_{xx} + \delta_{21}u + \delta_{22}v + \delta_{23}w + \tau_2 - \epsilon_2 v, \\ w_t &= \gamma w_{xx} + \delta_{31}u + \delta_{32}v + \delta_{33}w + \tau_3 - \epsilon_3 w, \end{aligned} \right\} \quad (5.4.10)$$

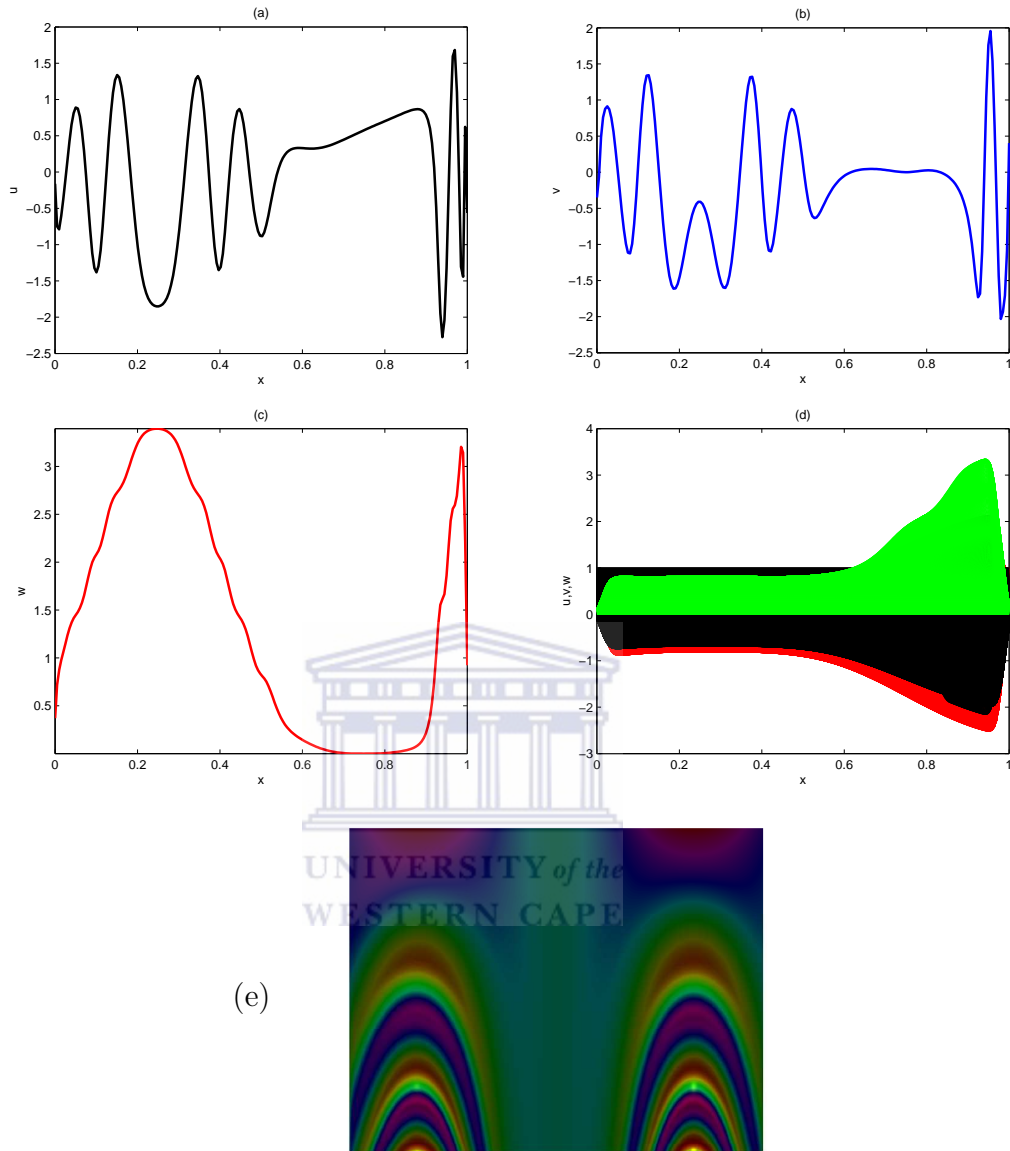


Figure 5.4.9: Concentration profiles in phase for the three species in case II of problem (5.4.5).

where $0 \leq x \leq l$ for some fixed l with boundary conditions taken as

$$u(0, t) = u(1, t) = 1, \quad v(0, t) = v(1, t) = w(0, t) = w(1, t) = 0, \quad (5.4.11)$$

the non-negative initial concentrations are taken in form of some small perturbations as

$$u(x, 0) = u_s(x), \quad v(x, 0) = v_s(x), \quad w(x, 0) = w_s(x), \quad (5.4.12)$$

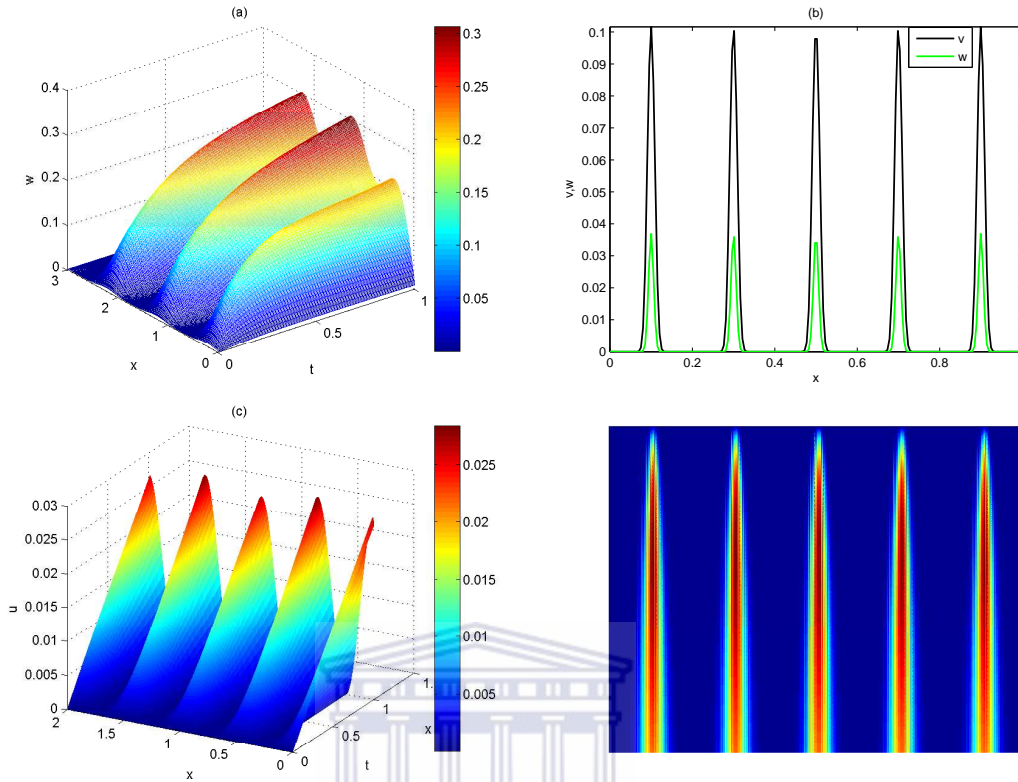


Figure 5.4.10: Various density profiles of equation (5.4.5) for the three species taken with $N = 250$ when a steady pattern has been obtained in the domain as a result of dynamic evolution from some initial perturbation. The parameters values are: (a) $\tau_1 = \tau_3 = 0.01$, $\tau_2 = \tau_4 = 0.15$, $\tau_5 = \tau_6 = 0.3$, $\alpha = \beta = \gamma = 0.05$, at $t = 1$; (b), (c) and (d) $\tau_1 = \tau_3 = 4 \cdot 10^{-2}$, $\tau_2 = \tau_4 = 10^4$, $\tau_5 = \tau_6 = 3 \cdot 10^7$, $\alpha = \beta = \gamma = 2 \cdot 10^{-2}$ at $t = 5 \cdot 10^{-4}$.

where subscript s accounts for the steady state. If the initial conditions (5.4.12), do not correspond to the steady state ($u_0 \neq u_s, v_0 \neq v_s, w_0 \neq w_s$), we expect that the system will evolve until it reaches a steady state.

This is a system of equations with widely varying diffusion coefficients. The initial and boundary conditions are mismatched, which produces spurious oscillations in most computational algorithms. In this case, $\alpha, \beta, \gamma > 0$ are the diffusion coefficients and $\epsilon_1, \epsilon_2, \epsilon_3 > 0$ are the respective decay rates of the species,

$$0 \leq \delta_{ij}(u + v + w) \leq l, \quad (5.4.13)$$

for each $i, j = 1, 2, 3$, account for the control parameter of each species growth in the chosen domain of length l .

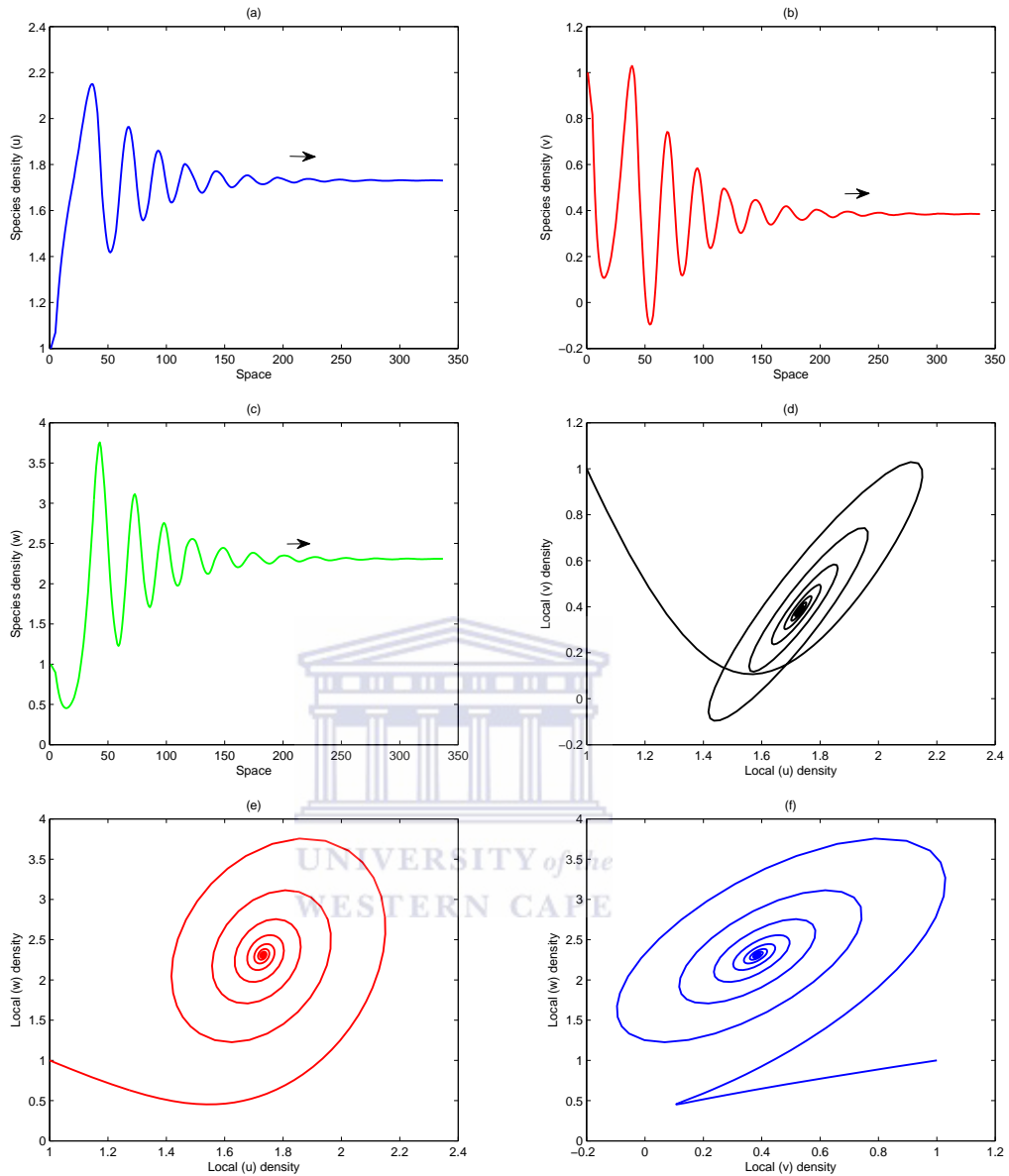


Figure 5.4.11: Plots showing the spatial distribution of (a) species u , (b) species v and (c) species w obtained at $t = 3000$ for parameters $\alpha = 0.0, \beta = 0.0, \gamma = 0.0, \delta_{11} = 0.01, \delta_{12} = 0.02, \delta_{13} = -0.01, \delta_{21} = 0.1, \delta_{22} = 0.0, \delta_{23} = 0.0, \delta_{31} = 0.1, \delta_{32} = 0.0, \delta_{33} = 0.01, \tau_1 = 0.05, \tau_2 = -0.15, \tau_3 = -0.15, \epsilon_1 = 0.03, \epsilon_2 = 0.06, \epsilon_3 = 0.02$ with initial size $u_0 = v_0 = w_0 = 1$. The local phase plane of model (5.4.10) is shown in plates (d)-(f). The parameter values are the same as above.

The behaviour of the species in problem (5.4.10) are well explored in figures 5.4.12 and 5.4.13. These simulations was performed for $0 < t < 1000$ in the interval of length $l = 40, 100, 200, \dots$. It is apparent from Figure 5.4.12 that the amplitudes of oscillations of the three species vary with time and the length of the computational domain. In

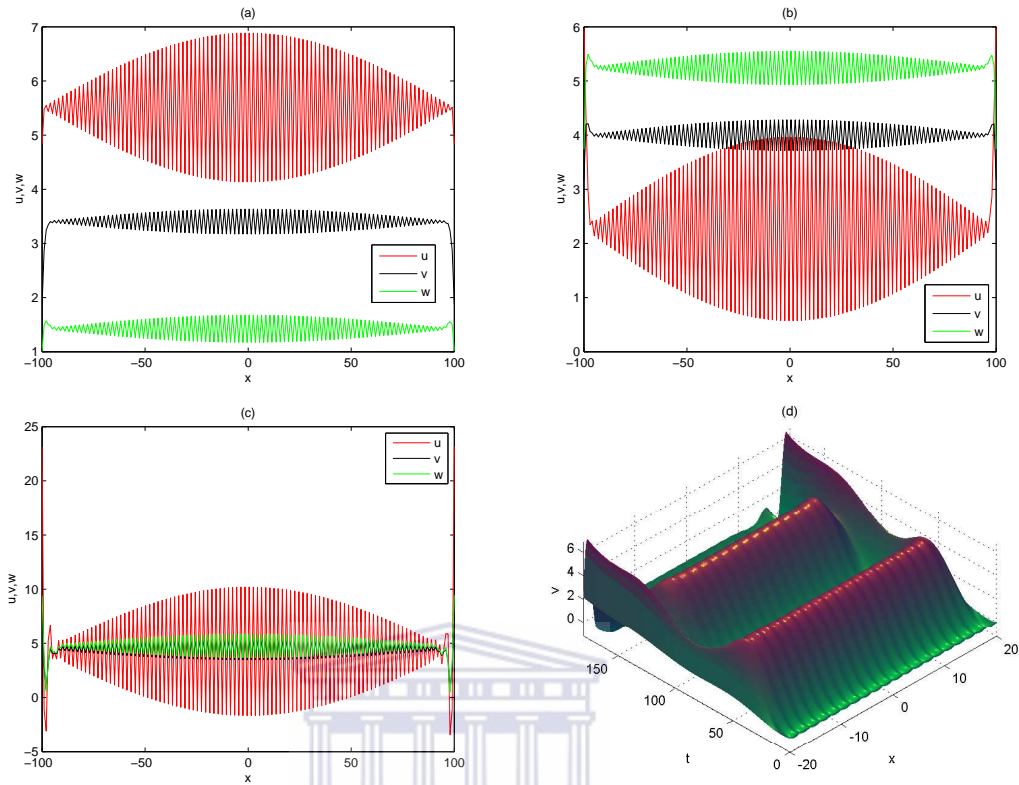


Figure 5.4.12: Density profiles for the three species, modelled through (5.4.10), taken at $t = 30, 60, 210$ for plots (a), (b) and (c) respectively. Panel (d) is showing the oscillation of v concentration at $t = 180$. Parameter values are: $\alpha = 0.005, \beta = 0.1, \gamma = 0.1, \delta_{11} = 0.08, \delta_{12} = -0.08, \delta_{13} = -0.01, \delta_{21} = -0.1, \delta_{22} = 0.0, \delta_{23} = 0.0, \delta_{31} = 0.1, \delta_{32} = 0.0, \delta_{33} = 0.01, \tau_1 = 0.05, \tau_2 = -0.15, \tau_3 = -0.25, \epsilon_1 = 0.03, \epsilon_2 = 0.06, \epsilon_3 = 0.02$.

panels (a), (b) and (c), all the three components oscillate in phase but in (a), species u (red) possess higher amplitude of oscillation between $t = 30$ and $t = 53$, at $t < 30$, species v and w oscillate in opposite phase. Clearly from panel (b), as time increased from $t = 53$ to $t = 77$, species w enjoyed high amplitude dominance forcing species u to oscillates in opposite phase. The three species oscillate within themselves as $t \geq 180$, with structures overlapped. Oscillatory amplitude of v is shown in Figure 5.4.12 (d) at $t = 180$ and the computational domain of length $l = 40$. It was observed that species v never attains high amplitude at any time t in the domain but maintains an intermediate position between the remaining two species.

Figure 5.4.13 presents various surface plot patterns obtained as a result of the dynamical evolution from some small initial perturbations of (5.4.12) up to a steady

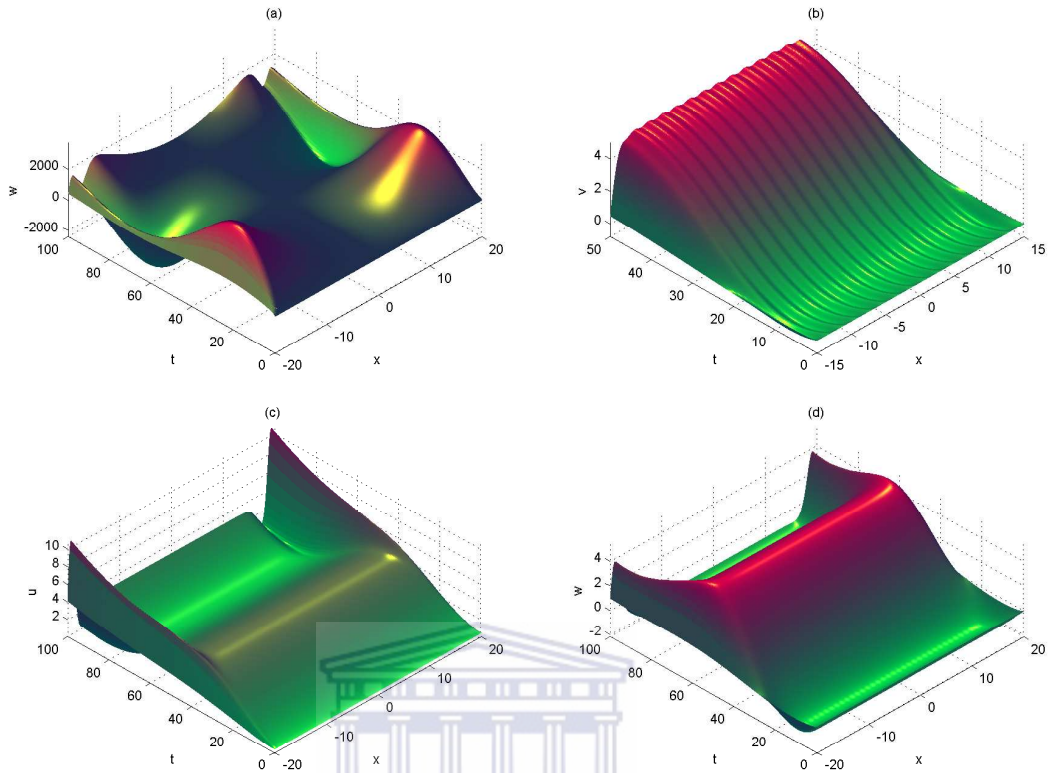


Figure 5.4.13: Plots showing the dynamical evolution of the three species in (5.4.10), obtained as a result of some small initial perturbations of (5.4.12) to obtain a steady (periodic) state. The parameter values here are same to those used for Figure 5.4.12 but notice the scales on the vertical axes for different amplitudes in the surface plot panels.

structures. Obviously, it can be deduced that the patterning process is greatly influenced by choices of the bounds in (5.4.13) and the length of the computational domain, result of Figure 5.4.14 is a proof to this assertion, we have been able to obtain steady and non-oscillatory profiles for the three species.

Panels (a), (b) in Figure 5.4.14 are the space-time and surface plots indicating when the concentrations of the three species oscillate in phase. As a result of further perturbation of the initial conditions (5.4.12) and the diffusion coefficients, the dynamic evolution of system (5.4.10) is stable and free of oscillations in panels (c) and (d). Notice also the scales on the vertical axes for different amplitudes in the panels.

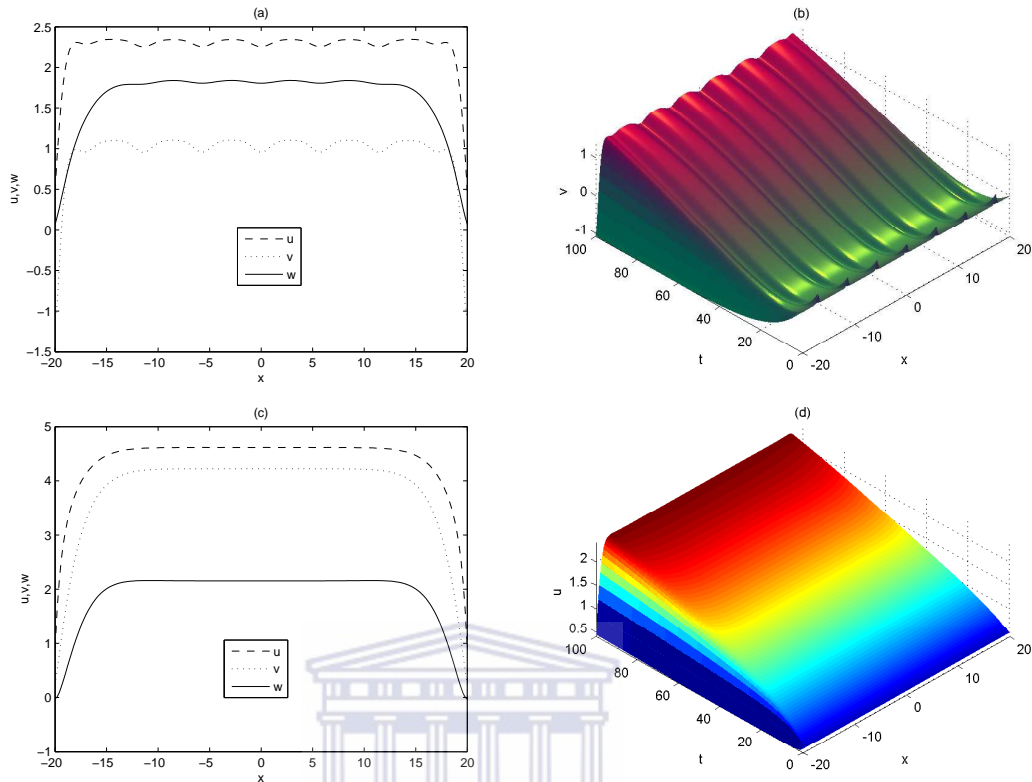


Figure 5.4.14: Concentration profiles for the three species model (5.4.10) taken at (a) $t = 80$ (b) $t = 100$ (c) $t = 100$ and (d) $t = 100$. Parameter values are: $\alpha = 0.007$, $\beta = 0.001$, $\gamma = 0.2$, $\delta_{11} = 0.01$, $\delta_{12} = 0.02$, $\delta_{13} = -0.01$, $\delta_{21} = 0.1$, $\delta_{22} = 0.0$, $\delta_{23} = 0.0$, $\delta_{31} = 0.1$, $\delta_{32} = 0.0$, $\delta_{33} = 0.01$, $\tau_1 = 0.05$, $\tau_2 = -0.15$, $\tau_3 = -0.15$, $\epsilon_1 = 0.03$, $\epsilon_2 = 0.06$, $\epsilon_3 = 0.02$.

5.5 Summary and discussions

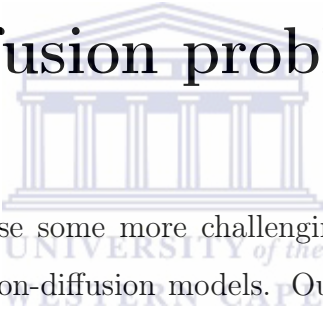
In this chapter, we have considered some systems of reaction-diffusion equations that explains the competition involving the interaction of three species in line with Turing's theory of pattern formation (spatiotemporal structures). Anomaly behaviour of the three examples considered in this chapter have further shown that chaos and hyperchaos can occur in systems of autonomous ordinary differential equations (ODE's) with at least three variables and two quadratic nonlinearities. These amazing structures occur due to proper selection of model parameters and suitable initial conditions. We further demonstrates in this work the compatibility of finite difference with higher order time stepping methods such as ETDRK4, IMEXLM4, IMEXRK4 and IMEXPC4. The result of the computational experiment obtained in Figure 5.4.6 demonstrates that

there is a wide difference between the fourth-order exponential time differencing Runge-Kutta on combination with fourth-order finite difference scheme in terms of supremacy over the family of fourth orders implicit-explicit methods used in this chapter. Finally in the next chapter, we shall further extends our numerical approach to solve some time-stepping stiff higher-order PDEs that are of parabolic types.



Chapter 6

Further exploration of higher order numerical methods for other classes of reaction-diffusion problems



In this chapter, we propose some more challenging numerical methods that can be tested for a class of reaction-diffusion models. Our method of solution connects two classic mathematical ideas since the semi-linear partial differential equations (PDEs) we are considering can be split into a linear, which contains the stiffest part of the problem, and a nonlinear part, that is expected to vary more slowly than the linear part. For simulation tests, we choose periodic boundary conditions and apply fourth-order central finite difference approximation for the spatial discretization. We first employ the first and second order family of implicit-explicit (IMEX) schemes and compare their performances. Later, we use the family of exponential time differencing (ETD) schemes as discussed in earlier chapters to integrate in time. The problems considered in this chapter are the higher order time-dependent Burgers-Fisher, Burgers, Fisher, Korteweg-de Vries, Allen-Cahn and Kuramoto-Sivashinski equations, all in a bounded one-dimensional domain. Numerical simulations of these time-dependent nonlinear PDEs revealed some of the spatiotemporal behavioural patterns. The result of error comparison with other more standard exponential time differencing (ETD) approaches show that the ETDRK4 method is efficient, accurate and more reliable.

6.1 Introduction

Nonlinear time-dependent parabolic partial differential equations (PDEs) (Allen-Cahn, Burgers, Burgers-Fisher, Korteweg-de Vries (KDV), Fisher-KPP, Navier-Stokes and Schrödinger) are often applied in various fields of science and engineering such as chemical kinetics, fluid mechanics, celestial mechanics, control theory, plasma physics, transverse motion and other areas of applied mathematics to mention a few. In this chapter, we are concerned with the numerical behavior of solutions of Burgers-Fisher, Burgers and Fisher-KPP equations.

We are motivated with the desire to use implicit-explicit schemes to explore the anomaly behavior of the generalized Burgers-Fisher equation (cf. [61, 90, 99]).

$$\frac{\partial u}{\partial t} = \nu \frac{\partial^2 u}{\partial x^2} - \alpha u^\delta \frac{\partial u}{\partial x} + \beta u(1 - u^\delta), \quad x \in \Omega, \quad 0 \leq t \leq T, \quad (6.1.1)$$

with initial condition

$$u(x, 0) = \phi(x), \quad x \in \Omega, \quad (6.1.2)$$

and the boundary conditions

$$u(0, t) = g_a(t), \quad 0 \leq t \leq T \quad (6.1.3)$$

and

$$u(l, t) = g_b(t), \quad 0 \leq t \leq T. \quad (6.1.4)$$

where t and x are the time and spatial coordinate respectively, $\phi(x)$, $g_a(t)$ and $g_b(t)$ are the specified initial and boundary conditions, α , β and δ are the varying parameters in the bounded domain Ω and ν is a nonnegative parameter describing the viscosity, in mathematical context [10, 11] it is seen as the coefficient that controls the diffusion. Numerical solution of equation (6.1.1) has been the subject of activity in the current field of scientific research, many researchers have used different methods to integrate Burgers-Fisher equation, among which is the spectral domain decomposition method of Golbabai and Javidi [61], where fourth order Runge-Kutta method is used in time

coupled with spectral collocation method using Chebyshev polynomial for the spatial derivatives. Chen et al. [34] proposed the use of an exponential function (Exp-function) method with the aid of symbolic computational system in a view to obtain a generalized traveling wave solutions of a Burgers-Fisher equation with variable coefficients, in a similar manner, Xu and Xian [197] used the approach of Exp-function method for finding simultaneously exact solutions expressed by various exponential functions to nonlinear evolution equations. Kaya and El-Sayed [94] introduced a numerical simulation and explicit solutions of the generalized form of Burgers-Fisher equation.

A well-known Burgers equation is obtained when $\beta = 0$, $\alpha = \delta = 1$ in equation (6.1.1) to yield

$$\frac{\partial u}{\partial t} = \nu \frac{\partial^2 u}{\partial x^2} - u \frac{\partial u}{\partial x}, \quad x \in \Omega, \quad t > 0, \quad (6.1.5)$$

which was introduced in the twenties as a model of turbulence by Burgers [24] and solved explicitly by Hopf [82] and Cole [35] in terms of the initial condition $u(x, t = 0)$, has led to a total understanding of the behavior properties of individual solutions in the inviscid limit when $\nu \rightarrow 0$. In fluids and gases, equation (6.1.5) can be interpreted as modeling the effect of viscosity, and so Burgers equation represents a simplified version of the equations of viscous flow.

By Hopf-Cole transformation in the limit $\nu \rightarrow 0$, the Burgers equation (6.1.5) becomes the inviscid Burgers equation which is standard diffusion equation

$$\frac{\partial u}{\partial t} + u \frac{\partial u}{\partial x} = 0, \quad x \in \Omega, \quad t > 0, \quad (6.1.6)$$

and also a prototype equation for which the solution can develop discontinuities (shock waves). We can also express (6.1.1) in terms of heat conduction equation when the parameter values $\alpha = \beta = 0$, to yield

$$\frac{\partial u}{\partial t} - \nu \frac{\partial^2 u}{\partial x^2} = 0, \quad x \in \Omega, \quad t > 0, \quad (6.1.7)$$

where ν is taken as diffusion coefficient.

In addition, setting $\alpha = 0$ and $\delta = 1$, it is obvious that equation (6.1.1) reduces to

a reaction-diffusion equation with quadratic kinematics

$$\frac{\partial u}{\partial t} = \nu \frac{\partial^2 u}{\partial x^2} + \beta u(1 - u), \quad x \in \Omega, \quad t > 0, \quad (6.1.8)$$

called Fisher-KPP (Kolmogorov, Petrovskii, and Piskunov) equation, $\nu > 0$ is regarded as diffusion coefficient. The Fisher equation (6.4.6) is regarded as the simplest model of spatial dynamics in which competitive interactions between individuals occur local medium. This type of reaction-diffusion equation has a long standing history in mathematical modeling describing the propagation of phenomena in dissipative dynamical models.

Equation (6.4.6) was earlier proposed by Fisher (1937) as a model applied to study population dynamics, with u representing the density of an advantageous gene, and the traveling wave solutions representing the spread of this gene in space. It also has a wide important applications areas such as flame propagation, branching Brownian motion processes, logistic population growth, autocatalytic chemical reactions and nuclear reactor theory. It universally agreed that nonlinear reaction-diffusion equations play some important roles in various fields of physics, chemistry, biology and ecology where developmental process appears in the form of a traveling wave of chemical concentration. Subsequent applications of Fisher equation have been varied and extended to many research areas. For instance, in ecology for modeling waves of an invading population, Holmes [80], wound healing models by Sherratt and Murray [179] with solutions representing healing waves of cells in the skin.

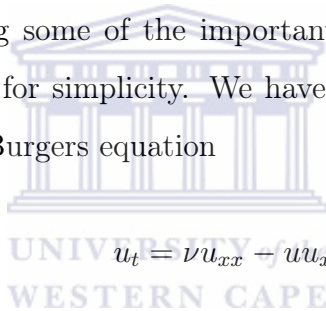
The details qualitative analysis in the phase plane and traveling wave solutions of equation (6.4.6) have been examined. Feng [49] investigates the behavior of a generalized form of Fisher equation with a view of obtaining a class of traveling solitary wave solutions. Sherratt [178] examines the traveling waves in Fisher equation using a transition from an initial data, Brazhnik and Tyson [22] examined the traveling wave solutions of (6.4.6) in two spatial dimensions. Finding the numerical solutions of nonlinear models is a difficult and has since become the major challenge of many researchers, several analytical methods have been sought to obtain the wave solutions

for pure dispersive nonlinear systems in one spatial dimension: the sinc collocation method [4] and pseudospectral method of solution [147] among others.

The chapter is organized into some sections. In Section 6.2, we briefly discuss the qualitative analysis of the Burgers-Fisher equation. In Section 6.3 we present the numerical methods and their formulations in both space and time. Numerical results based on some existing problems are well studied in Section 6.4. We give summary of the main outcomes in Section 6.5.

6.2 Qualitative analysis of model problems

We describe briefly in this section the qualitative behavior analysis of nonlinear equation (6.1.1) by considering some of the important evolution equations (Burgers and Fisher) that arise from it for simplicity. We have shown in section one that Burgers Fisher equation turns to Burgers equation



$$u_t = \nu u_{xx} - uu_x, \quad (6.2.1)$$

(6.1.5) when $\beta = 0, \alpha = \delta = 1$. Since equation (6.2.1) is first order in t , it means that their solutions can be predicted uniquely by their initial values. We assume that,

$$u(x, 0) = \psi(x), \quad (6.2.2)$$

here, the boundary effects are ignored. The easiest explicit solutions are the traveling waves, for which $u(x, t) = \mu(\xi) = \mu(x - ct)$, for $\xi = x - ct$, stands for a fixed profile moving towards the right with a constant speed c . With the application of chain rule,

$$u_t = -c\mu'(\xi), \quad u_x = \mu'(\xi), \quad u_{xx} = \mu''(\xi). \quad (6.2.3)$$

Putting these expressions into (6.2.1), we obtain a nonlinear second order ordinary differential equation

$$-c\mu' + \mu\mu' = \nu\mu''. \quad (6.2.4)$$

On integration of both sides with respect to ξ , we have

$$\nu\mu' = k - c\mu + \frac{1}{2}\mu^2, \quad (6.2.5)$$

where k is a constant, the quadratic polynomial on the right hand side is expected to have two roots which requires $k < \frac{1}{2}c^2$. We can also find the linear analysis of (6.1.5) by ignoring the second term which invariably yields inviscid Burgers equation (6.1.6).

$$u_t = \alpha uu_x, \quad \alpha > 0, \quad (6.2.6)$$

whose general solution is of the form

$$u(x, t) = \zeta(x - \alpha ut), \quad (6.2.7)$$

with ζ being an arbitrary function. We demonstrate further here that the wave profile undergoes deformation when t is increased. By taking a close look at the method of analysis adopted in [19], we differentiate (6.2.7) once with respect to x

$$u_x(x, t) = (1 - \zeta u_x(x, t)t)\zeta_\xi, \quad \xi = x - \alpha ut, \quad (6.2.8)$$

which we simplify further to have

$$u(x, t) = \frac{\zeta_\xi}{1 + t\alpha\zeta_\xi}. \quad (6.2.9)$$

Equation (6.2.9) describes the slope of the u -profile at x, t in terms of the initial profile at ξ for $\xi = x$, when $t = 0$. If the value of ζ_ξ is negative, then $u_x(x, t)$ is infinite at $t = -1/\alpha\zeta_\xi$ which implies that the solution ceases to be single valued in the neighborhood of $x_0 = \xi_0 + \alpha T\zeta(\xi_0)$, ξ_0 is the point at which $-1/\alpha\zeta_\xi$ attains a minimum value. We can as well investigate the changes in the slope of at $\xi = \xi_0$ whenever $t > T$. Assuming

$$t = T + \tau = \left(\frac{-1}{\alpha\zeta_\xi} \right)_{min} + \tau, \tau \ll 1 \quad (6.2.10)$$

we have

$$u_x(X_0(t), T + \tau) = \left(\frac{\zeta_\xi}{1 + t\alpha\zeta_\xi} \right)_{\xi=\xi_0, t=T+c}, \quad (6.2.11)$$

$X_0(t)$ is the position of ξ at any time t . We therefore obtain

$$u_x(X_0(t), T + \tau) = \frac{1}{\zeta\tau}. \quad (6.2.12)$$

As a result, we obtain $u_x(X_0(T - 0), T - 0) = -\infty$ and $u_x(X_0(T + 0), T + 0) = +\infty$, this shows that as t increases, the wave profile undergoes a progressive deformation.

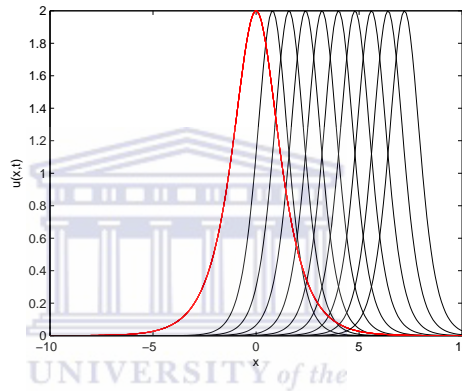


Figure 6.2.1: Solution of (6.1.1), with $\nu = 0.0015$, $\alpha = \beta = 0$, $t = 0.2(0.2)1.8$, $N = 200$ and $x \in [-10, 10]$.

The medium described by (6.4.6) is often referred to as a bistable medium because it has two homogeneous stationary states, at $u = 0$ and $u = 1$. For convenience, we rewrite (6.4.6) in the form

$$u_t = u_{xx} + u(1 - u), \quad (6.2.13)$$

the traveling wave solution can be written in the form $u(x, t) = u(\xi = x - ct)$, c is the propagating wave speed, we have ordinary differential equation

$$-cu_\xi = u_{\xi\xi} + u(1 - u) \quad (6.2.14)$$

where $u(\xi) > 0$ and bounded with the boundary conditions for the traveling wave solution $u(\xi \rightarrow -\infty) \rightarrow 1$ and $u(\xi \rightarrow \infty) \rightarrow 0$, which are respectively stable and unstable. Since (6.2.13) is invariant if $x \rightarrow -x$, and the value of c is either positive or

negative, specifically, we assume $c \geq 0$. This suggest that we should look for traveling wave solutions to (6.2.13) for which $0 \leq u(x, 0) \leq 1$ since $u(x, 0) < 0$ has no physical meaning. The speed of the waves has to be sought as solution for the eigenvalue problem (6.2.14) subject to conditions [23, 139]

$$\lim_{\omega \rightarrow -\infty} u(\xi) = 1, \quad \lim_{\omega \rightarrow \infty} u(\xi) = 0.$$

We let $u(\xi)$ be $U(\xi)$ in the phase plane (U, V) , where

$$U' = V, \quad V' = -cV - U(1 - U), \quad (6.2.15)$$

which results to the solutions of the phase plane trajectories

$$\frac{dV}{dU} = \frac{-cV - U(1 - U)}{V}. \quad (6.2.16)$$

This equation has steady states at the two singular points, say, $\xi_1 = (0, 0)$ and $\xi_2 = (1, 0)$ for (U, V) . The eigenvalues λ for the singular points are given as

$$\xi_1 : \lambda_{\pm} = -\frac{c}{2} \pm \frac{\sqrt{c^2 - 4}}{2}, \quad \xi_2 : \lambda_{\pm} = -\frac{c}{2} \pm \frac{\sqrt{c^2 + 4}}{2}, \quad (6.2.17)$$

if $c^2 > 4$, $c \geq c_{min} = 2$, just as earlier pointed out by Fisher that (6.2.13) has an infinite number of traveling wave solutions for which $0 \leq u(x, 0) \leq 1$, we see from (6.2.17) that the origin is a stable node, the case $u(x, 0) = 1$ for $x < a$, and $u(x, 0) = 0$ for $x > b$, results to a unique solution that evolves into a travelling monotonic wave solution with $c = c_{min}$. If $c^2 < 4$ it is stable spiral that oscillates in the neighborhood of the origin. It has been shown by Mckean [121] that any traveling wave speed with $c > 2$ is stable, for instance, Ablowitz and Zeppetella [2] present an explicit form of a traveling wave solution for (6.2.13) as

$$u(x, t) = \left(1 + \exp \left(\frac{\xi}{\sqrt{6}} \right) \right)^{-2}, \quad (6.2.18)$$

with a speed $c = 5/\sqrt{6}$. Readers are referred to [2, 21, 22, 121, 139] for further analysis.

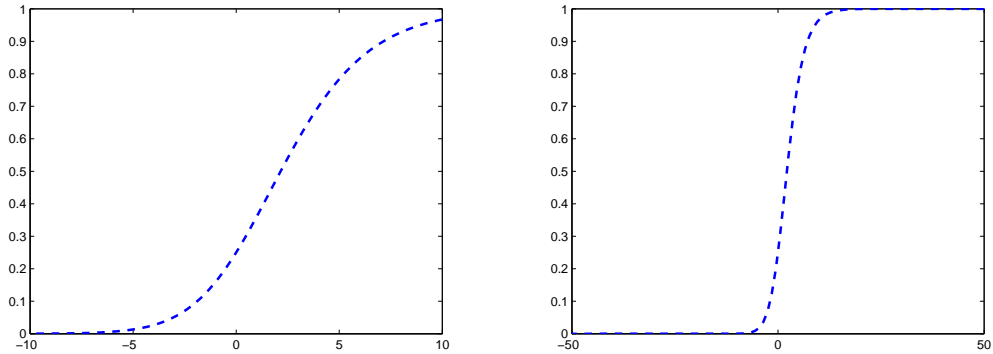


Figure 6.2.2: Traveling wave solution for equation (6.2.13).

Other important time-dependent problems we are considering in this chapter include the general third-order KdV equation with periodic boundary conditions,

$$u_t + uu_x + \beta u_{xxx} = 0, \quad x \in [-\pi, \pi], \quad (6.2.19)$$

and the fourth-order Kuramoto-Sivashinsky equation.

$$u_t = -uu_x - u_{xx} - u_{xxxx}, \quad x \in [0, L], \quad (6.2.20)$$

details of these models shall be discuss later in this chapter.

6.3 Numerical method

The method of solution of nonlinear PDEs of the form (6.1.1) are also in two parts, we first apply fourth-order central difference scheme to discretize the spatial derivatives in (6.1.1), and then use implicit-explicit (IMEX) schemes for the numerical integration of systems of ordinary differential equations arising from the spatial discretization of partial differential equations of parabolic type. We shall briefly discuss the steps involved.

Higher order spatial discretization:

The spatial discretization for all the equations studied in this chapter is done using fourth-order central finite difference schemes whose derivations are based on Taylor's series expansion techniques for the first and second derivatives in (6.1.1). Many researchers have used finite difference methods in various forms (see for example, [59, 103, 112, 126, 131, 149]).

The fourth-order central finite difference approximations used for the first, second, third and fourth order partial derivatives in this chapter are:

$$\frac{\partial u}{\partial x} \approx \frac{u_{i-2,j} - 8u_{i-1,j} + 8u_{i+1,j} - u_{i+2,j}}{12h}, \quad (6.3.1)$$

$$\frac{\partial^2 u}{\partial x^2} \approx \frac{-u_{i-2,j} + 16u_{i-1,j} - 30u_{i,j} + 16u_{i+1,j} - u_{i+2,j}}{12h^2}. \quad (6.3.2)$$

$$\frac{\partial^3 u}{\partial x^3} \approx \frac{u_{i-3,j} - 8u_{i-2,j} + 13u_{i-1,j} - 13u_{i+1,j} + 8u_{i+2,j} - u_{i+3,j}}{8h^3}, \quad (6.3.3)$$

$$\frac{\partial^4 u}{\partial x^4} \approx \frac{-u_{i-3,j} + 12u_{i-2,j} - 39u_{i-1,j} + 56u_{i,j} - 39u_{i+1,j} + 12u_{i+2,j} - u_{i+3,j}}{6h^4}. \quad (6.3.4)$$

As usual, we shall write the general Burgers-Fisher equation(6.1.1) in the form

$$u_t = \nu Lu + F(u, t), \quad (6.3.5)$$

where ν is the viscosity or simply diffusion coefficient term in mathematical context, L and F represent the linear and nonlinear operators respectively. When discretize in space, the result is a large system of ordinary differential equations (ODEs) of the form

$$u_t = \nu \mathbf{L}u + \mathbf{F}(u, t), \quad (6.3.6)$$

where

$$\mathbf{L}_1 = \frac{1}{12h} \begin{pmatrix} 0 & 8 & -1 & \dots & 0 & 0 & 0 \\ -8 & 0 & 8 & \dots & 0 & 0 & 0 \\ 1 & -8 & 0 & \dots & 0 & 0 & 0 \\ \vdots & \vdots & \vdots & \ddots & \vdots & \vdots & \vdots \\ 0 & 0 & 0 & \dots & 0 & 8 & -1 \\ 0 & 0 & 0 & \dots & -8 & 0 & 8 \\ 0 & 0 & 0 & \dots & 1 & -8 & 0 \end{pmatrix}_{(N-1) \times (N-1)} \quad (6.3.7)$$

$$\mathbf{L}_2 = \frac{1}{12h^2} \begin{pmatrix} 30 & 16 & -1 & \dots & 0 & 0 & 0 \\ 16 & 30 & 16 & \dots & 0 & 0 & 0 \\ -1 & 16 & 30 & \dots & 0 & 0 & 0 \\ \vdots & \vdots & \vdots & \ddots & \vdots & \vdots & \vdots \\ 0 & 0 & 0 & \dots & 30 & 16 & -1 \\ 0 & 0 & 0 & \dots & 16 & 30 & 16 \\ 0 & 0 & 0 & \dots & -1 & 16 & 30 \end{pmatrix}_{(N-1) \times (N-1)} \quad (6.3.8)$$

$\mathbf{L}_1, \mathbf{L}_2 \in \mathbf{L}$, it shows that the resulting differentiation matrix representing the second derivative in (6.3.5) is a pentadiagonal type which we compute as toeplitz matrix. Experiments have shown that solving a linear system is nearly always less computationally expensive than solving a nonlinear system of the form (6.3.6) since it contains \mathbf{F} that represents a non-stiff or mildly stiff part and \mathbf{L} is a stiff term requiring implicit integration, so it is reasonable to propose a method that will reduce the time step constraint as imposed by the linear term, this task is achieved by the use implicit-explicit (IMEX) methods that consist of using explicit multi-step formula to advance the nonlinear part of equation (6.3.6) and an implicit scheme to integrate the linear part (for thorough

discussion see [10, 66]).

Implicit-explicit (IMEX) schemes for discretization in time:

We want to discuss briefly here the implicit-explicit schemes for computing approximate solutions to large system of ordinary differential equations (6.3.6) arise from the spatial discretization by central finite difference of the time-dependent partial differential equations (6.3.5). The first- and second-order schemes to be considered are derived from general linear multi-step IMEX schemes [10] written in the form

$$\frac{1}{k}u_{n+1} + \frac{1}{k} \sum_{j=0}^{s-1} \alpha_j u_{n-j} = \sum_{j=0}^{s-1} \beta_j \mathbf{F}(u_{n-j}, t_{n-j}) + \nu \sum_{j=-1}^{s-1} \gamma_j \mathbf{L}(u_{n-j}), \gamma_{-1} \neq 0, \quad (6.3.9)$$

where ν is a nonnegative parameter referred earlier as viscosity or the diffusion coefficient term, k is the constant discretization step-size, and u_n is the numerical approximation at $t_n = k_n$. Given an extension to the various schemes in [10, 103, 112], the first-order IMEX scheme is presented as

$$u_{n+1} = (\mathbf{I} - \nu k \mathbf{L})^{-1} [u_n + k \mathbf{F}(u_n, t_n)], \quad (6.3.10)$$

is named in this chapter as (IMEXLM1), this scheme applies backward differentiation formula to the linear part \mathbf{L} to estimate the nonlinear part \mathbf{F} at time step $n + 1$. The second-order IMEX scheme which we called (IMEXLM2), applies Crank-Nicolson to stiff part which we treated implicitly and second-order Adams-Bashforth to the non-stiff part for which an explicit method is proposed.

$$u_{n+1} = \left(\mathbf{I} - \frac{\nu k \mathbf{L}}{2} \right)^{-1} \left[\left(\mathbf{I} + \frac{\nu k \mathbf{L}}{2} \right) u_n + \frac{3k}{2} \mathbf{F}(u_n, t_n) - \frac{k}{2} \mathbf{F}(u_{n-1}, t_{n-1}) \right], \quad (6.3.11)$$

where \mathbf{I} is the identity matrix of size $(N - 1) \times (N - 1)$.

In a similar way, first- and second-order IMEX predictor corrector schemes are equally considered by applying s -step IMEX scheme [112] to (6.3.6) yields,

one-step methods (IMEXPC1):

$$\bar{u}_{n+1} = (\mathbf{I} - \nu k \mathbf{L})^{-1} [(\mathbf{I} + (1 - \nu \alpha) k \mathbf{L}) u_n + k \mathbf{F}(u_n, t_n)], \quad (6.3.12)$$

as predictor, and

$$u_{n+1} = (\mathbf{I} - \nu k \mathbf{L})^{-1} [(\mathbf{I} + (1 - \nu \alpha) k \mathbf{L}) u_n + k((1 - \alpha) \mathbf{F}(u_n, t_n) + \alpha \mathbf{F}(u_{n+1}, t_{n+1}))], \quad (6.3.13)$$

as the corrector.

Two-step methods (IMEXPC2):

$$\begin{aligned} \bar{u}_{n+2} = & \left[\left(\alpha + \frac{1}{2} \right) \mathbf{I} - \left(\alpha + \frac{\nu \beta}{2} \right) k \mathbf{L} \right]^{-1} ([2\alpha \mathbf{I} + (1 - \alpha - \nu \beta) k \mathbf{L}] u_{n+1} + \\ & \left[\left(\frac{1}{2} - \alpha \right) \mathbf{I} + \frac{\nu \beta k \mathbf{L}}{2} \right] u_n + \\ & (\alpha + 1) k \mathbf{F}(u_{n+1}, t_{n+1}) - \alpha k \mathbf{F}(u_n, t_n)), \end{aligned} \quad (6.3.14)$$

as predictor, and

$$\begin{aligned} u_{n+2} = & \left[\left(\alpha + \frac{1}{2} \right) \mathbf{I} - \left(\alpha + \frac{\nu \beta}{2} \right) k \mathbf{L} \right]^{-1} ([2\alpha \mathbf{I} + (1 - \alpha - \nu \beta) k \mathbf{L}] u_{n+1} + \\ & \left[\left(\frac{1}{2} - \alpha \right) \mathbf{I} + \frac{\nu \beta k \mathbf{L}}{2} \right] u_n + \left(\alpha + \frac{\beta}{2} \right) k \mathbf{F}(\bar{u}_{n+2}, t_{n+2}) + \\ & (1 - \alpha - \beta) k \mathbf{F}(u_{n+1}, t_{n+1}) + \frac{\alpha}{2} k \mathbf{F}(u_n, t_n)), \end{aligned} \quad (6.3.15)$$

as corrector. The choices of free parameters ($0 \leq \alpha, \beta \leq 1$) in the schemes (6.3.12 - 6.3.15) allow us to generate varieties of methods.

Stability analysis of IMEX schemes:

For notational convenience, we write our Burger-Fisher equation (6.1.1) in the form

$$u_t = \nu Lu + F(u, t), \quad (6.3.16)$$

where $Lu = u_x x$, the linear term and $F(u, t) = \alpha u^\delta \frac{\partial u}{\partial x} + \beta u(1 - u^\delta)$, is classified as nonlinear term. Also, α, β, δ and ν are positive constants, subject to periodic boundary conditions. On applying the general IMEX scheme (6.3.9) to a test equation

$$\chi' = A\chi + iB\chi \quad (6.3.17)$$

yields

$$\frac{1}{k}\chi_{n+1} + \frac{1}{k} \sum_{j=0}^{s-1} \alpha_j \chi_{n-j} = \sum_{j=0}^{s-1} \beta_j B(\chi_{n-j}, t_{n-j}) + \nu \sum_{j=-1}^{s-1} \gamma_j A(\chi_{n-j}), \gamma_{-1} \neq 0. \quad (6.3.18)$$

The solution of difference equation (6.3.18) can be written in the form

$$\chi_{n+1} = \varrho_1 \tau_1^n + \varrho_2 \tau_2^n + \cdots + \varrho_s \tau_s^n$$

where τ_j , for $j = 1, 2, \dots, s$ is the j th root of the characteristic equation given by

$$\Gamma(z) = (1 - \gamma_{-1} Ak)z^s + \sum_{j=0}^{s-1} (\alpha_j - \beta_j iBk - \gamma_j Ak)z^{s-j-1} \quad (6.3.19)$$

and ϱ_j is a constant for which τ_j is simple. Stability holds for $|\tau_j| \leq 1$. For instance, considering the first-order scheme IMEXLM1, when equation (6.3.17) is applied, the general IMEX schemes (6.3.9) yields

$$\chi_{n+1} = \xi(A, B)\chi^n,$$

where

$$\xi(A, B) = \frac{1 + kA(1 - \gamma) + ikB}{1 - k\gamma A}.$$

Thus, the stability region of (A, B) is such that $|\xi(A, B)| \leq 1$.

In a similar manner, we can also obtain the conditions for IMEXPC methods by using the scalar test equation (6.3.16) [54, 112]. That is, to analyze the stability of the

IMEXPC schemes, we linearize the autonomous ODE

$$u'(t) = \nu u(t) + F(u(t), t), \quad (6.3.20)$$

about a fixed point u_0 , so that $\nu u_0 + F(u_0) = 0$. We obtain

$$u'(t) = \nu u(t) + \lambda u(t), \quad (6.3.21)$$

where $u(t)$ is the perturbation to u_0 and $\lambda = F'(u_0)$ is a diagonal or block matrix containing the eigenvalues of F .

In our computation, transformation [112] is taken for (6.3.9), to obtain the following predictor

$$\bar{u}_{n+s} = [(\alpha_s \mathbf{I} - \nu \beta k \mathbf{L})]^{-1} \sum_{j=0}^{s-1} (-\alpha_j u_{n+j} + \nu k \beta_j \mathbf{L} u_{n+j} + k \gamma_j \mathbf{F}(u_{n+j}, t_{n+j})), \quad (6.3.22)$$

and the corrector

$$u_{n+s} = [(\alpha_s \mathbf{I} - \nu \beta k \mathbf{L})]^{-1} \sum_{j=0}^{s-1} (-\alpha_j u_{n+j} + \nu k \beta_j \mathbf{L} u_{n+j} + k \beta_j \mathbf{F}(u_{n+j}, t_{n+j})) + k \beta_s \mathbf{F}(u_{n+j}, t_{n+j}), \quad (6.3.23)$$

schemes. Since matrix \mathbf{L} in (6.3.6) owns negative real eigenvalues, we are permitted to set $\lambda < 0$, letting also $\lambda = k\lambda$ and $\nu = k\nu$, and substitute them for the test equation (6.3.21) in the schemes (6.3.22) and (6.3.23) to give

$$u_{n+s} = [(\alpha_s - \lambda \beta_s)]^{-1} \sum_{j=0}^{s-1} \left[-\alpha_j + \lambda \beta_j + \nu \beta_j + \frac{\nu \beta_s}{\alpha_s - \lambda \beta_s} (-\alpha_j + \lambda \beta_j + \nu \gamma_j) \right] u_{n+j}, \quad \beta \neq 0. \quad (6.3.24)$$

Using Von Neumann stability analysis idea, we can now determine the stability region of (6.3.24) by the characteristic equation

$$(\alpha_s - \lambda \beta_s) \xi^j = \sum_{j=0}^{s-1} \left[-\alpha_j + \lambda \beta_j + \nu \beta_j + \frac{\nu \beta_s}{\alpha_s - \lambda \beta_s} (-\alpha_j + \lambda \beta_j + \nu \gamma_j) \right] \xi^j. \quad (6.3.25)$$

The IMEXPC scheme (6.3.12)-(6.3.13) is stable if no root of the characteristic equation (6.3.25) has modulus greater than one and if every root with modulus one is simple (that is, if all the roots of (6.3.25) lie in or on the unit circle).

So, the first-order IMEXPC schemes is stable if

$$\left| \frac{1 + \lambda + \nu - \lambda^2\gamma^2 - (\lambda(\lambda + 2) - \nu^2)\gamma}{\lambda^2\gamma^2 - 2\lambda\gamma + 1} \right| \leq 1.$$

Based on the roots condition in (6.3.25), we can easily verify that

$$\xi = \frac{1 + \lambda + \nu - \lambda^2\gamma^2 - (\lambda(\lambda + 2) - \nu^2)\gamma}{\lambda^2\gamma^2 - 2\lambda\gamma + 1},$$

hence, $\xi \leq 1$. This process can be repeated for the higher order IMEXPC schemes depending on the choices of the parameters.

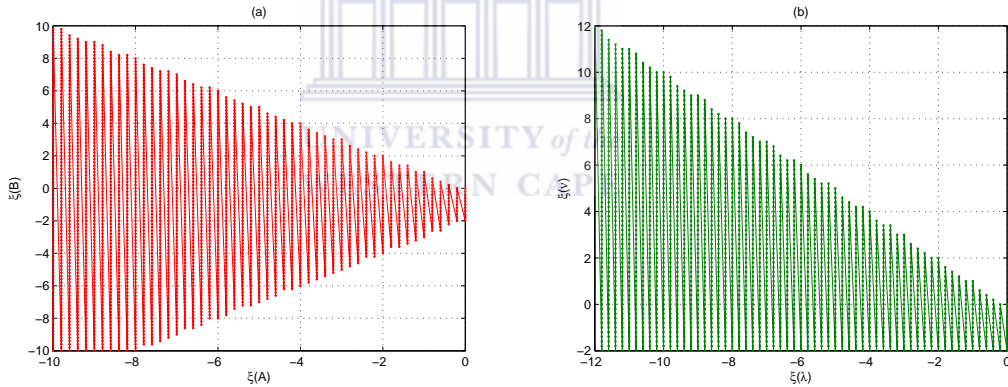


Figure 6.3.1: Stability regions of (a) IMEXLM1 (6.3.10) and (b) IMEXPC1 (6.3.12)-(6.3.13).

6.4 Numerical results

Effectiveness and accuracy of the methods discussed above are demonstrated with some numerical examples. In our computation, we measure the accuracy in terms of the maximum absolute relative error defined by

$$\text{absolute relative error} = \frac{\max_{1 \leq j \leq N} |u_j - \bar{u}_j|}{\max_{1 \leq j \leq N} |u_j|}, \quad (6.4.1)$$

where u_j and \bar{u}_j are the exact and computed values of solution u , and N is the number of interior points defined on the collocation interval

$$\{x_1 = a, \dots, x_i = a + (i - 1)h, \dots, x_N = b\}, \quad h = \frac{|b - a|}{N - 1}. \quad (6.4.2)$$

Burgers-Fisher equation:

In Figure 6.4.1, we present numerical result of Burgers-Fisher equation (6.1.1) subject to initial and boundary conditions

$$\left. \begin{aligned} \phi(x) = u(x, 0) &= \left\{ \frac{1}{2} + \frac{1}{2} \tanh \left(\frac{-\alpha\delta}{2(\delta+1)} x \right) \right\}^{1/\delta}, \\ u(0, t) &= \left\{ \frac{1}{2} + \frac{1}{2} \tanh \left[\frac{-\alpha\delta}{2(\delta+1)} \left(- \left(\frac{\alpha}{\delta+1} + \frac{\beta(\delta+1)}{\alpha} \right) t \right) \right] \right\}^{1/\delta}, \quad t \geq 0, \\ u(l, t) &= \left\{ \frac{1}{2} + \frac{1}{2} \tanh \left[\frac{-\alpha\delta}{2(\delta+1)} \left(1 - \left(\frac{\alpha}{\delta+1} + \frac{\beta(\delta+1)}{\alpha} \right) t \right) \right] \right\}^{1/\delta}, \quad t \geq 0, \end{aligned} \right\} \quad (6.4.3)$$

with exact solution

$$u(x, t) = \left\{ \frac{1}{2} + \frac{1}{2} \tanh \left[\frac{-\alpha\delta}{2(\delta+1)} \left(x - \left(\frac{\alpha}{\delta+1} + \frac{\beta(\delta+1)}{\alpha} \right) t \right) \right] \right\}^{1/\delta}, \quad t \geq 0, \quad (6.4.4)$$

for various parameter values of δ , α and β .

Burgers equation:

We present the numerical solution of Burgers equation

$$\frac{\partial u}{\partial t} = \nu \frac{\partial^2 u}{\partial x^2} - \beta u \frac{\partial u}{\partial x}, \quad x \in \Omega, \quad t > 0, \quad (6.4.5)$$

for various initial conditions $u(x, 0) = \phi(x)$, $x \in \Omega$, $0.001 \leq \nu \leq 1$, $\beta > 0$.

Fisher equation:

In Figure (6.4.7), we present the numerical results of well-known Fisher's equation

$$\frac{\partial u}{\partial t} = \nu \frac{\partial^2 u}{\partial x^2} + \beta u(1 - u), \quad x \in \Omega, \quad t > 0, \quad (6.4.6)$$

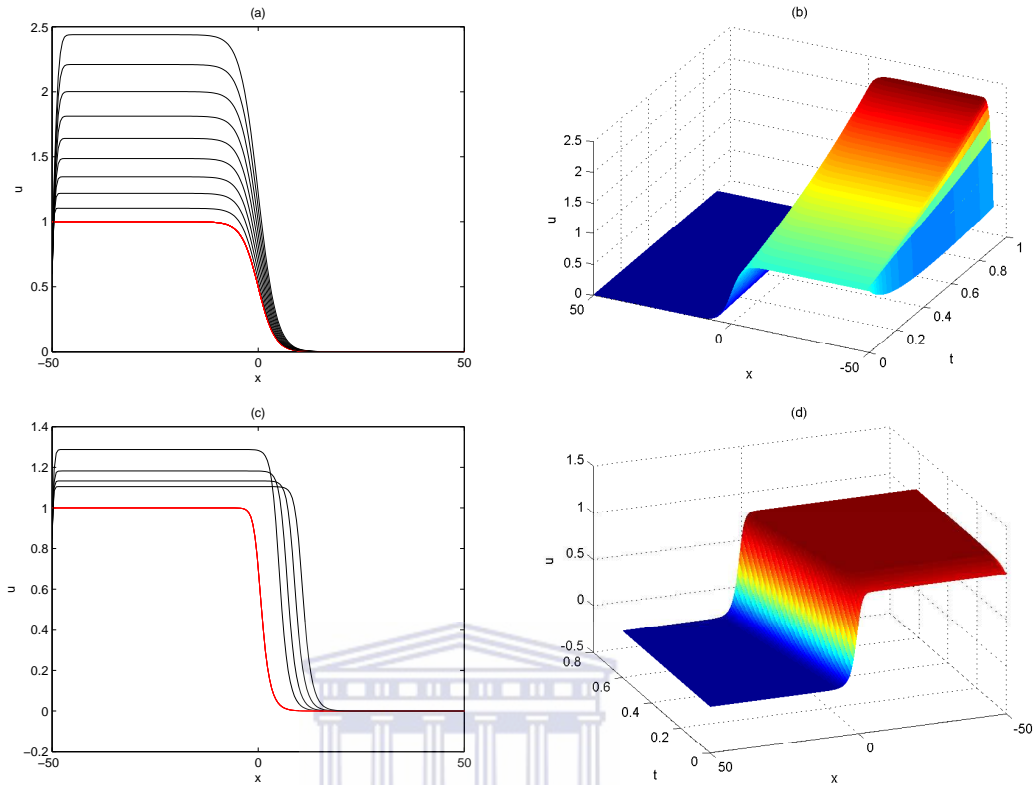


Figure 6.4.1: Numerical solution for Burgers-Fisher equation (6.1.1) at different parameter values for $N = 200$ with time-step $k = 0.0001$, (a) $\alpha = 1, \beta = 1, \delta = 1, \nu = 1, t = 0.1, 0.2, \dots, 0.9$, (b) surface plot at time $t = 0.9, \alpha = 1, \beta = 1, \delta = 1, \nu = 1$. Panel (c) is obtained at $t = 0.6, \beta = 5, 7, 9, 11, \nu = 1, \alpha = 2$ and $\delta = 2$. Surface plot (d) shows solution at time $t = 0.6, \beta = 11, \delta = 2, \nu = 1$ and $\alpha = 2$.

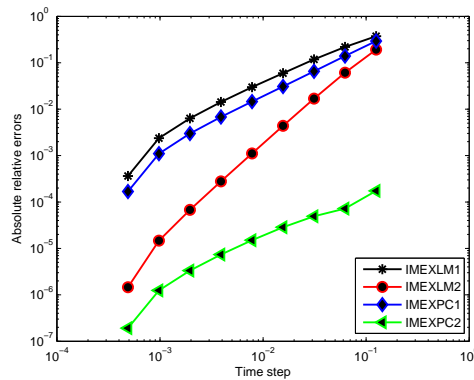


Figure 6.4.2: Performance of IMEXLM1, IMEXLM2, IMEXPC1 and IMEXPC2 when applied to solve Burger's-Fisher equation (6.1.1) at parameter values $\nu = 0.5, \alpha = 2, \beta = 5, \delta = 2, t = 1$, and $N = 250$ for $x \in [-50, 50]$.

subject to periodic boundary conditions in the interval $-L \leq x \leq L$ and some initial conditions

$$u(x, 0) = \phi(x), \tag{6.4.7}$$

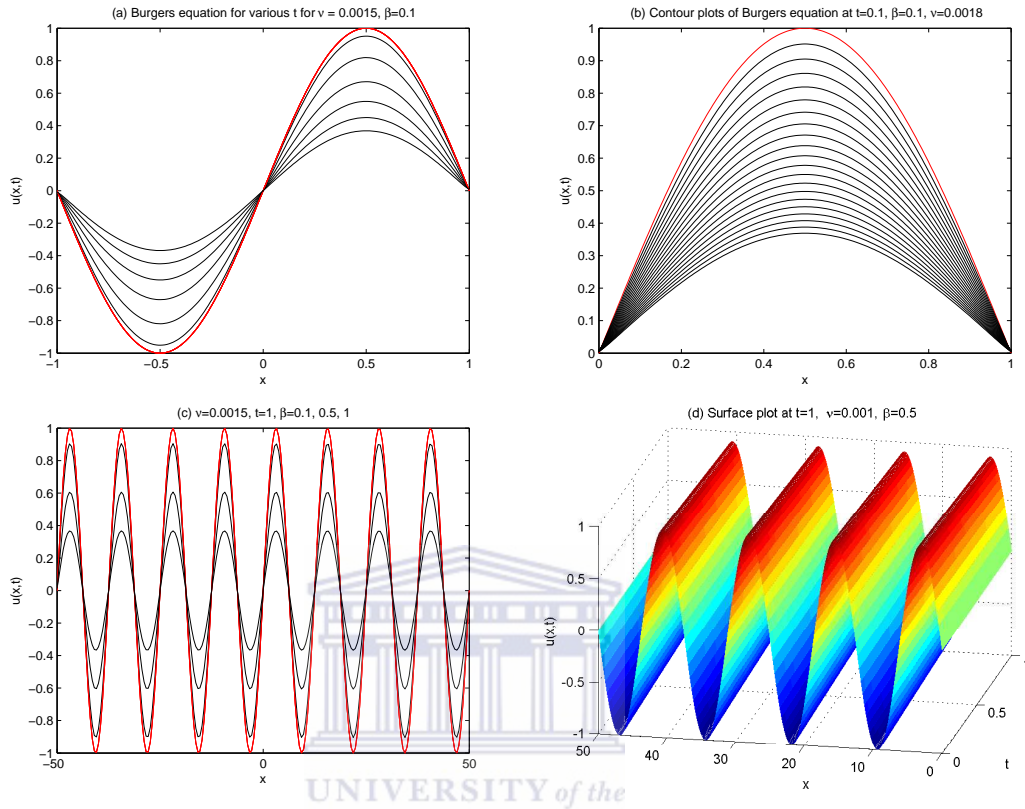


Figure 6.4.3: Numerical solution of Burgers equation (6.4.5) at different parameter values and for $u(x, 0) = \sin(32\pi x)$.

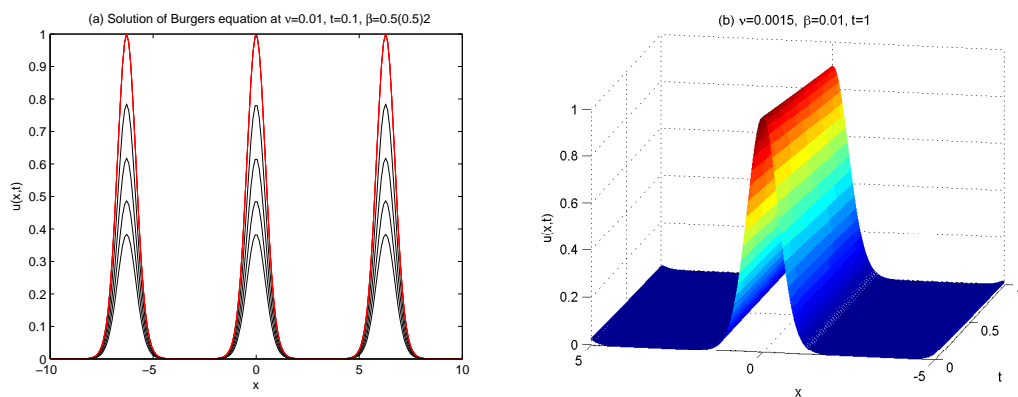


Figure 6.4.4: Numerical solution of Burgers equation (6.4.5) for different parameter values and $u(x, 0) = e^{-10 \sin(\frac{\pi}{2})^2}$.

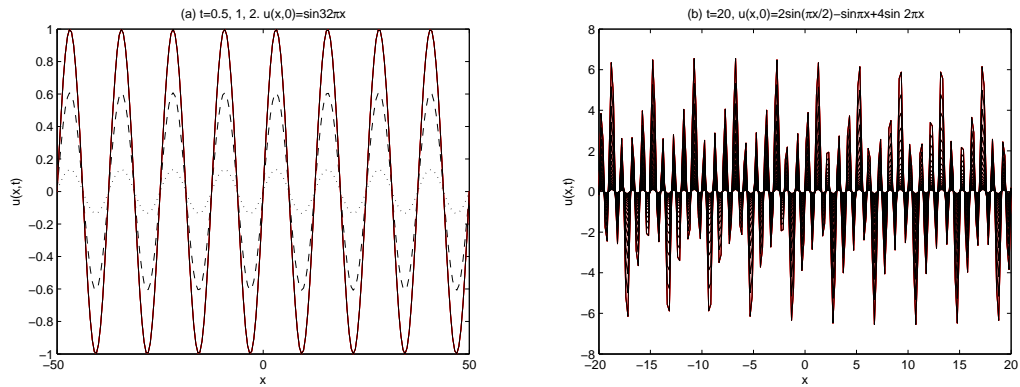


Figure 6.4.5: Solution of inviscid Burgers equation (6.1.6) for different parameter values and different initial conditions.

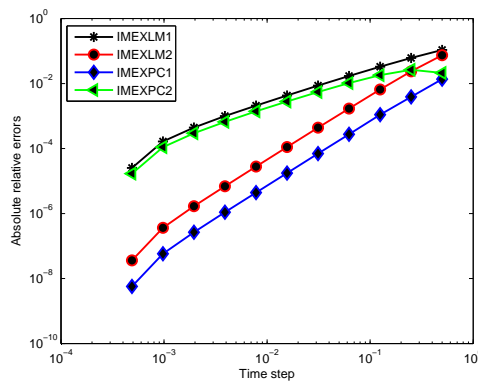


Figure 6.4.6: Performance of IMEXLM1, IMEXLM2, IMEXPC1 and IMEXPC2 when applied to solve Burgers equation (6.4.5). Other parameter values are $\nu = 0.001$, $\beta = 0.2$, $t = 1$, and $N = 200$ for $x \in [-20, 20]$.

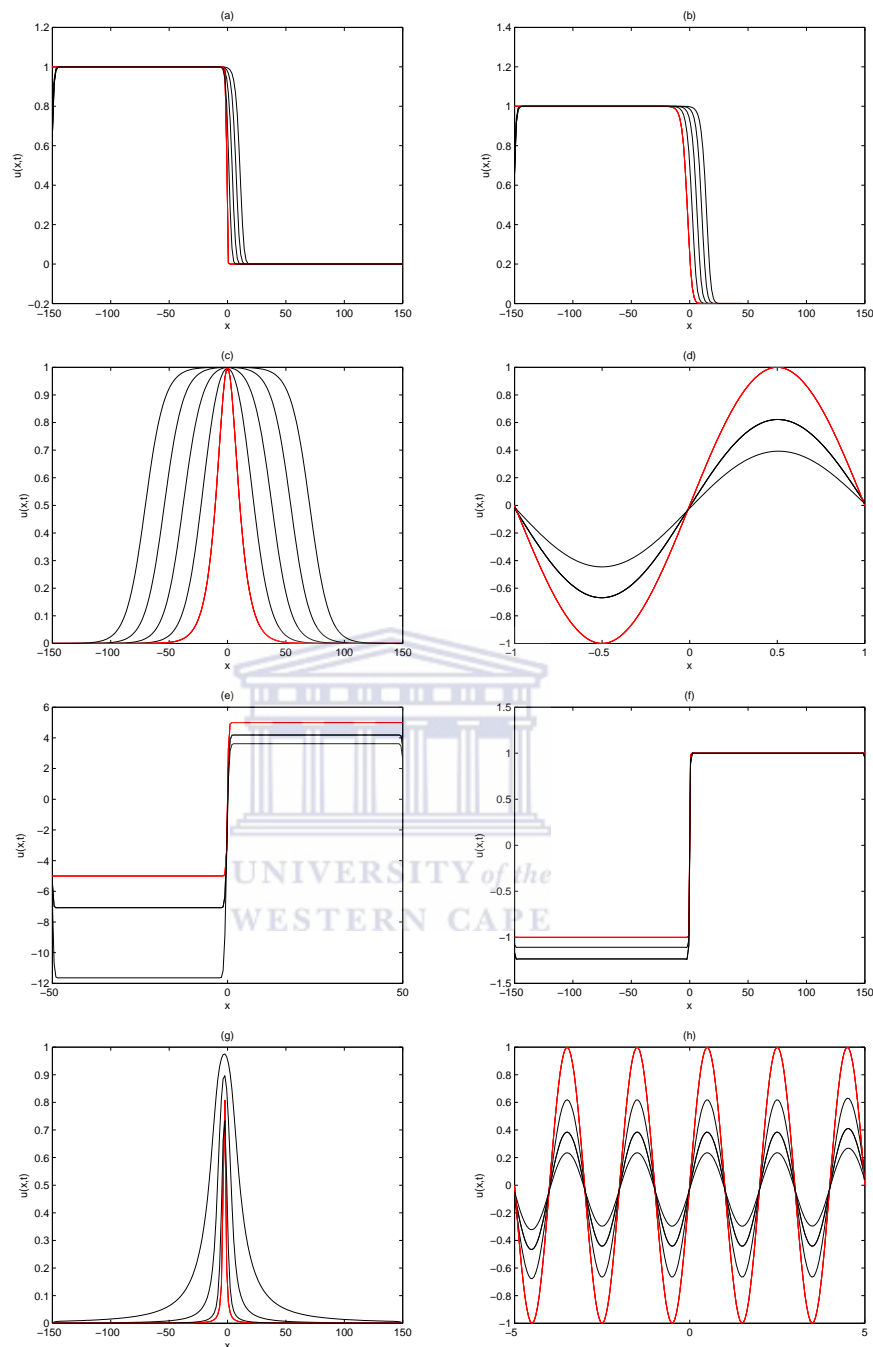


Figure 6.4.7: Numerical solution of Fisher's equation (6.4.6) for various initial conditions.

In Figure 6.4.7, we present the solution of Fisher equation (6.4.6). The parameter values are: (a) $\phi(x) = [1 + 5/6 \exp(6x/\sqrt{6})]^{-2}$, $t = 2, 4, 6, 8$ and $L = 150$; (b) $\phi(x) = [1 + \exp(x/\sqrt{6})]^{-2}$, $t = 2, 4, 6, 8$ and $L = 150$; (c) $\phi(x) = 1/\cosh \delta x$, $\delta = 0.125$, $t = 1, 2, 3, 4$, and $L = 150$; (d) $\phi(x) = \sin \pi x$, $t = 0.04, 0.08$ and $L = 1$; (e) $\phi(x) =$

5 $\tanh \pi x$, $t = 0.04, 0.08$ and $L = 50$; (f) $\phi(x) = \tanh x$, $t = 0.04, 0.08$ and $L = 150$; (g) $\phi(x) = 1/1 + (x + 2.75)^{-2}$, $t = 1, 3, 5$ and $L = 150$; (h) $\phi(x) = \sin \pi x$, $t = 0.04, 0.08, 0.16$ and $L = 5$.

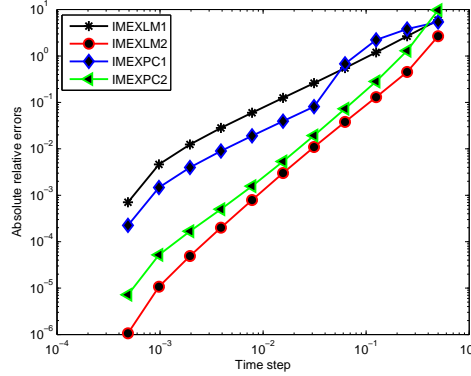


Figure 6.4.8: Performance of IMEXLM1, IMEXLM2, IMEXPC1 and IMEXPC2 when applied to solve Fisher's equation (6.4.6) for parameter values $\nu = 0.5$, $\beta = 0.15$, $t = 1$, and $N = 250$ for $x \in [-5, 5]$.

Korteweg-de Vries equation:

The Korteweg-de Vries (KdV) equation has a long standing history dating back to 1895, when Korteweg and his associate, de Vries developed an important equation known as KdV [101]. The equation was used to describe the theory of water waves in shallow channels. KdV equation is a nonlinear equation that exhibits special solutions referred to as solitons, it is the simplest model of the dispersive waves which under certain simplifying conditions covers cases of surface waves of long wavelength in liquids, plasma waves [87], lattice waves, weakly nonlinear magneto-hydrodynamic waves, acoustic waves in an inharmonic crystal [200] and ion-acoustic waves [148, 164]. KdV equation in modified form incorporates both convection and diffusion properties in fluid mechanics to illustrate shock waves [196]. The wide applicability of KdV equations is the main reason why over many years, they have attracted so much attentions in various fields of mathematics, physics and engineering.

We investigate the general third-order KdV equation with periodic boundary conditions,

$$u_t + uu_x + \beta u_{xxx} = 0, \quad x \in [-\pi, \pi], \quad (6.4.8)$$

for the dispersive waves in one and two and three soliton solutions. β is nonnegative diffusion coefficient. By neglecting the reaction term in (6.4.8), we have the linearized form of the KdV equation

$$u_t + \beta u_{xxx} = 0, \quad (6.4.9)$$

for which the dispersion relation takes the form $\omega = -\beta\gamma^3$ (say, a function of γ). Since $\omega''(\gamma) \neq 0$, it implies that the wave is dispersive.

By using the following transformation,

$$x \rightarrow \beta^{\frac{1}{3}}x, \quad u \rightarrow -6\beta^{\frac{1}{3}}u, \quad t \rightarrow t.$$

Equation (6.4.8) becomes

$$u_t - 6uu_x + u_{xxx} = 0. \quad (6.4.10)$$

Next, we sought for solution of (6.4.8) that is transported in the general form

$$u(x, t) = \phi(x - ct),$$

where c is the wave speed. On substituting in (6.4.20), we have

$$-c\phi = -\phi''' + 6\phi\phi',$$

which on integration yields

$$-c\phi = -\phi'' + 3\phi^2 + \frac{1}{2}A.$$

On multiplying through by $2\phi'$ and then integrate to give

$$\phi'^2 = 2\phi^3 + c\phi^2 + A\phi + B,$$

where A and B are the constants of integration. We assumed that the initial condition $u(x, 0) = u_0(x)$ is to be bounded and continuously differentiable, we want a solution for which $u, u_x, u_{xx} \rightarrow 0$ as $x \rightarrow \infty$. Under these boundary conditions the solitary wave

solution of (6.4.10) is

$$u(x, t) = \phi(x - ct) = -\frac{c}{2} \operatorname{sech}^2 \left(\frac{\sqrt{c}}{2} (x - ct) + C \right), \quad (6.4.11)$$

where C is constant. Readers are referred to [19] for further analysis.

We subject (6.4.8) to initial conditions

$$u(x, 0) = \frac{c}{2} \operatorname{sech} \left(\frac{\sqrt{c}}{2} (x + 8) \right)^2, \quad (6.4.12)$$

and

$$u(x, 0) = B \tanh(\nu(x + 1)), \quad (6.4.13)$$

for one soliton solutions.

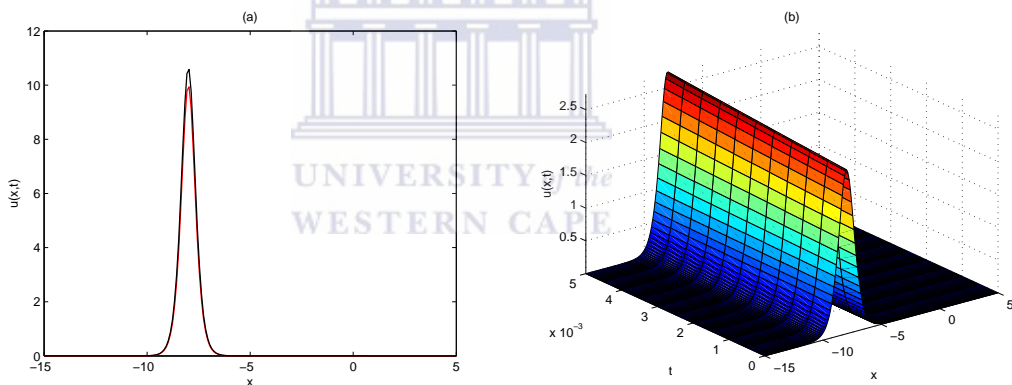


Figure 6.4.9: One soliton solution for KdV equation (6.4.8), using initial condition (6.4.12) and with $N = 200$, $x \in [-15, 5]$. The parameter values used are: (a) $t = 0.0005$, $c = 20$ and $\beta = 1$, (b) $t = 0.005$, $c = 5$ and $\beta = 0.05$.

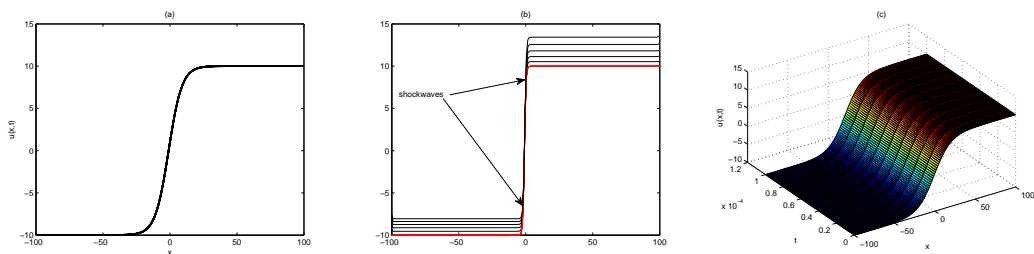


Figure 6.4.10: One soliton solution for KdV equation (6.4.8) using initial condition (6.4.13), for $\beta = 1, B = 20$ and with parameter values (a) $t = 0.00005$, $\nu = 0.1$, (b) $t = 0.01, \dots, 0.05$, $\nu = 0.9$ and (c) $t = 0.005$, $\nu = 0.05$.

Likewise, we consider initial conditions

$$u(x, 0) = 3A^2 \operatorname{sech} \left(\frac{A(x+2)}{2} \right)^2 + 3B^2 \operatorname{sech} \left(\frac{B(x+1)}{2} \right)^2 \quad (6.4.14)$$

and

$$u(x, 0) = 2 \operatorname{sech}(x)^2 + 0.5 \operatorname{sech}(0.5(x - 4\pi))^2, \quad (6.4.15)$$

for two soliton solutions.

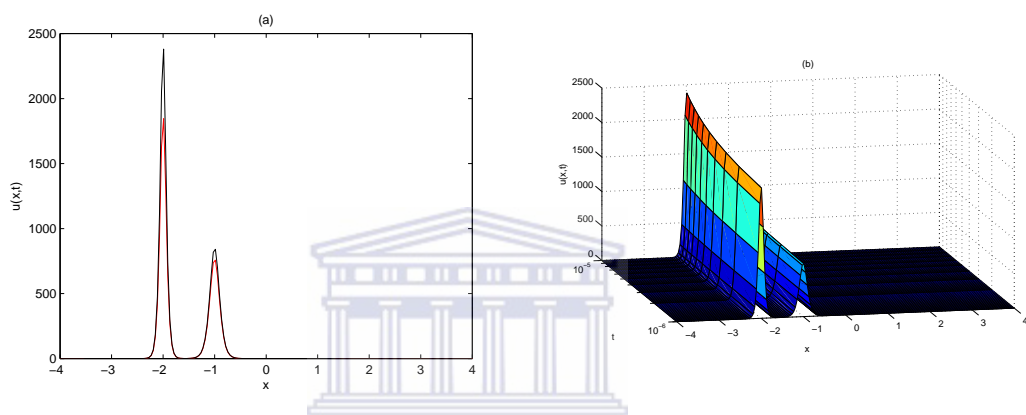


Figure 6.4.11: Two soliton solutions for KdV equation (6.4.8), for $t = 0.0001$, $A = 25$, $B = 16$ and $\beta = 1$, and using initial condition (6.4.14).

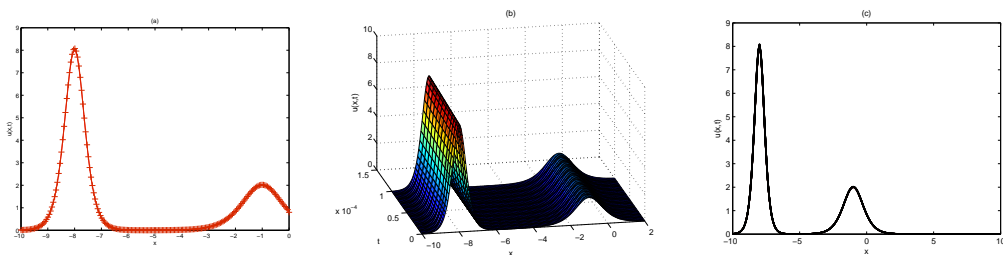


Figure 6.4.12: Two soliton solutions for KdV equation (6.4.8) using initial condition (6.4.15), for $\beta = 1$.

The variability in the positions of the smaller soliton along the space interval $[-10, 10]$ is shown in Figure 6.4.12.

We finally conclude based on the results obtained in figures 6.4.9-6.4.13 above, that soliton travelling from $x = -\infty$ to $x = \infty$ except that they differ in phase. In case of two solitons, a double wave solution which breaks into two solitons as $t \rightarrow -\infty$ and as $t \rightarrow \infty$. According to KdV equation, the effect of nonlinear interaction between them

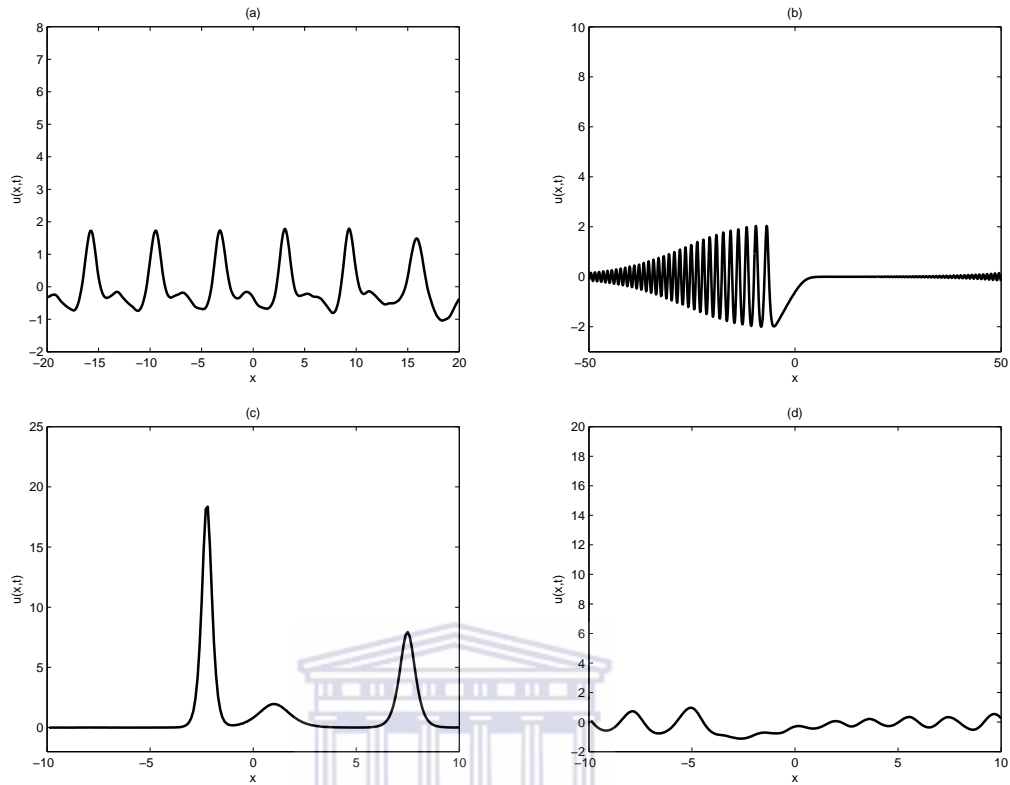


Figure 6.4.13: Solitons travelling from $x = -\infty$ to $x = \infty$ with different phase for KdV equation (6.4.8).

simply displaces their relative position. This is much evident in Figure 6.4.14 (b) that represents interaction of two disparate solitons with different velocities and amplitudes starting from $t = -\infty$, the bigger following the smaller. The actual interaction takes place mainly from $t = -10$ to $t = 10$. We can see clearly that at first the bigger soliton begins to swallow the smaller one, at $t = 0$ they both combine to form a single double wave, then the bigger soliton emerges out leaving the smaller soliton behind. As t is increased say, $t = 0.62$, both appear as separate solitons.

For the three solitons, we consider the initial condition

$$u(x, 0) = 3 \exp(-20(x + 4)^2) + \exp(-20(x + 1)^2) + 2.05 \exp(-10(x - 4)^2). \quad (6.4.16)$$

Numerical solutions are represented for $0 \leq t \leq 3.5$ in Figure 6.4.15.

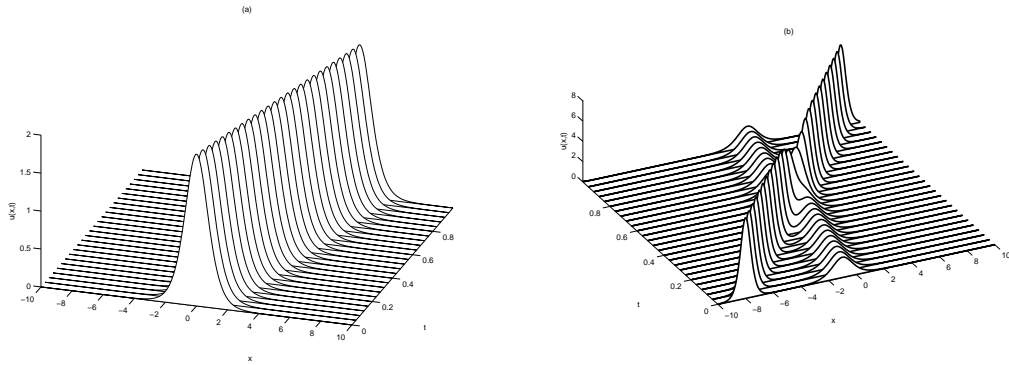


Figure 6.4.14: Interaction of (a) one and (b) two solitons for KdV equation (6.4.8).

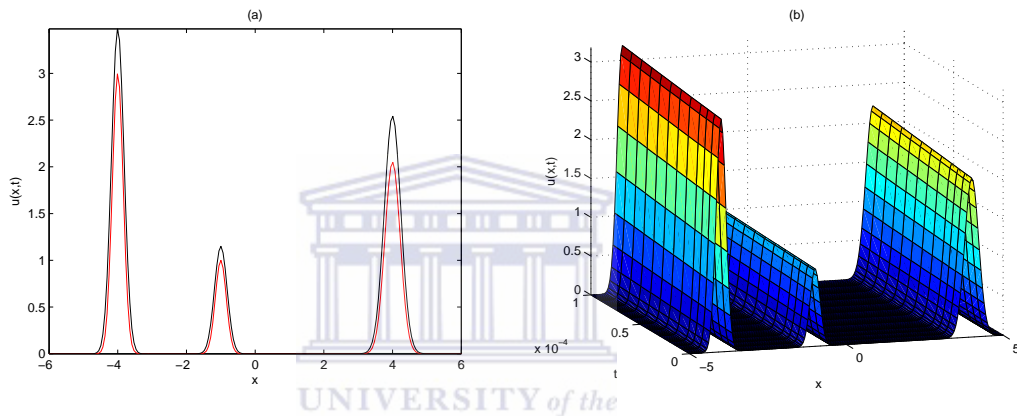


Figure 6.4.15: Three solitons solutions for KdV equation (6.4.8): (a) $t=0.005$, (b) $t=0.0001$.

Allen-Cahn (bistable) equation:

Allen-Cahn equation was earlier introduced in the combined work of Allen and Cahn [6] to give a description of the motion of anti-phase boundaries in crystalline solids and other phase transition problems. Allen-Cahn equation have been widely studied in various forms for many complex and rigorous moving interface problems in application areas of materials science and fluid dynamics via a phase-field technique (see for example, [84, 113]. Various numerical methods have been used to solve Allen-Cahn equation [3, 48, 85, 177, 202].

We consider Allen-Cahn equation

$$u_t = \delta u_{xx} + u - u^3, \quad x \in [-l, l], \quad (6.4.17)$$

subject to initial conditions

$$u(x, 0) = \frac{1}{100} \left[53x + 47 \sin \left(\frac{-3\pi x}{2} \right) \right], \quad x \in [-l, l], \quad (6.4.18)$$

with constant dirichlet boundary conditions,

$$u(-l, t) = -1, \quad u(l, t) = 1, \quad (6.4.19)$$

where δ is a positive parameter value. This equation has three steady states, $u = -1$ and $u = 1$ are stable, $u = 0$ is unstable. The states $u = \pm 1$ are attracting, meaning that any solution will converge either to -1 or 1 and makes the region $-1 \leq x \leq 1$ invariant. The solutions tend to exhibit flat areas close to the values separated by interfaces that may amalgamate or vanish on a long time scale, this phenomenon is referred to as metastability [187].

Compared to the Fisher equation, the bistability equation uses an improvement of the logistic growth term $u(1-u)$; for instance, if the population density $u(x, t)$ is too low, it could lead to an extinction by lack of encounters between individuals, this is termed Allee effect [23, 102, 139, 140].

At first, in Figure 6.4.16 the solution displays sinusoidal-like pattern but sometimes, the periodic oscillation becomes less strong, dampens and then turns flat, which we referred to as a steady state profile.

Kuramoto-Sivashinsky equation:

The Kuramoto-Sivashinsky (KS) [187], equation in one space dimension is given by

$$u_t = -uu_x - u_{xx} - u_{xxxx}, \quad x \in [0, L], \quad (6.4.20)$$

where L is periodic with initial condition

$$u(x, 0) = \cos \left(\frac{x}{16} \right) \left(1 + \sin \left(\frac{x}{16} \right) \right). \quad (6.4.21)$$

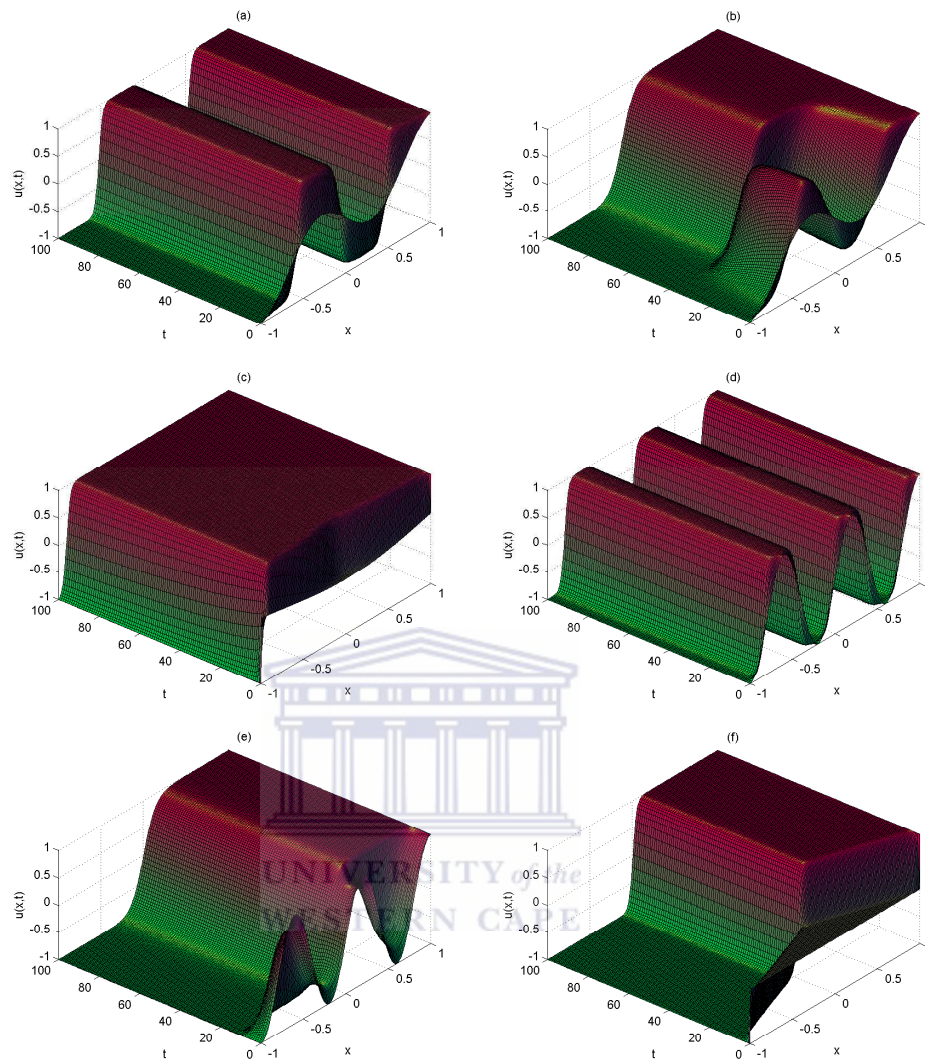


Figure 6.4.16: Time evolution for the Allen-Cahn equations (6.4.17)-(6.4.19), for $\omega = 16$, $0 \leq t \leq 100$, the x -axis runs from $x = -1$ to $x = 1$ with diffusion coefficient in the range $[0.001, 0.01]$.

The three terms on the right hand side of (6.4.20), correspond in a unique way to nonlinear advection term that acts as medium of transfer of energy from low to high wave numbers, energy input at large scales that posses the destabilizing effect and dissipation at small scales with stabilizing effect respectively. The KS equation dates back to mid-1970s, it was first derived by Kuramoto in the study of reaction-diffusion and later considered in higher space dimensions by Sivashinsky to model small thermal diffusive instabilities in laminar flame fronts. The KS equation arises primarily in the description of stability of flame fronts and solidification problems in reaction-diffusion

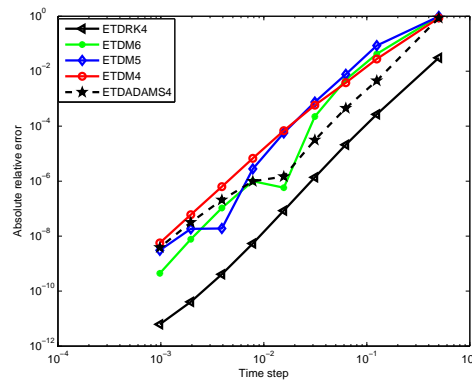


Figure 6.4.17: Performance of ETDRK4, ETDM4, ETDM5, ETDM6 and ETDADAMS4 methods for solving the Allen-Cahn equation with $N = 200$, $\delta = 0.5$ and $T = 1$ on $[-1,1]$.

systems, it was described as one of the simplest and most interesting nonlinear PDEs whose behaviour exhibit spatiotemporally chaotic solutions. Numerical solution of KS equation has generated a lot of attentions [92, 96] because of the fourth-order term present in it.

In this context, we present only the numerical study of KS equation (6.4.20), to display various chaotic structures and pattern formations subject to the periodic boundary condition with initial data L . Readers are referred to [39, 65, 105, 109], for further analytical study, structure, stability and bifurcation characteristics.

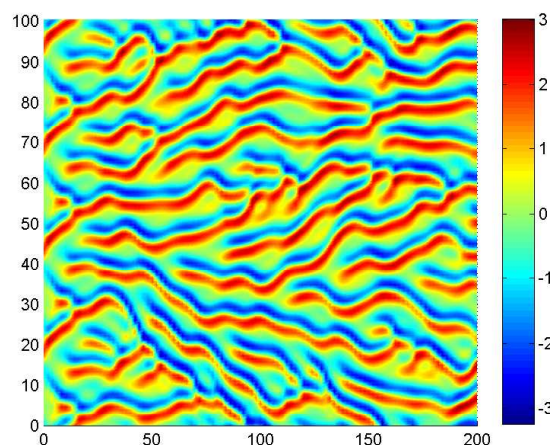


Figure 6.4.18: A typical spatiotemporally chaotic structure of the solution of the Kuramoto-Sivashinsky equation (6.4.20) emerging from smooth initial data on interval of length $L = 32\pi$.

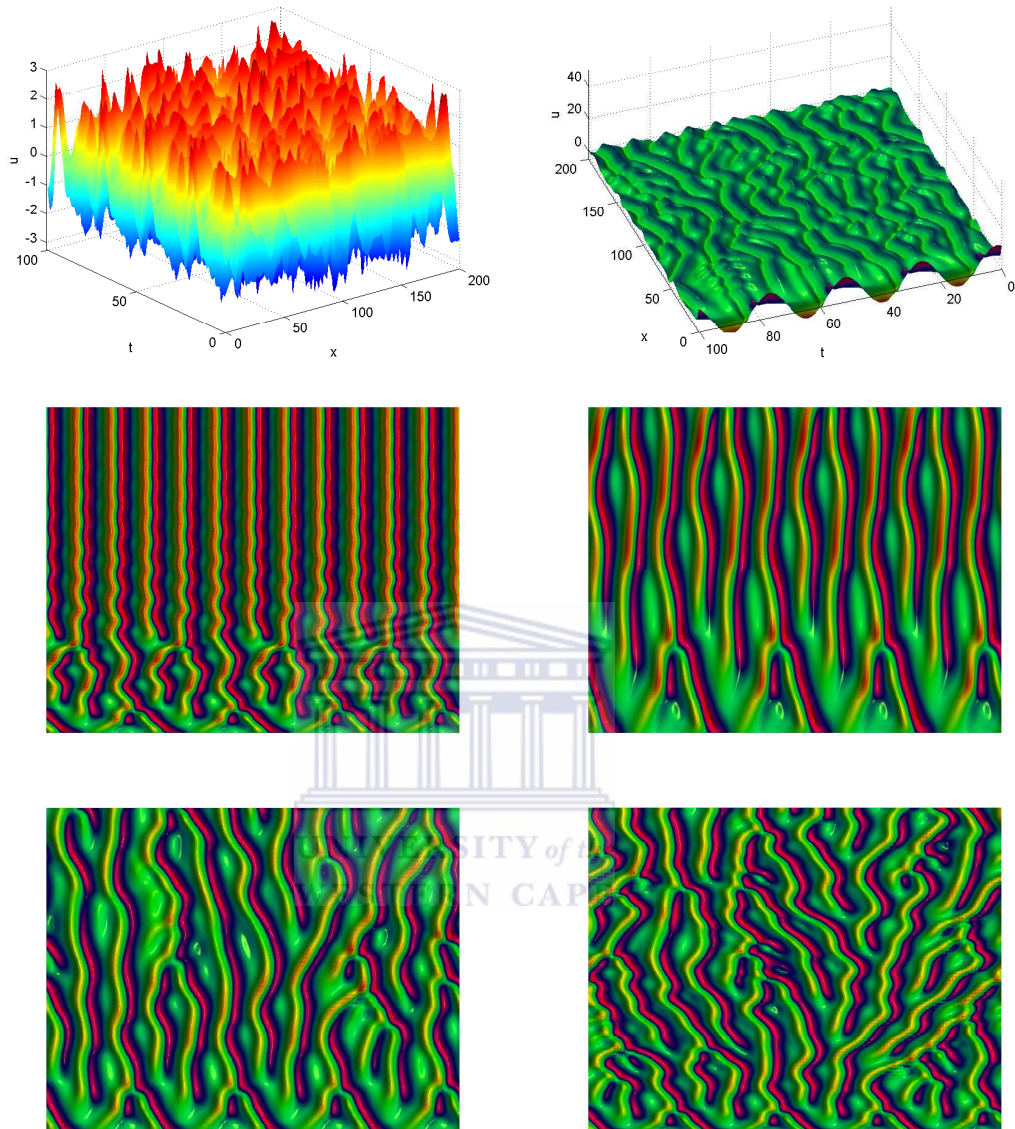


Figure 6.4.19: Time evolution of the Kuramoto-Sivashinsky equation (6.4.20) at some initial conditions for $L = 32\pi$.

The plots in Figure 6.4.19 demonstrate how each initial data evolves into a much more complicated structure.

6.5 Summary and discussions

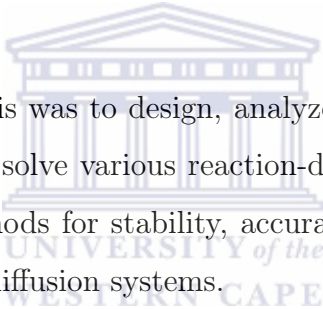
In this chapter, four implicit-explicit (IMEXLM1, IMEXLM2, IMEXPC1, IMEXPC2) schemes have been used for the time integration in conjunction with fourth-order cen-

tral finite difference in space for the numerical exploration of various features and patterns in the solution of the popular Burgers-Fisher equation. In figures 6.4.2, 6.4.6 and 6.4.8, we illustrate the tradeoff between the time step and the accuracy, with a gold-standard run (computed with IMEXLM1, IMEXLM2, IMEXPC1, IMEXPC2 and $\Delta t = 10^{-4}$), the absolute relative errors are displayed as a function of the time step. One observes that the convergence of the schemes is mostly influenced by the choice of the parameters because it is very difficult to say decide which scheme has the best convergence, for instance, IMEXPC2 appears best for Burgers-Fisher equation, IMEXPC1 takes the lead for the Burgers equation while IMEXLM2 shines for the Fisher equation. All the codes run faster under two seconds. Another benefit of our approach is that the schemes used here, with some modifications, can be extended to solve nonlinear reaction-diffusion equations.

Later, we considered the use of higher-order exponential time differencing schemes for the numerical solution of nonlinear time-dependent stiff PDE problems such as the Korteweg de Vries (KdV) equation, Allen-Cahn equation and the Kuramoto-Sivashinsky (KS) equation. Comparing with the existing exponential time differencing (ETD) schemes, such as the multi-step methods of orders 4,5,6, discussed in the previous chapter, we can deduce from the results obtained in Figure 6.4.17 that ETDRK4 provides a better accuracy over its higher-order time-stepping counterparts. Compatibility and accuracy of our approach are justified via numerical experiments.

Chapter 7

Concluding remarks and scope for future research



The main aim of this thesis was to design, analyze and implement several high order time stepping methods to solve various reaction-diffusion problems through a careful examination of these methods for stability, accuracy and practicability when applied to very complex reaction-diffusion systems.

We explored the use of higher-order finite difference approximations in space in conjunction with ETD schemes in time to provide an accurate and reliable numerical results. The derivation of the explicit exponential time differencing (ETD) of Adams-type, denoted as ETDADAMS4, and those of Runge-Kutta type, abbreviated as ETDRK4 are both of order four. These schemes are used as our time-stepping methods for the numerical integration of large system of ODEs arising from the space discretization method. Stability properties of these methods were illustrated through several figures where we plotted the boundaries of the stability regions in two dimensions for negative and purely real values of the stiffness parameters in the test problems. Our findings revealed that these methods possess different features in terms of stability. For instance, as the order of ETDRK schemes increases, their stability regions are also increased. One may note that even though the lower order ETD schemes are not used in this work but we carried out their stability analysis for us to have full comparative understanding of their behaviours.

We have also discussed the stability properties of ETDADAMS4 in both complex and real planes. In case of complex plane, the ETDADAMS4 has the largest stability region in which the lower order counterparts are enclosed. This is in contrast to the stability regions in the real (x, y) plane as the stability regions of ETDADAMS4 scheme is reduced as the order of the method is increased.

We have provided further justification to the assertion made by Kassam and Trefethen [92] on the efficiency and suitability of ETDRK4 schemes in conjunction with spatial discretisation methods by comparing it with exponential time differencing method (ETDADAMS4) of Adams type and exponential time differencing multi-step (ETDM4, ETDM5, ETDM6) methods. This approach was tested by considering the nonlinear form of reaction-diffusion equations. Regarding accuracy and computational (CPU) time in the solving such nonlinear equations, we found that the ETDRK4 method is the best among above mentioned methods. This method maintains good stability properties and produces high accuracy with reasonable computational effort.

In the same manner, further numerical simulations of the scalar type of reaction-diffusion problems are also considered. We have studied the Fisher equation (to examine the rate of diffusivity, logistic growth and speed selection process) and the density dependent Nagumo equation. We believe also that the work done in Chapter 2 could grant an insight to the understanding of pattern formation in scalar reaction-diffusion systems. In comparison with other existing numerical methods that solve Fisher equation, our approach compared favourably. The ETDRK4 method demonstrates its superiority over of the existing ETD schemes used in terms of accuracy and convergence. The most amazing factor is the fact that the ETDRK4 is found to be much more accurate than fifth and sixth order ETD multi-step schemes. Biologically, the result presented in this chapter are found interesting and seen as means of displaying the complexities that nonlinearity has introduced into the simplest equations of population biology.

In Chapter 3, we considered two-system of reaction-diffusion equations. This type of equations could yield some interesting phenomena, such as, pattern formation far from equilibrium, pulse splitting and shedding, reactions and competitions in excitable

systems, nonlinear waves and spatiotemporal chaos. Our results have sparked renewed interest in reaction-diffusion models for biological pattern formation and, in particular, the roles that domain growth and diffusion coefficient played in the pattern formation mechanism.

The dynamic complexities of some other reaction-diffusion models consisting of prey-predator systems, competitive systems, and mutualism systems are studied in Chapter 4. Both the cases, with and without diffusions, are well discussed in this chapter.

In Chapter 5, some stiff systems of reaction-diffusion equations that explains the competition involving the interaction of three species in line with Turing's theory of pattern formation are solved. Anomaly behaviour of the three examples considered have further shown that chaos and hyper-chaos can occur in systems of autonomous ordinary differential equations with at least three variables and two quadratic nonlinearities. These amazing structures occur due to proper selection of model parameters and suitable initial conditions.

We further demonstrated the compatibility of high accuracy finite difference discretizations with higher-order time stepping IMEX methods. We are not surprised with the ill-performance of the IMEX schemes. Despite their simplicity and frequent usage, they are restricted from having an order higher than two if A-stability (which indicates the property that physically decaying solutions are numerically damped for any choice of time-step) is required. Such schemes are then extended to solve a number of nonlinear problems in Chapter 6.

In summary, the methods developed and implemented in this thesis gave us very robust results.

As far as the **scope for future research is concerned**, we are currently exploring the following:

- Firstly, we aim to develop a robust time-discretization methods that can enhance numerical studies of higher-order problems with linear and nonlinear stiff terms present in other complex models in mathematical biology.

- We are also extending our numerical methods to solve some reaction-diffusion models covering a diverse range of physical phenomena.
- Proposed numerical methods in this thesis can also be extended to solve reaction-diffusion problems in two-dimensional space.
- It should be noted that we have used higher order finite difference approximations for spatial discretizations in this thesis. To this end, we are currently working on the use of spectral methods for spatial discretization in conjunction with the exponential time-differencing integrators as well as, spectral discretizations for both time and space discretizations.



Bibliography

- [1] U.G. Abdullaev, Stability of symmetric traveling waves in the cauchy problems for the KPP equation, *Journal of Differential Equation* **30** (1994) 377-386.
- [2] M.J. Ablowitz and A. Zeppetella, Explicit solution of Fisher's equation for a special wave speed, *Bulletin of Mathematical Biology* **41** (1970) 835-840.
- [3] I. Ali, S. Islam, I. Siddique and N. Min-Allah, Some efficient numerical solutions of Allen-Chan equation with non-periodic boundary conditions, *International Journal of Nonlinear Science* **11** (2011) 380-384.
- [4] K. Al-Khaled, Numerical solution of Fisher's reaction-diffusion equation by the sinc collocation method, *Journal of Computational and Applied Mathematics* **137** (2000) 245-255.
- [5] W.C. Allee, *The Social Life of Animals*, Norton, New York, 1938.
- [6] S.M. Allen and J.W. Cahn, A microscopic theory for antiphase boundary motion and its application to antiphase domain coarsening, *Acta Metallurgica* **27** (1979) 1085-1095.
- [7] L.J.S. Allen, *An Introduction to Mathematical Biology*, Pearson Education, Inc., New Jersey, 2007 .
- [8] P. Amarasekare, Interactions between local dynamics and dispersal: insights from single species models, *Theoretical Population Biology* **53** (1998) 44-59.
- [9] R. Aris, *The Mathematical Theory of Diffusion and Reaction in Permeable Catalysts, Vols. I and II*, Oxford University Press (Clarendon), New York, 1975.

- [10] U.M. Ascher, S.J. Ruth and B.T.R. Wetton, Implicit-explicit methods for time-dependent partial differential equations, *SIAM Journal on Numerical Analysis* **32** (1995) 797-823.
- [11] U.M. Ascher, S.J. Ruth and R.J. Spiteri, Implicit-explicit Runge-Kutta methods for time-dependent partial differential equations, *Applied Numerical Mathematics* **25** (1997) 151-167.
- [12] H.A. Ashi, *Numerical Methods for Stiff Systems*, PhD thesis, University of Nottingham, 2008.
- [13] H. Baek, D.I. Jung and Z. Wang, Pattern formation in a semi-ratio-dependent predator-prey system with diffusion, *Discrete Dynamics in Nature and Society* (2013). Doi:10.1155/2013/657286.
- [14] K.A. Bagrinovskii and S.K. Gudunov, Difference schemes for multi-dimensional problems, *Doklady Akademii Nauk* **115** (1957) 431-433.
- [15] N.J. Balmforth, R.V. Craster and S.J.A. Malham, Unsteady fronts in an autocatalytic system, *Proceedings of the Royal Society of London A* **455** (1999) 1401-1433.
- [16] H. Berland and B. Skaflestad, Solving the nonlinear schrodinger equation using exponential integrators, *Norwegian Society of Automatic Control* **27** (2006) 201-217.
- [17] A.A. Berryman, *Population Systems: A General Introduction*, Plenum Press, New York, 1981.
- [18] G. Beylkin, J.M. Keiser and L. Vozovoi, A new class of time discretization schemes for the solution of nonlinear PDEs, *Journal of Computational Physics* **147** (1998) 362-387.
- [19] P.L. Bhatnagar, *Nonlinear Waves in One-dimensional Dispersive Systems*, Oxford Mathematical Monographs, 1979.

- [20] J. Billingham and A.C. King, *Wave Motion*, Cambridge Text in Applied Mathematics, Cambridge University Press, Cambridge, 2000.
- [21] P.K. Brazhnik and J.J. Tyson, Nonspiral excitation waves beyond the eikonal approximation, *Physics Review E* **54** (1999) 4338-4346.
- [22] P.K. Brazhnik and J.J. Tyson, On Traveling wave solutions of Fisher's equation in two spatial dimensions, *SIAM Journal of Applied Mathematics* **60** (1999) 371-391.
- [23] N.F. Britton, *Reaction-diffusion Equations and their Applications to Biology*, Academic Press, London, 1986.
- [24] J.M. Burgers, On the application of statistical mechanics to the theory of turbulent fluid motion, *Proceedings of the Royal Netherlands Academy Society* **32** (1929) 414-425.
- [25] R.L. Burden and J.D. Faires, *Numerical Analysis*, Wadsworth Group, 2001.
- [26] J.C. Butcher, Implicit Runge-Kutta processes, *Mathematics of Computation* **18** (1964) 50-64.
- [27] J.C. Butcher, On Runge-Kutta processes of high order, *Journal of the Australian Mathematical Society* **4** (1964) 179-194.
- [28] J.C. Butcher, A history of Runge-Kutta methods, *Applied Numerical Mathematics* **20** (1996) 247-260.
- [29] J.C. Butcher and G. Wanner, Runge-Kutta methods: some historical notes, *Applied Numerical Mathematics* **22** (1996) 113-151.
- [30] M.P. Calvo, J. de Frutos and J. Novo, Linearly implicit Runge-Kutta methods for advection-reaction-diffusion equations, *Applied Numerical Mathematics* **37** (2001) 535-549.
- [31] M. Calvo and C. Palencia, A class of explicit multi-step exponential integrators for semi-linear problems, *Numerical Mathematics* **102** (2006) 367-381.

- [32] V. Castets, E. Dulos, J. Boissonade and P. De Kepper, Experimental evidence for a sustained Turing-type nonequilibrium chemical pattern, *Physical Review Letters* **64** (1990) 2953-2956.
- [33] J. Certaine, The Solution of Ordinary Differential Equations with Large Time Constants. In A. Ralston and H.S. Wilf (eds.): *Mathematical Methods for Digital Computers*, 128-132, Wiley, New York, 1960.
- [34] B. Chen, Y. Li, H. Chen and B. Wang, Exp-function method for solving the Burgers-Fisher equation with variable coefficients; <http://arxiv.org/abs/1004.1815v1>, (2010).
- [35] J.D. Cole, On a quasi linear parabolic equation occurring in aerodynamics, *Quarterly of Applied Mathematics* **9** (1951) 225-236.
- [36] S.M. Cox and P.C. Matthews, Exponential time differencing for stiff systems, *Journal of Computational Physics* **176** (2002) 430-455.
- [37] R.V. Craster and R. Sassi, Spectral algorithms for reaction-diffusion equations, *Technical report, Note del Polo – Ricerca N. 99* Universita di Milano, 2006.
- [38] M. Crouzeix, Une méthode multipas implicite-explicite pour l'approximation des équations d'évolution paraboliques, *Numerical Mathematics* **35** (1980) 257-276.
- [39] P. Cvitanovic, R.L. Davidchack and E. Siminos, On the state space geometry of the Kuramoto-Sivashinsky flow in a periodic domain, *SIAM Journal on Applied Dynamical Systems* **9** (2010) 1-33.
- [40] M. del Pino, M. Kowalczyk and J. Wei, Multi-bump ground states of the Gierer-Meinhardt system in R^2 , *Annales de l'Institut Henri Poincaré (C) Non Linear Analysis* **20** (2003) 53-85.
- [41] B. Dennis, Allee effects: population growth, critical density, and the chance of extinction, *Natural Resource Modeling* **3** (1989) 481-538.

- [42] A. Doelman, T.J. Kaper and P.A. Zegeling, Pattern formation in the one-dimensional Gray-Scott model, *Journal of Nonlinear Science* **10** (1997) 523-563.
- [43] A. Doelman, R.A. Gardner and T.J. Kaper, Stability analysis of singular patterns in the 1D GS model: a matched asymptotic approach, *Physica D: Nonlinear Phenomena* **122** (1998) 1-36.
- [44] A. Doelman and H. van der Ploeg, Homoclinic stripe patterns, *SIAM Journal on Applied Dynamical Systems* **1** (2002) 65-104.
- [45] A. Doelman, T.J. Kaper and H. van der Ploeg, Spatially periodic and aperiodic multi-pulse patterns in the one-dimensional Gierer-Meinhardt equation, *Methods and Applications of Analysis* **8** (2001) 387-414.
- [46] Q. Du and W. Zhu, Analysis and applications of the exponential time differencing schemes and their contour integration modifications, *BIT Numerical Mathematics* **45** (2005) 307-328.
- [47] E. Dulos, J. Boissonade, J.J. Perraud and B. Rudovics, Chemical morphogenesis: Turing patterns in an experimental chemical systems, *Acta Biotheoretica* **44** (1996), 249-261.
- [48] X. Feng and A. Prohl, Numerical analysis of the Allen-Cahn equation and approximation for mean curvature flows. *Numerische Mathematik* **94** (2003) 33-65.
- [49] Z. Feng, Traveling wave behaviour for a generalized fisher equation, *Chaos, Solitons and Fractals* **38** (2008) 481-488.
- [50] P.C. Fife, *Mathematical Aspects of Reacting and Diffusing systems*, Lecture Notes in Biomathematics, Vol. 28, Springer-Verlag, New York, 1979.
- [51] R.A. Fisher, The wave of advance of advantageous genes, *Annals of Eugenics* **7** (1937) 353-369.
- [52] B. Fornberg and Driscoll, A fast spectral algorithm for nonlinear wave equations with linear dispersion, *Journal of Computational Physics* **155** (1999) 456-467.

- [53] B. Fornberg, Finite difference method, *Scholarpedia* **6** (2011) (10) 9685.
- [54] J. Frank, W. Hundsdorfer and J.G. Verwer, On the stability of implicit-explicit linear multistep methods, *Applied Numerical Mathematics* **25** (1997) 193-205.
- [55] A. Friedli, Verallgemeinerte Runge-Kutta Verfahren zur Lösung steifer Differentialgleichungssysteme, In *Numerical treatment of differential equations (Mathematical Conference Proceedings Forschungsinst, Oberwolfach, 1976)* **631** 35-50, Lecture Notes in Mathematics, Springer, Berlin, 1978.
- [56] S. Gakkhar and R.K. Naji, Order and chaos in a food web consisting of a predator and two independent preys, *Communications in Nonlinear Science and Numerical Simulation* **10** (2005) 105-120.
- [57] M. Garvie, Finite-difference schemes for reaction-diffusion equations modeling predator-prey interactions in MATLAB, *Bulletin of Mathematical Biology* **69** (2007) 931-956.
- [58] M. Garvie and C. Trenchea, Finite element approximation of spatially extended predator-prey interactions with the Holling type II functional response, *Numerische Mathematik* **107** (2007) 641-667.
- [59] M. Garvie and C. Trenchea, Spatiotemporal dynamics of two generic predator-prey models, *Journal of Biological Dynamics* **4** (2010) 559-570.
- [60] A. Gierer and H. Meinhardt, A theory of biological pattern formation, *Kybernetik* **12** (1972) 30-39.
- [61] A. Golbabai and M. Javidi, A spectral domain decomposition approach for the generalized Burger's-Fisher equation, *Chaos Solitons and Fractals* **39** (2009) 385-392.
- [62] P. Gray and S.K. Scott, Autocatalytic reactions in the isothermal, continuous stirred tank reactor: Isolas and other forms of multistability, *Chemical Engineering Science* **38** (1983) 29-43.

- [63] P. Gray and S.K. Scott, Autocatalytic reactions in the isothermal, continuous stirred tank reactor: oscillations and instabilities in the system $A + 2B \rightarrow 3B, B \rightarrow C$, *Chemical Engineering Science* **39** (1984) 1087-1097.
- [64] P. Gray and S.K. Scott, Sustained oscillations and other exotic patterns of behaviour in isothermal reactions, *Journal of Physical Chemistry* **89** (1985) 22-32.
- [65] J.M. Greene and J.S. Kim, The steady states of the Kuramoto-Sivashinsky equation, *Physica D* **33** (1988) 99-120.
- [66] I. Grooms and K. Julien, Linearly implicit methods for nonlinear PDEs with linear dispersion and dissipation, *Journal of Computational Physics* **230** (2011) 3630-3560.
- [67] M. Gyllenberg, J. Hemminki and T. Tammaru, Allee effects can both conserve and create spatial heterogeneity in population densities, *Theoretical Population Biology* **56** (1999) 231-242.
- [68] H. Haario and T.I. Siedman, Reaction and diffusion at a gas/liquid interface, *SIAM Journal on Mathematical Analysis* **25** (1994) 1069-1084.
- [69] E. Hairer and G. Wanner, *Solving Ordinary Differential Equations II: Stiff and Differential-Algebraic Problems*, Springer-Verlag, New York, 1991.
- [70] J.P. Harmon and D.A. Andow, Indirect effects between shared prey, predictions for biological control, *Biological control* **49** (2004) 605-625.
- [71] K. Heun, Neue Methode zur approximativen Integration der Differentialgleichungen einer unabhängigen Veränderlichen, *Zeitschrift für angewandte Mathematik und Physik* **45** (1900) 23-38.
- [72] F. Hildebrand, *Finite-difference Equations and Simulations*. Prentice-Hall, Englewood Cliffs, New Jersey, (1968).
- [73] M. Hochbruck and C. Lubich, On Krylov subspace approximations to the matrix exponential operator, *SIAM Journal of Numerical Analysis* **34** (1997) 1911-1925.

- [74] M. Hochbruck, C. Lubich, and H Selhofer, Exponential integrators for large systems of differential equations, *SIAM Journal of Scientific Computing* **19** (1998) 1552-1574.
- [75] M. Hochbruck and A. Ostermann, Exponential Runge-Kutta methods for parabolic problems, *Applied Numerical Mathematics* **53** (2005) 323-339.
- [76] M. Hochbruck and A. Ostermann, Explicit exponential Runge-Kutta methods for semilinear parabolic problems, *SIAM Journal on Numerical Analysis* **43** (2005) 1069-1090.
- [77] Hochbruck and A. Ostermann, Exponential multistep methods of Adams-type, *BIT Numerical Mathematic* **51** (2011) 889-908.
- [78] J. Hofbauer and K. Sigmund, *The Theory of Evolution and Dynamical Systems*, Cambridge University Press, Cambridge, 1988.
- [79] J. Hofbauer and J.W. So, Multiple limit cycles for three dimensional competitive Lotka-Volterra equations, *Applied Mathematics Letters* **7** (1994) 65-70.
- [80] E.E. Holmes, M.A. Lewis, J.E. Banks and R.R. Veit, Partial differential equations: Spatial interactions and population dynamics, *Ecology* **75** (1994), 17-29.
- [81] R.D. Holt, Predation, apparent competition, and the structure of prey communities, *Theoretical Population Biology* **12** (1977) 197-229.
- [82] E. Hopf, The partial differential equation $u_t + uu_x = \mu u_{xx}$, *Communications on Pure and Applied Mathematics* **3** (1950) 201-230.
- [83] F. de la Hoz and F. Vadilo, An exponential time differencing method for the nonlinear schrodinger equation, *Computer Physics Communications* **179** (2008) 449-456.
- [84] Z. Hu, S.M. Wise, C. Wang and J.S. Lowengrub, Stable and efficient finite-difference nonlinear-multigrid schemes for the phase field crystal equation, *Journal of Computational Physics* **228** (2009) 5323-5339.

- [85] P. Huang and A. Abduwali, A numerical method for solving Allen-Chan equation, *Journal of Applied Mathematics and Informatics* **29** (2011) 1477-1487.
- [86] W. Hundsdorfer and S.J. Ruuth, Imex extensions of linear multistep monotonicity and boundedness properties, *Journal of Computational Physics* **225** (2007) 2016-2042.
- [87] E. Infeld and G. Rowlands, *Nonlinear Waves, Solitons and Chaos*, Cambridge University Press, Cambridge, 2002.
- [88] M.K. Jain, S.R.K. Iyengar and R.K. Jain, *Computational Methods for Partial Differential Equations*, Wiley Eastern Limited, New Delhi, 1994.
- [89] D.H. Janzen, The natural history mutualisms. In D.H. Boucher (ed.), *Biology of Mutualism*, Oxford University Press, Oxford, pp. 44-99, 1985.
- [90] M. Javidi, Modified pseudospectral method for generalized Burger's-Fisher equation, *International Mathematical Forum* **32** (2006) 1555-1564.
- [91] G. Karniadakis, M. Israeli and S. Orszag, Higher-order splitting methods for the incompressible Navier-Stokes equation, *Journal of Computational Physics* **91** (1991) 414-443.
- [92] A.K. Kassam and L.N. Trefethen, Fourth-order time-stepping for stiff PDEs. *SIAM Journal of Scientific Computing* **26** (2005) 1214-1233.
- [93] K. Kawasaki, A. Mochizuki, M. Matsushita, T. Umeda and N. Shigesada, Modeling spatio-temporal patterns generated by *Bacillus subtilis*, *Journal of Theoretical Biology* **188** (1997) 177-185.
- [94] D. Kaya and M.S. El-Sayed, A numerical simulation and explicit solutions of the generalized Burgers-Fisher equation, *Applied Mathematics and Computation* **152** (2004) 403-413.

- [95] C. Kennedy and M. Carpenter, Additive Runge-Kutta schemes for convection-diffusion-reaction-diffusion equations, *Applied Numerical Mathematics* **44** (2003) 139-181.
- [96] I.G. Kevrekidis, B. Nicolaenko and J.C. Scovel, Back in the saddle again: a computer assisted study of the Kuramoto-Sivashinsky equation, *SIAM Journal on Applied Mathematics* **50** (1990) 760-790.
- [97] H. Kierstead, L.B. Slobodkin, The size of water masses containing plankton blooms, *The Journal of Marine Research* **12** (1953) 141-147.
- [98] E. Kilic and M. El-Milkkawy, A computational algorithm for special n th-order pentadiagonal Toeplitz determinants, *Applied Mathematics and Computation* **199** (2008) 820-822.
- [99] D. Kocacoban, A.B. Koc, A. Kurnaz and Y. Keskin, A better approximation to the solution of Burger-Fisher equation, *Proceedings of the World Congress on Engineering*, Vol I, WCE (2011), London, U.K.
- [100] A. Kolmogoroff, I. Petrovskii and N. Piscounoff, Etude de l'équation de la diffusion avec croissance de la quantité de matière et son application à un problème biologique, *Moscow University Bulletin of Mathematics* **1** (1937) 1-25.
- [101] D.J. Korteweg and H. de Vries, On the change of form of long waves advancing in a rectangular canal, and on a new type of long stationary waves, *Philosophical Magazine* **39** (1895) 422-443.
- [102] M. Kot, *Elements of Mathematical Ecology*, Cambridge University Press, United Kingdom, 2001.
- [103] T. Koto, IMEX Runge-Kutta schemes for reaction-diffusion equations, *Journal Computational Applied Mathematics* **215** (2008) 182-195.
- [104] S. Krogstad, Generalized integrating factor methods for stiff PDEs, *Journal of Computational Physics* **203** (2005) 72-88.

- [105] M. Krupa, Bifurcations of relative equilibria, *SIAM Journal on Mathematical Analysis* **21** (1990) 1453-1486.
- [106] W. Kutta, Beitrag zur näherungsweise Integration totaler Differentialgleichungen, *Zeitschrift für Angewandte Mathematik und Physik* **46** (1901) 435-453.
- [107] J.D. Lambert, *Computational Methods in Ordinary Differential Equations*, John Wiley and Sons, London, UK, 1973.
- [108] J.D. Lambert, *Numerical Methods for Ordinary Differential Systems, The Initial Value Problem*, Chichester John Wiley and Sons, 1991.
- [109] Y. Lan and P. Cvitanovic, Unstable recurrent patterns in Kuramoto-Sivashinsky dynamics, *Physical Review E* **78** (2008) 026208.
- [110] J.M. Lee, T. Hillen and M.A. Lewis, Pattern formation in prey-taxis systems, *Journal of Biological Dynamics* **3** (2009) 551-573.
- [111] K.J. Lee and H.L. Swinney, Lamellar structures and self-replicating spots in a reaction-diffusion system, *Physical Review E* **51** (1995) 1899-1915.
- [112] D. Li, C. Zhang, W. Wang and Y. Zhang, Implicit-explicit predictor-corrector schemes for nonlinear parabolic differential equations, *Applied Mathematical Modelling* **35** (2011) 2711-2722.
- [113] C. Liu and J. Shen, A phase field model for the mixture of two incompressible fluids and its approximation by a Fourier-spectral method, *Physica D* **179** (2003) 211-228
- [114] D.J. Logan, *An Introduction to Nonlinear Partial Differential Equations*, Wiley, New York, 1994.
- [115] A.J. Lotka, *The Elements of Physical Biology*, Williams and Wilkins, Baltimore, 1952.

- [116] A.J. Lotka, The growth of mixed populations, two species competing for a common food supply, *Journal of the Washington Academy of Sciences* **22** (1932) 461-469.
- [117] R.L. Luther, Rauemliche fortpflanzung Chemischer reaktionen, *Z. für Elektrochemie und Angew. Physikalische Chemie* **12** (1906) 506-600. English translation: R. Arnold, K. Showalter and J.J. Tyson, Propagation of chemical reactions in space, *Journal of Chemical Education* **64** (1987) 740-742.
- [118] H. Malchow, Spatio-temporal pattern formation in nonlinear nonequilibrium plankton dynamics, *Proceedings of the Royal Society of London B* **251** (1993) 103-109.
- [119] H. Malchow, S.V. Petrovskii and E. Venturino, *Spatiotemporal Patterns in Ecology and Epidemiology: Theory, Models, and Simulations*, Chapman and Hall/CRC Press, London, 2008.
- [120] R.M. May and W.J. Leonard, Nonlinear aspects of competition between three species, *SIAM Journal on Applied Mathematics* **29** (1975) 243-253.
- [121] H.P. McKean, Nagumo's equation, *Advances in Mathematics* **4** (1970) 209-223.
- [122] A.B. Medvinsky, S.V. Petrovskii, I.A. Tikhonova, H. Malchow and B.L. Li, Spatiotemporal complexity of plankton and fish dynamics, *SIAM Reviews* **44** (2002) 311-370.
- [123] H. Meinhardt, *Models of Biological Pattern Formation*, Academic Press, London, 1982.
- [124] H. Meinhardt, *The Algorithmic Beauty of Sea Shells*, Springer, Berlin, Heidelberg, 1998.
- [125] M.J. Metcalf, J.H. Merkin and S.K. Scott, Oscillating wave fronts in isothermal chemical systems with arbitrary power of autocatalysis *Proceedings of the Royal Society of London A* **477** (1994) 155-174.

- [126] R. Mickens, A nonstandard finite difference scheme for a Fisher PDE having nonlinear diffusion, *Computers and Mathematics with Applications* **45** (2003) 429-436.
- [127] M. Mimura, H. Sakaguchi and M. Matsushita, Reaction-diffusion modelling of bacterial colony patterns, *Physica A* **282** (2000) 283-303.
- [128] B.V. Minchev and W.M. Wright, A review of exponential integrators for first order semi-linear problems, *Technical Report NTNU*, Department of Mathematical Sciences, Norwegian University of Science and Technology, 2005.
- [129] M.H. Mohd and Y.A. Hasan, Pattern formation in a two-dimensional space diffusive prey-predator model, *Journal of Applied Science* **12** (2012) 2016-2025.
- [130] D.R. Mott, E.S. Oran and B.V. Leer, A quasi-steady-state solver for the stiff ordinary differential equations of reaction kinetics, *Journal of Computational Physics* **164** (2000) 407-428.
- [131] K. Morton and D. Meyers, *Numerical Solution of Partial Differential Equations*, Cambridge University Press, Cambridge, 1996.
- [132] H. Munthe-Kaas, High order Runge-Kutta methods on manifolds, *Applied Numerical Mathematics* **29** (1999) 115-127.
- [133] A. Munteanu and R.V. Sole, Pattern formation in noisy self-replicating spots, *International Journal of Bifurcation and Chaos* **16** (2006) 3679.
- [134] C.B. Muratov and V.V. Osipov, Spike autosolitons and pattern formation scenarios in the two-dimensional Gray-Scott model, *European Physical Journal B* **22** (2001) 213-221.
- [135] C.B. Muratov and V.V. Osipov, Stability of the static spike autosolitons in the two-dimensional Gray-Scott model, *SIAM Journal Applied Mathematics* **62** (2002) 1463-1487.

- [136] J.D. Murray, *Lectures on Nonlinear Differential Equation Models in Biology*, Oxford University Press, New York, 1977.
- [137] J.D. Murray, *Mathematical Biology*, Springer-Verlag, Berlin, 1989.
- [138] J.D. Murray, *Mathematical Biology*, Biomathematics Texts, Springer, Berlin, 1993.
- [139] J.D. Murray, *Mathematical Biology I: An Introduction*, Springer-Verlag, New York, 2002.
- [140] J.D. Murray, *Mathematical Biology II: Spatial Models and Biomedical Applications*, Springer-Verlag, New York, 2003.
- [141] J. Nagumo, S. Arimoto and S. Yoshizawa, An active pulse transmission line simulating nerve axon, *Proceedings of the Institute of Radio Engineers* **50** (1962) 2061-2070.
- [142] S.P. Nørsett, An A-stable modification of the Adams-Bashforth methods, In *Conference on Numerical Solution of Differential Equations* Lecture Notes in Math.109/1969, 214-219, Springer-Verlag, Berlin, 1969.
- [143] E.J. Nyström, Ueber die numerische Integration von Differentialgleichungen, *Acta Societatis Scientiarum fennicae* **50** (1925) 1-54.
- [144] T. Ohta, Y. Hayase and R. Kobayashi, Spontaneous formation of concentric waves in a two-component reaction-diffusion system, *Physical Review B* **54** (1996) 6074-6082.
- [145] A. Okubo, Horizontal dispersion and critical scales of phytoplankton patches. In: J.H. Steele (ed.): *Spatial Patterns in Plankton Communities*, New York, (1978), 21-42.
- [146] A. Okubo, P.K. Maini, M.H. Williamson and J.D. Murray, On the spatial spread of the grey squirrel in Britain, *Proceedings of the Royal Society of London B* **238** (1989) 113- 125.

- [147] D. Olmos and B.D. Shizgal, A pseudospectral method of solution of Fisher's equation, *Journal Computational and Applied Mathematics* **193** (2006) 219-242.
- [148] T. Ozis and S. Ozer, A simple similarity transformation iterative scheme applied to Korteweg-de Vries equation, *Journal of Computational and Applied Mathematics* **173** (2006) 19-32.
- [149] C. Pao, Finite difference reaction-diffusion systems with coupled boundary conditions and time delays, *Journal of Mathematical Analysis and Applications* **272** (2002) 407-434.
- [150] J.E. Pearson, Complex patterns in a simple system, *Science* **261** (1993) 189-192.
- [151] S. Petrovskii, K. Kawasaki, F. Takasu and N. Shigesada, Diffusive waves, dynamic stabilization and spatio-temporal chaos in a community of three competitive species, *Japan Journal of Industrial and Applied Mathematics* **18** (2001) 459-481.
- [152] S. Petrovskii and H. Malchow, Wave of chaos: new mechanism of pattern formation in spatio-temporal population dynamics, *Theoretical Population Biology* **59** (2001) 157-174.
- [153] S. Petrovskii, A.Y. Morozov and E. Venturino, Allee effect makes possible patchy invasion in a predator-prey system, *Ecology Letter* **5** (2002) 345-352.
- [154] S. Petrovskii, B. Li and H. Malchow, Quantification of the spatial aspect of chaotic dynamics in biological and chemical systems, *Bulletin of Mathematical Biology* **65** (2003) 425-446.
- [155] D. Qiang and Z. Wenxiang, Analysis and applications of the exponential time differencing schemes and their contour integration modifications, *BIT Numerical Mathematics* **45** (2005) 307-328.
- [156] J.I. Ramos, Exponential methods for one-dimensional reaction-diffusion equations, *Applied Mathematics and Computation* **170** (2005) 380-398.

- [157] S.C. Reddy and L.N. Trefethen, Lax-stability of fully discrete spectral methods via stability regions and pseudo-eigenvalues, *Computer Methods in Applied Mechanics and Engineering* **80** (1990) 147-164.
- [158] S.C. Reddy and L.N. Trefethen, Stability of the method of lines, *Numerische Mathematik* **62** (1992) 235-267.
- [159] W.N. Reynolds, J.E. Pearson and S. Ponce-Dawson, Dynamics of self-replicating patterns in reaction diffusion systems, *Physical Review Letters* **72** (1994) 1120-1123.
- [160] W.N. Reynolds, S. Ponce-Dawson and J.E. Pearson, Self-replicating spots in reaction-diffusion systems, *Physical Review E* **56** (1997) 185-198.
- [161] H.H. Robertson, The solution of a set of reaction rate equations, *Journal of Numerical Analysis*, Academic Press, London, (1966) 178-182.
- [162] J. Roessler and H. Hussner, Numerical solution of the 1 + 2 dimensional Fisher's equation by finite elements and the galerkin method, *Mathematical and Computer Modelling* **25** (1997) 57-67.
- [163] A. Rovinsky and M. Menzinger, Interaction of Turing and Hopf bifurcation in chemical systems, *Physical Review A* **46** (1992) 6315-6322.
- [164] O.V. Rudenko and S.I. Soluyan, *Theoretical Basis of Nonlinear Acoustics*, Nauka, Moscow, 1975.
- [165] C. Runge, Ueber die numerische Auflösung von Differentialgleichungen, *Mathematische Annalen* **46** (1895) 167-178.
- [166] R.D. Ruth, A canonical integration technique, *IEEE Transactions on Nuclear Science* **30** (1938) 2669-2671.
- [167] S. Ruuth, Implicit-explicit methods for reaction-diffusion problems in pattern formation, *Journal of Mathematical Biology* **34** (1995) 148-176.

- [168] Y. Saad, Analysis of some Krylov subspace approximations to the matrix exponential operator, *SIAM Journal of Numerical Analysis* **131** (1992) 209-228.
- [169] J.M. Sanz-Serna and M.P. Calvo, *Numerical hamiltonian problems*, Chapman and Hall, London, 1994.
- [170] E.N. Sarmin and L.A. Chudov, On the stability of the numerical integration of systems of ordinary differential equations arising in the use of the straight line method, *USSR Computational Mathematics and Mathematical Physics* **3** (1963), 1537-1543.
- [171] R.A. Satnoianu, M. Menzinger and P.K. Maini, Turing instabilities in general systems, *Journal of Mathematical Biology* **41** (2000) 493-512.
- [172] M. Schatzman, Toward non-commutative numerical analysis: Higher order integration in time, *Journal of Scientific Computing* **17** (2002) 99-116.
- [173] W.E. Schiesser, *Numerical Method of Lines Integration of Partial Differential Equations*, Academic Press, San Diego, 1991.
- [174] W.E. Schisser and G.W. Griffiths, *A Compendium of Partial Differential Equation Models: Method of Lines Analysis with Matlab*, Cambridge University Press, Cambridge, 2009.
- [175] T. Schmelzer and L.N. Trefethen, Evaluating matrix functions for exponential integrators via Carathéodory-Fejér approximation and contour integrals, *Electronics Transactions on Numerical Analysis* **29** (2007) 1-18.
- [176] T.I. Seidman and L.V. Kalachev, A one-dimensional reaction/diffusion system with a fast reaction, *Journal of Mathematical Analysis with Applications* **209** (1997) 392-414.
- [177] J. Shen and X. Yang, Numerical approximations of Allen-Cahn and Cahn-Hilliard equations, *AIMS Discrete and Continuous Dynamical Systems - Series A* **28** (2010) 1669-1691.

- [178] J.A. Sherratt, On the transition from initial data to traveling waves in the Fisher-KPP equation, *Dynamics and Stability of Systems* **13** (1998) 167-175.
- [179] J.A. Sherratt and J.D. Murray, Models of epidermal wound healing, *Proceedings of the Royal Society London A* **80** (1990) 29-36.
- [180] J. Sherratt, Periodic travelling waves in cyclic predator-prey systems *Ecology Letter* **4** (2001) 30-37.
- [181] J.G. Skellam, Random dispersal in theoretical populations, *Biometrika* **38** (1951) 196-218.
- [182] A.M. Soane, M.K. Gobbert and T.I. Seidman, Numerical exploration of a system of reaction-diffusion equations with internal and transient layers, *Nonlinear Analysis* **6** (2005) 914-934.
- [183] J.C. Strikwerda, *Partial Difference Schemes and Partial Differential Equations*, SIAM, Philadelphia, 2004.
- [184] L.N. Trefethen and H.M. Gutknecht, The Carathéodory-Fejér method for real rational approximation, *SIAM Journal on Numerical Analysis* **20** (1983) 420-436.
- [185] L.N. Trefethen, Lax-stability vs. eigenvalue stability of spectral methods. In K.W. Morton and M.J. Baines, *Numerical Methods in Fluid Dynamics III*, Clarendon Press, Oxford, 1988.
- [186] L.N. Trefethen, *Finite Difference and Spectral Methods for Ordinary and Partial Differential Equations*, Upson Hall Cornell University Ithaca, New York, 1996.
- [187] L.N. Trefethen, *Spectral Methods in MATLAB*, SIAM, Philadelphia, 2000.
- [188] L.N. Trefethen and M. Embere, *Spectra and Pseudospectra: The Behavior of Non-normal Matrices and Operators*, Princeton University Press, New Jersey, 2005.
- [189] A.M. Turing, The chemical basis for morphogenesis. *Philosophical Transactions of the Royal Society* **237** (1952) 37-72.

- [190] V. Volpert and S. Petrovskii, Reaction-diffusion waves in biology, *Physics of Life Reviews* **6** (2009) 267-310.
- [191] V. Volterra, Fluctuation in abundance of the species considered mathematically, *Nature* **118** (1926) 558-560.
- [192] V. Volterra, *Variations and Flunctuations of the Numbers of Individuals in Animal and Species Living together* , Reprinted in 1931 in R.N. Chapman, *Animal Ecology*, McGraw-Hill, New York, 1926.
- [193] W. Wang, Q. X. Liu and Z. Jin, Spatiotemporal complexity of a ratio-dependent predator-prey system, *Physical Review E* **75** (2007) 1539-3755.
- [194] W. Wang, L. Zhang, H. Wang and Z. Li, Pattern formation of a predator-prey system with Ivlev-type function response, *Ecological Modelling* **221** (2010) 131-140.
- [195] M.J. Ward, Asymptotic methods for reaction- diffusion systems: Past and present, *Bulletin Mathematical Biology* **68** (2006) 1151-1167.
- [196] A.-M. Wazwa, The variational iteration method for rational solutions for KdV, K(2,2) Burgers and cubic Boussinesq equations, *Journal of Computational and Applied Mathematics* **207** (2007) 18-23.
- [197] Z. Xu and D. Xian, Application of exp-function method to generalized Burgers-Fisher equation, *Acta Mathematicae Applicatae Sinica* **26** (2010) 669-676.
- [198] N. Yasumasa and U. Ueyama, A skeleton structure of self-replicating dynamics, *Physica D* **130** (1999) 73-104.
- [199] H. Yu, S. Zhong and R.P. Agarwal, Mathematics and dynamic analysis of an apparent competition community model with impulsive effect, *Mathematical and Computer Modelling* **52** (2010) 25-36.

- [200] N.J. Zabusky, A synergetic approach to problems of nonlinear dispersive wave propagation and interaction. In W.F. Ames (ed.), *Nonlinear Partial Differential Equations*, Academic Press, New York, (1967) 223-258.
- [201] M.L. Zeeman, Hopf bifurcations in competitive three-dimensional Lotka-Volterra systems, *Dynamics and Stability of Systems* **8** (1993) 189-217.
- [202] J. Zhang and Q. Du, Numerical studies of discrete approximations to the Allen-Cahn equation in the sharp interface limit, *SIAM Journal on Scientific Computing* **31** (2009) 3042-3063.
- [203] B. Zinner, Existence of traveling wavefront solutions for the discrete Nagumo equation, *Journal of Differential Equations* **96** (1992) 1-27.

